Soils and Rocks

Volume 39, N. 3

2016

ISSN 1980-9743

Soils and Rocks

Soils and Rocks

An International Journal of Geotechnical and Geoenvironmental Engineering

Volume 39, N. 3
September-December 2016

Soils and Rocks is an International Journal of Geotechnical and Geoenvironmental Engineering published by

ABMS - Brazilian Association for Soil Mechanics and Geotechnical Engineering
Av. Queiroz Filho, 1700 – Torre A Sky, Sala 106 – Vila Hamburguesa
05319-000, São Paulo, SP
Brazil

SPG – Portuguese Geotechnical Society
LNEC, Avenida do Brasil, 101
1700-066 Lisboa
Portugal

Issue Date: *December 2016*

Issue: *400 copies and 800 online-distributed copies*

Manuscript Submission: *For review criteria and manuscript submission information, see Instructions for Authors at the end.*

SOILS and ROCKS

An International Journal of Geotechnical and Geoenvironmental Engineering

Editor Waldemar Coelho Hachich - University of São Paulo, Brazil

Co-editor José Couto Marques - University of Porto, Portugal

"Ad hoc" Reviewers (2015-2016)

Soils and Rocks publishes papers in English in the broad fields of Geotechnical Engineering, Engineering Geology and Geo-environmental Engineering. The Journal is published in April, August and December. Subscription price is US$ 90.00 per year. The journal, with the name "Solos e Rochas", was first published in 1978 by the Graduate School of Engineering, Federal University of Rio de Janeiro (COPPE-UFRJ). In 1980 it became the official magazine of the Brazilian Association for Soil Mechanics and Geotechnical Engineering (ABMS), acquiring the national character that had been the intention of its founders. In 1986 it also became the official Journal of the Brazilian Association for Engineering Geology and the Environment (ABGE) and in 1999 became the Latin American Geotechnical Journal, following the support of Latin-American representatives gathered for the Pan-American Conference of Guadalajara (1996). In 2007 the journal acquired the status of an international journal under the name of Soils and Rocks, published by the Brazilian Association for Soil Mechanics and Geotechnical Engineering (ABMS), Brazilian Association for Engineering Geology and the Environment (ABGE) and Portuguese Geotechnical Society (SPG). In 2010, ABGE decided to publish its own journal and left the partnership.

Soils and Rocks

1978,	1 (1, 2)
1979,	1 (3), 2 (1,2)
1980-1983,	3-6 (1, 2, 3)
1984,	7 (single number)
1985-1987,	8-10 (1, 2, 3)
1988-1990,	11-13 (single number)
1991-1992,	14-15 (1, 2)
1993,	16 (1, 2, 3, 4)
1994-2010,	17-33 (1, 2, 3)
2011,	34 (1, 2, 3, 4)
2012-2015,	35-38 (1, 2, 3)
2016,	**39 (1, 2, 3)**

ISSN 1980-9743 CDU 624.131.1

ISSN 1980-9743

SOILS and ROCKS
An International Journal of Geotechnical and Geoenvironmental Engineering

Publication of
ABMS - Brazilian Association for Soil Mechanics and Geotechnical Engineering
SPG - Portuguese Geotechnical Society
Volume 39, N. 3, September-December 2016

Table of Contents

Victor de Mello Lecture

The Victor de Mello Lecture was established in 2008 by the Brazilian Association for Soil Mechanics and Geotechnical Engineering (ABMS), the Brazilian Association for Engineering Geology and the Environment (ABGE) and the Portuguese Geotechnical Society (SPG) to celebrate the life and professional contributions of Prof. Victor de Mello. Prof. de Mello was a consultant and academic for over 5 decades and made important contributions to the advance of geotechnical engineering. Every second year a worldwide acknowledged geotechnical expert is invited to deliver this special lecture, on occasion of the main conferences of ABMS and SPG.

The fifth Victor de Mello Lecture is delivered by Prof. J.P. Giroud, an internationally renowned professor, author, consultant, practitioner and researcher. Prof. de Mello established, during his term as president of the ISSMGE, the Technical Committee that started to study the behaviour and the contributions of geosynthetics to the diverse fields of geotechnical engineering. The challenges of introducing a synthetic material for the crucial task of filtering or waterproofing an interface of soils of different grain size distributions needed sound concepts and a focused research effort. Prof. Giroud shares with us, in his lecture, the rationale behind reliable engineering solutions using geomembrane liners.

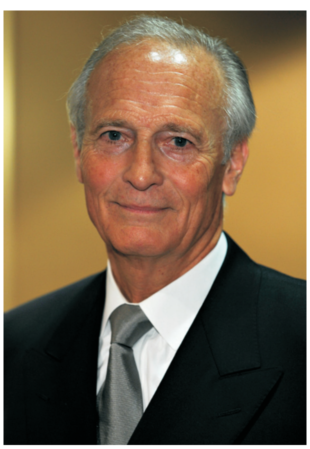

Prof. J.P. GIROUD, a consulting engineer, is a former professor of geotechnical engineering. He is chairman of the editorial board of *Geosynthetics International* and past president of the International Geosynthetics Society (the IGS). Dr. Giroud is a member of the US National Academy of Engineering and Chevalier in the Order of the Légion d'Honneur. He has authored over 400 publications and he coined the terms "geotextile" and "geomembrane" in 1977. Dr. Giroud has 54 years of experience in geotechnical engineering and he has developed many of the design methods used in geosynthetics engineering. The IGS has named its highest award "The Giroud Lecture", "in recognition of the invaluable contributions of Dr. J.P. Giroud to the technical advancement of the geosynthetics discipline". A Giroud Lecture is presented at the opening of each International Conference on Geosynthetics by a lecturer selected by the IGS. Dr. Giroud has delivered prestigious lectures, such as the Vienna Terzaghi Lecture, the Mercer Lecture and the Terzaghi Lecture of the American Society of Civil Engineers.

Leakage Control using Geomembrane Liners

J.P. Giroud

Abstract. Geomembrane liners are used in all types of containment structures. Evaluating the performance of a geomembrane liner is a challenge. While zero leakage into the ground is a legitimate goal if the leaking liquid may pollute the ground and the ground water, or if the soil integrity can be impaired, zero is unrealistic and impossible to measure. Furthermore, zero leakage is not an appropriate goal in some applications such as geomembrane-lined dams. In this paper, it is shown that the difference between acceptable and unacceptable leakage should result from a rational analysis of the potentially detrimental consequences of leakage. Also, it is shown that the specified leakage must be achievable and measurable. Therefore, emphasis is placed on the quantitative evaluation of leakage. Practical guidance is provided for leakage reduction at construction stage and design stage; and typical leakage rates are mentioned. Potential failures associated with leakage control measures are described. Case histories illustrate both failures in case of misuse of geomembranes and the durability of geomembranes. This paper is intended to contribute to the appropriate design and the safety of geomembrane-lined structures.

Keywords: geosynthetics, geomembranes, drainage, liners, leakage, reservoirs, dams.

1. Introduction

1.1. The Fifth Victor de Mello Lecture

Victor de Mello was a visionary. In the 1980s, he encouraged the use of geotextiles and geomembranes and created the first Technical Committee on Geotextiles of the International Society for Soil Mechanics and Geotechnical Engineering and he appointed the author of this paper as chairman of this committee. The author of this paper is both indebted to Victor de Mello and very honored to present the Fifth Victor de Mello Lecture. The information presented in this paper is consistent with the interest of Victor de Mello for innovative materials as evidenced by the following words, "Engineering creativity is vital and of the essence in geotextiles and geomembranes technology", from the foreword Victor de Mello wrote for the paper summarizing the work of the Technical Committee on Geotextiles (Giroud *et al.*, 1985).

1.2. This paper

This paper is devoted to leakage control using geomembranes. To that end, this paper will address various topics pertaining to leakage such as liner materials, terminology, influence of parameters on leakage, measures taken at design and construction stages to reduce leakage, leakage detection and measurement, and leakage prediction. The discussions presented in this paper are relevant to containment structures lined with geomembranes, such as landfills, reservoirs and dams.

2. General Introduction to Leakage

2.1. Leakage happens and must be addressed

"All liners leak": this was stated by Giroud & Bonaparte (1989a) at the beginning of their paper. This should not be construed as meaning that there is no way to safely store liquids. In fact, recognizing that all liners may leak is the first step to the safe design of liquid containment systems. The design of a containment structure cannot be safe if the possibility of leakage is not recognized in the first design step. Depending on the desired degree of leakage control, there is a choice of adequate solutions using geomembrane liners, including single geomembrane liner, composite liner (*i.e.* geomembrane associated with clay), and double liner. This paper will show that, with a realistic goal regarding acceptable leakage rate, it is possible to achieve the desired level of leakage control using appropriate design and construction methods.

2.2. Terminology related to leaks, leakage and leakage rate

Adapting from several dictionaries, and restricting the discussion to liquids, it can be said that the word "leak" has two meanings: (i) a passageway through which liquid can unintentionally escape; and (ii) the liquid that escapes through a passageway, such as liquid flowing unintentionally out of a reservoir. To avoid possible confusion due to this dual meaning of the word "leak", the word "hole" is used herein to mean a passageway through the liner such as a puncture, tear or crack, or a passageway at the periphery

J.P. Giroud, PhD., E.C.P., Consulting Engineer, JP GIROUD, INC., Miami, FL, USA. e-mail: jpg@jpgiroud.com.
Intited Lecture, no discussions.

of the liner such as a gap between the liner and an appurtenance.

The word "defect" is often used to designate a hole that makes a leak possible. In fact, the use of "defect" to designate a hole should be avoided, because many types of defects do not constitute a passageway for liquid. All holes associated with a liner are defects (either defects in the liner or inadequate connections between the liner and adjacent structures), but not all defects are holes.

The word "leakage" designates the amount of liquid that escapes from a containment structure. The term "leakage rate" designates the amount of leakage per unit of time. Sometimes, the term "leakage rate" is also used to designate what is more accurately called "leakage rate per unit area", which implies "per unit area of liner", a concept applicable to some, but not all, containment structures. The distinction between "leakage rate" and "leakage rate per unit area" appears in the units.

2.3. Units use for leakage rate

The following units are used for leakage rate:

1 m^3/s = 1000 liters per second = 60,000 liters per minute

The following units are used for leakage rate per unit area:

1 liter per hectare per day (lphd) = 1.157×10^{-12} m/s = 1.157×10^{-10} cm/s.

A liquid level drop of 1 mm per day is equal to 10,000 lphd.

A rate of leakage of 1 m^3/s in one hole per ha is equivalent to 8.64×10^7 lphd $\approx 1 \times 10^8$ lphd.

2.4. Zero leakage, a desirable goal but an inappropriate specification

Zero leakage is a desirable target. However, "zero" is impossible to measure in engineering. Since zero leakage cannot be measured, it is inappropriate to specify zero leakage. Therefore, a small, but rationally established, maximum leakage rate should be specified. One of the goals of this paper is to provide guidance for the selection of a rational maximum leakage rate.

If zero leakage is detected in the monitoring of a containment structure, it is recommended to draw careful conclusions:

- The zero-leakage detection may, indeed, result from excellent performance, but it is only representative of the current situation and there is no guarantee that the performance will continue to be excellent. Monitoring should continue.
- The zero-leakage detection may result from incorrect or inaccurate measurement. The method used for leakage detection and measurement should be scrutinized using as a guide the review of potential errors in leakage rate measurement, which is presented hereafter in Section 8.3.

Another reason for selecting a rational value for the specified maximum leakage rate is the following: when zero or excessively small values of maximum leakage rates are specified, extensive investigations to find holes in the geomembrane and extensive geomembrane repairs may be required to try to meet the specified leakage rate. The investigation and repair activities may cause collateral damage to the liner, which has resulted in higher leakage rates in several instances (see Sections 8.3.1 and 8.3.3).

From the foregoing discussion, it is clear that, rather than pursing the unrealistic goal of zero leakage, it is preferable to follow the rational approach that consists in discussing the limit between acceptable and unacceptable leakage, which requires an understanding of the potentially detrimental consequences of leakage.

2.5. Potentially detrimental consequences of leakage

2.5.1. Review of the potentially detrimental consequences of leakage

Leakage can be potentially detrimental for several reasons, including economic loss, environmental damage, perceived damage, geotechnical damage, and liner damage or disturbance, as described below:

- Economic loss including: (i) loss of water (an increasingly valuable liquid), or loss of other valuable liquids (*e.g.* chemical liquids in industrial reservoirs, and pregnant solutions in mining ponds); (ii) loss of generated power in the case of massive leakage in reservoirs for pump-storage stations; (iii) difficulty in maintaining an acceptable liquid level (*e.g.* in decorative ponds, reservoirs for recreation or sport activities); and (iv) cost associated with the following four items.
- Environmental damage due to: (i) contamination of soils, water streams and ground water by chemical components of the leaking liquids; and (ii) flooding due to massive leakage.
- Perceived damage, such as visible leakage through the downstream face of a concrete dam, which may be technically safe and, therefore, technically acceptable, but is detrimental regarding public perception
- Geotechnical damage by: (i) deterioration of the material supporting the liner by intrusion of leakage in the soil supporting the liner (*e.g.* erosion of the ground under the geomembrane, formation of solution cavities, internal erosion of an embankment (dam or dike), softening of the soil supporting the geomembrane causing soil deformation thereby inducing strains in the geomembrane, erosion and/or softening of the soil supporting the geomembrane bringing stones in contact with the geomembrane, physical and/or chemical deterioration of concrete in the case of concrete dams); and (ii) instability of the soil or structure supporting the liner (*e.g.* due to phreatic surface buildup and pore water pressure increase in the ground supporting the liner, due to excessive pore water

pressure in embankment dam or dike, due to water pressure in cracks or joints of concrete dams).

- Liner damage or disturbance, such as: (i) damage to the liner (and consequently increase in leakage rate) caused by the liquid flow pressure (*e.g.* erosion of a clay liner or increase of geomembrane hole size); and (ii) uplifting of liner (which, in the case of a geomembrane, reduces the reservoir capacity, induces tensile stresses in the geomembrane, exposes the geomembrane to mechanical damage and weather-generated deterioration).

Examples of consequences of leakage are summarized in Table 1. It appears in Table 1 that the risk of geotechnical damage may be more frequent than other risks. Therefore, engineers designing liner systems should pay special attention to the potential deterioration of geotechnical conditions due to leakage, rather than focusing exclusively on economic loss and contamination of ground, as they often do.

2.5.2. Acceptable leakage based on the detrimental consequences of leakage

As often mentioned by the author of this paper, it must be recognized that "all liners leak, or may leak" and that "a leak should only be a leak", *i.e.* a loss of liquid without unacceptable consequences. In other words, a leak should not trigger an unacceptable problem, *i.e.* one of the detrimental consequences mentioned above in Section 2.5.1.

As discussed above in Section 2.4, zero leakage is an inappropriate requirement. Therefore, the only relevant approach is, for each specific case, to determine the limit between acceptable and unacceptable leakage based on an evaluation of the detrimental consequences of leakage listed above in Section 2.5.1. As adapted from Giroud (1984a) and Peggs & Giroud (2014), leakage from a geomembrane-lined reservoir can be acceptable if the following five requirements are met: (i) the loss of liquid remains small enough to be economically acceptable; (ii) the leaking liquid does not cause unacceptable pollution of the ground or the ground water; (iii) the leakage is not perceived by the public as unacceptable; (iv) the leaking 1liquid does not cause a degradation of the soil or the structure supporting the geomembrane; and (v) the leaking liquid does not uplift the geomembrane liner or otherwise damage the liner.

2.5.3. Acceptable leakage based on achievability and measurability

The specified leakage rate must be achievable and measurable. Specifying a leakage rate that cannot be achieved is counterproductive because it will trigger endless investigations and repairs that often result in causing damage to the liner, hence more leakage (see Sections 2.4, 8.3.1 and 8.3.3).

In order to adequately specify, it is necessary to be able to predict, and to predict it is necessary to be able to quantify. Accordingly, guidance will be provided to evaluate leakage (see Section 8). This is essential, because engineering is essentially done with numbers.

3. Liners and Liquid Migration

3.1. Geomembranes and other liner materials

3.1.1. Presentation of geomembranes

The term "geomembrane" proposed by the author of this paper (Giroud & Perfetti, 1977) has been adopted worldwide. Geomembranes are quasi-impermeable membranes ("membrane" implying continuity and flexibility) used in geotechnical engineering applications as a barrier to the migration of fluids. Geomembranes are mostly used as barriers to contain liquids, redirect their flow or prevent their migration, in particular in reservoirs, canals, dams, hydro tunnels, tailings dams, leach pads, waste storage landfills, and underground structures (tunnels, below-ground buildings, etc.). The quasi-impermeable component of geomembranes is either a polymer or bitumen. A variety of chemical and mineral additives are incorporated in the polymer or the bitumen to improve some of their properties.

Geomembranes are un-reinforced or reinforced. Reinforced geomembranes are reinforced using a woven fabric or a nonwoven fabric:

- A woven fabric is used to reinforce some polymeric geomembranes. It is then placed inside the geomembrane.
- A nonwoven fabric impregnated and coated with bitumen is used to manufacture bituminous geomembranes. Some bituminous geomembranes are reinforced with glass fibers, in addition to the nonwoven fabric.
- A nonwoven fabric bonded to a geomembrane (Fig. 1) forms a type of reinforced geomembrane called "composite geomembrane"; in this case the nonwoven fabric

Table 1 - Examples of detrimental consequences of leakage.

Detrimental consequence	Containment of water	Containment of mining pregnant solution	Containment of wasted liquid
Loss of valuable liquid	Yes	Yes	No
Contamination of ground	No	Yes	Yes
Geotechnical damage	Yes	Yes	Yes

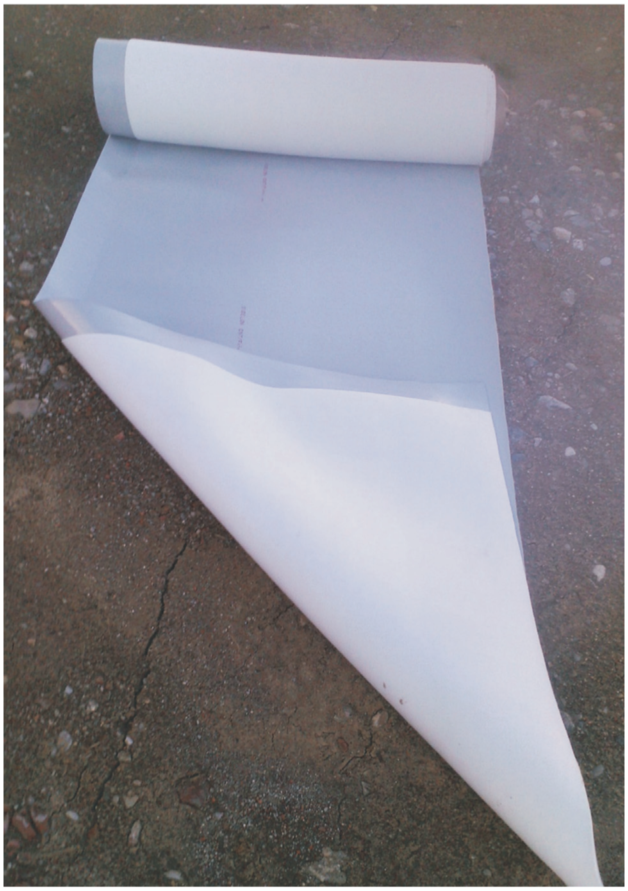

Figure 1 - Composite geomembrane composed of a geomembrane (grey color) bonded to a nonwoven geotextile (white color). The selvage with no geotextile is reserved for seaming the geomembrane to the adjacent panel [Courtesy Carpi].

(which is, in fact, a nonwoven geotextile) is outside the geomembrane.

The thickness of geomembranes is typically from approximately 1 to 5 mm. Geomembranes are available in rolls (typically 2 to 10 m wide), which are assembled by seaming to form large liners.

All the geomembranes considered herein are made in a manufacturing plant. It is generally considered that geomembranes made in situ by spraying a low-permeability compound onto a geotextile or directly on the ground are not sufficiently reliable to be used for high-performance leakage control.

Since the 1970s, geomembranes have progressively replaced traditional liner materials in many applications.

3.1.2. Presentation of liner materials other than geomembranes

Traditional liner materials include cement concrete, bituminous concrete, and compacted clay. Typical thicknesses for liners made using these traditional materials are 0.1-0.2 m for cement concrete and bituminous concrete, and 0.3-1.0 m for compacted clay.

There is a category of geosynthetic liner material whose low-permeability component is bentonite, a variety of clay with very low permeability: the bentonite geocomposites, also called geosynthetic clay liners. Typically, a bentonite geocomposite consists of a layer of bentonite between two layers of fabric. The thickness of bentonite geocomposites is typically 5-7 mm when the bentonite is dry and of the order of 10 mm when the bentonite is hydrated.

All of the above materials can be associated with geomembranes to form composite liners (see Section 6). This is typically done with compacted clay and bentonite geocomposites.

3.2. Liquid migration through liners

3.2.1. Modes of liquid migration

Leakage associated with any type of liner include:

- Liquid migration through the liner via the following mechanisms:
    - diffusion (which takes place at the molecular scale),
    - advective flow, which includes laminar flow (through a porous medium, and through thin cracks and very small holes) and non-laminar flow through cracks and holes.
- Liner bypass (*i.e.* flow at and around the periphery of the liner).

These mechanisms are discussed in the following sections, with particular emphasis on the case of geomembranes.

3.2.2. Diffusion

Diffusion through geomembranes occurs essentially in the case of some volatile organic compounds, such as benzene, toluene, trichloroethylene, and xylene. Diffusion through geomembranes is negligible in the case of water and non-organic compounds such as chlorides. In the case of compounds that could migrate through geomembranes by diffusion, the migration can be reduced by proper selection of the type of geomembrane, and the effect on the ground of compounds that migrate by diffusion can be alleviated by placing a thick layer of fine-grained soil under the geomembrane. This layer, called "attenuation layer", is typically made of clay or silt and it is typically more than 1 m thick.

Diffusion will not be discussed further in this paper. Leakage through holes in the geomembrane is the only mode of leakage through the geomembrane that will be discussed in this paper. In addition, leakage due to flow at and around the periphery of the geomembrane will be addressed later in this paper (see Section 5.2).

3.2.3. Laminar advective flow

All liner materials except geomembranes are porous media. Furthermore, when these materials are intact, the pores are so small that the flow is generally laminar. Therefore, Darcy's equation, which is strictly applicable to laminar flow through porous media, can be used for these liners. As a result, a hydraulic conductivity (*i.e.* coefficient of permeability) can be defined and measured for these liners.

Strictly speaking, the coefficient of permeability cannot be used for liquid migration through geomembranes because geomembranes are not porous media. However, some standard tests conducted to evaluate geomembrane acceptance can be interpreted by deriving an "equivalent coefficient of permeability". In the case of good-quality modern geomembranes the equivalent coefficient of permeability is typically less than 10^{-14} m/s.

The equivalent coefficient of permeability is a convenient way to compare geomembranes to other liner materials. Typical orders of magnitude of the coefficient of permeability (for liners others than geomembranes) and the equivalent coefficient of permeability (for geomembranes) are as follows:

- Cement concrete: 10^{-12} m/s in ideal laboratory conditions.
- Cement concrete: 10^{-10} m/s to 10^{-8} m/s in the field.
- Roller compacted concrete: 10^{-8} m/s to 10^{-6} m/s.
- Bituminous concrete: 10^{-9} m/s in ideal laboratory conditions.
- Bituminous concrete: 10^{-8} m/s in the field.
- Compacted clay layer: 10^{-9} m/s with excellent construction and quality control.
- Compacted clay layer: 10^{-8} m/s with ordinary construction and quality control.
- Bentonite geocomposite 10^{-11} m/s (when hydrated and not exposed to calcium cations).
- Geomembranes: < 10^{-14} m/s (when intact).

These orders of magnitude show that geomembranes can be considered quasi-impermeable materials while other liner materials are low-permeability materials. However, it is not because geomembranes are quasi impermeable that geomembrane-lined containment structures do not leak. Impermeability of an intact geomembrane on a small scale does not guarantee impermeability on a large scale under field conditions.

3.2.4. Non-laminar advective flow through holes

When a geomembrane with holes rests on a highly permeable material such as coarse gravel (possibly stabilized with a small amount of cement or bitumen), the flow of liquid through the holes is non-laminar and the equation for free flow through an orifice is applicable (see Section 8.2.2) The leakage rate is then high.

The rate of leakage through a hole in a geomembrane can be drastically reduced by placing the geomembrane on another liner material such as a compacted clay layer or a bentonite geocomposite. A "composite liner" is thus formed. An entire section will be devoted to this important way of using geomembranes, which has significant advantages but requires precautions for a safe use (see Section 6).

In modern geomembranes, there are no holes in the geomembranes made in a manufacturing plant. The development of holes during construction (geomembrane installation and, more importantly, subsequent construction activities such as placement of materials on top of the geomembrane) and in service depend in great part on the mechanical properties of the geomembrane. Thus, tensile characteristics, puncture resistance and tear resistance of a geomembrane are essential properties (see Section 5.2.2).

3.2.5. Conclusion on liquid migration

In conclusion, it is not appropriate to characterize a geomembrane using a coefficient of permeability (except for a simplistic comparison with other types of liners). As leakage through geomembranes occurs essentially through holes, it is more important to characterize a geomembrane by the size and frequency of holes. This will be discussed in Section 8.1.

Leakage through geomembrane liners can be reduced by actions taken during construction (such as construction quality assurance and electric leak location survey) and decisions made at the design stage (such as geomembrane damage control, use of composite liner, use of double liner). These important aspects will be addressed in subsequent sections: leakage reduction by measures taken during construction (Section 4), leakage reduction by controlling geomembrane damage (Section 5), leakage reduction by using composite liners (Section 6), and leakage reduction by using double liners (Section 7).

4. Leakage Reduction by Measures Taken During Construction

4.1. Detection of holes during construction

The usual way to improve liner quality and, in particular, to find holes is by implementing a construction quality assurance plan. In the case of geomembrane liners, construction quality assurance consists of inspections and measures taken by a team independent from the geomembrane installer during installation of the geomembrane and associated materials, including overlying materials. Indeed, damage to geomembrane liners is often caused by the placement of materials (in particular soil layers) on top of the geomembrane.

Typical construction quality assurance activities aimed at finding holes in the geomembrane include:

- Nondestructive tests on seams to find gaps in seams.
- Visual inspection of the entire geomembrane liner to find: (i) punctures and tears in the geomembrane, and (ii) gaps in attachments of geomembrane to appurtenant structures.

These typical construction quality assurance activities (seam testing and visual inspection) may be sufficient in the case of first-class projects, characterized by: excellent workmanship; and excellent working conditions. This is the case for sophisticated applications, such as geomembrane-lined dams. But, experience shows that these typical construction quality assurance activities (seam testing and visual inspection) are not sufficient in the case of usual projects, such as landfills and many reservoirs where they miss a number of holes. In such projects, it is recommended to perform electric leak location surveys in addition to the implementation of construction quality assurance.

4.2. Electric leak location survey of geomembranes

4.2.1. Definition

The modern technology for finding holes in geomembrane liners is the electric method designated by "electric leak location survey" or "electric liner integrity survey" or similar terms (such as "electric hole-detection survey", which indicates that the method detects holes, not leaks, according to the terminology presented in Section 2.2). When it is applicable, this technology makes it possible to detect a significant number of holes that are not typically detected by visual inspection. After repair of the detected holes, the geomembrane liner has been significantly improved, because the number and size of holes has been significantly reduced.

The principle of electric leak location surveys is simple. Most geomembranes are electrical insulators. Therefore, electric current will pass if there is a hole in the geomembrane or a gap in an attachment of the geomembrane to an appurtenant structure. The electric liner integrity survey requires a conductive layer immediately beneath the geomembrane. Therefore, the electric liner integrity survey is not effective if the geomembrane is not in contact with the underlying soil unless a conductive-backed geomembrane is used (*i.e.* a geomembrane with a thin conductive layer along its lower face). In particular, with ordinary geomembranes (*i.e.* geomembranes with no conductive layer), the electric leak location technique is not effective at locations where the geomembrane exhibits wrinkles.

4.2.2. Performance and sensitivity

In the past two decades, the electric leak location technology has made significant progress. Today, electric leak location can be performed on a bare geomembrane, on a geomembrane under water, or on a layer of soil overlying a geomembrane.

When a geomembrane is to be covered by a layer of soil, it is important to perform electric leak location survey, not only after geomembrane installation, but also after placement of the soil layer because holes in the geomembrane are often caused by soil placement.

The sensitivity of electric leak location survey (*i.e.* the size of holes that can be found by electric leak location survey) depends on the amount of material covering the geomembrane when the survey is performed. With current technology (2016), the sensitivity limit of the electric leak location technique (*i.e.* the minimum size of holes that can be found) is approximately: (i) 1 mm for a bare geomembrane; and (ii) 6 mm under 0.6 m of soil. Clearly, electric leak location can find small holes, but not all. This leads to the following discussion on the limitation of this technology.

4.2.3. Limitation of the technology

The same leakage rate may result from one hole (easy to find by electric survey) or several small holes that are difficult to find. Therefore, if the specified maximum leakage rate can be generated by small holes, much time could be wasted and much expenses could be incurred using the electric liner survey technique to try unsuccessfully to find holes that are too small to be detected. A similar concern has been expressed by Darilek & Laine (2013). Furthermore, excessive activity on a geomembrane liner to try to find holes may result in additional damage to the geomembrane liner, as illustrated in the case history presented in the Section 8.3.3.

This situation shows the limit of the electric survey technology and is a reminder that electric survey does not replace geomembrane installation by a skilled crew with strict construction quality assurance, which is the best way to minimize the risk of holes before performing an electric liner integrity survey. This situation is also a reminder that the specified maximum leakage rate must be selected rationally (see Section 2.5.3).

4.2.4. Use of the electric leak location survey technology

An inquiry based on data collected by two suppliers of electric leak location surveys (Beck & Darilek, 2016) and summarized by the author of this paper has shown that 2% of the geomembrane liner surface area installed in the United States in 2014 was subjected to electric leak location survey, which is very small, compared to 21% in the province of Quebec in 2014 (Charpentier *et al.*, 2016).

4.3. Conclusion on leakage reduction by measures taken during construction

The measures taken during construction to reduce the number and size of holes (and therefore, reduce leakage) are useful but not sufficient. These measures do not replace good workmanship in geomembrane liner installation, and they do not replace adequate design.

Measures at the design stage are often necessary in addition to the measures taken at the construction stage. A general characteristic of these measures is that they generally associate complementary materials:

- Association geomembrane/geotextile, the geotextile protecting the geomembrane from adjacent materials (see Section 5).
- Association geomembrane/clay to form a composite liner (see Section 6).
- Association geomembrane/drainage layer/geomembrane thereby forming a double liner (see Section 7).

5. Leakage Reduction by Controlling Geomembrane Damage

5.1. Geomembrane protection using a geotextile

Holes in geomembranes car result from geomembrane puncture by sharp objects (generally stones) during construction and in service. The state of practice is to use nonwoven geotextiles for geomembrane protection, a technique initiated by the author of this paper in 1971 (Giroud, 1973).

Nonwoven geotextiles are available with different masses per unit area. There is currently wide discrepancy between practices in different countries: for example, nonwoven geotextiles with a mass per unit area of the order of 500 g/m^2 are typically used in North America to protect geomembranes compared to 1000 g/m^2 frequently used in Europe. In technically advanced cases, a mass per unit area of the order of 2000 g/m^2 is not uncommon. This was done, for example, for the rehabilitation of several masonry dams with a very rough upstream face. An example is illustrated in Figs. 2 and 3.

Figure 2 - Face of a masonry dam on which a nonwoven geotextile with a mass per unit area of 2000 g/m^2 was placed prior to installing a geomembrane, Covão do Ferro Dam, Portugal [Courtesy Carpi].

5.2. Attachment to appurtenant structures

5.2.1. Statement of the problem

Good installers know how to make attachments to appurtenant structures that are leak-proof provided the structure has a simple geometry. However, geomembrane liners can rupture while in service next to their attachment to a rigid structure. In fact, a significant fraction of observed leakage of geomembrane-lined facilities occurs at or near the attachments between the geomembrane and rigid appurtenant structures.

Causes of geomembrane failure next to attachment to a rigid structure include:

- Geomembrane failure due to stresses induced by large differential settlement between the embankment that supports the geomembrane and the rigid structure.
- Geomembrane failure due to stresses induced by repeated displacement of geomembrane by wind action, by wave action, or by cycles of filling-emptying of the reservoir.

Two failure modes are observed: (i) tensile rupture of the geomembrane; and (ii) failure of the geomembrane seam that is closest to the attachment. Indeed, seams are generally weaker that the geomembrane and the seam geometry causes stress concentration by a factor of the order of 2 (Giroud *et al.*, 1995). This is particularly true in the case of polyethylene geomembranes when the seam closest to the attachment is an extrusion seam, which is weaker that the fusion seam.

The first of the above mentioned two causes (differential settlement) is well known. In contrast, the second cause (repeated displacement of the geomembrane) has not received sufficient attention. Repeated displacement of the geomembrane is, in fact, a major cause of geomembrane seam failure located next to an attachment. The geomembrane being restrained on one side of the seam and free to move on the other side, the seam is subjected to repeated tension and bending, which progressively causes fatigue of the seam and, eventually, cracking, especially in the case of extrusion seams of HDPE geomembranes. The author of this paper works on a large reservoir where several tens of extrusion seams have thus failed as a result of repeated wind action.

The two aspects to be considered when dealing with attachments are: (i) geomembrane selection, and (ii) geometric considerations, *i.e.* shape of the rigid structure and configuration of the geomembrane in the vicinity of the attachment.

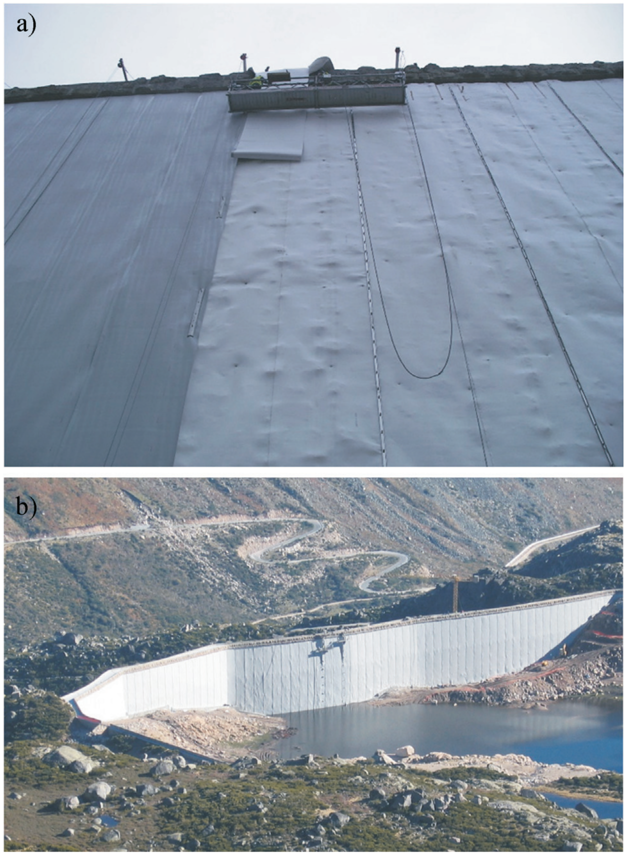

Figure 3 - Rehabilitation of a masonry dam: (a) placement of the geomembrane on the geotextile on the upstream face of Covão do Ferro Dam, Portugal, and (b) view of the completely rehabilitated dam [Courtesy Carpi].

5.2.2. Selection of the geomembrane for withstanding differential settlement at attachment

A theoretical analysis of the case of differential settlement between an embankment and the rigid structure to which a geomembrane is attached has been conducted (Giroud & Soderman, 1995, Giroud, 2005). The analysis demonstrates that the factor of safety against geomembrane rupture in this case is the square root of the ratio of the ultimate co-energy of the geomembrane and the required co-energy:

- The ultimate co-energy is the area between the tension-strain curve of the geomembrane and the tension axis (*i.e.* the vertical axis). This is the area hatched in red in Fig. 4, *i.e.* area ADE, with E being the end of the tension-strain curve (or, more strictly, the end of the useful portion of the tension-strain curve considered in design).
- The required co-energy depends on the magnitude of the settlement, the pressure of the contained liquid, and the interface friction angle between the geomembrane and the embankment soil. The required co-energy can be calculated for each specific case. The required co-energy is represented by the shaded area in Fig. 4 (*i.e.* area ABC).

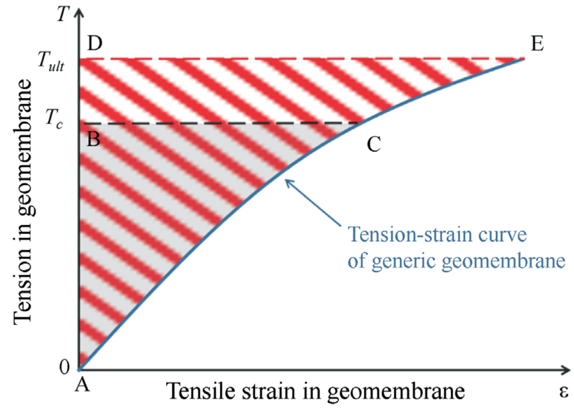

Figure 4 - Required co-energy (grey area, ABC) *vs.* maximum co-energy (area with red stripes).

It is limited by the calculated tension in the geomembrane, Tc.

The factor of safety (which is the square root of the ratio of the hatched area and the shaded area, as indicated above) can be determined graphically. It can also be determined analytically if the equation of the geomembrane tension-strain curve is known. This has been done for HDPE geomembranes (4th degree parabola) and composite geomembranes that consist of a PVC geomembrane bonded to a nonwoven geotextile (straight line).

While the various available geomembranes are all quasi-impermeable and, therefore, quasi-equivalent from the viewpoint of impermeability, their tension-strain curves are very different as illustrated in Fig. 5. Based on the analysis, the geomembranes that have tension-strain curves close to the vertical axis (*i.e.* the geomembranes that have a small co-energy) are the most likely to rupture next to their attachments to rigid structures in case of differential settlement.

5.2.3. Shape of the structure and configuration of the connection

Two geometric measures can be taken to prevent geomembrane rupture in the vicinity of a rigid structure to

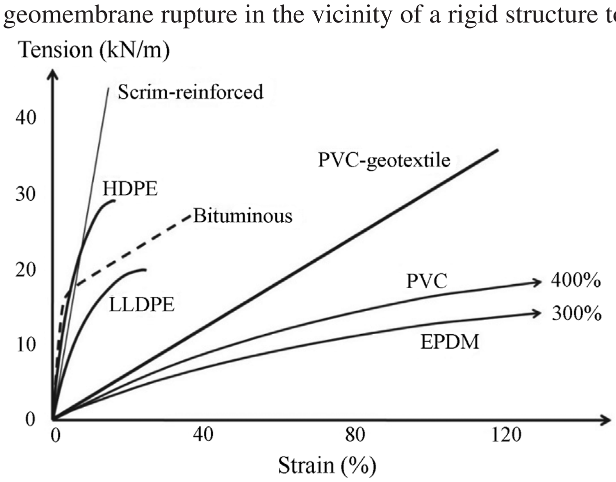

Figure 5 - Tension-strain curves of various geomembranes.

which the geomembrane is attached: (i) eliminating the abrupt differential settlement by an appropriate shape of the structure (Fig. 6); and (ii) providing an extra length ("slack") to the geomembrane such that the geomembrane is not under tension after settlement of the embankment has taken place (Fig. 7). This solution has been used, in particular, in the Water Saving Basins of the Panama Canal Locks in 2016 (Fig. 8).

6. Leakage Reduction by Using Composite Liners

6.1. The concept of composite liner

6.1.1. Definition of composite liner

The term "composite liner" could have several meanings. It is generally used to designate a liner composed of two complementary materials: a synthetic component and a mineral component. The most frequent type of composite liner consists of a geomembrane and a layer of low-permeability soil, with the geomembrane overlying the low-permeability soil (Fig. 9). The low-permeability soil component of a composite liner is generally either a compacted clay layer or a bentonite geocomposite. The thickness of a compacted clay layer is typically between 0.3 and 1.5 m whereas the thickness of a hydrated bentonite geocomposite depends on the compressive stress applied during hydration and is typically approximately 10 mm after hydration under load. Whereas a compacted clay layer is two orders of magnitude greater than the thickness of a bentonite geocomposite, the permeability of bentonite is two orders of magnitude lower than the permeability of compacted clay.

6.1.2. Effectiveness of composite liners

A composite liner is effective, because, if there is a hole in the geomembrane (which should always be assumed at the design stage), the leakage rate is low because of the presence of the low-permeability soil next to the hole.

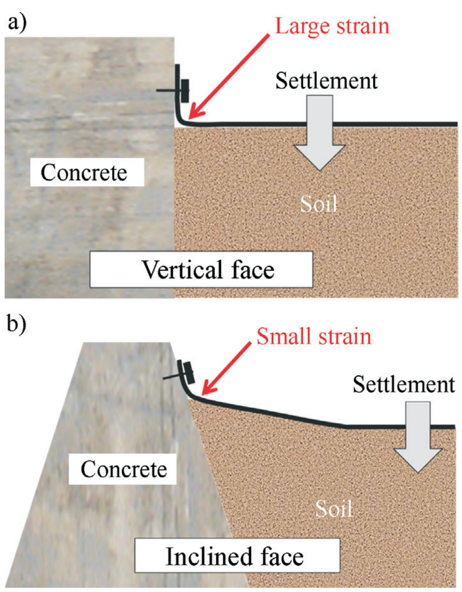

Figure 6 - Impact of the shape of a rigid structure on the tensile stress and strain in the geomembrane next to the attachment, in case of differential settlement between concrete and soil: the stress and strain in the geomembrane are (a) large if the face of the structure is vertical, and (b) small if the face is inclined.

Figure 8 - Slack in the geomembrane next to a rigid structure in the Water Saving Basins of the Panama Canal Locks, 2016 [Courtesy Carpi].

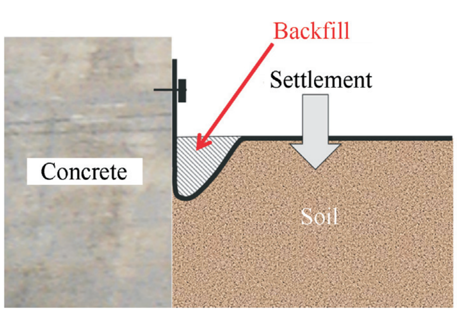

Figure 7 - Slack in the geomembrane to reduce the tensile stress next to a rigid structure in case of differential settlement between concrete and soil [Courtesy Carpi].

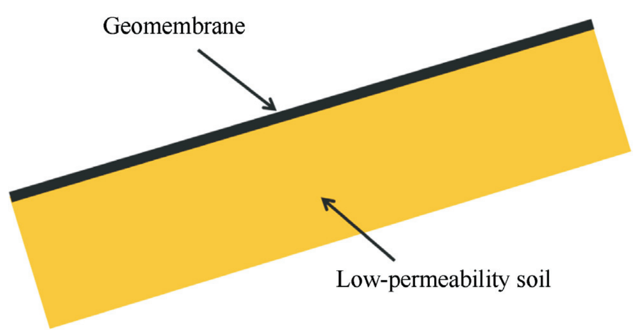

Figure 9 - Composite liner.

This assumes that there is intimate contact between the geomembrane and the low-permeability soil. This intimate contact concept (Giroud & Bonaparte, 1989b) is the cornerstone of the effectiveness of composite liners. There is no intimate contact at locations where geomembrane exhibits wrinkles, which happens with geomembranes that have both high stiffness and high coefficient of thermal expansion. Therefore, when a composite liner is used, it is important to minimize wrinkles by good installation practice.

Composite liners are very effective in reducing leakage. As shown by Giroud & Bonaparte, (1989b) and others (*e.g.* Rowe, 1998, Touze-Foltz *et al.*, 2008), the rate of leakage through a composite liner is typically two to four orders of magnitude less than the rate of leakage through a geomembrane alone with the same hole size and frequency.

6.1.3. A special type of composite liner

In some technically advanced cases, a manufactured liner that consists of a layer of bentonite encapsulated between two geomembranes has been used. This is a special type of composite liner where the intimate contact between the two components exists even in case of wrinkles.

6.2. Precautions with the association of two liners

6.2.1. Risk of uplift of the geomembrane component of a composite liner

Composite liners are used extensively in landfills. However, composite liners should be used with caution in reservoirs and dams. A composite liner should not be directly exposed to the impounded liquid. As pointed out by Giroud & Bonaparte (1989a, p. 37): "Composite liners must be used with caution in liquid containment facilities. If the geomembrane component of the composite liner is directly in contact with the contained liquid (in other words, if the geomembrane is not covered with a heavy material such as a layer of earth or concrete slabs), and if there is leakage through the geomembrane, liquids will tend to accumulate between the low-permeability soil (which is the lower component of the composite liner) and the geomembrane, since the submerged portion of the geomembrane is easily uplifted. Then, if the impoundment is rapidly emptied, the geomembrane will be subjected to severe tensile stresses because the pressure of the entrapped liquids is no longer balanced by the pressure of the impounded liquid. Therefore, a composite liner should always be loaded, which is automatically the case in a landfill or in a waste pile, and which must be taken into account in the design of a liquid containment facility."

According to Thiel & Giroud (2011), "there would be a significant potential that a hole in the primary geomembrane could allow some liquid to get between the geomembrane and the underlying mineral component, and cause uplifting of the geomembrane due to gas formation, liner buoyancy, or unbalanced liquid pressure in case of fluctuation of the liquid level or turbulence in the pond. In general, unballasted (exposed) composite primary liners in ponds cannot be expected to perform as true composite liners. While the mineral component of such a primary composite liner system would serve to impede the leakage rate into the leakage collection layer, it may tend to act alone as a single mineral liner as the geomembrane uplifts, and equations for predicting leakage through holes in composite liners cannot be used with these systems. If an exposed primary composite liner is proposed, the owner should strongly consider minimizing the risk of holes in the geomembrane by having a first-rate construction quality assurance program and an electric hole-detection survey performed, and be committed to emptying the pond and repairing the geomembrane at the first sign of any leakage or geomembrane displacement. Considering these constraints, the authors do not generally recommend this configuration. Furthermore, the authors would recommend against using this configuration in cases where the geomembrane could be exposed to expected mechanical damage, and cases where there are conditions of quickly-fluctuating water levels and turbulence (*e.g.* pumped-storage projects, and ponds with aerators)."

The above comments make it clear that the problem is not the potential uplift of the composite liner as a whole, but the potential uplift of the geomembrane, resulting in separation of the geomembrane component of the composite liner from the low-permeability soil component. The above comments are so important that they are repeated below for the case of dams.

A composite liner should not be used on the upstream slope of an embankment dam. This is because during normal operation, in case of a leak, even small, through the geomembrane, water may accumulate in the space between the geomembrane and the soil component of the composite liner. In case of rapid drawdown of the reservoir, the pressure of the water entrapped between the two components of the composite liner is no longer balanced by the pressure of the water in the reservoir. Depending on the amount of water entrapped between the two components of the composite liner, and the weight of material (if any) above the composite liner, instability of the upstream slope may occur at the interface between the two components of the composite liner. Even if instability does not occur, the geomembrane and the materials (if any) above the geomembrane may be uplifted, which may have detrimental consequences such as permanent deformations or cracking.

Therefore, if a composite liner is used in a dam, the weight of materials on top of the geomembrane should be sufficient to exceed the pressure of the water likely to be entrapped between the two components of a composite liner. From a practical standpoint, this means that, if a composite liner is used in a dam, it should be inside the dam rather than being at the upstream face. As an additional benefit, the normal stress applied by the materials located on top of the geomembrane, reduces the amount of water likely to be entrapped between the two components of the composite liner. However, it should be pointed out that the use of composite liners is very rare in dams; the usual design consists of a geomembrane liner associated with a drainage layer (see Section 9.1.2).

The conclusion of this discussion is that a composite liner (or any two superposed liners) can be used in reservoirs and dams only if sufficient load is placed on the upper liner. This conclusion applies to all cases where a liner is placed on top of another liner (which should not be done, as a general rule).

As a consequence of the fact that two low-permeability layers should not be placed on each other (unless they are sufficiently ballasted), in dams, the layers underlying the geomembrane liner should be sufficiently permeable to avoid accumulation of water. Indeed, drainage layers are generally associated with geomembranes in dams (see Sections 9.1.2 and 9.3.4).

6.2.2. Risk of desiccation of the low-permeability soil component of a composite liner

When a composite liner is not covered with a protective soil layer, it is exposed to cycles of high and low temperatures, such as day-night cycles. As a result, the geomembrane temperature fluctuates. When the ambient temperature is high, the geomembrane temperature may reach 80 °C if the geomembrane is black. As a result, moisture from the low-permeability soil component evaporates. At the same time, wrinkles may be formed and vapor accumulates in the wrinkles and in the small space, if any, between the relatively flat portions of the geomembrane and the underlying material. At night, when the geomembrane cools down, the entrapped vapor condenses on the lower face of the geomembrane in the form of drops of water. If the geomembrane is on a slope, the drops of water flow downslope along the lower face of the geomembrane. After a number of day-night cycles, water is transferred from the upper part of a slope to the lower part of the slope. As a result, the low-permeability soil is desiccated in the upper part of the slope. The consequences of this desiccation are:

- If the low-permeability soil is compacted clay, the clay cracks and no longer performs its function of liner component.
- If the low-permeability soil is a bentonite geocomposite, the tendency of the bentonite to crack is counteracted by the geotextile components of the bentonite geocomposite. As a result, the bentonite geocomposite shrinks and adjacent panels get separated unless they were installed with generous overlaps.

Both mechanisms hamper the composite liner effect. The cracking and related shrinkage mechanisms can be prevented by covering the composite liner by a protective soil layer within a few weeks after installation of the geomembrane, in particular on slopes. This recommendation is particularly important in the case of the side slopes of landfills. Indeed, several instances of clay desiccation and bentonite geocomposite shrinkage have been observed on the side slopes of landfills where a composite liner had been left uncovered for months because the placement of waste was delayed.

6.2.3. Conclusion on composite liners

Composite liners are very effective because they reduce the leakage rate by orders of magnitude compared to a geomembrane used alone. However, the foregoing discussions show that there are two important risks with exposed composite liners: geomembrane uplift and low-permeability soil desiccation.

The case of a double liner discussed below is different from a composite liner. In a double liner the two liners are not in contact because there is a leakage detection layer in between. In other words, a double liner associates two liners that are not in contact, whereas a composite liner associates two liners that are in contact.

7. Leakage Reduction Using Double Liners

7.1. Definition and concept of double liner

7.1.1. Definition and terminology

Recognizing that individual liners may leak has led to the development of the concept of the double liner system, which is a very safe way to contain liquids with negligible leakage into the ground, even though individual liners may leak. The concept was presented by Giroud (1973) and used for the first time with two geomembranes in 1974, as described by Giroud & Gourc, (2014) (see Section 7.3).

In the terminology of geosynthetics engineering, a double liner consists of two liners separated by a drainage layer (Fig. 10). The upper liner is called the "primary liner" and the lower liner is called the "secondary liner". The purpose of the drainage layer is to collect, convey, detect and remove leakage that may occur through the primary liner, hence the terminology "leakage collection, detection and removal layer" or, more simply, "leakage collection layer" or "leakage detection layer".

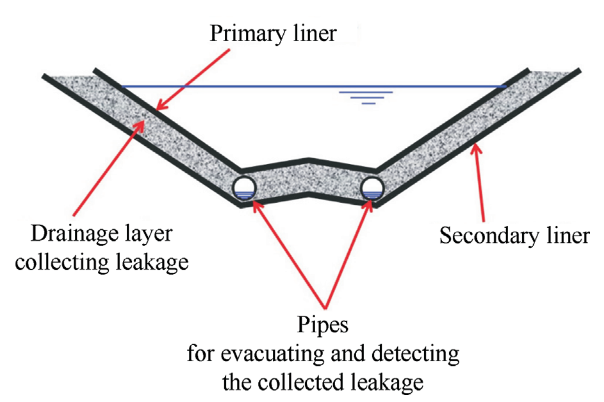

Figure 10 - Double liner concept.

7.1.2. The double liner concept

The essential aspect of the double liner concept is that the thickness of liquid flow in the leakage detection layer must be as small as possible and less than the thickness of the leakage detection layer. As a result, there is no pressure buildup in the leakage detection layer and the hydraulic head on the secondary liner is small. Consequently, there is little leakage into the ground, even if there are some holes in the secondary liner.

Another aspect of the double liner concept is that leakage through the primary liner can be detected at the outlet of the leakage detection layer. It should be noted that the leakage detection layer is not a leak detection layer: it detects leakage, it does not find the leaks.

7.2. Functioning of a double liner

7.2.1. Primary liner

Theoretically, any type of liner can be used as the primary liner of a double liner. However, since the goal of a double liner is to minimize leakage, the rate of leakage through the primary liner should be as small as possible. To that end, a geomembrane or a composite liner should be used. The leakage rate through the primary liner is much lower if the primary liner is a composite liner than if the primary liner is a geomembrane.

Here, it is important to remember that composite liners should only be used if they are sufficiently ballasted to prevent the geomembrane component of the composite liner from being uplifted (see Section 6.2). As a result, the use of composite liners as primary liners is practically limited to landfills (since the weight of the waste ensures ballasting). In landfills, it should be remembered that the composite liner should be promptly covered by a protective soil layer, in particular on the side slopes, to prevent desiccation and related shrinkage of the low-permeability soil component of the composite liner (see Section 6.2.2).

Rough orders of magnitude of typical leakage rates through the primary liners of landfills are: 100 to 1000 lphd (10^{-10} to 10^{-9} m/s) for geomembrane alone; 0.1 to 1 lphd (10^{-13} to 10^{-12} m/s) for composite liner with compacted clay layer as the low-permeability soil component; and 0.01 to 0.1 lphd (10^{-14} to 10^{-13} m/s) for composite liner with bentonite geocomposite as the low-permeability soil component.

As indicated in Section 6.1, a composite liner consists of a geomembrane underlain by a low-permeability soil layer. In general, the low-permeability soil layer component of a composite liner can be a layer of compacted clay or a bentonite geocomposite. However, if a composite liner is used as the primary liner of a double liner system, it is not recommended to use a layer of compacted clay as the low-permeability soil component of the primary liner, because the discharge of water expelled from the clay (when the clay compresses under load) can be of the same order of magnitude as, and even greater than, leakage through the primary liner. As a result, the liquid detected by the leakage detection layer can be incorrectly considered to be due to leakage only.

The rate at which water is expelled from a clay layer subjected to a load applied progressively (such as waste disposal in a landfill, or filling of a reservoir) can be calculated using equations for the consolidation of soil subjected to a load applied linearly with time (Giroud, 1983). Calculations done using these equations by Gross *et al.* (1990) gave the following rough orders of magnitude for typical landfill cases: 10 to 1000 lphd. These values are significantly higher than the typical leakage rate of 0.01 to 1 lphd for composite liners mentioned above. Clearly, leakage monitoring cannot be done using a leakage detection layer overlain by a primary liner where the low-permeability soil component is a compacted clay layer. Therefore, when the primary liner of a double liner is a composite liner (which is a good design to reduce leakage), the low-permeability component of the composite liner should be a bentonite geocomposite (or the special composite liner described in Section 6.1.3).

7.2.2. Functioning of the leakage collection and detection layer

The flow capacity of the leakage collection and detection layer is essential. This layer must have an appropriate slope and the material of this layer must have high hydraulic conductivity to rapidly convey the flow with a hydraulic head as small as possible. Indeed, rapid flow ensures rapid leakage detection and small hydraulic head is required to ensure small leakage rate through the secondary liner, *i.e.* small rate of leakage into the ground. The leakage collection and detection layer must be designed with a high factor of safety, for example with a flow capacity at least ten times the expected leakage rate through the primary liner, to ensure that there will be no pressure buildup in the leakage collection and detection layer unless there is a catastrophic failure of the primary liner. In that case, warning will be provided by the abnormally high detected leakage rate, the double-lined containment facility should then be put out of service, and the liner should be repaired.

Adequate leakage detection layer materials are gravel and geosynthetic drainage layers with low compressibility, such as geonets and drainage geocomposites with a geonet core. Sand is not adequate because it is not sufficiently permeable to ensure rapid flow and it retains water by capillarity.

The risk of clogging is a legitimate concern regarding all drainage layers. Because of the very small flow rate, clogging by migrating particles is not typically expected in leakage collection and detection layers, unless sand is used as the drainage material and geotextile filters are misused. Another possibility is clogging by precipitation of calcium carbonate, which may happen in the presence of concrete (for example for drainage associated with concrete dams or concrete-faced dams). In these dams, the drainage system can be washed periodically in case of evidence of flow capacity reduction.

The above discussion is related to the requirements to ensure there is a low hydraulic head on the secondary liner. Requirements for accurate leakage detection are presented in Section 8.3.2.

7.2.3. Important requirement for the secondary liner

The secondary liner of a double liner system plays an essential role. The only suitable material for a secondary liner is a geomembrane because the leakage rate through the primary liner is generally so small that, if the secondary liner is a soil, even a low-permeability soil such as clay, much of the leakage collected will flow through the soil rather than being conveyed, detected and removed.

The secondary liner is not simply a back-up to the primary liner. It has an essential role for proper leakage collection and measurement. As indicated in Section 7.2.1, typical leakage rate per unit area through a geomembrane-only primary liner is of the order of 10^{-10} to 10^{-9} m/s in a landfill and 10^{-9} to 10^{-8} m/s in a reservoir. As also indicated in Section 7.2.1, smaller leakage rates can be expected with a composite liner primary liner. These leakage rates per unit area are of the same order as the vertical flow rate through compacted clay with a hydraulic gradient of 1. Clearly, if the secondary liner is made of clay only (rather than geomembrane or clay overlain by a geomembrane), at least a large fraction of the collected leakage will infiltrate into the clay and, therefore, will not be detected. If the secondary liner is made of only a bentonite geocomposite, most of the liquid leaking through the primary liner will be used to hydrate the bentonite. In other words, if the leakage detection layer does not rest on a geomembrane, the rate of leakage through the primary liner will not be measured.

7.3. Case history: the first double liner

The first double liner with two geomembranes was constructed in 1974 and has been in continuous service since then (Giroud & Gourc, 2014). The lined structure is a 10 m deep, 195 m long and 55 m wide water reservoir, located on top of a 50 m high 33° slope. The geotechnical study concluded that the slope was stable, but could become unstable in case of major leakage of water from the reservoir. Any risk of instability was unacceptable because a large chemical plant was, and still is, located at the toe of the slope. Because safety was essential, a double liner was recommended by the author of this paper. It is interesting to note that the need for strict leakage control resulted from the risk of geotechnical deterioration, which was emphasized in Section 2.5.1.

The primary liner is a 1.5 mm thick butyl rubber geomembrane. It is exposed (in other words, it is not covered with a protective layer). The secondary liner is a bituminous geomembrane. The leakage detection layer between the two liners is made of gravel stabilized with mortar. The reservoir has been monitored since the end of construction. No leakage was detected until 2004, *i.e.* 30 years after construction, when a trickle of water appeared at the outlet of the leakage detection layer. This indicates that the leakage collection and detection system performed its function.

The leak was repaired under water. It is interesting to note that the leak took place at the seam closest to the concrete intake structure. This confirms the fact that high stresses can develop next to rigid structures and that failure is likely to take place at seams due to stress concentration (see Section 5.2.1). It should be noted that the reservoir was not subjected to filling-emptying cycles, which could have caused greater stresses and more seam failures (see Section 8.3.3).

This case history shows that a butyl rubber geomembrane can last more than 40 years when it is exposed (*i.e.* with no protection) in a temperate climate with hot summers, which is remarkable. Ironically, the use of butyl rubber geomembranes has been practically discontinued in the 1990s, in part because they were thought to have insufficient durability. Indeed, several types of modern geomembranes would last longer than butyl rubber, *i.e.* longer than 40 years under the same conditions, which confirms the durability of modern geomembranes.

8. Quantitative Evaluation of Leakage

8.1. Data on holes in geomembranes

8.1.1. Data on frequency of holes in geomembranes

The frequency of holes is the number of holes per unit area (usually per hectare). Since the first publication presenting data on frequency and size of holes in installed geomembrane liners (Giroud & Bonaparte, 1989a), a number a studies have been published. It would be beyond the scope of this paper to review these studies. A summary was published by Giroud & Touze-Foltz, (2003) who stated “(i) The number of holes at the end of geomembrane installation with construction quality assurance is typically believed to be from 1 to 5 holes per hectare; these holes are generally small, and their number is smaller for large liners (*e.g.* greater than 2 ha) than for small liners. (ii) The number of holes caused by the placement of soil on top of the geomembrane varies in a wide range, from very few to 20 per hectare, depending on the amount of care taken during placement of soil on top of the geomembrane and the type of geomembrane protection used; these holes can be large (and often are).”

More recently, the author of this paper has reviewed data (Beck & Darilek, 2016) from more than 150 cases of electric liner integrity surveys performed on more than 250 hectares of HDPE geomembranes. This review has provided 5.4 holes/ha for HDPE geomembranes installed in the Unites States with typical construction quality assurance.

In conclusion, a number of holes of 5 or 6 per hectare can be considered typical at the end of geomembrane installation with construction quality assurance. In the case where there is no construction quality assurance, a greater hole frequency can be expected, as pointed out by Giroud & Bonaparte (1989a, p. 65), as follows: "A frequency of 25 holes per hectare or more is possible when quality assurance is limited to an engineer spot-checking the work done by the geomembrane installer".

8.1.2. Data on size of holes in geomembranes

Typical sizes of holes in geomembranes are summarized below:

- Holes smaller than 1 mm^2 cannot be detected by electric leak location survey with the current technology (2016).
- Minimum hole sizes that can be detected by electric leak location survey are of the order of: (i) 1 mm^2 under the low depth of water required to perform the electric leak location survey under optimum conditions; (ii) 10 mm^2 under a soil layer up to 0.3 m thick; (iii) 30 mm^2 under a soil layer up to 0.6 m thick, and (iv) 100 mm^2 under a soil layer up to 1.0 m thick.
- A crack due to stress cracking may have an area of the order of 10 mm^2. However, it may increase to 100 mm^2 or more if the geomembrane remains under tension after the opening of the crack.
- The size of holes due to puncture by stones may be of the order of 10 mm^2 or more.
- Holes in the geomembrane due to tears by construction equipment during placement of a layer of soil on top of the geomembrane are generally large, *e.g.* 100 cm^2 or even 1000 cm^2 (*i.e.* 10,000 or even 100,000 mm^2).

8.1.3. Relationship between frequency and size of holes in geomembranes

Holes present in a geomembrane at the end of installation of the geomembrane subjected to strict construction quality assurance are less numerous and smaller than assumed in the past and reported in papers published in the 1990s and even in the early 2000s.

After reviewing published data and recent data provided to the author of this paper by suppliers of electric liner integrity surveys (Beck & Darilek, 2016), the hole size distribution presented in Table 2 has been established by the author of this paper for the case of strict construction quality assurance with a 2 mm thick HDPE geomembrane. The following comments can be made on Table 2:

- The hole size ranges have been selected to be such that the spatial frequency is the same for each hole size range: one hole per hectare.
- The hole sizes are expressed as areas (mm^2) rather than as diameter (mm) because the area is generally used in leakage calculations.
- This hole size distribution has been established by the author of this paper to be slightly conservative for liner systems subjected to strict construction quality assurance. This level of conservativeness has been confirmed by a provider of electric liner integrity survey with outstanding experience.

The following comments can be made on the data presented in Table 2:

- The frequency of geomembrane holes that corresponds to strict construction quality assurance is 6 per hectare. This is consistent with the 5.4/ha mentioned Section 8.1.1, but it has been rounded.
- Among those 6/ha, 4 holes per hectare can be detected by electric liner integrity survey because they are equal to or larger than 1 mm^2. This assumes that the electric liner integrity survey is effective, which depends on either intimate contact between the geomembrane and the underlying soil or the use of a geomembrane with a thin conductive layer at its lower face (see Section 4.2). Therefore, if an effective electric leak location survey is performed at the end of geomembrane installation and the detected holes are repaired, the remaining hole frequency is 2/ha, and these holes are small (*i.e.* smaller than 1 mm^2).
- However, if a soil layer is placed on top of a geomembrane that has been subjected to electric leak location survey, new holes will be created depending on the level of care used for soil placement and the level of construction quality assurance associated with this opera-

Table 2 - Geomembrane hole size distribution for 2 mm thick HDPE geomembrane installed with strict construction quality assurance.

Possibility of detection by electric liner integrity survey	Hole size range	Hole spatial frequency for the considered hole size range
Detectable	5-10 mm^2	1 hole/hectare
	3-5 mm^2	1 hole/hectare
	2-3 mm^2	1 hole/hectare
	1-2 mm^2	1 hole/hectare
Not detectable	0.1-1 mm^2	1 hole/hectare
	< 0.1 mm^2	1 hole/hectare

tion. A second round of electric leak location survey can then be performed. For example, if the soil layer is 0.6 m thick, holes greater than 30 mm^2 can then be detected and repaired.

As seen below in Section 8.2, the rate of leakage is proportional to the hole area in the case of a geomembrane resting on a permeable soil, but it is not proportional to the hole area in the case of a composite liner. Therefore, averaging the data presented in Table 2 is delicate.

Tentatively, it can be said that the data presented in Table 2 can be combined in the following statement: A geomembrane liner at end of installation with construction quality assurance can be expected to have 4 holes per hectare with a hole area of 4 mm^2. This is not far from the recommendation made in 1989 by Giroud & Bonaparte (1989a, p.64): 2.5 holes per hectare with a hole size of 3.1 mm^2 (*i.e.* a diameter of 2 mm).

In 1989, Giroud & Bonaparte (1989a) also made a recommendation for design calculations: 2.5 holes per hectare with a hole size of 100 mm^2. This recommendation is still followed with a slight modification: over the years, the practice for engineers as well as researchers has been to consider 5 holes per hectare with a hole size of 100 mm^2. This practice may be considered to include some holes caused by the placement of soil on top of the geomembrane. (However, it should be noted that, in 1989, it was not realized that a significant number of additional holes could be caused by placement of a soil layer on top of the geomembrane.) (See Section 8.1.1.)

8.2. Theoretical evaluation of leakage rate

8.2.1. Equations for leakage rate calculation

A number of equations have been proposed for the calculation of leakage rate through liners. Only typical equations are presented below. The equations make it possible to calculate a leakage rate assuming values for the various parameters, such as the number and size of geomembrane holes, which can be assumed from data presented above in Section 8.1. The equations depend on the type of geomembrane liner: geomembrane alone on permeable soil (Section 8.2.2); composite liner (Section 8.2.3); and geomembrane on a semi-permeable soil (Section 8.2.4). Also, the impact of wrinkles on the leakage rate can be quantified (Section 8.2.5) and the determination of leakage rate calculation in the case of double liners is addressed (Section 8.2.6).

Once leakage rate through a geomembrane hole, Q, has been calculated, the leakage rate per unit area, q, can be derived as follows (see Section 2.3):

$$q = 8.64 \times 10^7 NQ \tag{1}$$

with the leakage per unit area, q, in lphd, the frequency of holes, N, given as a number of holes per hectare, and the leakage rate in a hole, Q, in m^3/s.

8.2.2. Rate of leakage through geomembrane liners

In the case of a geomembrane liner resting on a permeable medium, such as a permeable ground or a leakage detection layer, the leakage rate can be calculated using Bernoulli's equation as suggested by Giroud (1984b):

$$Q = 0.6a\sqrt{2gh} \tag{2}$$

where Q = leakage rate, a = hole area, g = acceleration due to gravity, and h = hydraulic head. Eq. 2 can be used with any set of coherent units. The basic SI units are: Q (m^3/s), a (m^2), g (9.81 m/s^2), and h (m).

The leakage rate per unit area is given by the following equation derived from Eqs. 1 and 2:

$$q = 51.84aN\sqrt{2gh} = 230aN\sqrt{h} \tag{3}$$

with the leakage per unit area, q, in lphd, the hole size in mm^2, the frequency of holes, N, given as a number of holes per hectare, the hydraulic head, h, in meters, and g = 9.81 m/s^2.

8.2.3. Determination of the rate of leakage through composite liners

The usual equation for calculating the rate of leakage through of holes in the geomembrane component of a composite liner is (Giroud 1997):

$$Q = 0.21\left[1 + 0.1\left(\frac{h}{t}\right)^{0.95}\right]a^{0.1}h^{0.9}k^{0.74} \tag{4}$$

where Q = leakage rate through one hole, a = hole area, t = thickness of the low-permeability soil component of the composite liner, h = hydraulic head on top of the geomembrane, and k = coefficient of permeability of the low-permeability soil component of the composite liner. This equation is applicable only with the following units: Q (m^3/s), h (m), t (m), a (m^2), k (m/s).

Several equations derived from the above equation or presented with the same format have been proposed for several specific cases (Touze-Foltz & Giroud, 2003, Touze-Foltz *et al.*, 2008).

8.2.4. Determination of the rate of leakage in the case of semi-permeable soils

In the case where a geomembrane rests on a soil that is neither a high-permeability soil nor a low-permeability soil, a methodology has been developed by Giroud *et al.*, 1997b.

8.2.5. Impact of geomembrane wrinkles on the rate of leakage through a composite liner

The equations presented above in Section 8.2.3 are based on the assumption that there is intimate contact between the geomembrane and the low-permeability soil component of the composite liner. In the field, geomembranes often exhibit wrinkles.

Wrinkles have no impact on the leakage rate if the considered liner is a geomembrane alone on a permeable material. In contrast, in the case of a composite liner, the leakage rate can be significantly increased if the geomembrane exhibits wrinkles. This effect has been quantified by Rowe (2012), Giroud & Touze-Foltz (2005), and Giroud & Wallace (2016).

8.2.6. Determination of the rate of leakage in case of double liners

In the case of a double liner, the rate of leakage through the primary liner (which can be measured thanks to the leakage detection layer) can be calculated using the equations presented in Section 8.2.2 (if the primary liner is a geomembrane alone) or the equation presented in Section 8.2.3 (if the primary liner is a composite liner).

It is important to note that the rate of leakage through the primary liner is not the rate of leakage into the ground. In the case of a double liner, the determination of the rate of leakage into the ground requires three steps: (i) determination of the rate of leakage through the primary liner; (ii) analysis of the flow in the leakage detection layer and determination of the hydraulic head on the secondary liner; and (iii) determination of the rate of leakage through the secondary liner, which is the rate of leakage into the ground.

A methodology for the analysis of the liquid flow in the leakage detection layer and the determination of the resulting hydraulic head on the secondary liner is provided by Giroud *et al.* (1997a).

8.3. Leakage rate measurement

8.3.1. The two situations of leakage rate measurement

To measure the leakage rate, the containment structure (*e.g.* landfill, reservoir, dam) must be in service or under conditions similar to the conditions in service, such as in a test where a reservoir is filled with water up to the normal service level. Two cases can be considered for the measurement of the resulting leakage: the case where there is a double liner system (which makes it possible to directly measure the rate of leakage through the primary liner); and the case where a liner is used (which requires an indirect evaluation of the leakage rate).

8.3.2. Measurement of leakage rate in case of double liner

If there is a double liner system, the leakage rate is obtained by monitoring the outlet of the leakage detection layer. This method is reliable unless the leakage detection layer is not functioning properly. The functioning of leakage detection layers was addressed in Section 7.2.2. Possible errors in the measurement of leakage using the leakage detection layer of a double liner are summarized below. The leakage rate may be overestimated due to the following errors:

- In the first days following the filling of the reservoir, if the water impounded in the reservoir is relatively cold, condensation of water vapor entrapped in the leakage detection layer may result in liquid flow in the leakage detection layer. If this liquid flow is limited in time (*e.g.* a few days), it should not be interpreted as leakage (a case history is presented by Giroud & Gourc, 2014).
- Precipitation water entrapped into the leakage detection layer material during construction may flow toward the outlet after the reservoir is put in service. Such water, if any, should not be interpreted as leakage.
- If the primary liner is a composite liner that consists of geomembrane on clay, water expelled from the clay under compressive stress due to the weight of the impounded liquid (in the case of a reservoir) or the weight of waste (in the case of a landfill) may be falsely interpreted as leakage. As indicated in Section 7.2.2, composite liners where the low-permeability soil component is compacted clay should not be used as the primary liner of a double liner if accurate leakage rate measurement is desired.
- Precipitation and run-off water may percolate in an anchor trench where the primary liner, the leakage detection layer and the secondary liner are anchored. Part of this water may intrude into the leakage detection layer. To prevent such intrusion, it is necessary to seam together the primary and the secondary liners in the anchor trench. Also, the configuration of the anchor trench and surrounding soil should be such that precipitation and runoff waters do not penetrate into anchor trenches.
- In exceptional cases, there may be false leakage detection if high ground water percolates into the leakage detection layer through the secondary liner.

The above causes of error lead to an overestimation of the leakage rate. In contrast, a fraction, or all, of the leakage through the primary liner may not be detected for the following reasons:

- Some or all of the water collected by the leakage detection layer may leak through the secondary liner.
- Wrinkles in the geomembrane secondary liner may block the flow of water collected by the leakage detection layer.
- Water may be retained by capillarity in the leakage detection layer (for this reason sand should not be used as the leakage detection layer material).

Leakage rate measurement using a double liner is not perfect, but it is much more accurate than leakage rate measurement using a water balance test.

8.3.3. Water balance tests

If there is a single liner, the only way to measure leakage rate is a water balance test (also called “ponding test”). The water balance test consists in filling a reservoir with water to the normal service level and measuring the water level drop as a function of time during a certain period of time (*e.g.* 14 days). Corrections for evaporation, rainfall and runoff must be done, but it is difficult to make accurate corrections and errors are frequent. The corrected water level drop (in mm/day) can be converted into leakage rate (in lphd) as indicated in Section 2.3.

The water balance test has the merit of testing at once an entire reservoir. In particular, it detects and measures leakage due to all causes, not only holes in the geomembrane. However, the water balance test has many drawbacks:

- The water balance test is impractical due to large amount of water required,
- The water balance test is time consuming (it typically takes several weeks in a relatively small reservoir, *i.e.* 1 ha, and would take more time in a large reservoir).
- The water balance test is not accurate due to the difficulty in accurately evaluating evaporation.
- The water balance test lacks sensitivity due to the very small impact of leakage on water level. Thus, a level drop of only 1 mm/day, which is hardly measurable, is equivalent to 10,000 lphd, which is a significant rate of leakage.
- According to Darilek & Laine (2013), an error of 2 mm on water level is possible. Over 14 days, this amounts to an error of about 1400 lphd. If the specified maximum leakage rate is 2000 lphd, the error is 70%, and more if there are errors on evaporation and rainfall corrections.
- The water balance test does not find leaks, but only measures leakage. Therefore, it does not find holes in the geomembrane. However, some of the holes can be found by a subsequent visual inspection guided by the results of the water balance test.
- Performing the water balance test may damage the liner if it has not been designed for filling/emptying cycles.
- Activities of the crew involved in conducting the test, inspecting the liner and repairing the detected geomembrane holes may cause additional damage to the geomembrane liner.

The limitations of the water balance test are illustrated by the following case history (Peggs, 2014). A single liner (0.91 mm thick reinforced polypropylene geomembrane placed on a needle-punched nonwoven geotextile on subgrade) was installed in a typical rectangular reservoir with a water depth in service of 4.5 m. The reservoir size was 7,000 m^2. There were four penetrations (*e.g.* pipe boots), including a complex one. The specified maximum water level drop was 6 mm in 14 days (which is equivalent to 4.8×10^{-9} m/s = 4170 lphd). The sequence of events was as follows:

- The water balance test was performed with the reservoir filled to the service level. The drop in water level over the 14 day test period was more than 10 times higher than the specified 6 mm. (It was about 66 mm /14 days = 47,000 lphd = 5.5×10^{-8} m/s.)
- The reservoir was emptied, the liner visually inspected, and repairs made.
- The reservoir was filled, and the water balance test redone. There was insufficient improvement (21 mm/14 days).
- Three more times, the reservoir was emptied, inspection and repairs were made, and the 14-day water balance test was performed, but the measured leakage rate remained high (112 mm/14 days, 23 mm/14 days, and finally more than 130 mm/14 days).
- After several months thus wasted, the geomembrane liner was removed. A second contractor was hired to install a completely new liner identical to the preceding liner. The new liner easily passed its first water balance test (in fact, the leakage rate was so small that it was not measurable).

It should be noted that there were three other similar reservoirs in the same facility with only one or two penetrations each (compared to four penetrations in the considered reservoir). These three reservoirs passed the water balance test the first or second time.

The leakage was increasing in spite of repairs. The leakage increased for at least two reasons:

- Additional damage to the geomembrane liner was caused by the team walking on the geomembrane to perform the visual inspection, and by the crew performing the repairs.
- The cycles of emptying-filling of the reservoir caused repeated displacement of the geomembrane, which resulted in fatigue of the geomembrane at the attachments between the free-to-move geomembrane and the fixed appurtenant structures.

The following additional comments can be made about this case history:

- Visual inspection does not find all holes.
- A number of holes were found at the geomembrane attachments to penetrations (*e.g.* pipe boots).
- Based on observations and comparison with the three other reservoirs, filling/emptying cycles induced stresses in the geomembrane, next to appurtenant structures and pipes.
- It is possible to think that the large fluctuations in the measured water level drops observed on this reservoir are due to the potential errors associated with the interpretation of the water balance test.

The following lessons can be learned from this case history:

- Good workmanship in liner installation is essential to ensure a small rate of leakage.
- Measures taken to find and repair holes in geomembranes are useful, but they do not replace good workmanship.

- The difference between good workmanship and poor workmanship in terms of leakage rate can be very significant. Indeed, in the foregoing case history, the difference was by about two orders of magnitude, between a measured leakage rate much less than the specified value and a measured leakage rate 20 times more than the specified value.
- The number of geomembrane holes caused by excessive activity on a geomembrane liner (by the team performing visual inspection and by the crew repairing the detected holes) may be greater than the number of repaired holes. If inspections and repairs are not properly done, the procedure may, in fact, increase the leakage rate. Therefore, if inspections and repairs are needed, they must be performed with great care.
- The number of appurtenances (*e.g.* pipe boots and various penetrations, ancillary concrete structures) should be minimized.
- Appurtenances must be designed with a geometry that ensures long-term performance of the attached geomembrane.
- If a reservoir is subjected to frequent filling/emptying cycles, the liner should be designed accordingly. In particular, attachments of the geomembrane to appurtenant structures should be such that the geomembrane is not damaged by expected displacements.
- In conclusion, the water balance test is not only prone to errors but also potentially destructive.

Above, there are good lessons for design engineers: they must treat geomembrane liners as seriously as they treat geotechnical issues. Design engineers, who carefully take into account the impact of rapid drawdown on slope stability, should take into account the impact of multiple filling/emptying cycles on geomembrane liners. Also, design engineers should understand that attaching geomembranes to appurtenant structures in a waterproof manner (which geomembrane installers generally do well) is not sufficient. The geometry of the appurtenant structure and the configuration of the geomembrane liner in the vicinity of the appurtenant structure should be designed to ensure long-term performance, as discussed in Section 5.2. This is the responsibility of the design engineer.

8.4. Typical leakage rates for geomembrane-lined landfills and reservoirs

8.4.1. Typical leakage rates for geomembrane-lined landfills

In landfills in the United States a maximum leakage rate of 200 lphd is often specified for the primary liner of double-lined landfills. As indicated in by Peggs & Giroud (2014), the average hydraulic head on the primary liner of landfills during the active leachate production can be considered to be approximately 30 mm. Calculations, performed with Eq. 3 (*i.e.* for a geomembrane-alone primary liner) and a hydraulic head of 30 mm, show that:

- With holes larger than a few mm^2, the leakage rate through a geomembrane is significantly higher than 200 lphd even under the small hydraulic head that exists in properly designed landfills.
- If the hole size is 1 mm^2, a leakage rate of 200 lphd is obtained with 5 holes per hectare.

The 1 mm^2 hole size shows that a maximum leakage rate of 200 lphd for a typical landfill hydraulic head can be achieved only by a very high-quality geomembrane liner installed with strict construction quality assurance and, preferably, subjected to an electric liner integrity survey (see Sections 1.10 and 3.3). This is why, in landfills, a composite primary liner is generally used to meet the 200 lphd maximum leakage rate specification; a leakage rate through the primary liner of the order of 1 lphd can then be achieved.

8.4.2. Typical leakage rates for geomembrane-lined reservoirs

Typically observed leakage rates for a 5 m deep reservoir range from 5000 to 100,000 lphd and beyond. Calculations done using Eq. 3 (*i.e.* for a geomembrane-alone liner) show that 5000 lphd (*i.e.* a water level drop of 0.5 mm/day) correspond to a geomembrane with 5 holes per hectare having a hole area of 2 mm^2. Such a high quality geomembrane can only be achieved under perfect conditions during construction, which can be described as follows:

- Firm and smooth supporting soil;
- Geotextile protection as needed;
- Dry and clean working conditions;
- Moderate temperature and no wind;
- No interference from the general contractor and other contractors;
- No appurtenant structures;
- Cooperation between good geomembrane installer and good quality assurance team; and
- Electric leak location followed by repair of detected holes.

In contrast, a rate of leakage higher than 5000 lphd and as high as 100,000 lphd (10 mm/day water level drop) or even higher may happen in many typical projects where one or more of the above "perfect conditions" are not met.

9. Leakage Control in Geomembrane-Lined Dams

9.1. Overview of uses of geomembranes in dams

9.1.1. Types of dams where geomembranes are used

Geomembranes have been used in more than 200 large dams, mostly in the past four decades. Geomembrane-lined dams include tailings dams and a variety of hydraulic dams:

- Embankment dams: (i) rockfill dams; and (ii) earth dams;
- Concrete-related dams: (i) roller compacted concrete dams; (ii) conventional concrete dams; and (iii) masonry dams.
- Cemented-material dams (such as hardfill dams).

Geomembranes have been used in new embankment dams and new roller compacted concrete dams, as well as in the rehabilitation of all types of dams: concrete-faced rockfill dams, bituminous concrete-faced rockfill dams, wood-faced rockfill dams, earth dams, conventional concrete dams, masonry dams, and roller compacted concrete dams.

9.1.2. Typical configuration

In most cases, the geomembrane is used at the upstream face of the dam. Fig. 11 illustrates schematically the typical configuration applicable to both embankment dams and concrete dams. It is important to note that a drainage layer is always associated to the geomembrane (see Sections 6.2.1 and 9.3.4). This figure will be useful to follow the subsequent discussions.

9.2. Leakage control goals specific to dams

9.2.1. Differences between dams and other liquid containment structures

So far in this paper, the emphasis was on landfills and reservoirs, because this is where most work on leakage control has been done in the field of geosynthetic engineering. Hereafter, aspects of leakage control specific to dams are addressed. This is interesting because the approach to leakage control is different in dams than in other liquid containment structures.

The goal and practice of controlling leakage in the case of dams is not exactly the same as the goal and practice of controlling leakage in the case of landfills and reservoirs.

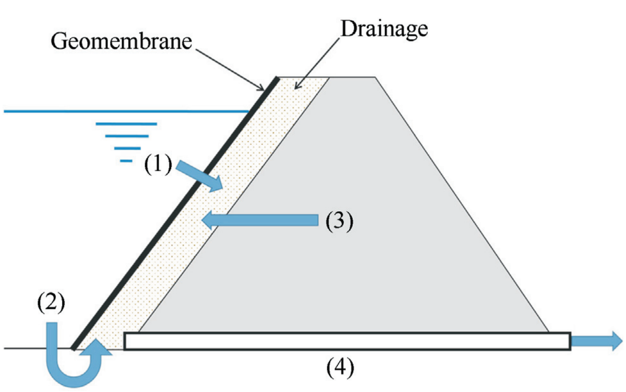

Figure 11 - Schematic configuration of a geomembrane-lined dam. The drainage system collects (1) water leaking through the geomembrane, (2) water flowing around the geomembrane, and (3) water (if any) drained from the dam, and (4) conveys the collected water to the downstream side of the dam.

The two differences are: (i) a zero-leakage goal is not relevant to dams; and (ii) controlling the presence and flow of water in the body of the dam is an essential consideration.

It should be noted that the discussions presented hereafter, which are specific to dams, are in part applicable to reservoirs surrounded by dikes or embankments.

9.2.2. Irrelevance of the zero-leakage goal in dams

Both geometric and environmental conditions that are specific to dams have an impact on the goal of leakage control goal in dams.

The geometry of geomembrane-lined dams is different from the geometry of geomembrane-lined landfills and reservoirs:

- In the case of landfills and reservoirs, the liquid is completely contained by the liner.
- In the case of dams, the liquid is, in great part, in contact with the natural ground and, therefore, a significant fraction of leakage takes place into the ground.

In addition to the fact that, in the case of geomembrane-lined dams, a significant fraction of the leakage takes place around the liner and not through the liner, a minimum flow rate should be kept in the river downstream of the dam, in particular for environmental considerations. For these two reasons, a zero-leakage goal is not relevant to geomembrane-lined dams. In other words, geomembranes are used in dams for leakage reduction, but the goal is not necessarily zero leakage.

9.2.3. Essential impact of dam body performance on leakage control goal in dams

The flow of water through dams, or simply the presence of water in the body of a dam, can be detrimental as a result two mechanisms: (i) progressive deterioration of the dam material, due to erosion and/or chemical reactions; and (ii) instability of the dam due to water pressure. Therefore, the flow and presence of water in a dam should be controlled.

To control the flow and presence of water in a dam, three actions are required: (i) minimizing leakage through the liner; (ii) preventing water that leaks through and flows around the liner from infiltrating into the dam body; and (iii) removing excess water from the dam body. The first action requires a good liner (essentially a geomembrane), while the second and third actions require a drainage system.

9.2.4. Leakage control approach for dams

Based on the foregoing discussions, the approach for leakage control in dams includes the association of the liner (for leakage reduction) and a drainage system (to prevent deterioration of the dam body). The drainage system conveys the collected water to the downstream side of the dam, which is consistent with the environmental requirement of keeping minimum flow in the river downstream of the dam.

Furthermore, as pointed out in Section 9.3.4, a drainage layer is also needed behind the geomembrane to prevent the presence of water, which could uplift the geomembrane in case of rapid drawdown of the reservoir water.

9.3. Influence of the type of dam on leakage control in dams

The relative importance of the two leakage control goals, leakage reduction and prevention of deterioration of the dam body, depends on the type of dam.

9.3.1. Leakage control approach in the case of embankment dams

In the case of embankment dams, the two potential mechanisms of dam body deterioration by water (material deterioration and instability) are as follows:

- Progressive material deterioration, if it occurs, is by internal erosion ("piping").
- Instability of the dam, if it occurs, is caused by high pore water pressure in the body of the dam.

It is not safe to rely only on a geomembrane liner to prevent internal erosion and instability in an embankment dam. As a general rule, a dam lined with a geomembrane should be designed in such a way that no catastrophic failure should occur in the case of a major breach in the geomembrane liner, at least during the time necessary to repair the geomembrane (if this can be done under water) or to empty the reservoir if this needs to be done for safety and/or to repair the geomembrane.

To prevent failure of an embankment dam:

- It is important to eliminate leakage through the dam, thanks to the geomembrane, which reduces leakage, and thanks to the drainage system associated with the geomembrane that collects the leakage that flows through holes in the geomembrane and leakage coming from the geomembrane periphery, and conveys it downstream of the dam.
- It is important to design a dam structure (*e.g.* with appropriate materials, filters and drains) that can function safely during a period of time sufficient to perform repairs if there is a major failure of the geomembrane liner and/or the drainage system associated with the geomembrane.
- It is useful to monitor leakage, which is possible thanks to the drainage system associated with the liner. This is possible in the case of concrete dams, because the drainage layer behind the geomembrane is generally vertical or quasi-vertical and the concrete that is backing the drainage layer has a relatively low permeability. As a result, the collected leakage is conveyed to the outlet. In contrast, in the case of embankment dams, part or all of the collected leakage may be lost in permeable zones of the dam.
- It is important to promptly repair the geomembrane if leakage has been detected, which is possible underwater.

In the case of well-designed rockfill dams: (i) the risk of dam body deterioration by water (internal erosion and instability) is low; and (ii) the permeability of the dam materials is high. Therefore, the main goal of the lining system is leakage reduction.

In the case of those earth dams that are sufficiently permeable to justify the use of a geomembrane liner for leakage reduction, the risk of internal erosion and instability (both related to water in the dam body) may be high. Therefore, the two goals of leakage control (leakage reduction and prevention of deterioration of the dam body) are both important in the case of those earth dams.

9.3.2. Leakage control approach in the case of conventional concrete dams

In concrete dams, deterioration of the dam body can result from the following mechanisms:

- Deterioration of the dam material may be due to: (i) leaching of cement by seeping water; (ii) freeze-thaw cycles (obviously linked to water); and (iii) alkali-aggregate reaction in the presence of water.
- Instability of the dam may be caused by water pressure in cracks and lift joints.

Alkali-aggregate reaction deserves a discussion. In modern concrete, aggregate is generally inert. However, some aggregate (especially those containing silica) reacts with alkali hydroxide in concrete, thereby forming a gel that swells when it absorbs water. The swelling pressure progressively deteriorates the concrete.

In conclusion, in the case of concrete dams, for all of the reasons mentioned above (alkali-aggregate reaction, leaching of cement, freeze thaw, instability due to water pressure) the body of the dam must be kept as dry as possible. This is achieved by associating a geomembrane and a drainage system. The drainage system collects leakage water and water drained from the dam body (if any); and it conveys the collected water to the downstream side of the dam.

Based on the preceding discussion, it is important to keep the dam body dry in concrete dams, in particular when there is a risk of alkali-aggregate reaction. This is particularly true in the case of the rehabilitation of old concrete dams where alkali-aggregate reaction has started a long time before rehabilitation is undertaken.

In the case of the rehabilitation of old concrete dams, keeping the dam body dry means: not only, to drain the water leaking through holes in the geomembrane and the water seeping from the periphery of the geomembrane; but, also, to progressively drain water that has accumulated in the dam over the years.

In conclusion, in the case of the rehabilitation of conventional concrete dams, the emphasis is on drainage.

However, it should be noted that drainage can only function behind a waterproof barrier.

9.3.3. Roller compacted concrete dams

In roller compacted concrete dams, the potential for leakage through the dam is high, because:

- the permeability of the dam material is high since roller compacted concrete typically has a cement content lower than that of conventional concrete;
- water tightness of the contraction joints is difficult to achieve; and
- the interfaces between lifts of compacted concrete provide preferential paths for water.

Therefore, leakage reduction is an essential goal of the geomembrane facing of roller compacted concrete dams. But, in roller compacted concrete dams, there is a risk of progressive degradation of concrete due to leaching of cement by seeping water and, in some cases, by alkali-aggregate reaction.

Therefore, in roller compacted concrete dams, the two goals of a lining system are both essential: (i) leakage reduction; and (ii) prevention of dam body deterioration.

9.3.4. Importance and design of the drainage layer in the case of concrete dams

The foregoing discussions have shown the importance of a drainage system associated with a geomembrane liner in dams.

Based on the foregoing discussions, there is generally a drainage system associated with a geomembrane on the upstream face of dams, including: (i) a drainage layer under the geomembrane; and (ii) collector pipes leading to a gallery or an outlet.

The flow capacity of the drainage system should be sufficient to convey with no excessive pressure buildup:

- water leaking through geomembrane holes;
- water leaking through the attachments of the geomembrane to the peripheral plinth;
- water seeping from the abutments; and
- water that progressively drains from the dam body.

The drainage layer associated with the geomembrane should have a high resistance to compressive stress to ensure the required flow capacity under the high pressure that exists at the toe of the dam.

In fact, a drainage layer behind the geomembrane is also needed for another reason. In all cases where a geomembrane is located at, or near, the upstream face of a dam, a drainage layer is necessary beneath the geomembrane to prevent the presence of water under the geomembrane, which could uplift the geomembrane in case of rapid drawdown of the reservoir water.

One may expect that the drainage system can be used to monitor leakage through the geomembrane liner. However, the situation is complex.

9.4. Leakage monitoring in dams

Water collected in the drainage system associated with the geomembrane liner of a dam is not only leakage through the geomembrane or leakage at the geomembrane connections with appurtenant structures, but also (and in great part) seepage from the abutments. In some dams with a drainage system composed of independent sections, careful analyses have shown that up to 90% of the collected water is, in fact, flowing from the abutments (Machado do Vale, 2016). Therefore, the amount of water collected by the drainage system of a dam cannot be interpreted as leakage through the geomembrane, unless there is a sophisticated drainage system where waters from different sources are identified.

An idea of the effectiveness of geomembranes used at the upstream face of dams can be obtained by reviewing data from dam rehabilitation. Data from eight dams rehabilitated using a geomembrane (Wilkes & Schlosser, 2015), analyzed by the author of this paper, show that: (i) the leakage rate ratio before and after rehabilitation ranges between 4 and 1200; and (ii) most typical ratios are between 10 and 100. The wide range is probably due to different conditions at the geomembrane periphery. These data show that there is a significant reduction in leakage when a geomembrane is used at the upstream face of a dam, but it should be remembered that another benefit, which is often the main benefit, is that, in great part thanks to the drainage system, the leakage is not seeping through the dam body and the dam body is drained, so the dam body is dry.

10. Summary and Conclusion

10.1. Summary of information presented in this paper

The following has been shown in this paper:

- Leakage must be minimized because it is detrimental due to loss of precious liquid and/or damage to ground and ground water.
- Leakage is inevitable, even when a quasi-impermeable liner, such as a geomembrane, is used.
- When a geomembrane liner is used, leakage occurs through holes in the geomembrane and/or defective connections with appurtenant structures.
- Geomembrane holes and defective connections are minimized in number and size by appropriate design and specifications, professional installation, construction quality assurance, and electric hole detection.
- The impact of geomembrane holes on leakage rate can be greatly reduced by associating a geomembrane with a layer of low-permeability material (typically clay) to form a composite liner. However, composite liners must be ballasted to prevent the geomembrane from being uplifted, in particular in case of rapid drawdown. Therefore, composite liners are mostly used in landfills.
- Leakage can be reduced if a double liner is used, which includes a leakage collection and detection layer be-

tween the two liners. As a result, leakage through the primary liner is detected while the hydraulic head is maintained extremely low on the secondary liner, which results in negligible leakage through the secondary liner into the ground.

- Mechanical properties of the geomembrane are essential for minimizing the risk of puncture and the risk of tensile rupture at attachments of the geomembrane to appurtenant structures. The tensile strength of the geomembrane is not the relevant property. An appropriate (and quantifiable) balance of strength and extensibility is required. From this view point, optimum tensile behavior is achieved with a geomembrane reinforced with a nonwoven geotextile.
- Geomembrane liners are often associated with drainage layers.
- The goal and practice of leakage control depends on the type of containment structure. In dams, a geomembrane liner typically reduces leakage while preventing the deterioration of the dam body, functioning in association with a drainage system.
- Leakage monitoring is difficult and sometimes inaccurate. However, available leakage monitoring data confirm the effectiveness of geomembrane liner systems in reducing leakage by a significant factor.

10.2. Conclusion

This paper shows that the use of geomembranes, has significantly improved the performance of liquid containment structures. However, using geomembrane liners without appropriate design and adequate workmanship can lead to failures. Too many users think that the mere fact of using a geomembrane will solve all containment problems. Too many engineers have learned about geomembranes while designing landfills, an application where the use of geomembranes is strictly regulated. Then, they design reservoirs and dams without addressing the problems specific to these applications. Geotechnical engineering is not about cutting and pasting; geotechnical engineering is about thinking. This paper should encourage thinking by providing the rationale that supports engineering solutions related to geomembrane liners. The author of this paper believes that this approach is consistent with the spirit of Victor de Mello.

Acknowledgments

The author is grateful to José Luís Machado do Vale who provided invaluable information and comments. The author is also grateful to Gabriella Vaschetti for her careful review.

This paper is dedicated to Victor de Mello who inspired many of us by sharing his vision of an ever evolving discipline, in particular by encouraging the use of geosynthetics.

References

Beck, A. & Darilek, G. (2016) Personal Communication.

Charpentier, C.; Jacquelin, T.; Rollin, A.L. & Bremner, H. (2016) Statistics on ell surveys compared to the overall geomembrane covered area in the province of Quebec in 2014. Proc. Third PanAmerican Conference on Geosynthetics, GeoAmericas 2016, Miami Beach, 10 p.

Darilek, G.T. & Laine, D.L. (2013) Specifying allowable geomembrane leakage rates based on available technology. Proc. Geosynthetics 2013, Long Beach, p. 180-185.

Giroud, J.P. (1973) L'étanchéité des retenues d'eau par feuilles déroulées. Annales de l'ITBTP, 312, TP 161, Paris, p. 94-112 (in French).

Giroud, J.P. & Perfetti, J. (1977) Classification des textiles et mesure de leurs propriétés en vue de leur utilisation en geotechnique. Proc. International Conference on the Use of Fabrics in Geotechnics, Session 8, Paris, p. 345-352 (in French).

Giroud, J.P. (1983) Geotextile drainage layers for soil consolidation. In: Civil Engineering for Practicing and Design Engineers, Volume II, Pergamon Press, USA, p. 275-295.

Giroud, J.P. (1984a) Geomembrane liners: Accidents and preventive measure. Proc. Second International Symposium on Plastic and Rubber Waterproofing in Civil Engineering, Session 4, Liege, v. 1, p. 4.2.1-4.2.6.

Giroud, J.P. (1984b) Impermeability: The myth and a rational approach. Proc. International Conference on Geomembranes, Denver, v. 1, p. 157-162.

Giroud, J.P.; Arman, A. & Bell, J.R. (1985) Geotextiles in Geotechnical Engineering, Practice and Research, with Foreword by V.B de Mello. Geotextiles & Geomembranes, Vol. 2, No. 3, p. 179-242.

Giroud, J.P. & Bonaparte, R. (1989a) Leakage through liners constructed with geomembranes, Part I: Geomembrane liners. Geotextiles & Geomembranes, 8(1):27-67.

Giroud, J.P. & Bonaparte, R. (1989b) Leakage through liners constructed with geomembranes, Part II: Composite liners. Geotextiles & Geomembranes, 8(2):71-111.

Giroud, J.P. & Soderman, K.L. (1995) Comparison of geomembranes subjected to differential settlement. Geosynthetics International, Special Issue on Design of Geomembrane Applications, 2(6):953-969.

Giroud, J.P.; Tisseau, B.; Soderman, K.L. & Beech, J.F. (1995) Analysis of strain concentrations next to geomembrane seams. Geosynthetics International, Special Issue on Design of Geomembrane Applications, 2(6):1049-1097.

Giroud, J.P. (1997) Equations for calculating the rate of liquid migration through composite liners due to geomembrane defects. Geosynthetics International, Special Issue on Liquid Migration Control Using Geosynthetic Liner Systems, 4(3-4):335-348.

Giroud, J.P.; Gross, B.A.; Bonaparte, R. & McKelvey, J.A. (1997a) Leachate flow in leakage collection layers due to defects in geomembrane liners. Geosynthetics International, Special Issue on Liquid Migration Control Using Geosynthetic Liner Systems, 4(3-4):215-292.

Giroud, J.P.; King, T.D.; Sanglerat, T.R.; Hadj-Hamou, T. & Khire, M.V. (1997b) Rate of liquid migration through defects in a geomembrane placed on a semi-permeable medium. Geosynthetics International, Special Issue on Liquid Migration Control Using Geosynthetic Liner Systems, 4(3-4):349-372.

Giroud, J.P. & Touze-Foltz, N. (2003) Geomembranes for landfills. Geosynthetics International, 10(4):124-133.

Giroud, J.P. (2005) Quantification of geosynthetics behavior. Geosynthetics International, Special Issue on Giroud Lectures, 12(1):2-27.

Giroud, J.P. & Gourc, J.P. (2014) The first double geomembrane liner forty years later. Proc. 10th International Conference on Geosynthetics, Berlin, 8 p.

Giroud, J.P. & Wallace, R.B. (2016) Quantified impact of geomembrane wrinkles on leakage through composite liners. Proc. Third PanAmerican Conference on Geosynthetics, GeoAmericas 2016, Miami Beach, 10 p.

Gross, B.A.; Bonaparte, R. & Giroud, J.P. (1990) Evaluation of flow from landfill leakage detection layers. Proc. Fourth International Conference on Geotextiles, Geomembranes and Related Products, The Hague, v. 2, p. 481-486.

Machado do Vale, J.L. (2016) Personal Communication.

Peggs, I.D. (2014) Personal Communication.

Peggs, I.D. & Giroud, J.P. (2014) Action leakage rate for reservoir geomembrane liners. Proc. 10th International Conference on Geosynthetics, Berlin, 10 p.

Rowe, R.K. (1998) Geosynthetics and the minimization of contaminant migration through barrier systems beneath solid waste. Keynote Paper, Proc. 6th International Conference on Geosynthetics, v. 1, p. 27-103.

Rowe, R.K. (2012) Short- and long-term leakage through composite liners. The 7th Arthur Casagrande Lecture. Canadian Geotechnical Journal, 49:141-169.

Thiel, R.S. & Giroud, J.P. (2011) Important considerations for leakage control of exposed geomembrane-lined ponds. Proc. 13th International Waste Management and Landfill Symposium, Sardinia, 12 p.

Touze-Foltz, N. & Giroud, J.P. (2003) Empirical equations for calculating the rate of liquid flow through composite liners due to geomembranes defects. Geosynthetics International, 10(6):215-233.

Touze-Foltz, N.; Lupo, J. & Barroso, M. (2008) Geoenvironmental applications of geosynthetics. Keynote Paper. Proc. EuroGeo4, Edinburgh, 98 p.

Wilkes, J. & Schlosser, E. (2015) Personal Communication.

Articles

Shear Strength of Tropical Soils and Bentonite Mixtures for Barrier Design

T.L.C. Morandini, A.L. Leite

Abstract. Compacted clayey tropical soils have great potential to be used as barriers in waste disposal facilities, considering that some technical requirements are fulfilled (*e.g.* hydraulic conductivity; compatibility after disposal; shear strength; swelling/cracking, etc). In turn, the bentonite addition is relevant for the cases where the hydraulic conductivity must be lowered, and therefore investigations on the changes of the mechanical parameters of tropical soils induced by the bentonite addition are of great interest. This paper presents the results of a laboratory investigation on the shear strength of different samples of tropical soils and their mixtures with bentonite in the proportions of 0, 3, 6, 9 and 12% (dry weight basis). The tropical soil samples were collected considering the lateritic, transitional and non-lateritic behavior according to the MCT-M (Modified-Miniature-Compacted-Tropical) classification. The laboratory tests consisted of *CU* (Consolidated-Undrained) triaxial tests under the confining stresses of 100, 200 and 400 kPa. The results have showed that the addition of bentonite produced a significant increase in the plasticity of the tropical soil samples (*PI* increases 4 to 6 times), considerably reduced their friction angle (by as much as 11°) and stiffness at peak (modulus reductions of 2.5 to 4 MPa) and gave rise to a slight increase in their cohesion (up to 12 kPa). These facts must be considered in the barrier stability analyses when heavy loads are applied. The important role of the shear strength on barrier design is highlighted.

Keywords: tropical soils, bentonite, clayey barriers, shear strength, stiffness.

1. Introduction

To be used as liners on barrier design for waste disposal facilities, soils must suit geotechnical criteria such as low hydraulic conductivity, long-term compatibility with the disposed liquid, adequate swelling/cracking properties and adequate shear strength (Shackelford, 1994).

In fact, the shear strength was highlighted once the weight on designs of solid waste landfill barriers (urban and industrial) has been steadily increasing as a response to the lack of sites for waste disposal facilities.

The hydraulic behavior of different clayey soils for barrier purposes was investigated by Eklund (1985), Chapuis (1990), Sivapullaiah *et al.* (1998), Shackelford (1994), Gleason *et al.* (1997), Rowe (2001), Koch (2002), Laird (2006) and Shackelford & Sample-Lord (2014), among others.

The hydraulic adequacy of tropical soils and their admixtures to be used on barrier design was evaluated by Anderson & Hee (1995), Osinubi & Nwaiwu (2002) and Amadi & Eberemu (2012).

In turn, the shear strength of geosynthetic clay liners (GCL) was assessed by Stark & Eid (1996), Chiu & Fox (2004), Fox *et al.* (2006), Fox & Kim (2008), Chen *et al.* (2010) and Eid (2011). Some other papers report studies of the shear strength of soils for barrier purposes such as Heineck (2002), Hueckel & Pellegrini (2002), Santamarina (2003), Sunil *et al.* (2009) and Batista & Leite (2010). In these papers, the addition of bentonite led to a decrease in the resistance to shear of the soil as a whole. Particularly, a reduction of the friction angle (ϕ) and an increase of the cohesion (c) was observed.

Considering the absence of research on the matters of using tropical soils and their admixtures with bentonite, this study was proposed to cover most of the geotechnical criteria referred in the first paragraph, such as hydraulic conductivity, shear strength and long-term compatibility. The tropical soil samples investigated were classified as lateritic, transitional and non-lateritic according to the MCT-M Classification as proposed by Vertamatti (1998). Morandini & Leite (2013 and 2015) report part of the results of this research, focused on the hydraulic behavior of admixtures of tropical soils and 0, 3, 6, 9, and 12% of bentonite (dry weight basis).

In particular, the present paper focuses on the shear strength of admixtures of tropical soils with bentonite in the same proportions investigated by Morandini & Leite (2013 and 2015). Laboratory works involved triaxial shear strength tests under different confining stresses. The long-term compatibility issue will be reported elsewhere.

2. Soil Characterization

The tropical soil samples were collected as an attempt to represent lateritic (SL sample), transitional (ST sample) and non-lateritic (SN sample) behavior according to the MCT-M Classification (Vertamatti, 1998). The sampling

Thiago Luiz Coelho Morandini, Doctor, Departamento de Engenharia Civil, Centro Federal de Educação Tecnológica de Minas Gerais, Belo Horizonte, MG, Brazil. e-mail: thiagomorandini@des.cefetmg.br.
Adilson do Lago Leite, Doctor, Departamento de Engenharia Civil, Universidade Federal de Ouro Preto, Ouro Preto, MG, Brazil. e-mail: alleite@em.ufop.br.
Submitted on October 7, 2015; Final Acceptance on November 27, 2016; Discussion open until April 28, 2017.

locations in the state of Minas Gerais, Brazil can be seen on Fig. 1.

The evaluated tropical soils were collected from the geological formation denominated "Iron Quadrangle". This type of soil is formed from igneous rocks (mostly basalt) or metasedimentary rock from Precambrian orogenetic cycles. It is characterized as residual soil formed by pedogenetic process known as laterization, in which the hot and humid climate and the profile of high draining favors the processes of hydrolysis, hydration and oxidation. After the formation of sediments, the silica particles are highly leached to lower layers and consequently the iron and aluminum oxides remain in the surface layers.

The main factor responsible for the contrast between the classes of the studied tropical soils is their position on the pedological layer: the laterite soil was collected at the top of a slope (theoretically with high concentration of oxides); the non-lateritic soil was collected at the foot of a cut slope (with characteristics of the parent rock and a high concentration of silica); the transitional soil was collected at the foot of a hill, in a spot with process of erosion and transport of different pedological layers.

The mixtures were prepared by hand and the proportions of bentonite Brasgel-PA® (X-ray diffraction presented by Morandini & Leite, 2015) were 0, 3, 6, 9 and 12% (dry weight basis), which received the designations expressed in Table 1. Recent studies indicate the use of bentonite in content between 2 and 20% mixed with sand and other soils, such as Chapuis (1990), Shackelford (1994), Anderson & Hee (1995), Batista & Leite (2010) and Amadi and Eberemu (2012). The complete characterization procedures and results for all these samples were firstly presented by Morandini & Leite (2015). Table 2 shows only a summary of their geotechnical properties. The parameters presented in Table 2 were tested according to the procedures of the standards ABNT NBR 6459 (1984), ABNT NBR 7180 (1984), ABNT NBR 7181 (1984) and ABNT NBR 7182 (1986). The SL, SL and SN samples refer to the original soils and BB sample refers to Brasgel Bentonite.

The mineralogy of the SL sample is mainly composed of kaolinite, quartz, gibbsite and hematite. The ST sample presents kaolinite, illite, chlorite and smectite, while the SN sample is composed of kaolinite, quartz and goethite. The chemical composition of these samples indicates high contents of Fe and Al oxides in the following order: sample SL > sample ST > sample SN.

3. Methods

Ordinary triaxial soil tests were used to determine the shear strength, axial deformation and pore pressure in-

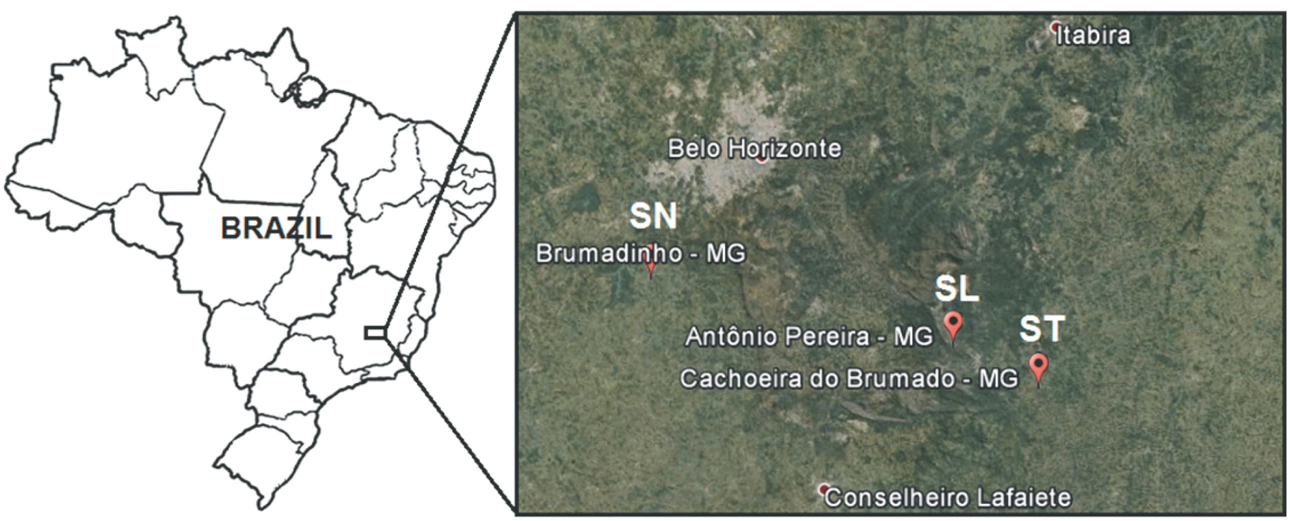

Figure 1 - Soil sampling locations (Source: Google Earth®).

Table 1 - Sample designation and bentonite proportions (dry weight basis).

Designation	Content (%)	Designation	Content (%)	Designation	Content (%)
SL	0.0	ST	0.0	SN	0.0
SL03	3.0	ST03	3.0	SN03	3.0
SL06	6.0	ST06	6.0	SN06	6.0
SL09	9.0	ST09	9.0	SN09	9.0
SL12	12	ST12	12	SN12	12

Table 2 - Summary of the geotechnical properties (Source: Morandini & Leite, 2015).

Property	Sample															
	SL[1]	SL03	SL06	SL09	SL12	ST[1]	ST03	ST06	ST09	ST12	SN[1]	SN03	SN06	SN09	SN12	BB[2]
Atterberg limits																
w_L (%)	23	42	57	72	87	52	78	96	117	156	56	76	96	116	136	683
w_P (%)	12	21	23	26	27	30	28	29	27	28	31	34	37	40	44	91
PI (%)	11	21	34	46	60	22	50	67	90	128	25	42	59	76	92	592
Grain size																
Clay (%)	29	29	30	30	31	41	39	41	41	42	36	38	42	44	46	91
Silt (%)	16	18	17	20	17	9	10	9	9	8	10	11	11	11	12	9
Fine Sand (%)	35	34	34	29	28	36	17	17	18	19	23	20	20	19	20	0
Medium Sand (%)	16	15	15	15	17	8	27	26	25	24	18	19	19	17	14	0
Coarse Sand (%)	3	3	4	5	7	5	6	6	6	6	10	9	6	6	6	0
Gravel (%)	1	1	0	1	0	1	1	1	1	1	3	3	2	3	2	0
USCS	CL	CL	CH	CH	CH	MH	CH	CH	CH	CH	MH	CH	CH	CH	CH	CH
Normal proctor compaction																
$\rho_{dmáx}$ (g/cm^3)	1.82	1.81	1.79	1.78	1.76	1.62	1.65	1.62	1.60	1.58	1.62	1.61	1.59	1.58	1.57	N[3]
w_{opt} (%)	12.5	14.5	16.2	17.8	19.1	21.5	22.5	23.3	24.0	24.8	22.2	23	23.6	24.4	25.1	N[3]
Cation exchange capacity and specific surface																
CEC (cmol/kg)	3.6	6.2	9.8	12.9	15.7	6.9	13.5	18.6	25.3	36.0	7.9	11.6	16.0	20.3	24.8	99.4
SS (m^2/g)	28	48	76	100	122	54	105	145	197	281	61	90	124	158	193	776

[1]Results of original soil samples.
[2]Results of pure Bentonite Brasgel.
[3]Not available.

crease of the compacted soil samples of Table 2. Consolidated-Undrained (CU) test was chosen, as an attempt to represent a fast loading condition over low-permeability soils, as usually is the case of clayey barriers.

According to the procedures indicated by ASTM-D4767 (1995), soil specimens were firstly compacted under Normal Proctor energy (moisture content 2% above the optimum moisture). The sample was then trimmed to a final geometry of 50 ± 2 mm diameter (D) and 100 ± 4 mm height (H). These dimensions are close to the specifications indicated by the standard ASTM-D4767 (1995): H = 2.0 to 2.5D. Three soil specimens were used for each triaxial test, leading to a final number of 45.

The confining stresses (σ_3) of 100, 200 and 400 kPa have been applied to represent the field reality of bottom liners loaded with Municipal Solid Waste (MSW). For exemple, a landfill 100 m high and a density of 1.2 kN/m^3, would be a confining pressure of about 60 kPa. General procedures involve saturation, consolidation and shearing of the soil specimens. Since this is a current geotechnical laboratory test, some brief description of these methods is given next:

- Saturation. Counter pressure method, as suggested by Head (1986). Small pressure gradients are applied according to the following premise: confining stress > pore pressure at the base of the soil specimen > counter pressure at the top of the soil specimen. Counter pressure difference between the top and bottom of the sample never exceeds 20 kPa. Confining pressure was applied by adding the counter pressure without the necessity of retained counter pressure, resulting in effective stress of 100, 200, and 400 kPa. Samples were considered saturated when the parameter *B* of Skempton was above 95%.
- Consolidation. Confining stress application and free drainage of the soil specimens until the pore pressure decreases until equalization. The consolidation was measured by evaluating the volume variation *vs.* the square root of time.
- Shearing. The axial load (deviator stress) was applied through controlled deformation at a constant velocity of 0.0025 mm/s during 65 min, leading to a maximum axial deformation of 20%. This rate of axial loading was established according to the criteria suggested by Head (1986) for fine soil, with 5% of the axial strain being reached at 50% of the estimated time for soil consolidation.

The friction angle (φ) and cohesion (c) were determined by the stress path approach (Lambe, 1964), using the diagram of mean total stress (p) or mean effective stress (p') *vs.* the deviator total stress (q) or deviator effective stress (q'), as expressed by Eqs. 1 through 4.

$$p = \frac{\sigma_1 + \sigma_3}{2} \tag{1}$$

$$q = \frac{\sigma_1 - \sigma_3}{2} \tag{2}$$

$$p' = p - u \tag{3}$$

$$q' = q \tag{4}$$

where σ_1 is the axial stress, σ_3 the confining stress and u the pore pressure.

The shear strength envelope in the p-q or p'-q' space is represented by the Eqs. 5 and 6, respectively.

$$q = a + p \tan\alpha \tag{5}$$

$$q' = a' + p' \tan\alpha' \tag{6}$$

where p, p' and q, q' are parameters that represent the average stress and deviator total stress, respectively. And a, a' and α, α' are modified parameters obtained from the strength envelope at failure. In turn, the parameters φ and c (Mohr-Coulomb envelope) are related to the referred modified parameters by Eqs. 7 through 10, in terms of total and effective stresses.

$$\varphi = \sin^{-1}(\tan\alpha) \tag{7}$$

$$c = \frac{a}{\cos\varphi} \tag{8}$$

$$\varphi' = \sin^{-1}(\tan\alpha') \tag{9}$$

$$c' = \frac{a'}{\cos\varphi'} \tag{10}$$

Additionally, Eqs. 11 and 12 were used to estimate the modulus of elasticity at peak (taken across the line connecting the origin to the peak resistance) and the *A* parameter (Skempton, 1954), respectively. The *A* parameter was measured to represent the effect of the axial load on the generation of pore pressure, a fundamental parameter for the study of low permeability soils.

$$E_P = \frac{\sigma_d}{\varepsilon_a} \tag{11}$$

$$\Delta u = B[\Delta\sigma_3 + A([\Delta\sigma_d)] \tag{12}$$

where σ_d is the deviator stress at peak ($\Delta\sigma_1$ - $\Delta\sigma_3$), ε_a is the axial strain at peak and Δu the pore pressure variation.

4. Results and Discussion

The influence of the bentonite addition on the stiffness of the mixtures is illustrated on Figs. 2, 3 and 4, which show the deviator stress ($\sigma_d = \Delta\sigma_1 - \Delta\sigma_3$) *vs.* axial strain ($\varepsilon_a$) curves. It is quite clear that the bentonite addition reduced the peak deviator and residual stresses of the samples.

Higher values for the peak deviator stresses were found for the SL sample compared to ST and SN samples for all the confining stresses used in the tests. This fact is due in part to the coarser grain size of the SL sample compared to ST and SN samples, and also to the cementation (micro concretions) often found in lateritic soils, as mentioned by Nogami & Villibor (1985).

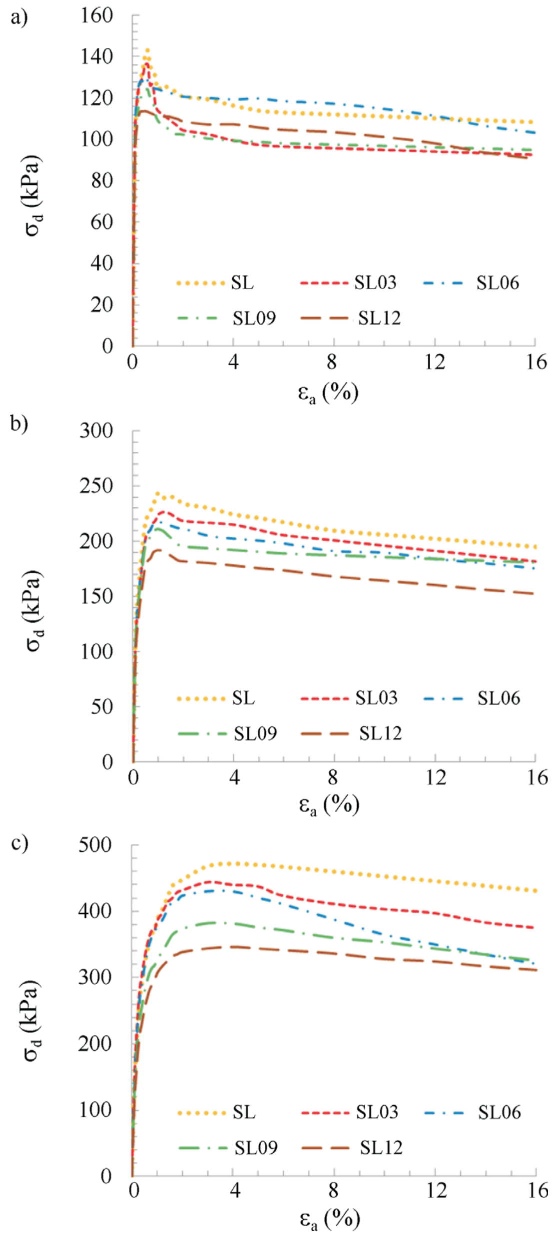

Figure 2 - Deviator stress *vs.* axial strain for the sample SL under the following confining stresses: (a) 100 kPa, (b) 200 kPa and (c) 400 kPa.

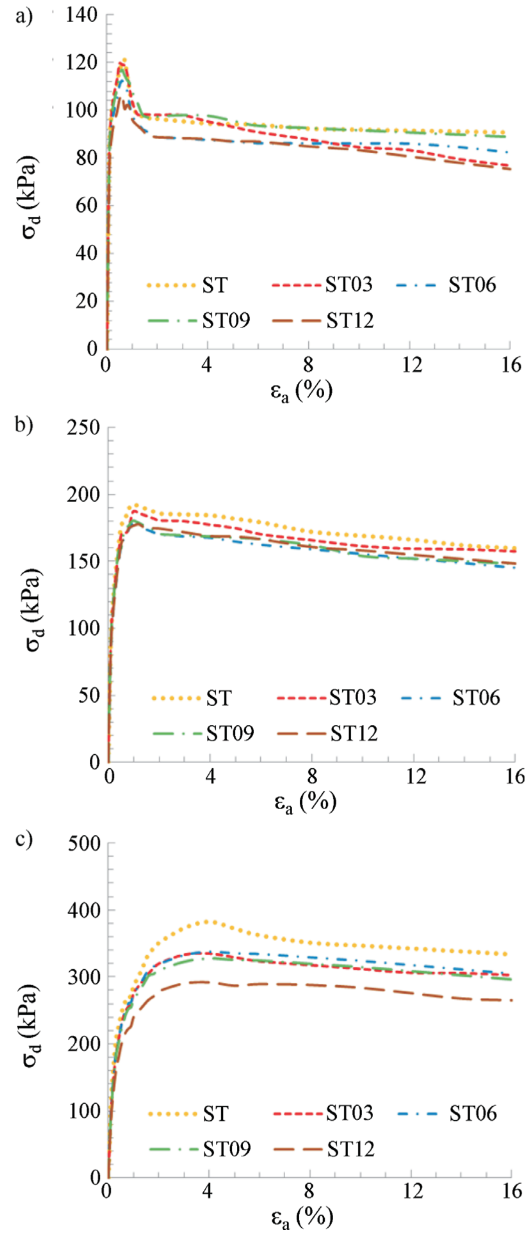

Figure 3 - Deviator stress *vs.* axial strain for the sample ST under the following confining stresses: (a) 100 kPa, (b) 200 kPa and (c) 400 kPa.

As expected, peak axial deformations increased with increasing confining stresses for all samples. However, that peak axial deformation did not vary significantly among the soils and bentonite contents.

Particularly, the peak axial strains were: sample SL = 0.6% (σ_3 = 100 kPa), 1.2% (σ_3 = 200 kPa) and 3.0% (σ_3 = 400 kPa); sample ST = 0.7% (σ_3 = 100 kPa), 1.2% (σ_3 = 200 kPa) and 3,1% (σ_3 = 400 kPa); sample SN 0.9% (σ_3 = 100 kPa), 1.4% (σ_3 = 200 kPa) and 3.9% (σ_3 = 400 kPa).

The moduli at peak (E_p) were estimated from the peak axial stresses and strains, and are presented in Fig. 5 as a function of the bentonite content for all samples. As also expected, there was a reduction on the modulus at peak with the addition of bentonite. For instance, 12% of bentonite caused a reduction of 4 MPa on E_p of the SL sample and 2.5 MPa for the ST and SN sample.

As expected, for all the soil samples there was a significant decrease in the friction angle as a response to the increase of the bentonite content, as shown on Figs. 6 and 7. However, the rate of this decrease was very similar for the SL and ST samples, and more accentuated for the SN sample. For instance, the value of φ' = 34° for the natural

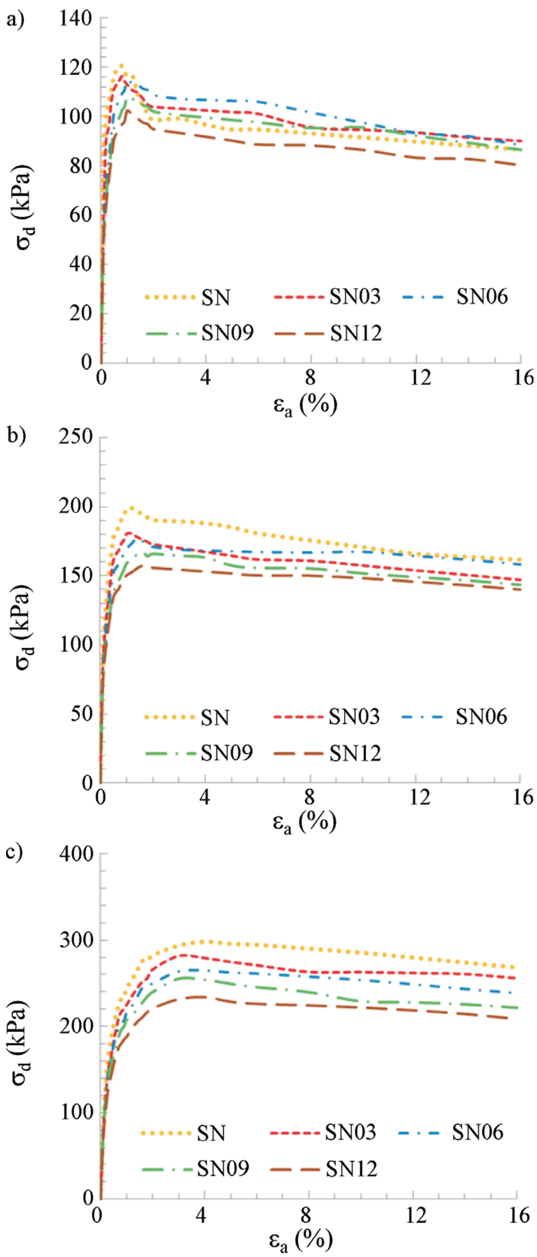

Figure 4 - Deviator stress *vs.* axial strain for the sample SN under the following confining stresses: (a) 100 kPa, (b) 200 kPa and (c) 400 kPa.

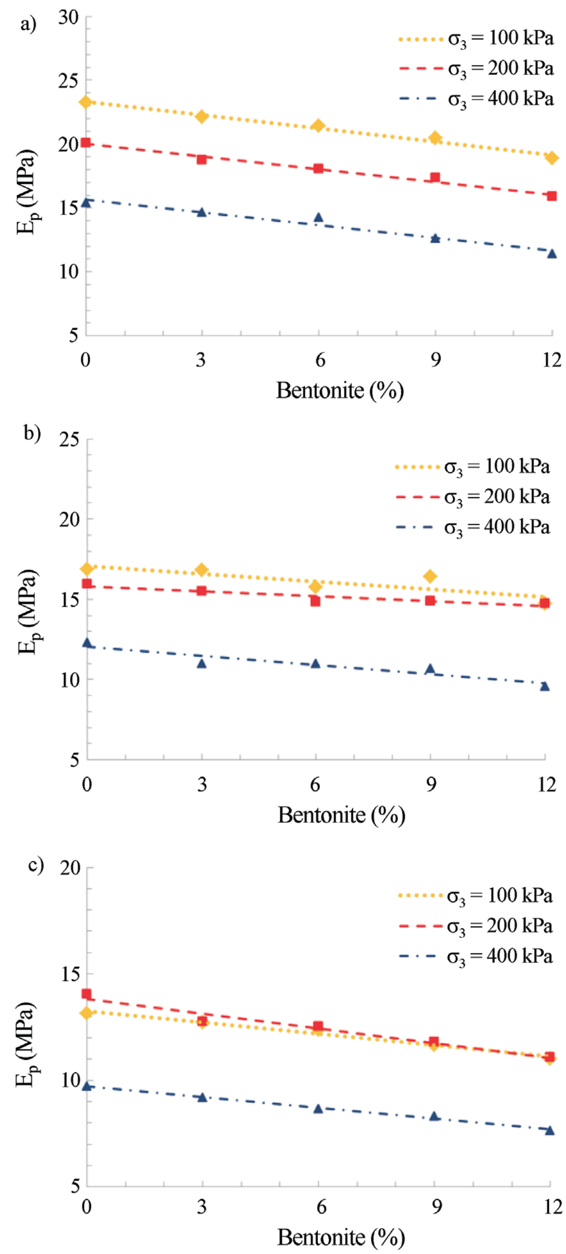

Figure 5 - Modulus at peak (E_p = *maximum deviator stress / maximum axial strain*) as a function of the bentonite content: (a) SL sample; (b) ST sample and (c) SN sample.

lateritic sample (sample SL) reduced to φ' = 29° when 12% of bentonite was considered (sample SL12).

Mesri & Olson (1971) reported a significant reduction of the friction angle of pure montmorillonite clays by increasing the effective stress. Therefore, it would be expected that besides the addition of bentonite, the variation of the confining stresses (σ_3) from 100 to 400 kPa could also exert some influence on the friction angles, which was not confirmed, considering the linearity observed in the curves of Fig. 7.

As also expected, cohesion experimented linear increase with the bentonite addition (Fig. 7) for all samples. For instance, cohesion increased from 6 to 12 kPa considering the addition of 12% of bentonite for all samples.

As general remark about the influence of the addition of bentonite on the strength parameters (*c* - *c*' and φ - φ'), it can be said that the decrease in the friction angle can be compensated by the increase in the cohesion, depending on the loading conditions. Under light loading (*e.g.* at the beginning of operation of a landfill site), the mobilization of the friction angle is small and the increase in the cohesion may be sufficient to compensate for the loss in the global

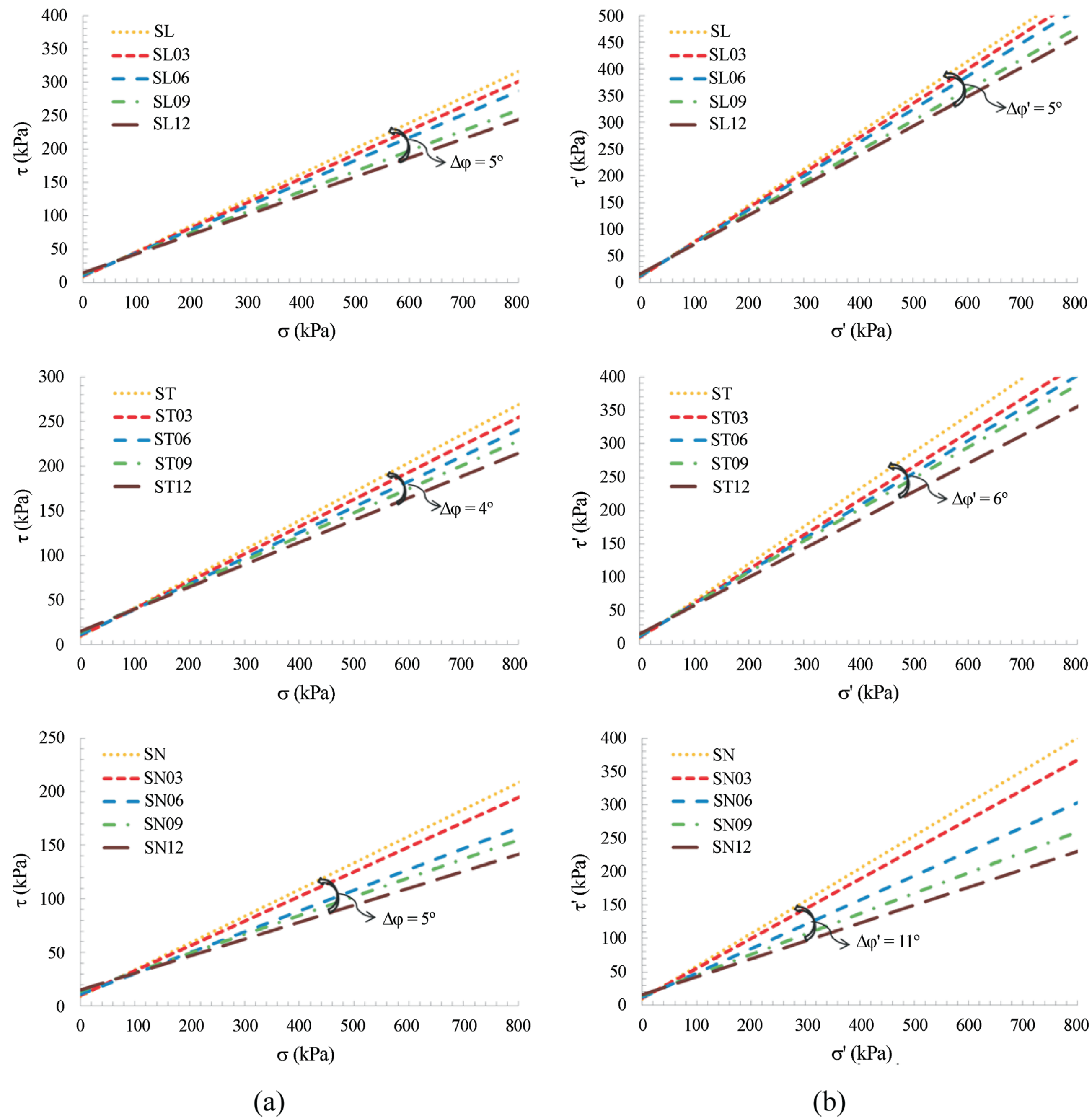

Figure 6 - Shear strength envelopes for total (a) and effective (b) stresses.

shear strength. On the other hand, under heavy loading (*e.g.* at the end of operation of a landfill site), the mobilization of the friction angle is high and so is the loss in shear strength. However, friction angle values and cohesion of the SL and of the ST + 12% of bentonite would not be likely to lead to soil failure.

Figure 8 shows that the parameter *A* at failure increases as a function of the bentonite content for all samples and all confining pressures, especially for the confining stress of 400 kPa. Morandini & Leite (2015) report the significant reduction of the hydraulic conductivity caused by the addition of bentonite in the same soil samples and mixtures, which might be responsible for this increase in the pore pressure during the application of the deviator stress.

A higher parameter A means that the barrier would be subject to higher pore pressure generation during the loading phase. Under such circumstances, and if liners are installed deep in the landfill, special care must be taken in the rising rate of the landfill.

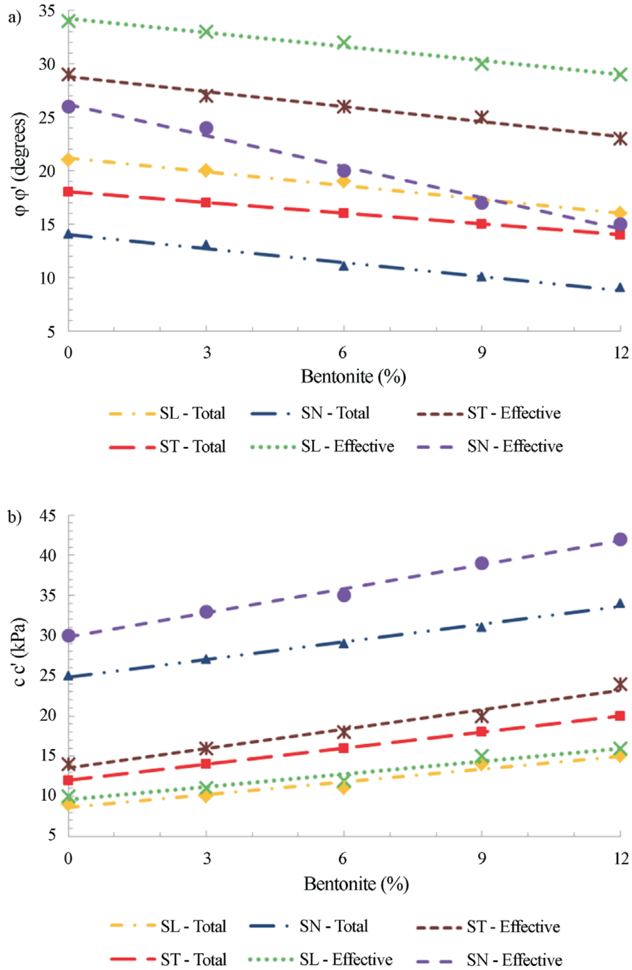

Figure 7 - Variation of the friction angle (a) and cohesion (b) with bentonite content (total and effective stresses).

5. Conclusions

As a general remark, for the evaluated soils in this study, it is concluded that the lateritic character has minor influence on the mechanical behavior when bentonite is applied.

In turn, the changes in the mechanical behavior of the tropical soil samples (in different magnitudes according to the class SL, SN and ST) induced by the addition of bentonite are summarized next:

- A significant increase in the plasticity;
- A decrease in the peak stress at failure, with no influence on the subsequent deformations;
- A significant reduction in the stiffness;
- The pore pressure considerably increased during the shear stress application, as suggested by successive increases in the parameter *A*;
- Significant reduction of the friction angle and a slight increase in the cohesion.

At first, the above conclusions seem to be obvious, considering the high plasticity of the bentonite. Nevertheless, the high magnitude of the mechanical changes imposed by the bentonite addition was relevant and must be taken into consideration for barrier design. In terms of effective friction angle, there was a decrease of approximately 14%, 20% and 40% respectively for the SL, ST and SN samples and these samples with addition of 12% of bentonite. The stiffness declines up to 25% compared to pure soils and soils with 12% of bentonite. Therefore, bentonite plays an important role in reducing the hydraulic conductivity of tropical soils, but caution should be exercised about the quantities of this material to be used.

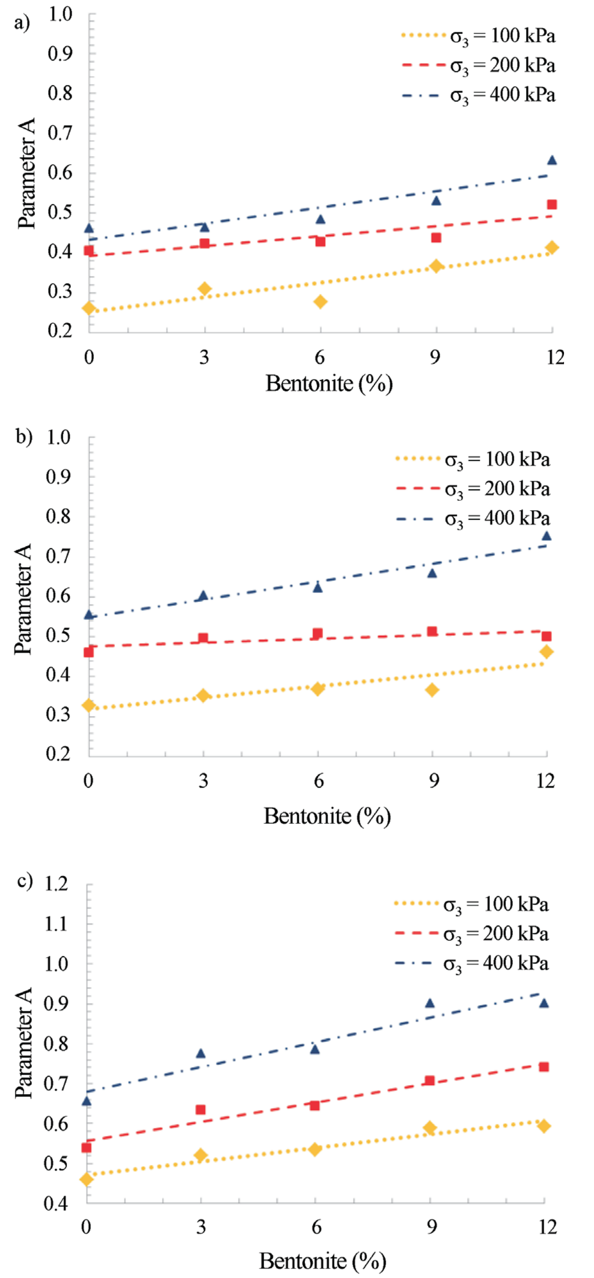

Figure 8 - Parameter *A* (Skempton, 1954) at failure as a function of the bentonite content: (a) Sl sample; (b) ST sample and (c) SN sample.

Acknowledgments

The authors give special acknowledgments to the Fundação de Amparo à Pesquisa do Estado de Minas Gerais (FAPEMIG) for supporting this research (grant number TEC-APQ02502-12) and for providing a full scholarship to the first author during his Ph.D. course. The company Bentonit União Nordeste Ltda gently donated the bentonite samples used in laboratory tests. Part of these tests was executed in the company Diefra Engineering and Consultants, and the authors thank the owners of this company for their support.

References

ABNT (1984). NBR 6459 - Determination of Liquid Limit. Rio de Janeiro (In Portuguese).

ABNT (1984). NBR 7180 - Determination of Plastic Limit. Rio de Janeiro (In Portuguese).

ABNT (1984). NBR 7181 - Particle Size Analysis. Rio de Janeiro (In Portuguese).

ABNT (1986). NBR 7182 - Soil - Compaction Test. Rio de Janeiro (In Portuguese).

Amadi, A.A. & Eberemu, A.O. (2012). Delineation of compaction criteria for acceptable hydraulic conductivity of lateritic soil-bentonite mixtures designed as landfill liners. Environmental Earth Sciences, 67(4):999-1006.

Anderson, S.A. & Hee, B.H. (1995). Hydraulic conductivity of compacted lateritic soil with bentonite admixture. Environmental and Engineering Geoscience, 1(3):299-312.

ASTM (1995). D 4767/95 - Standard Test Method for Consolidated Undrained Triaxial Compression Test for Cohesive Soils. West Conshohocken.

Batista, P. & Leite, A.L. (2010). Mixtures of a laterite with cement and bentonite to be used in vertical blinds. REM. Magazine School of Mines, 63(2):255-263 (In Portuguese).

Chapuis, R.P. (1990). Sand-bentonite liners: Predicting permeability from laboratory tests. Canadian Geotechnical Journal, 27(1):47-57.

Chen, Y.-M.; Lin, W.-A. & Zhan, T.L.T. (2010). Investigation of mechanisms of bentonite extrusion from GCL and related effects on the shear strength of GCL/GM interfaces. Geotextiles and Geomembranes, 28(1):63-71.

Chiu, P. & Fox, P.J. (2004). Internal and interface shear strengths of unreinforced and needle-punched geosynthetic clay liners. Geosynthetics International, 11(3):176-199.

Eid, H.T. (2011). Shear strength of geosynthetic composite systems for design of landfill liner and cover slopes. Geotextiles and Geomembranes, 29(3):335-344.

Eklund, A.G. (1985). A laboratory comparison of the effects of water and waste leachate on the performance in soil liners. Hydraulic Barriers in Soil and Rock, ASTM STP 874, Johnson, A.I.; Frobel, R.K.; Cavalli N.J. & Pettersson, C.B. (eds) American Society for Testing and Materials, Pennsylvania, pp. 188-202.

Fox, P.J.; Nye, C.J.; Morrison, T.C.; Hunter, J.G. & Olsta, J.T. (2006). Large dynamic direct shear machine for geosynthetic clay liners. Geotechnical Testing Journal, 29(5):392-400.

Fox, P.J. & Kim, R.H. (2008). Effect of progressive failure on measured shear strength of geomembrane/GCL interface. Journal of Geotechnical and Geoenvironmental Engineering, 134(4):459-469.

Gleason, M.K.; Daniel, D.E. & Eykholt, G.R. (1997). Calcium and sodium bentonite for hydraulic containment applications. Journal of Geotechnical and Geoenvironmental Engineering, 123(5):438-445.

Head, K.H. (1986). Manual of Soil Laboratory Testing: Effetive Stress Tests. John Wiley and Sons, London, v. 3.

Heineck, K.S. (2002). Study of the Hydraulic and Mechanical Behavior of Geotechnical Materials to Waterproof Horizontal Barriers. Doctoral Thesis, Universidade Federal do Rio Grande do Sul, Porto Alegre (In Portuguese).

Hueckel, T. & Pellegrini, R. (2002). Reactive plasticity for clays: Application to a natural analog of long-term geomechanical effects of nuclear waste disposal. Engineering Geology, 64(2):195-215.

Koch, D. (2002). Bentonites as a basic material for technical base liners and site encapsulation cut-off walls. Applied Clay Science, 21(1):1-11.

Laird, D.A. (2006). Influence of layer charge on swelling of smectites. Applied Clay Science, 34(1):74-87.

Lambe, T.W. (1964). Methods of Estimating Settlement. Journal of the Soil Mechanics and Foundation Division, ASCE, 90(SMS):47-74.

Mesri, G. & Olson, R.E. (1971). Shear strength of montmorillonite. Geotechnique, 20(3):261-270.

Morandini, T.L.C. & Leite, A.L. (2013). Hydraulic conductivity and compatibility of mixtures of tropical soil and bentonite for barrier usage purpose. Soils and Rocks, 35(3):267-278.

Morandini, T.L.C. & Leite, A.L. (2015). Characterization and Hydraulic Conductivity of some Tropical Soils Samples and Bentonite Mixtures for CCL Purposes. Engineering Geology, 196(1):251-267.

Nogami, J.S. & Villibor, D.F. (1985). A new classification of soils for road purposes. Proc. Brazilian Symposium on Tropical Soils Engineering, Rio de Janeiro, p. 30-41 (In Portuguese).

Osinubi, K.J. & Nwaiwu, C.M.O. (2002). Compacted lateritic soils as hydraulic barriers in waste containment systems. Proc. 4th International Congress on Environmental Geotechnics, Rio de Janeiro, p. 225-230.

Rowe, R.K. (2001). Barrier systems. Proc. Geotechnical and Geoenvironmental Engineering Handbook. Kluwer Academic, New York, p. 739-788.

Santamarina, J.C. (2003). Soil behavior at the microscale: particle forces. Proc. Soil Behavior and Soft Ground Construction. ASCE, Massachusetts, p.25-56.

Shackelford, C.D. (1994). Waste-Soil Interactions that Alter Hydraulic Conductivity. Hydraulic Conductivity and Waste Contaminant Transport in Soil. ASTM STP1142, Philadelphia, p. 111-166.

Shackelford, C.D. & Sample-Lord, K.M. (2014). Hydraulic conductivity and compatibility of bentonite for hydraulic containment applications. In: Soil Behavior Fundamentals to innovations in Geotechnical Engineering. Iskander, M.; Garlanger, J. & Hussein, M. (eds) Geotechnical Special Publication 233, Honoring Roy E. Olson, ASCE, Reston, p. 370-387.

Sivapullaiah, P.V.; Sridharan, A. & Stalin, V.K. (1998). Evaluation of bentonite and sand mixtures as liners. Proc. 3rd International Congress on Environmental Geotechnics, Lisboa, p. 17-21.

Skempton, A.W. (1954). The pore water coefficients A and B. Geotechnique, 4(1):143-147.

Stark, T.D. & Eid, H.T. (1996). Shear behavior of reinforced geosynthetic clay liners. Geosynthetics International, 3(6):771-786.

Sunil, B.M.; Nayak, S. & Shrihari, S. (2009). Shear strength characteristics and chemical characteristics of leachate-contaminated lateritic soil. Engineering Geology, 106(1):20-25.

Vertamatti, E. (1998). New considerations for Amazonian tropical soils of fine texture classification. Proc. 23th Annual Congress of Paving, Florianópolis, p. 533-564 (In Portuguese).

Electrokinetic Remediation of Tropical Soils: Effect of the Electric Potential Difference

R.Z. Velten, D.C. Lima, M.P.F. Fontes, C.A.B. Carvalho

Abstract. This paper addresses the influence of electric potential difference on the electroosmotic decontamination of two tropical soils from Brazil. The laboratory testing program encompassed: (i) two residual soils of gneiss, a C-horizon saprolite clayey silty sand (soil sample A) and a B-horizon sandy silty clay (soil sample B); (ii) mineralogical and chemical analysis of the soils; (iii) addition of an aqueous solution of cadmium nitrate in the concentration of 100 $mg.L^{-1}$ to the soil samples; (iv) compaction of the mixtures specimens at the Standard AASHTO; (v) electroosmotic decontamination tests applying 5, 15 and 30 V; (vi) application of a modified sequential extraction analysis adapted to tropical soils. The results support that the PZC of soils influenced the direction of cadmium migration and that the increase in the applied electric potential difference led to the increase in the amount of extractable contaminant.
Keywords: electrokinetic remediation, tropical soils, electric potential difference, sequential extraction.

1. Introduction

Soil and groundwater contaminations are major problems for public health and the environment. The contaminants present in these polluted areas include metals, volatile and semi-volatile organic compounds which can be found alone, or co-existing with metals and organic contaminants (Cameselle & Reddy, 2012). Because of these environmental problems, techniques of soil decontamination have been developed and applied over the years on a worldwide basis, such as the electrokinetic remediation of soils contaminated with heavy metals. In this case, efforts have been directed to the mobility, interaction and absorption of the contaminant in the soil matrix, mainly in its clayey fraction.

Lestan *et al.* (2008) and Thomé *et al.* (2013) emphasize that there is a great environmental concern in many parts of the world about soils contaminated with heavy metals, mainly due to fast industrialization, growing urbanization, agricultural practices, and inappropriate waste disposal methods. Regarding the application of the electroosmotic decontamination technique, researchers have been analyzing the mobility of these metals and how they are held in the soil matrix, mainly in the clayey fractions (Christensen, 1989; Boekhold *et al.*, 1993; Naidu *et al.*, 1994; Pombo, 1995; Pierangeli *et al.*, 2005; Velten, 2012; Giannis *et al.*, 2010; Cameselle & Reddy, 2012; Rojo *et al.*, 2014).

Electrokinetic remediation is a technique for treating heavy metal polluted soils by applying a low direct current (in the order of $mA.cm^{-2}$ of the cross-sectional area) or a low potential gradient (in the order of $V.cm^{-1}$ of the distance between the electrodes) at electrodes that are inserted into the ground. In the application of this technique, contaminants are transported by electroosmosis and electromigration to either the cathode or the anode, where they can be extracted.

According to Rojo *et al.* (2014) in the electrokinetic remediation process, water is electrolyzed by the electric field electrodes and oxidation at the anode and reduction at the cathode generate, respectively, an acid and a base front in the soil mass. The acid generated at the anode moves through the soil towards the cathode by electromigration and electroosmosis, while the base generated at the cathode moves towards the anode by electromigration and diffusion. Acid production generally enhances the process, and a high pH zone adversely affects the extraction of heavy metals from soils. In relative terms, the acid front dominates the base front due to the greater mobility of H^+ ion and backflow due to electroosmosis that retards the base front.

New techniques to improve the extraction of heavy metals of soils have been suggested over the years, as follows (Giannis *et al.*, 2010): (i) the use of an electrolyte solution in order to control the electrolyte pH (Lee & Yang, 2000); (ii) sequential improvement by adding chemical reagents to enhance metal solubility (Reddy & Chinthamreddy, 2003); (iii) use of membrane ion selection to reduce or exclude the OH^- ions migration from the cathode to the interior of the soil (Kim *et al.*, 2005); and (iv) conditioning of the pH electrode compartments (Giradakos & Giannis, 2006) through the use of a new technique for electric decontamination of a silty sand with the addition of chelates

Rodrigo Zorzal Velten, M.Sc., Walm Engenharia, Rua Antônio de Albuquerque, 156, 13º andar, Funcionários, 30112-010 Belo Horizonte, MG, Brazil, e-mail: rodrigozorzal@hotmail.com.
Dario Cardoso de Lima, Ph.D., Departamento de Engenharia Civil, Universidade Federal de Viçosa, Av. P.H. Rolfs s/n, 36570-000 Viçosa, MG, Brazil. e-mail: declima@ufv.br.
Maurício Paulo Ferreira Fontes, Ph.D., Departamento de Solos, Universidade Federal de Viçosa, Av. P.H. Rolfs s/n, 36570-000 Viçosa, MG, Brazil. e-mail: mpfontes@ufv.br.
Carlos Alexandre Braz de Carvalho, D.Sc., Departamento de Engenharia Civil, Universidade Federal de Viçosa, Av. P.H. Rolfs s/n, 36570-000 Viçosa, MG, Brazil. e-mail: cabraz@ufv.br.
Submitted on October 20, 2015; Final Acceptance on November 27, 2016; Discussion open until April 28, 2017.

in order to change the chemical form of heavy metals and thus extract them more easily from the soil through the decontamination process.

More recently, Lu *et al.* (2012) proposed a new way to increase the efficiency during the electrokinetic soil remediation using the technique named polarity exchange, which basically consists on inversion of electrodes polarities during the process. According to these authors, the technique is easily applied, does not require the addition of chemical elements, is dependent on the distribution of heavy metal in the soil mass, but it has been tested only for contaminated soils with a single contaminant; therefore new studies are needed for multiple contaminants. The results obtained showed that the inversion of polarities greatly increased the extraction of the heavy metals cadmium and chromium, preventing both the absorption of Cr^{6+} in acidic conditions and the precipitation of Cd^{2+} and Cr^{3+} in alkaline media.

On the other hand, it should be emphasized that the inversion of polarities may result in a highly acidic environment that can lead to the destruction of soil minerals. So, Lu *et al.* (2012) state that researchers have given little attention to adsorption and desorption of heavy metals during electrokinetic remediation and especially to the removal of metal dependency upon its physicochemical form and the chemical prevailing conditions during the remediation process. In order to determine the nature of a system studied in terms of chemical forms present and their relative mobility, it is recommended to use sequential extraction analysis before and after the process, which consists of a sequence of extractions to determine the form of the metal present in the soil.

From a historical perspective, Darmawan & Wada (2002) analyzed the effect of soil clay mineralogy on the feasibility of electrokinetic remediation using the following sequential extraction analysis: (i) water extractors, in order to determine the soluble fractions; (ii) magnesium chloride, to determine the electrostatically fraction weakly adsorbed; and (iii) hydrogen peroxide digestion, followed by hydrochloric acid, to determine the fractions strongly adsorbed or those who presented complexation with the soil minerals. Another sequential extraction methodology was employed by Reddy *et al.* (2001), which was developed by Tessier *et al.* (1979), in which the analysis was divided into five phases, namely: (i) soluble or exchangeable forms; (ii) carbonates linked forms; (iii) iron and manganese oxides linked forms; (iv) organic matter linked forms; and (v) residual fraction. With respect to both sequential extraction methods here presented, the first one is usual and more complicated when compared with the second one, however it does not separate the metal strongly adsorbed from the residual fraction; on the other hand the second form has more acceptance by researchers, such as Kim *et al.* (2002), Chen *et al.* (2006), Giannis *et al.* (2010) and Cameselle & Reddy (2012).

In contrast, the two sequential extraction methodologies presented are not generally applied to tropical soils, who frequently do not present significant amounts of manganese oxides and carbonates. In addition, the amount of iron and aluminum oxides present in these soils is very high and they are predominantly in crystalline form, whereas in temperate soils they occur in smaller quantities and in amorphous form. Therefore, considering the limitations of the reported sequential extraction methods, Egreja Filho (2000) developed at the Federal University of Viçosa (UFV), Brazil, a new methodology of sequential extraction comprising four steps in order to extract the elements present in the following forms in soil: (i) soluble metals; (ii) exchangeable or weakly absorbed metals; (iii) specifically adsorbed metals (*i.e.*, strongly adsorbed); and (iv) residual fraction metals.

This methodology comprises the following steps: (i) in the first extraction, distilled water acts only as an agent that washes the soil and removes the metals that are in the soluble form; (ii) in the second extraction, calcium chloride, which is a soluble salt that releases the cation Ca^{2+} in solution, is used to displace the other metals or chemicals, in particular cations, which may be linked only electrostatically on the soil surface (weakly adsorbed); (iii) in the third extraction, the fluoride and phosphate anions, which have a strong specific adsorption, are used to compete for adsorption sites and thus release the surface metals present in the soil minerals without dissolution of the oxide; and (iv) in the fourth stage, there is the determination of the residual fraction (*i.e.*, the one that is ingrained in the soil minerals) using digestion with nitric and perchloric acid, which are strong acids that create an opening, leaving only the silicates of the source material.

Therefore, taking into account that tropical soils have geotechnical properties, electrochemical parameters, and mineralogy that differ substantially from temperate soils, this research was directed to the analysis of the influence of the application of electric potential differences to two tropical young soils contaminated with cadmium nitrate using the modified sequential extraction technique proposed by Egreja Filho (2000).

2. Experimental Protocols

2.1. Geotechnical, mineralogical and chemical characterization of soils

Two gneiss residual soil samples were collected on the UFV Campus, located in the North Forest Zone, Minas Gerais state, Brazil, as follows: (i) soil sample A is a clayey silty sand collected in the C-horizon of a soil profile located at the geographic position coordinates 20°46'48.2" of South latitude and 42°52'52" of West longitude, and classified as Saprolite; and (ii) soil sample B is a sandy silty clay soil collected at the B-horizon of a soil profile located at the geographic position coordinates 20°45'23.5" of South latitude and 42°50'22.4" of West longitude, and pedologically classified as Red-Yellow Argisol. Tables 1, 2, 3, 4 and 5 summarize data from Velten *et al.* (2012), regarding, respectively, the geotechnical, mineralogical and chemical soil parameters.

2.2. The contaminant

A cadmium mono-species solution with concentration of 100 $mg.L^{-1}$ of salt was added to the soil samples in different volumes, according to their original moisture contents and considering the water amounts required to make them reach the cadmium concentration of 10 to 12 $mg.kg^{-1}$ of dry soil mass, which are the minimum guiding values that require intervention in agricultural or residential contaminated areas (Cetesb-SP, 2001). The cadmium salt used was cadmium nitrate tetra hydrated [$Cd(NO_3)_2.4H_2O$] 99% from Riedel-de Haën with the molecular weight of 308.48 g.

2.3. Electroosmotic cell

Figure 1 introduces the electroosmotic cell used in the study, originally designed and built by Damasceno (2003), and now including graphite in substitution for copper electrodes.

2.4. Decontamination tests

2.4.1. Samples preparation

The soil samples were air-dried and passed through the 4.8 mm sieve. Then, compaction tests were carried out on the AASHTO Standard compaction effort (ABNT, 1986) in order to determine the soils samples optimum water content (w_{opt}) and maximum dry unit weight (γ_{dmax}). During soil sample preparation, water and cadmium nitrate solution were added to the air-dried samples, in order to reach the optimum moisture content previously determined in the compaction tests, as well as the cadmium concentration of 10 to 12 $mg.kg^{-1}$ of dry soil. Later, using incubation

Table 1 - Geotechnical characterization of soils.

Geotechnical parameters	Brazilian Standards (ABNT)	Soil sample A	Soil sample B
Sand – 2 mm < $\phi \leq$ 0.06 mm (%)	NBR 7181	57	8
Silt – 0.06 mm < $\phi \leq$ 0.002 mm (%)	NBR 7181	30	40
Clay – $\phi \leq$ 0.002 mm (%)	NBR 7181	13	52
Liquid limit – w_L (%)	NBR 6459	31	81
Plastic limit – w_P (%)	NBR 7180	19	58
Plasticity index – $I_{P(\%)}$	-	12	23
Specific gravity of soil solids	NBR 6508	2.679	2.812
Optimumwater content – w_{opt} (%)	NBR 6457 and NBR 7182	20.23	33.68
Maximum dry unit weight – γ_{dmax} ($kN.m^{-3}$)	NBR 6457 and NBR 7182	15.57	12.87

Table 2 -
Soil classification by the Transportation Research Board - TRB and Unified Soil Classification - USC Systems (DNIT, 2006), and the Miniature Compacted Tropical - MCT Methodology (Nogami & Villibor, 1995).

Soil	Geotechnical classifications		
	TRB	USC	MCT
A	A-6 (2)	SC-SM	NS' (Non-lateritic behavior)
B	A-7-5 (17)	MH	NG' (Non-lateritic behavior)

Table 3 - Mineralogy of soils A and B - Qualitative results.

Soil fraction	Soil A	Soil B
Fraction ≥ 53 μm	Quartz, Kaolinite, Mica, HIV	Quartz, Kaolinite, Mica
Fraction < 53 μm	Kaolinite, Goethite, Hematite, HIV	Kaolinite, Goethite, Gibbsite, HIV

HIV: Hydroxy-interlayered vermiculite.

Table 4 - Chemical characterization of soil samples A and B, following the standard procedures proposed by Embrapa (1997).

Soil sample	Chemical parameters											
	pH in H_2O	Point of Zero Charge - PZC	P ($mg.dm^{-3}$)	K ($mg.dm^{-3}$)	Na ($mg.dm^{-3}$)	Ca^{2+} ($cmol_c.dm^{-3}$)	Mg^{2+} ($cmol_c.dm^{-3}$)	Al^{3+} ($cmol_c.dm^{-3}$)	H + Al ($cmol_c.dm^{-3}$)	SB ($cmol_c.dm^{-3}$)	CEC – t ($cmol_c.dm^{-3}$)	CEC – T ($cmol_c.dm^{-3}$)
A	5.75	3.73	0.9	2	0.0	0.00	0.05	0.45	1.9	0.06	0.51	1.96
B	5.81	6.00	2.2	8	0.0	0.00	1.11	0.00	0.6	1.13	1.13	1.73

SB: Sum of exchangeable bases; CEC (t): Cationic exchange capacity; CEC (T): Cationic exchange capacity in pH 7.0.

Table 5 - Chemical characterization of soils samples A and B, following the standard procedures proposed by Embrapa (1997).

Soil sample	Chemical parameters										
	V (%)	m (%)	SSI (%)	OMC ($dag.kg^{-1}$)	P-rem ($mg.L^{-1}$)	Zn ($mg.dm^{-3}$)	Fe ($mg.dm^{-3}$)	Mn ($mg.dm^{-3}$)	Cu ($mg.dm^{-3}$)	B ($mg.dm^{-3}$)	S ($mg.dm^{-3}$)
A	3.1	88.2	0.00	0.00	13.0	7.18	14.4	7.2	0.09	-	-
B	65.3	0.0	0.00	0.38	4.0	5.39	44.2	16.2	1.13	-	-

V: Base saturation index; m: Aluminum saturation index; SSI: Sodium saturation index; OMC: Organic carbon x 1.724 - Walkley-Black; P-rem: Reminiscent phosphorus.

times determined previously by Velten *et al.* (2012), the contaminated soil samples A and B were incubated, respectively, during 10 and 20 days in a temperature controlled chamber (20 °C ± 1 °C).

2.4.2. Test procedure

After soils samples incubation, a small fraction of each of the contaminated soil sample was taken to the UFV's Laboratory of Mineralogy of the Department of Soils in order to perform sequential extraction test (Egreja Filho, 2000) and pH determination. From each remaining contaminated soil sample, specimens were molded at the AASHTO Standard optimum compaction parameters (w_{opt} and γ_{dmax}) using Plexiglas cylinders to be tested in the electroosmotic cell. After placing each specimen in the electroosmotic cell, its anode and cathode were filled with distilled water up to the desired level.

Decontamination tests were carried out under controlled temperature (20 °C ± 1 °C) for a period of time of 216 h, using electric potential differences of 5, 15 and 30 V, allowing the electric current to vary throughout the test. Considering that the electrodes of the electroosmotic cell were 180 mm apart, electric gradients of 0.28, 0.83 and 1.67 $V.cm^{-1}$, respectively, were generated. During the decontamination tests, solutions were collected each 3 days from the anode and cathode reservoirs, in order to determine their cadmium concentrations using the Flame Atomic Absorption Spectrophotometry technique from the UFV' Soils Laboratory. Finally, at the end of the decontamination tests, soils specimens were taken from the cell and subdivided into five equally apart layers, in order to determine their cadmium concentrations.

2.5. Sequential extraction analyses

After performing the decontamination tests, the soils specimens were subdivided into five equal parts, which were identified and submitted to the sequential extraction analysis proposed by Egreja Filho (2000) using different extractors in each step, as well as higher extraction power as the process advanced. In this test, the extractor acted by changing the interaction between the heavy metal and the solid phase, promoting solubilization to be dosed by a convenient analytic method. The sequential extraction was carried out in four steps, as illustrated in Table 6 (Velten *et al.*, 2012).

3. Results and Discussion

3.1. Evaluation of electric potential difference effect in the electroosmotic conductivity coefficient

Table 7 presents the geotechnical parameters of the tested soils before and after performing the electroosmotic decontamination tests in order to evaluate the effect of the electric potential difference in the coefficient of electroosmotic conductivity.

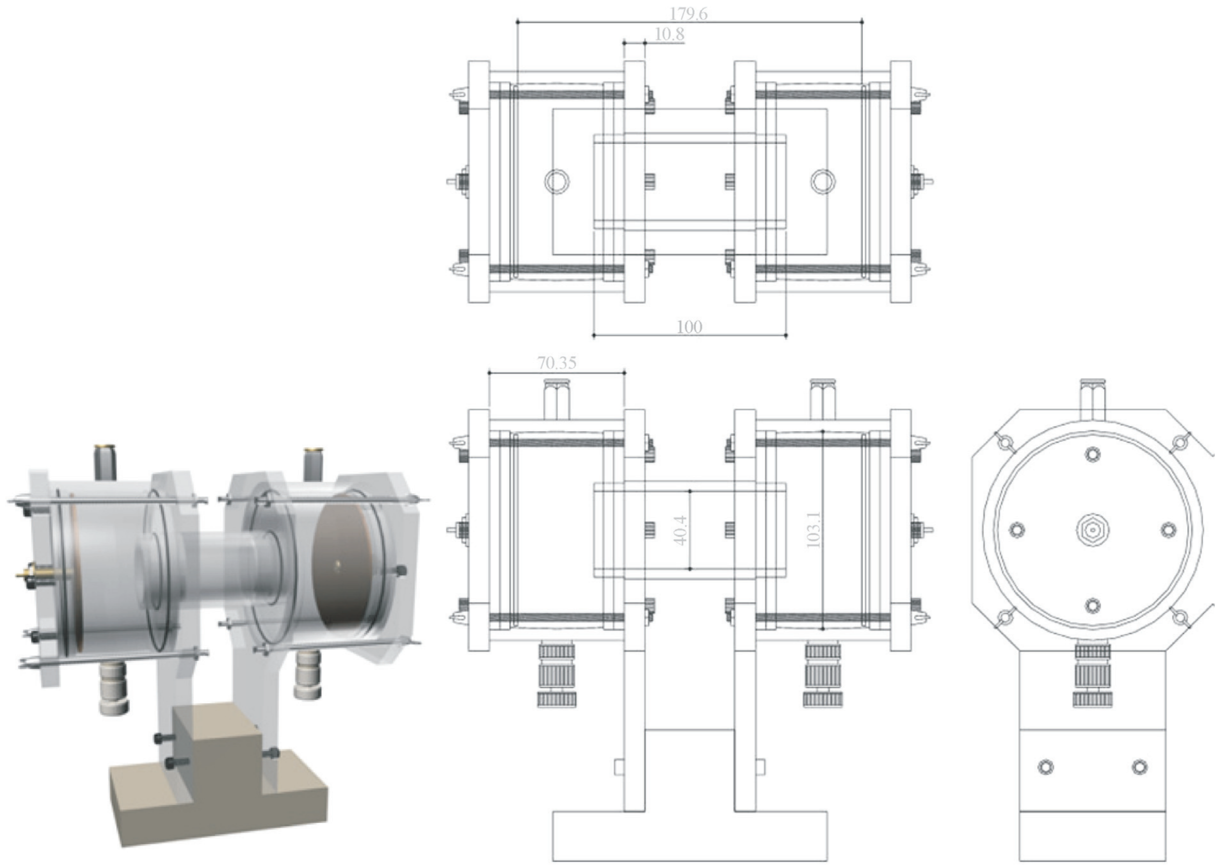

Figure 1 - Tridimensional view, layout, views and dimensions (in mm) of parts of the electroosmotic cell (Velten *et al.*, 2012).

Table 6 - Steps of the sequential extraction technique referring to the used extractor and to the determined chemical form.

Steps	Extractor	Determination
A	Distilled water	Soluble cadmium ion in the soil solution
B	0.1 $mol.L^{-1}$ of $CaCl_2$	Exchangeable cadmium ion (weakly absorbed)
C	Solution composed by 0.167 $mol.L^{-1}$ of Na_2HPO_4, 0.03 $mol.L^{-1}$ of NaF and 0.0083 $mol.L^{-1}$ of EDTA	Specifically absorbed cadmium ion (strongly adsorbed)
D	Nitric-perchloric digestion	Cadmium ion in the residual fraction

From the electroosmotic decontamination tests performed in the specimens of the tested soil samples, it was determined the coefficient of electroosmotic conductivity (k_e). During the tests, it was observed that the electric current decreased with time and the electroosmotic flow increased at the beginning of each test, tending to stabilize with time. In Table 7, it is also noticed that the coefficient of electroosmotic conductivity of soil sample A decreased slowly when increasing the applied electric potential difference, while in soil sample B this parameter increased slowly when increasing the applied electric potential difference. Results obtained by Chang & Liao (2006) using electric gradients of 2, 1 and 0.5 $V.cm^{-1}$ showed that the electroosmotic flow obtained at the electric gradient of 2 $V.cm^{-1}$ was two times and six times higher than those obtained at 1 and 0.5 $V.cm^{-1}$ respectively. However, independently of the applied electric gradient, in the present research the coefficient of electroosmotic conductivity showed values in the same order of magnitude, *i.e.* 10^{-6} $cm^2.s^{-1}.V^{-1}$.

3.2. Results from the electroosmotic decontamination tests

3.2.1. Cadmium concentration in the compartments and pH

Figures 2 and 3 present, respectively, the cadmium concentration in the anode and cathode compartments during decontamination tests and pH values determined before and after tests.

Table 7 - Results of geotechnical parameters of soils specimens submitted to the electroosmotic decontamination tests.

Soil sample	Electric potential difference applied (V)	Electroosmotic test duration (h)	w_o (%)	w_f (%)	Sr_o (%)	Sr_f (%)	k_{stable} ($cm^2.s^{-1}.V^{-1}$)
A	5	217.33	20.50	23.08	78.96	89.85	4.342×10^{-6}
	15	220.53	20.50	25.99	79.97	94.79	4.387×10^{-6}
	30	218.93	21.21	25.17	80.89	96.04	3.815×10^{-6}
B	5	216.67	33.68	39.35	85.62	96.13	2.060×10^{-6}
	15	223.25	36.51	44.47	99.79	100.00	2.791×10^{-6}
	30	216.78	36.51	41.39	86.43	95.39	2.992×10^{-6}

w_o - water content before test. w_f - water content after test. Sr_o - saturation degree before test. Sr_f - saturation degree after test. k_{stable} - coefficient of electroosmotic conductivity after flow stabilization.

It should be emphasized that during the decontamination tests, contrary to the behavior of soil sample A, soil sample B presented reverse electroosmotic flow direction, *i.e.*, from the cathode to the anode. In this case, the main explanation for the inversion in the direction of the electroosmotic flow can be related to the behavior of the electrochemical parameter PZC, in this case higher than the pH of the soil sample B, and in accordance with Cameselle & Reddy (2012) previous observation.

The results illustrated in Fig. 2 show that in soil sample A, a sandy soil with pH higher than its PZC, the cadmium concentration in both cell compartments decreased from 3 to 6 days, but increased again from 6 to 9 days, reaching values higher than those determined at 3 days. Regarding soil sample B, a clayey soil with pH smaller than its PZC, in Figure 3 it was observed that the cadmium concentration decreased with time in both cell compartments.

Besides, from Fig. 3 it was observed that the pH of soil samples A and B decreased from cathode to anode, in accordance with Yang & Lin (1998), and, in general, increased after application of the electroosmotic decontamination technique, independently of flow direction. Because of the induced electric potential in the tests, soil pH decreased close to the anode and increased close to the cathode, when H^+ ions created close to the anode compartment migrated to the cathode compartment (negative electrode) and OH^- generated close to the cathode migrated to the anode compartment (positive electrode). As a consequence, pH reached low values in the anode reservoir and high ones in the cathode and, according to Reddy *et al.* (2001), this pH difference distribution in the specimen created deep and different effects in the contaminant distribution and migration.

3.2.2. Sequential extraction data analysis

Figures 4 and 5 show the results of the sequential extraction analysis performed into the five vertical layers labeled 1 to 5 (2 cm long each) of the contaminated specimens taken before (named initial) and after performing the electroosmotic decontamination tests (named final). Regarding the tested soils and considering all cadmium extracted forms, these figures show that the behavior of the cadmium ion varied in the electroosmotic remediation process and with the applied electric potential difference. Analysis of the data presented in Figs. 4 and 5 support that:

- Soil sample A specimens: In general, from Fig. 4 it was noticed an increase in the amount of cadmium in the direction of the electroosmotic flow (anode to cathode) with the increase in the applied electric potential difference. The exception occurred for the electric potential difference of 5 V, because specifically adsorbed and residual cadmium fractions at the end of the decontamination process should not exist in the vicinity of the anode. At 5 V, it was observed that occurred accumulation of cadmium in sections close to the anode, resulting in low

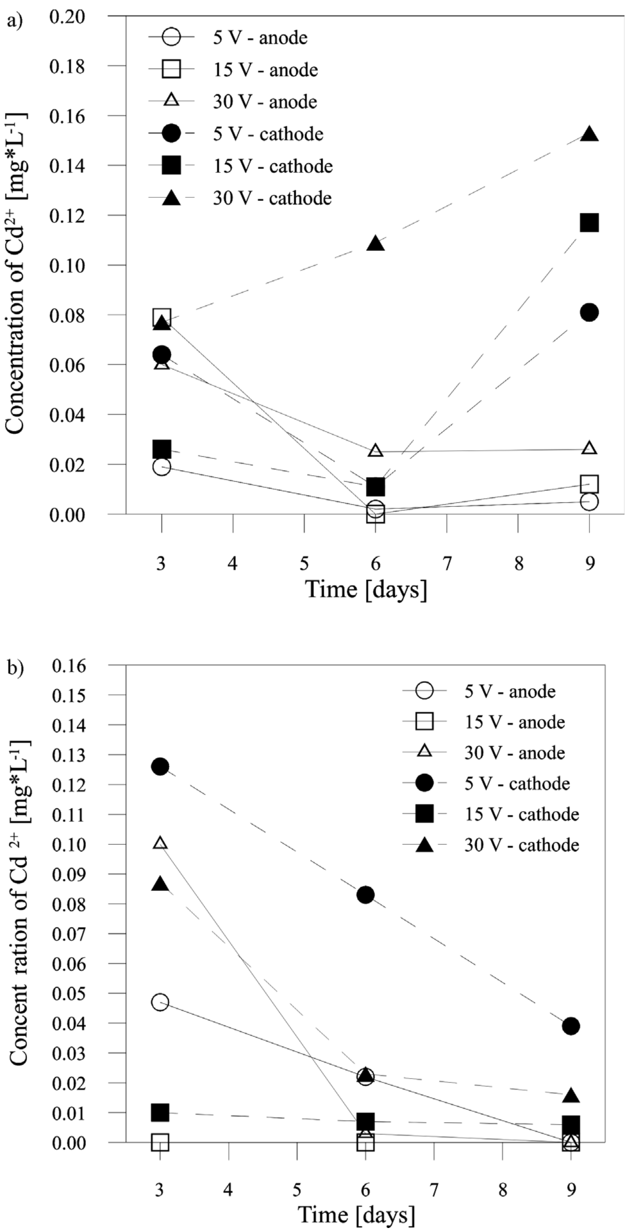

Figure 2 - Cadmium concentration in the anode and cathode compartments during decontamination tests: (a) soil sample A; and (b) soil sample B.

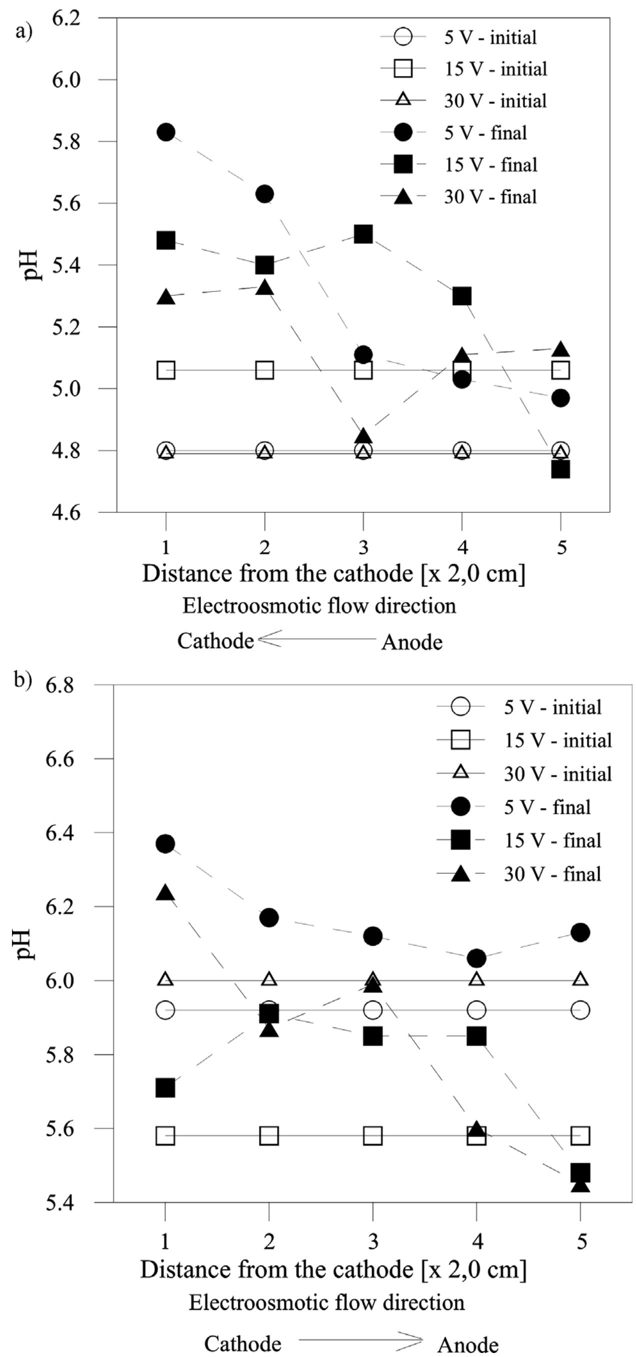

Figure 3 - pH values determined in the in the specimens before and after decontamination tests: (a) soil sample A; and (b) soil sample B.

contaminant removal from the soluble fraction. This behavior could be related to a possible accumulation of the metal in this fraction derived from other extractions that were not fully removed, as well as due to both the low intensity of the applied electric potential and the relatively short testing time. In all the contaminant forms in the soil A solid matrix, the contaminant migrated from the anode to the cathode, following the electroosmotic flow. In the vicinity of the cathode, an increase in the applied electric potential difference increased the concentration of cadmium ions, contrary to the behavior observed in the middle sections and in those close to the anode, which highlights the influence of the applied potential difference in removing the contaminant.

- Soil sample B specimens: As referred before, it was observed reversion of the electroosmotic flow direction, *i.e.* from cathode towards anode, as depicted in Fig. 5. In this case, the soluble fraction was barely detected, the electrostatically attracted fraction showed almost constant behavior in all sections of the specimen, and the cad-

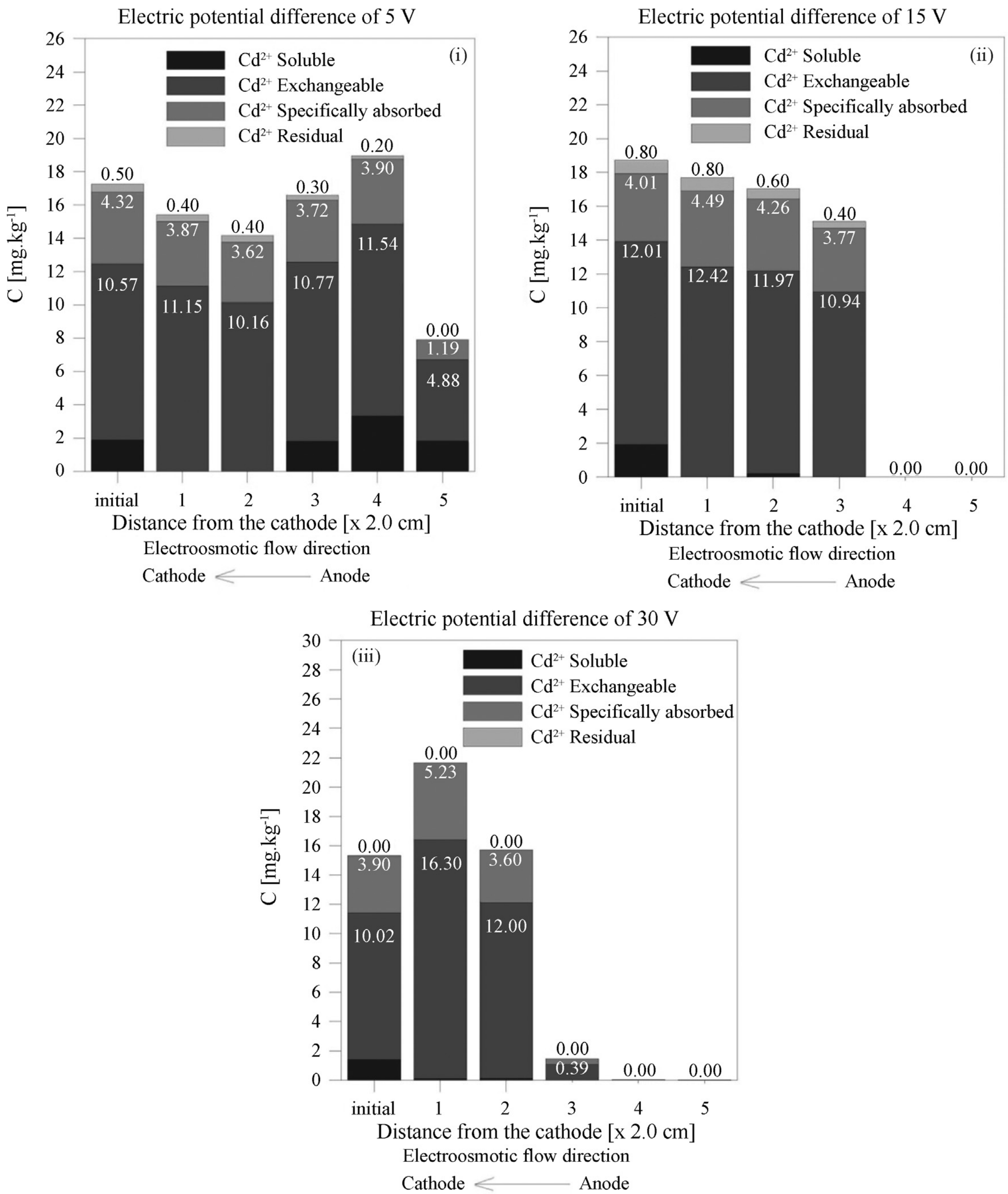

Figure 4 - Results from the sequential extraction analysis performed in the specimens from soil sample A before and after performing the electroosmotic decontamination tests: (i) incubation time of 10 days; (ii) application of the electric potential difference of 5, 15 and 30 V; and (iii) specimens divided into five vertical sections 2 cm long after the remediation tests.

mium concentration was higher than that determined by previous testing in some sections of the specimens, for 15 and 30 V. Regarding the strongly adsorbed and residual fractions, respectively, cadmium ion activity, respectively, increased and decreased in the vicinity of the cathode with the increase in the applied electric potential difference.

Table 8 shows the percentages of cadmium removed in each extraction phase in comparison with its initial value.

Data from this table support that:

- At the beginning of the decontamination process, each specimen slice presented the same cadmium concentration that could be represented by an area contained by a horizontal line in a figure that shows cadmium concentration in the ordinate axis (Y) and distance from the cathode in the abscissa axis (X). At the end of each phase of the sequential extraction analysis, the curve of cadmium concentration could be obtained from the amounts

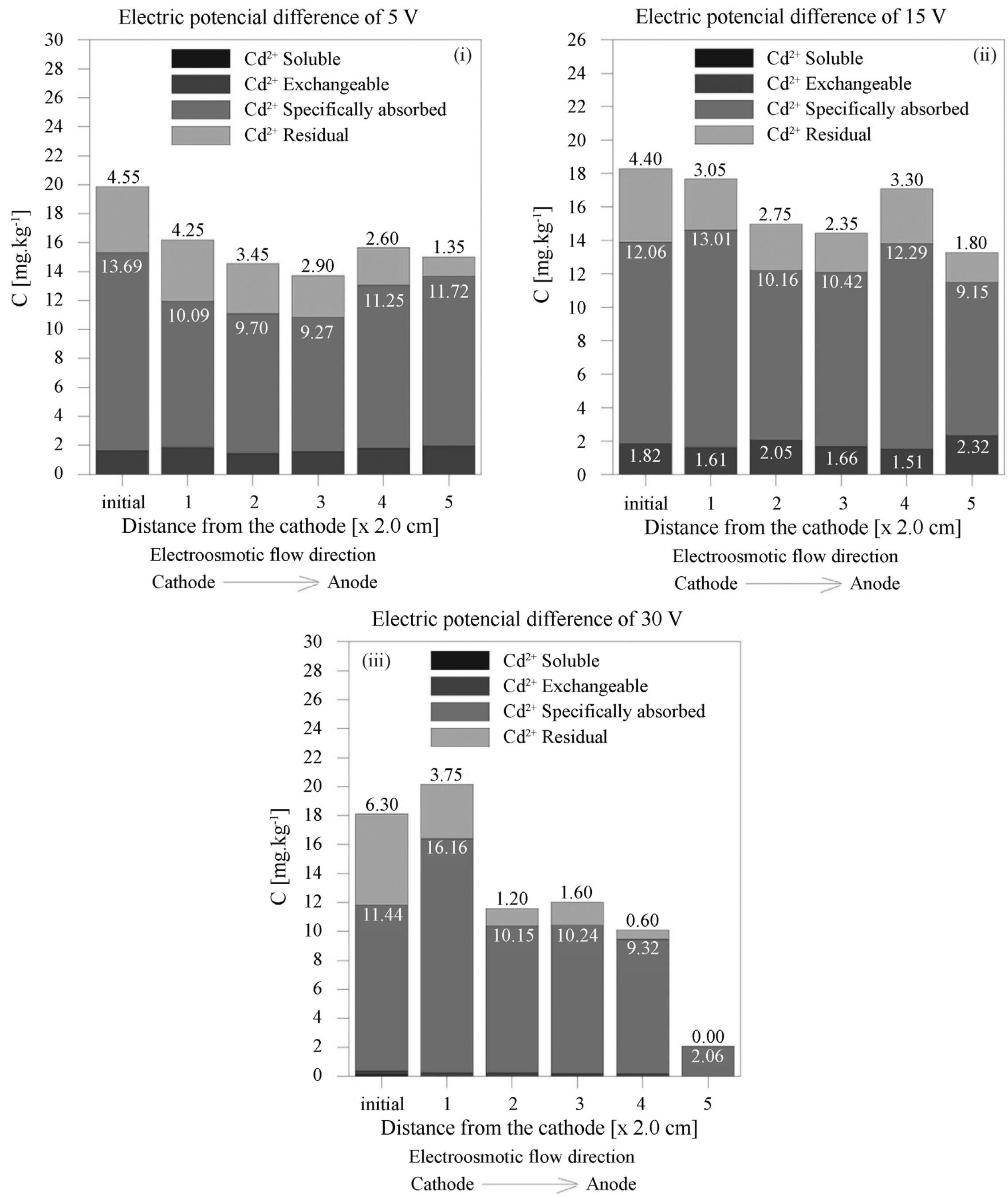

Figure 5 - Results from the sequential extraction analysis performed in the specimens from soil sample B before and after performing the electroosmotic decontamination tests: (i) incubation time of 20 days; (ii) application of the electric potential difference of 5, 15 and 30 V; and (iii) specimens divided into five vertical sections 2 cm long after the remediation tests.

of contaminant determined from each slice of the tested specimen. Therefore, from the comparison of these areas, it can be inferred the amount of cadmium extracted from the specimen during the electroosmotic decontamination test.

- Decontamination rates of soil samples A and B were strongly influenced by the applied electric potential difference, although the results obtained when applying 15 and 30 V to soil A specimens did not differ significantly when considering the soluble and exchangeable fractions. Therefore, application of an electric gradient of 0.50 V * cm^{-1} during the remediation process of soils similar to soil A contaminated with cadmium would be a fair estimate when there is no information available on theirs electroosmotic behavior, in agreement with Alshawabkeh *et al.* (1999) and Mitchell & Soga (2005).

Differences in the behavior of specimens from soil samples A and B during the decontamination tests could be

Table 8 - Percentage of cadmium removed from the analyzed soils by the electroosmotic process in each step of the sequential extraction.

Soil sample	Electric potential difference applied (V)	% of cadmium removed			
		Soluble	Exchangeable	Specifically absorbed	Residual
A	5	26.05	8.23	24.59	48.00
	15	97.92	41.16	37.54	55.00
	30	96.57	41.37	52.39	100.00
B	5	-	-5.66	24.02	36.04
	15	-	-0.48	8.76	39.77
	30	100.00	40.37	16.18	77.30

related to the differences in their mineralogy, in particular due to the large amount of iron oxides present in soil sample B, mainly in the form of goethite. The mobility of cadmium in this soil was greatest when applying 30 V, which was the test that presented final pH values generally smaller than the initial one, responding to the least amount of negative charges in the soil and, consequently, greater cadmium mobility. Therefore, the presence of goethite and other iron oxides such as hematite, and also oxides of aluminum, such as gibbsite, can influence considerably the phenomena of adsorption and removal of cadmium from the soils.

From Fig. 5, it was also noticed accumulation of cadmium in the residual fraction of specimens of soil sample B in the vicinity of the cathode, supporting that the strong acidification of the soil at the anode could be responsible for possible destruction of soil minerals in order to favor the removal of contaminants, as well as the strong alkalinization of the cathode may cause precipitation of contaminants in the form of insoluble salts or hydroxides, and may block the porous medium when pH reaches values near to 9.0.

Finally, it was observed in the tested soils that the application of electric potential difference of 30 V led to the highest cadmium decontamination rate.

4. Conclusions

The analysis of the results supports the following conclusions:

- The applied electric potential difference did not influence the value of the coefficient of electroosmotic conductivity of the tested soils, for engineering applications.
- The PZC of the tested soils influenced the cadmium direction migration. In soil A, the application of the electric potential differences generated cadmium migration in the electroosmotic flow direction. However, in soil B, the contaminant migrated in the anode-cathode direction, bringing up to attention the importance of the relationship between soil PZC and pH in the electroosmotic decontamination process.
- In general, the values of pH of all tested soils determined after decontamination tests were higher than those determined before, increasing from the anode to the cathode.
- The increase in the applied electric potential difference led to the increase in the amount of extractable contaminant.
- In soil B, the large presence of iron oxides in the form of goethite can be a preponderant factor in the removal of cadmium.
- In all decontamination tests, it was observed that cadmium in the residual fraction migrated from the anode towards the cathode, supporting that the strong acidification of the anode could have resulted in destruction of the constituents of the soil, thus facilitating the removal of chemical elements, as well as that alkalinization of the cathode, resulted in deposition and precipitation of the contaminant.

Acknowledgments

The authors thank the Brazilian National Council for Scientific and Technological Research (CNPq) for the financial resources invested in the development of this study (Grant No. 303143/2007-0), to CAPES for granting a master scholarship to the first author, and to the Departments of Civil Engineering and of Soils from the Federal University of Viçosa for supporting the development of this research.

References

ABNT (1984a). NBR 6508 - Grãos de solos que passam na peneira de 4,8 mm - Determinação da Massa Específica: Método de Ensaio. Rio de Janeiro, Brasil, 8 p.

ABNT (1984b). NBR 6459 - Solo - Determinação do limite de liquidez: método de ensaio. Rio de Janeiro, Brasil, 6 p.

ABNT (1984c). NBR 7180: Solo - Determinação do limite de plasticidade: método de ensaio. Rio de Janeiro, Brasil, 3 p.

ABNT (1984d). NBR 7181: Solo - Análise granulométrica: método de ensaio. Rio de Janeiro, Brasil, 13 p.

ABNT (1986a). NBR 6457: Amostras de solo - Preparação para ensaios de compactação e ensaios de caracterização: método de ensaio. Rio de Janeiro, Brasil, 9 p.

ABNT (1986). NBR 7182: Solo - Ensaio de compactação: método de ensaio. Rio de Janeiro, Brasil, 10 p.

Alshawabkeh, A.N.; Yeung, A.T. & Bricka, M.R. (1999). Practical aspects of in-situ electrokinetic extraction. Journal of Environmental Engineering, 125(1):27-35.

Boekhold, A.E.; Temminghoff, E.J.M. & van der Zee, S.E.A.T.M. (1993). Influence of electrolyte composition and pH on cadmium sorption by an acid sandy soil. Journal of Soil Science, 44(1):85-96.

Cameselle, C. & Reddy, K.R. (2012). Development and enhancement of electro-osmotic flow for the removal of contaminants from soils. Electrochimica Acta, 86:10-22.

Cetesb-SP (2001). Relatório de Estabelecimento de Valores Orientadores para Solos e Águas Subterrâneas no Estado de São Paulo. Companhia Ambiental do Estado de São Paulo, São Paulo, 232 p.

Chang, J-H. & Liao, Y-C. (2006). The effect of critical operational parameters on the circulation-enhanced electrokinetics. Journal of Hazardous Materials, 129(1-3):186-193.

Chen, X.; Shen, Z.; Lei, Y.; Ju, B. & Wang, W. (2006). Enhanced electrokinetic remediation of Cd and Pb-spiked soil coupled with cation exchange membrane. Aust. J. Soil Res., 44(5):523-529.

Christensen, T.H. (1989). Cadmium soil sorption at low concentrations: VIII. Correlation with soil parameters. Water Air, Soil Poll., 44(1):71-82.

Damasceno, V.M. (2003). Condutividade Eletrosmótica e Descontaminação de um Solo de Comportamento Laterítico da Zona da Mata Norte de Minas Gerais, Via Fenômenos Eletrocinéticos. Dissertação de Mestrado, Universidade Federal de Viçosa, 81 p.

Darmawan, S. & Wada, S.I. (2002). Effect of Clay Mineralogy on the Feasibility of Electrokinetic Soil Decontamination Technology. Elsevier Applied Clay Science, 20(6):283-293.

DNIT (2006). Manual de pavimentação. 3rd ed. IPR – Publicação 719, Departamento de Infraestrutura de Transportes, Rio de Janeiro, Brazil, 320 p.

Egreja Filho, F.B. (2000). Extração Sequencial de Metais Pesados em Solos Altamente Intemperizados: Utilização de Componentes – Modelo e Planejamento com Misturas Ternárias na Otimização do Método. Tese de Doutorado, Universidade Federal de Viçosa, 287 p.

Embrapa (1997). Manual de Métodos de Análises de Solos. Empresa Brasileira de Pesquisa Agropecuária, Rio de Janeiro, p. 212.

Giannis, A.; Pentari, D.; Wang, J.-Y. & Gidarakos, E. (2010). Application of sequential extraction analysis to electrokinetic remediation of cadmium, nickel and zinc from contaminated soils. Journal of Hazardous Materials, 184(1-3):547-554.

Giradakos, E. & Giannis, A. (2006). Chelate agents enhanced electrokinetic remediation for removal cadmium and zinc by conditioning catholyte pH. Water Air Soil Poll. 172(1):295-312.

Kim, S.; Kim, K. & Stuben, D. (2002). Evaluation of electrokinetic removal of heavy metals from tailing soils. Journal of Environmental Engineering, 128(8):705-715.

Kim, W.-S.; Kim, S.-O. & Kim, K.-W. (2005). Enhanced electrokinetic extraction of heavy metals from soils assisted by ion exchange membranes. Journal of Hazardous Materials, 118(1-3):93-102.

Lee, H.-H. & Yang, J.-W. (2000). A new method to control electrolytes pH by circulation system in electrokinetic soil remediation. Journal of Hazardous Materials, 77(1-3):227-240.

Lestan, D.; Luo, C.L. & Li, X.D. (2008). The use of chelating agents in the remediation of metal-contaminated soils, a review. Environmental Pollution, 153(1):3-13.

Lu, P.; Feng. Q.; Meng. Q. & Yuan, T. (2012). Electrokinetic remediation of chromium and cadmium contaminated soil from abandoned industrial site. Separation and Purification Technology 98(2012):216-220.

Mitchell, J.K. & Soga, S. (2005). Fundamentals of Soil Behavior. John Wiley & Sons, Inc., New York, 3rd ed., 558 p.

Naidu, R.; Bolan, N.S.; Kookana, R.S. & Tiller, K.G. (1994). Ionic-strength and pH effects on the sorption of cadmium and the surface charge of soils, Eur. J. Soil Sci., 45(4):419-429.

Nogami, J.S. & Villibor, D.F. (1995). Pavimentação de Baixo Custo com Solos Lateríticos. Ed. Villibor, São Paulo, 213 p.

Pierangeli, M.A.; Guilherme, L.R.G.; Curi, N.; Silva, M.L.N.; Lima, J.M. & Costa, E.T.S. (2005). Efeito do pH na adsorção e dessorção de cádmio em latossolos brasileiros. Revista Brasileira de Ciência do Solo, 29(4):523-532.

Pombo, L.C.A. (1995). Adsorção de cádmio em solos do Estado do Rio Grande do Sul. Revista Brasileira de Ciência do Solo, 19:19-24.

Reddy, K.R. & Chinthamreddy, S. (2003). Sequentially enhanced electrokinetic remediation of heavy metals in low buffering clayey soils. Journal of Geotechnical and Geoenvironmental Engineering, ASCE, 129(3):263-277.

Reddy, K.R.; Xu, C.Y. & Chinthamreddy, S. (2001). Assessment of electrokinetic removal of heavy metals from soils by sequential extraction analysis. Journal of Hazardous Materials, 84(2-3):279-296.

Rojo, A.; Hansen, H.K. & Monàrdez. O. (2014) Electrokinetic remediation of mine tailings by applying a pulsed variable electric field. Minerals Engineering, 55(2014):52-56.

Tessier, A.; Campbell, P.G.C. & Bisson, M. (1979). Sequential extraction procedure for the speciation of particulate trace metals. Anal. Chem., 51(7):844-851.

Thomé, A.; Korf, E.P.; Tímbola, R.S. & Consoli, N.C. (2013). Cadmium transport parameters in a clayey residual soil with different values of contaminant pH. Soil & Rocks, 36(3):311-316.

Yang, G.C.C. & Lin, S-L. (1998). Removal of lead from a silt loam soil by electrokinetic remediation. Journal of Hazardous Materials, 58(1):285-299.

Velten, R.Z.; Lima, D.C.; Fontes, M.P.F. & Carvalho, C.A.B. (2012). Electroosmosis in the remediation of tropical soils contaminated with cadmium: effect of the incubation time. Soils & Rocks, 35(1):39-49.

List of Symbols

AASHTO – American Association of State Highway and Transportation Officials
ABNT - Brazilian Technical Standards Association
CEC (t) - Cationic Exchange Capacity
CEC (T) - Cationic Exchange Capacity in pH 7.0
I_P - plasticity index
k_{stable} - electroosmotic conductivity coefficient after water flow stabilization
m - Aluminum Saturation Index
MCT - Miniature Compacted Tropical
OMC - Organic matter content, by Walkley-Black (OMC = Organic Carbon x k, where k = 1.724)
P-rem - Reminiscent Phosphorus
PZC - Point of Zero Charge
SB - Sum of Exchangeable Bases
Sr_o - initial degree of saturation
Sr_f - final degree of saturation
SSI - Sodium Saturation Index
TRB - Transportation Research Board
USC - Unified Soil Classification
V - Base Saturation Index
w_L - liquid limit
w_f - final moisture content
w_{opt} - optimum water content
w_P - plastic limit
w_o - initial moisture content
γ_{dmax} - maximum dry unit weight
ρ_s - density of solid particles

Use of Parallel-Seismic and Induction-Logging Tests for Foundation Depth Evaluation Under Difficult Conditions, a Root-Pile Foundation Embedded in Rock

T.J. Souza, P.S. Hemsi, O.C.B. Gandolfo, P.C. Aoki, A.F. Ribeiro

Abstract. A case study on the application of the parallel-seismic (PS) and induction-logging (IL) tests combined to evaluate the depth of a 25-cm diameter root-pile belonging to the foundations of a telecommunication tower located in Santana de Parnaíba, São Paulo, Brazil, is presented. The foundation element is embedded in a friable and altered meta-sandstone rock. The relatively small diameter of the pile and the presence of rock as surrounding material tend to limit the interpretation of the PS test. Nevertheless, the technique applied in this study showed satisfactory results. On the other hand, the existence of electromagnetic interference from the antenna itself limited the interpretation of the IL test in this case. The estimated depth of the foundation element was evaluated from the PS test as ranging from 6.5 to 7.5 m, which was later verified to be in agreement with the pile as-built documentation. When the possibility to drill boreholes at a site under investigation exists, the methods presented in this paper may become good options for the determination of the unknown depth of foundation elements in altered rock.
Keywords: foundations, induction logging test, meta-sandstone, parallel seismic test, telecommunication tower.

1. Introduction

The need for determining the unknown depth of existing foundation elements arises whenever a project requires the use of existing foundations under new loadings and design documentation is scarce or unavailable. The most common situation occurs when the retrofit and new use of a structure causes changes in the loads acting on the foundation, so that verifications need to be carried out. The stratigraphic profile, foundation type, dimensions and constructive method, as well as the depth of each of the foundation elements, are required as input information for bearing-capacity and settlements analyses traditional in foundation engineering practice.

With respect to foundations of telecommunication towers, such a situation occurs often as, due to cost optimization, additional or heavier and more robust antenna elements are frequently placed and installed on existing towers. Also, in this type of structures, some of the foundation elements are commonly subjected not to compression but to tension, as a result of the horizontal forces arising from wind action on the tower structure.

When foundations are shallow, direct methods for unveiling the foundations geometry and depth are likely viable. However, in the case of deep foundations, the use of an indirect method is required. To achieve this goal, various destructive and nondestructive tests have been developed.

Nondestructive tests based on geophysics methods have a high application potential, are damage-free, cost-effective and time-saving. Thus, they can be extended to a large population of tested elements reducing uncertainty at a given site. Most of the tests can be classified as either reflection or direct-transmission methods. Reflection methods are in general faster and more cost-effective, whereas direct-transmission methods allow better results for deeper elements.

An example of a non-destructive reflection method, the low deformation integrity testing methodology, commonly known as Pile Integrity Testing, or PIT (also known as sonic echo / impulse response test), has recently been used in Brazil for evaluating the depth of existing piles and caissons belonging to the foundations of telecommunication towers (Souza *et al.*, 2015). In the low deformation integrity testing, an impulse hammer generates a compressional wave (P-wave) which travels down the element until a change in acoustic impedance is encountered causing the wave to be reflected back and detected by a receiver placed next to the impact point, where the signal is recorded. The reflection of the wave occurs at the bottom of the tested element or at a depth corresponding to a discontinuity, such as a crack along the shaft. Based on the returning wave signal, the element depth, as well as the presence and location of a crack, may be determined since the velocity of an elastic

Tiago de Jesus Souza, American Tower do Brasil, Rua Olimpíadas 205, 04551-000 São Paulo, SP, Brazil. e-mail: tiago.souza@americantower.com.
Paulo Scarano Hemsi, Instituto Tecnológico de Aeronáutica, Praça Mal. Eduardo Gomes 50, 12228-900 São José dos Campos, SP, Brazil. e-mail: paulosh@ita.br.
Otávio Coaracy Brasil Gandolfo, Instituto de Pesquisas Tecnológicas de São Paulo, Av. Prof. Almeida Prado 532, Cidade Universitária, 05508-901 São Paulo, SP, Brazil. e-mail: gandolfo@ipt.br.
Paulo Cezar Aoki, American Tower do Brasil, Rua Olimpíadas 205, 04551-000 São Paulo, SP, Brazil. e-mail: paulo.aoki@americantower.com.
Alex Fortunato Ribeiro, Instituto de Astronomia, Geofísica e Ciências Atmosféricas, Universidade de São Paulo, Rua do Matão 1226, Cidade Universitária, 05508-090 São Paulo, SP, Brazil. e-mail: alex.fortunato@iag.usp.br.
Submitted on November 13, 2015; Final Acceptance on November 27, 2016; Discussion open until April 28, 2017.

wave travelling along a pile can be estimated. However, in the case of deep foundations partly embedded in rock, the low deformation integrity test has been reported to become erratic and difficult to interpret, restricting the applicability of this method (Cunha & Costa, 1998; Cunha *et al.*, 2002; Foá *et al.*, 2000).

The non-destructive direct-transmission geophysical methods rely on the use of one or more external boreholes drilled in the vicinity of the foundation element to be tested, and are, in general, capable of providing superior results in terms of the determination of the depth of longer foundation elements. Examples of tests include the borehole-based ground penetration radar, cross-hole sonic logging, the parallel seismic test and the induction logging test. The parallel seismic test has been used for determining the unknown depth of foundation elements for bridges and other structures in the USA for many years (Davis, 1995). On the other hand, the induction logging test has mostly been applied for subsurface mapping at environmentally-contaminated sites. Recently, an application of the PS test in the metropolitan area of São Paulo, Brazil, for evaluating the depth of a 230-cm diameter caisson without an enlarged base in a clayey-sandy silt provided good results when the obtained depth was compared to the depth depicted in the caissons documentation (Gandolfo *et al.*, 2015).

When the pile has a relatively small diameter (such as a root-pile) and the surrounding material is stiffer than soil, such as altered rock, the applicability of the PS test, which depends on the contrast in stiffness between the pile and surrounding material, may be limited. Additionally, when significant electromagnetic interference occurs at the site, the data obtained in the IL test may be of difficult interpretation.

This paper presents the results of an application of the parallel seismic and induction logging tests to determine the depth of a root-pile that is embedded in friable meta-sandstone. When the foundation element is partly embedded in rock, the methods chosen for this study become more appropriate than the low deformation integrity test, even though these methods are generally more expensive than the non-destructive reflection method.

2. Theoretical Background

As opposed to surface-based geophysics methods, borehole and logging tests are based on the use of drilled boreholes, in which probes (or sondes) and sensors are lowered to obtain data on geologic materials in depth and identify interfaces of different geophysical signatures (Ellis & Singer, 2008). In general, geophysical profiling is carried out in open wells, where different types of probes can be used, such as electrical, acoustic, or caliper (for measuring well diameter). When the borehole is cased, such as a polyvinyl chloride (PVC) casing, only probes based on electromagnetic induction and on the physical property of natural gamma radiation, or the parallel seismic test can be used.

2.1. Parallel seismic testing

The parallel seismic (PS) test is a geophysical technique developed in France several decades ago for the determination of the unknown depth of foundation elements, which has a methodology similar to that of the downhole test. Also, studies have been conducted to develop the PS test for evaluation of pile integrity (Liao *et al.*, 2006; Huang & Chen, 2007; de Groot, 2014). Practical advantages of the PS test are the applicability of the test for different foundation materials (*e.g.*, concrete, steel, wood and masonry) and the possibility of testing even when the pile head is not accessible.

The principle of the PS test is that a pulse is generated by the impact of a small hammer, equipped with a trigger switch, hitting against an exposed part of the structure connected to the foundation, or on the exposed top of the foundation element, if accessible. Elastic waves, predominantly of the compressional type (P-waves), are produced and propagate through the vertical element. If desired, shear waves (S-waves) may also be produced by laterally impacting the opposite sides of the block connected to the foundation.

Due to the great contrast between the elastic modulus of the foundation element (generally consisting of a reinforced-concrete element) and the surrounding soil materials, the P-waves are refracted and are detected by receivers such as three-component geophones or hydrophones placed within an encased borehole near the foundation element. The waves arriving at the geophones are recorded on a seismograph at regular intervals. The working principle of the PS test is illustrated in Fig. 1.

The preparation of the borehole to be used in the PS test should follow the guidance for the crosshole and downhole testings (ASTM D4428 and ASTM D7400). The vertical borehole must be drilled less than 1.5 m from one edge, and be encased with a PVC casing capped at the bottom. The annular space between the casing and the borehole wall must be grouted with cement to ensure good contact with the surrounding soil. In terms of depth, the borehole must be drilled to a depth that exceeds the expected foundation depth by at least 3 to 5 m. When using geophones, the casing must be kept dry, whereas when using hydrophones, the casing must be filled with water prior to testing. Also, another important consideration is to ensure the borehole verticality.

The PS measurements are usually recorded using a sequence of geophones vertically spaced along depth at 0.5- to 1.0-m regular intervals. A seismograph is used to record the signal, or seismic trace, from each geophone position. The time of first arrival of the P-wave at a geophone is obtained as the first break observed in the seismic trace (Fig. 2). Thus, the travel time of the wave from the source (*i.e.*, the point of impact of the hammer) to the corresponding geophone can be calculated. The set of all seismic traces results in a seismogram. Connecting the first-arrival points

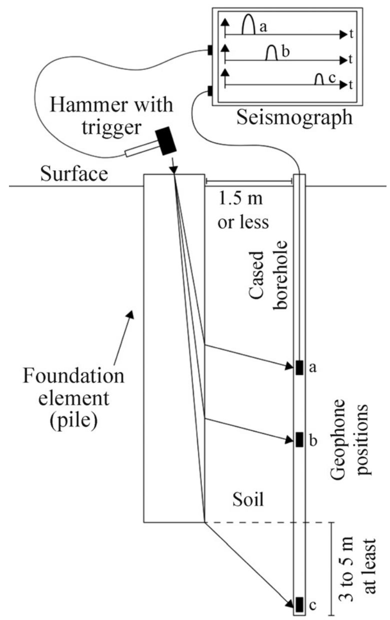

Figure 1 - Illustration of the working principle of the Parallel Seismic test (Niederleithinger, 2012).

for all geophones allows the fitting of two straight lines; the point of intersection of the two adjusted lines (the inflection point) corresponds to the interpreted depth of the foundation element. The slope of the top line provides an indication of the wave propagation velocity within the foundation element, whereas the slope of the bottom line indicates the velocity within the surrounding soil. Usually, the top line is steeper than the bottom line, due to the greater wave velocity in the more rigid material that constitutes the foundation element than in the soil. However, when the pile has a relatively small diameter and the surrounding material has a high modulus, the distinct pattern in Fig. 2 is not observed. In this case, the depth of the foundation element may still be determined by observing the depth at which there is a significant drop in signal amplitude (energy) of the traces, and diffraction of the wave energy (both occurring below the bottom of the foundation), as previously reported by Sack & Olson (2010).

2.2. Induction logging testing

Broadly, induction logging (IL) testings are based on Faradays laws of Electromagnetism whereby a transmitter

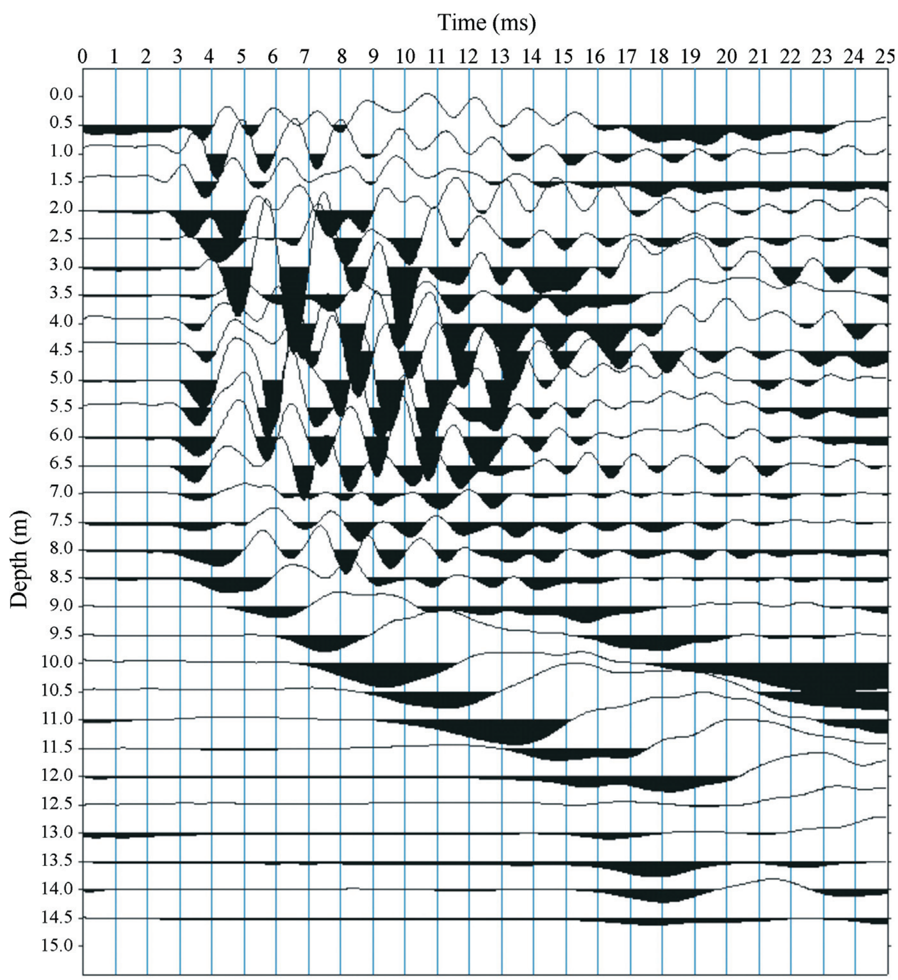

Figure 2 - Example of a seismogram for an array of various geophones installed at 0.5-m intervals in a PS test (Gandolfo *et al.* 2015).

coil inside a probe is energized with an alternating electric current at the audio frequency, originating a primary variable magnetic field which induces alternate-current flow in the vicinity, *i.e.*, in the surrounding conductive geologic materials, that, in turn, induce an electric potential (and secondary magnetic field) in one or more receptor coils placed also in the probe (Fig. 3).

Tests with Electromagnetic Induction measures are widely used to map groundwater contamination plumes, for groundwater exploration, and for general geological mapping. Surface inductive surveys for measuring layer conductivities are used to detect conductive features such as buried metal objects, ore bodies, and fluid-filled fractures, and to map conductive plumes of inorganic chemicals, such as landfill leachate, or saltwater intrusion (McNeill, 1980; Mondelli, 2008).

Induction Logging for measuring conductivity of the formation around the borehole can be used to identify the placement of screening in ground-water monitoring wells, monitor contamination levels outside of cased wells, and detect or monitor contamination plumes in the vadose zone. The use of two or more receiver coils allows the investigation at different radii from the well center.

The IL sonde operates at low values of induction number, as defined by McNeill (1980). Thus, the ratio of the secondary to the primary magnetic fields, or the intensity of the electric potential measured in the receiver coil, is assumed to be linearly proportional to the bulk apparent terrain electrical conductivity, such as (Doll, 1949; Moran & Kunz, 1962):

$$\sigma_a = \frac{4}{\omega \mu_0 s^2} \left(\frac{H_s}{H_p} \right) \tag{1}$$

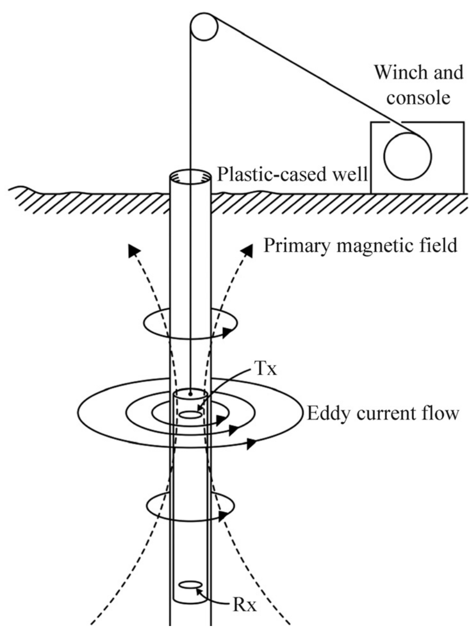

Figure 3 - Illustration of the working principle of the Induction Logging (McNeill, 1990).

where σ_a is the bulk apparent subsurface electrical conductivity (which has usually units of mS m^{-1}), ω is equal to $2\pi f$, where f is the frequency, μ_0 is the magnetic permeability in the vacuum, s is the intercoil spacing, and H_s and H_p are, respectively, the secondary and primary magnetic fields measured at the receiver coil. Equation 1 represents the conductivity in the isotropic, homogeneous semi-space. The apparent conductivity measured in a well can be found in McNeill (1990).

For some probes, the linear relationship is not valid when the media present high electric resistivity, *i.e.*, greater than 100 ohm-m (Scott *et al.*, 1986), and a non-linearity is observed between the electric potential and the conductivity of the medium.

Besides the electric conductivity, the induction probe is equipped with sensors that can record the logging of natural gamma ray in the surrounding formation, *i.e.*, the concentration in counts per second (CPS) of natural gamma ray emitting radioisotopes from the uranium (U) and thorium (Th) decay series, and potassium (K)-40. These radioisotopes tend to be more abundant in clays as a result of potassium-rich feldspar and mica decomposition, and of uranium and thorium concentrations in the clay due to adsorption and ion exchange. Gamma-emitting radioisotopes of anthropogenic origin cannot be differentiated from naturally occurring isotopes in natural-gamma ray logging. Variations in the gamma log are used to indicate lithologic changes in the formation surrounding a borehole, *i.e.*, the presence of clayey materials (Keys, 1989, Luthi, 2001).

More innovative than the aforementioned applications, is the use of the IL test to determine the depth of a steel or continuously-reinforced concrete foundation element based on the contrast between the magnetic field strength recorded along the element, and that occurring below the tip of the foundation element, *i.e.*, representative of the geologic material.

3. Materials and Methods

3.1. Site description

The PS and IL tests were performed at a telecommunication-tower site located in Santana de Parnaíba, São Paulo, Brazil (Fig. 4). Figure 4a shows a lateral view of the three-legged tower structure, and Fig. 4b depicts a plan-view schematic of the location of the tower in reference to the site.

A vertical borehole to be used for the PS and IL tests was drilled at the site at the position marked in Fig. 4b, 1.1 m apart from the foundation block. The borehole was drilled to a depth of 11.0 m, exceeding by 3 to 5 m the expected foundation depth. The borehole was encased with an 85-mm internal-diameter PVC tube, closed at the bottom, and the annular space was totally filled with cement grout.

The stratigraphic profile at the location of the borehole is depicted in Table 1, and includes a superficial 2.0-m

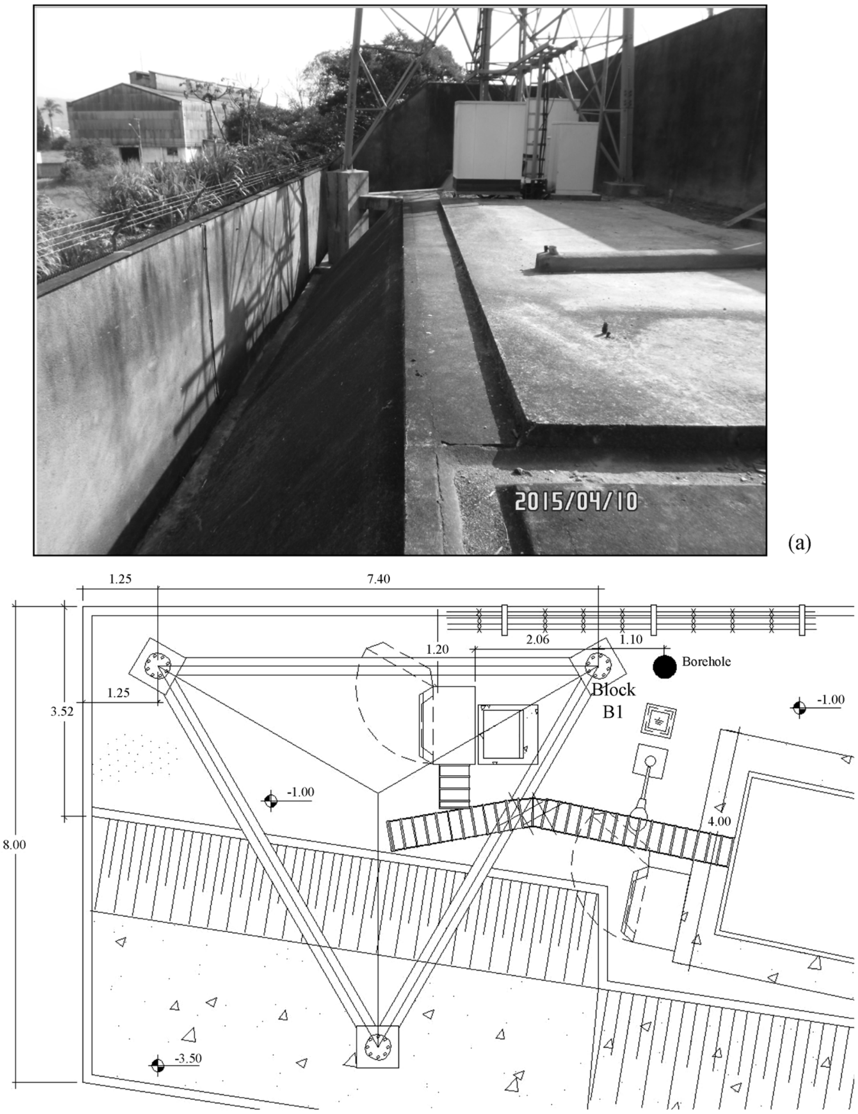

Figure 4 - Santana de Parnaíba site: (a) lateral view of the telecommunication tower at the testing site, and (b) plan-view location schematic.

Table 1 - Stratigraphic profile at the location of the borehole drilled at the site (SM-02).

SM-02			Elevation: 99.75 m		
Date: 06-August-2014					
Water table (m)	Layer depth (m)	Sample	Recovery (%)	RQD (%)	Classification
Not found	2	0	-	-	Sandy-silt Fill
		1			
	4	2	5	0	Meta-sandstone, sedimentary rock, cream color, friable (C4), significantly altered (A4), fragmented (F5), São Roque Group.
		3			
	6	4	5	0	
		5			
	8	6	4	0	
		7			
	10	8	7	0	
		9			
	12	10	7	0	
		11			

thick fill layer consisting of a brown sandy silt followed by a layer (2.0 to 11.0 m) of an altered meta-sandstone belonging to the São Roque Group, light brown in color, friable (C4), very altered (A4) and fragmented (F5). The local water table was not encountered above the depth of 11.0 m.

Each tower leg was supported by a block with four piles. The piles consisted of so-called root-piles, or micropiles, which were circular in cross-section, with 25-cm nominal diameter, and molded in-situ (Fig. 5). The constructive method involved drilling a cylindrical hole through the fill and meta-sandstone layers using high pressure hydraulics or pneumatics, inserting a reinforcing steel member, and injecting cement grout from the bottom up. Micropiles have mainly been used as foundation elements, as well as for the reinforcement of slopes and existing foundations. The foundation element tested belonged to foundation block "B1", so that the distance between the borehole and the element tested was 1.1 m (Fig. 4b).

3.2. Field tests

3.2.1. Parallel seismic testing

The following equipment was utilized for performing the PS test at the site (Fig. 6): a 12-channel seismograph (SmartSeis, Geometrics), a 1.8-kg sledgehammer with a trigger switch, and a set of 21 triaxial 8-Hz borehole geophones with a pneumatic clamping mechanism. A schematic of a geophone and the clamping mechanism is provided in Fig. 7.

The exposed top of foundation block "B1" was impacted vertically by the hammer, to generate a P-wave (Fig. 8). Also, in order to acquire S-waves, the structure was hit horizontally with the hammer, against two opposite sides of the block, a typical procedure to generate waves with opposite polarities. The seismic traces were recorded at regular 0.5-m intervals, from near the bottom of the borehole, at a depth of 10.5 m, to near the surface level, at a depth of 0.5 m.

3.2.2. Induction logging testing

The equipment utilized for performing the IL test consisted of a dual spaced induction sonde, model DUN 10290, made by Robertson Geologging (UK), connected to a register Micrologger II that was managed by the Winlogger 1.5 software, a mini winch provided with a 150-m long cable, and a tripod with encoder velocity transducer, as illustrated in Fig. 9.

The IL sonde utilized had a length of 225 cm, and contained two pairs of transmitting and receiving coils, the transmitting coil located 47 cm from the tip of the probe, and the receiving coil located 80 cm from the tip. The gamma-radiation sensor was located at a distance of 35 cm measured from the top of the sonde and contained a scintillation meter made of sodium iodide crystal. When the crystal is exposed to gamma rays, photons are emitted, which

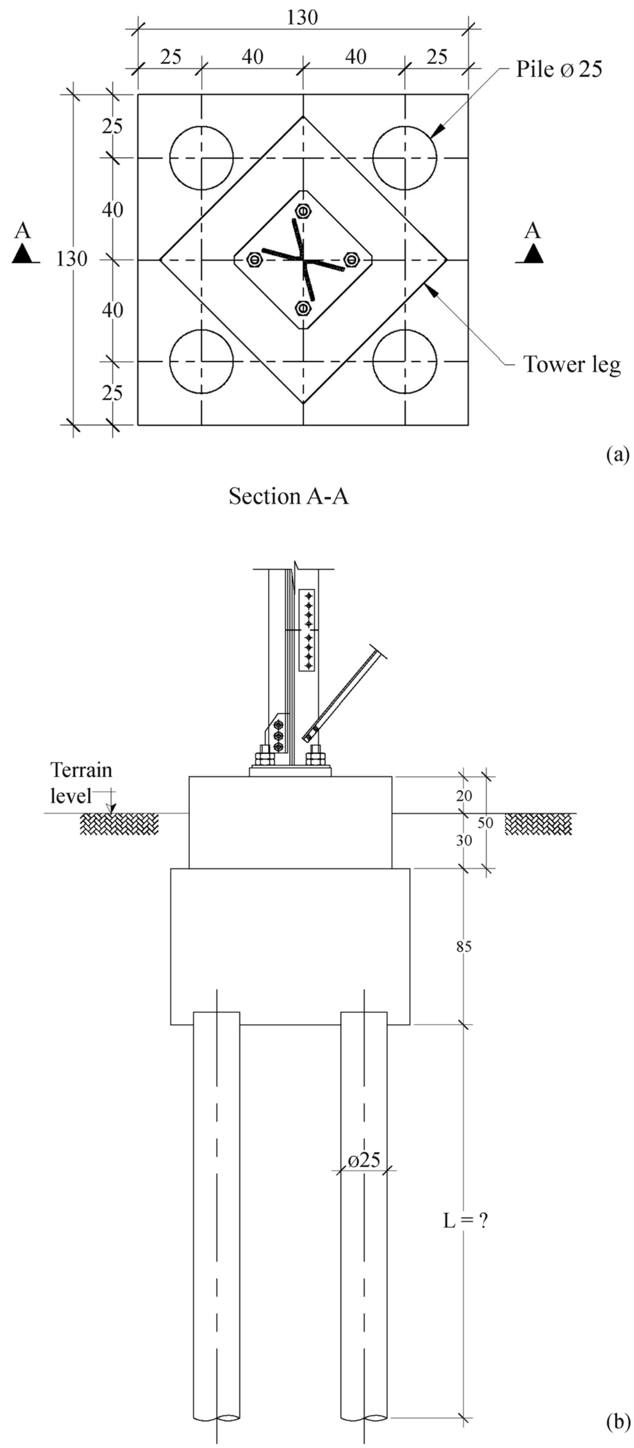

Figure 5 - Foundation block detail: (a) plan view of a block, and (b) elevation of the block depicting two root-piles.

are amplified and converted into electric pulses for register in the form of pulse counts per second.

The IL measurements could be taken with the sonde moving downwards or upwards along the borehole. Repeatability between measurements taken using both procedures indicates good quality data. In down hole measures,

(a)

(b)

(c)

Figure 6 - Equipment used for the PS test: (a) seismograph, (b) small sledgehammer with a trigger, and (c) borehole geophone.

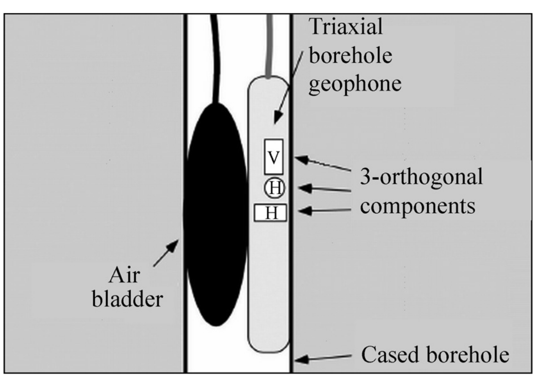

Figure 7 - Detail schematic showing the assemblage of a geophone and air bladder clamping mechanism.

the surface was used as depth reference, whereas in up hole measures the reference was the base of borehole. Both conditions can be accommodated by the Micrologger. However, the alternative modes entail different coverage of the sensors. For the gamma-radiation sensor located 35 cm below the top of the probe, the logs started at an initial depth of 45 cm, since normally the reference level was established when the top of the probe was at ground level. Different coverage also occurs when using the different types of probes (ILM and ILD). Due to the positioning of the sensors, gamma radiation data was collected when the sonde was moving downwards, whereas IL data when moving upwards. This way, each data type was collected under conditions of best possible sensor coverage.

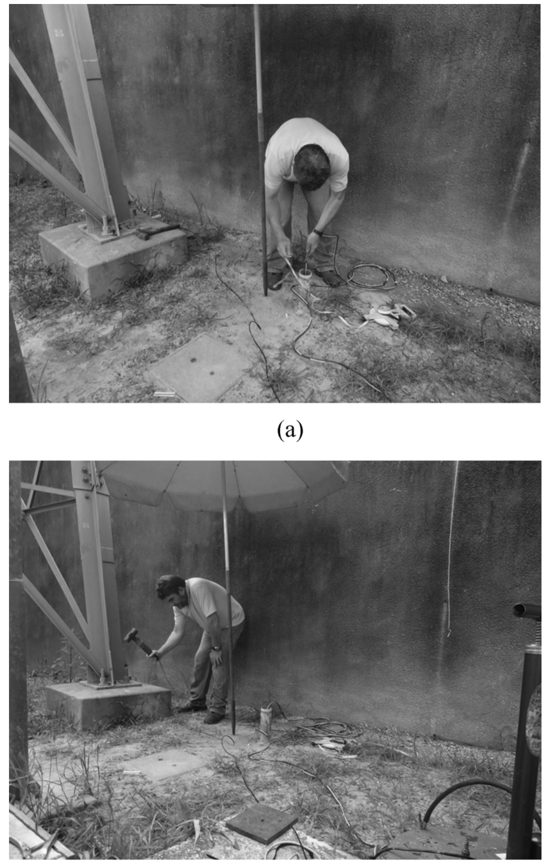

(a)

(b)

Figure 8 - Proceeding with the PS test at block "B1": (a) placement of the geophones inside the borehole, and (b) generation of a compressive wave.

4. Results and Discussion

4.1. Paralell seismic testing

The parallel seismic test results are presented in Fig. 10 showing the seismogram obtained from the record of one of the horizontal components of triaxial geophones. The criterion generally employed to interpret the seismogram and determine the depth of the foundation element, *i.e.*, the intercept point of the two fitting straight lines (Fig. 2), could not be applied in this case, since the first arrivals beyond the 7.5-m depth were not noticeable.

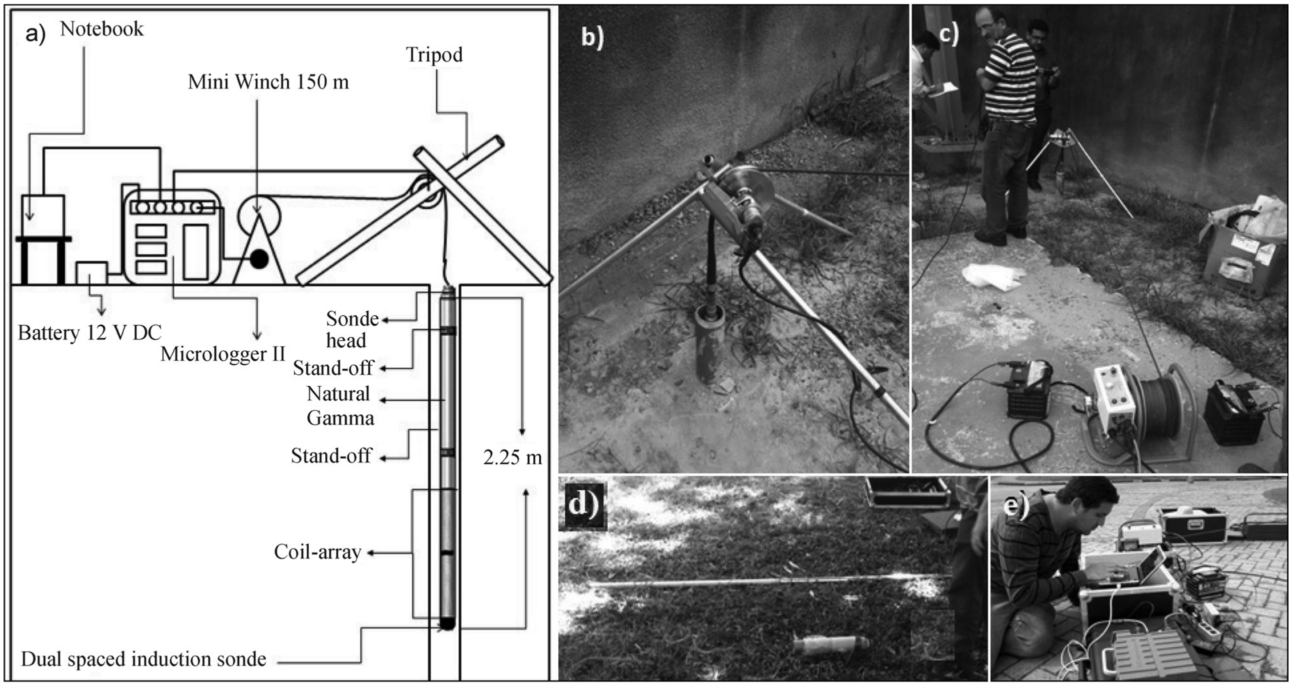

Figure 9 - (a) General layout of the IL test equipment, including the notebook and sonde, (b) pulley and tripod, (c) mini winch and batteries, (d) dual spaced induction sonde, and (e) micrologger.

In Fig. 10, the depth corresponding to the end of the foundation element (pile tip) was inferred based on the observation of the signal attenuation, *i.e.*, sharp decline, or drop, in signal amplitudes occurring at the depth of 7.5 m. When there is small stiffness contrast between the foundation element and the rock, this may become the significant criterion for pile depth estimation based on PS testing. On the other hand, Gandolfo *et al.* (2015) obtained a seismograph similar to that in Fig. 2 for a PS test performed on a 230-cm caisson embedded in a clayey-sandy silt.

Figure 11 presents the seismogram obtained from the record of the S-waves applied to block “B1”. The traces depicted show the inversion in signal polarity, corresponding to the seismic signals recorded for the two impacts applied. The seismogram for the S-waves revealed a drop in signal amplitudes occurring at the depth of 6.5 m.

Therefore, the data analyses based on the results obtained from the PS tests performed, using both P- and S-wave seismograms, allowed to estimate the depth of the tip of the foundation element as ranging from 6.5 to 7.5 m.

4.2. Induction logging testing

The results obtained with the IL and gamma-radiation sonde are shown in Fig. 12. These results include the stratigraphic description of the layers crossed by the probe (Fig. 12a), the profile of gamma-radiation, in counts per second (Fig. 12b), and the profiles of electric conductivity obtained by induction logging, in mS m^{-1} (Fig. 12c), which included short and long induction logging results (solid and dashed lines) and the amplitude-envelope profile (thicker solid line). The gamma-radiation value is an indicator of the content of clay minerals rich in potassium feldspars present in the soil or rock. As shown in Fig. 12b, an analysis of the gamma-radiation profile indicated that above the “Z1” level the count numbers were higher than below this level; the “Z1” level indicates the contact between the fill layer and the meta-sandstone. The acronyms in Fig. 12a correspond to “AT” for anthropogenic material (fill), and “MA” for meta-sandstone. The gradual variations in gama-radiation below the “Z1” level suggest texture or clay-content variations in the layer. The variations are interpreted as being inherent to the material and not affected by the foundation element, with no evidence that the longitudinal reinforcement of the foundation element might have affected the gamma-radiation counts, which, in general, are more affected by the materials (soils and rocks) surrounding the borehole. The two peaks in gamma radiation observed between levels “Z1” and “Z2” can be interpreted as indications of the presence of remnant clay deposited during the sedimentation.

As shown in Fig. 12c, the short and long induction-logging profiles displayed an oscillatory pattern. The IL amplitude envelope displayed a decaying pattern following approximately an exponential decay. With depth, the envelope amplitude declined from a maximum value of ~ 35 mS m^{-1} to an approximately constant value of 10 mS m^{-1} below the depth “Z2”. The fact that beyond the depth “Z2” the amplitude envelope remained nearly constant and at a lower value may correspond to the background value of electrical conductivity of the geological medium. In this

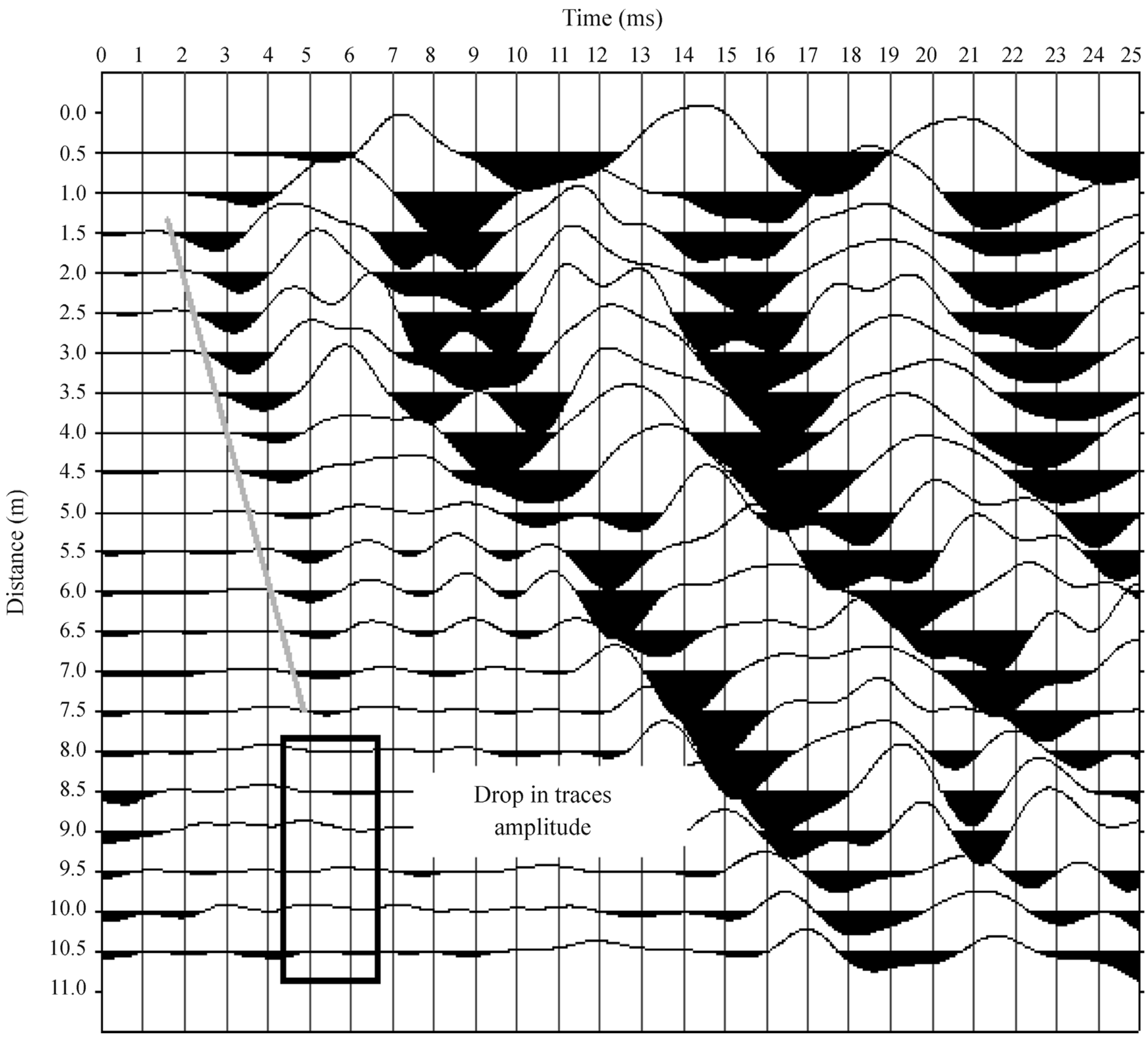

Figure 10 - Parallel seismic test results showing the seismogram for one horizontal component after the application of a P-wave, and visualization of a drop in trace amplitudes occuring at 7.5 m.

case, "Z2" may correspond to the position of the end of the pile. However, additional data, such as measurements of electrical conductivity of the altered rock, would be required to confirm this interpretation and the length of the pile in the IL test could not be defined with certainty.

Additionally, the exponential-decay pattern with depth observed in the amplitude envelope above the "Z2" level was not expected and is not compatible with the expected electromagnetic induction response in the vicinity of a metallic structure (Telford *et al.*, 1990). Preliminary tests conducted at a different site helped explain the reason for the amplitude envelope to decline exponentially with depth. These tests allowed to identify the interference of electromagnetic waves (plane waves) generated at the surface - probably by the antennas on the telecommunication tower itself - on the results. Given that the electromagnetic field generated by the sonde is not expected to decay with depth, the results in Fig. 12c indicate that the field generated by the sonde may be considered negligible in comparison to the surface field generated by the antennas. If confirmed, this hypothesis indicates that the sonde would have stopped working as a magnetic-field inducer to act only as a receptor.

In order to confirm these hypotheses, it would be necessary to conduct additional investigation, such as carrying out measurements along time with the probe in the air, and then at every meter in depth, and analyzing these measurements for differences in the obtained spectral contents. The only limitation to these measurements is the sampling rate of the sonde, which will not allow identification of high frequencies (MHz), but only frequencies within the kHz range. Another possible test is to utilize a portable spectral measuring device to measure the spectral content (kHz to MHz) from the surface down to the bottom of the borehole.

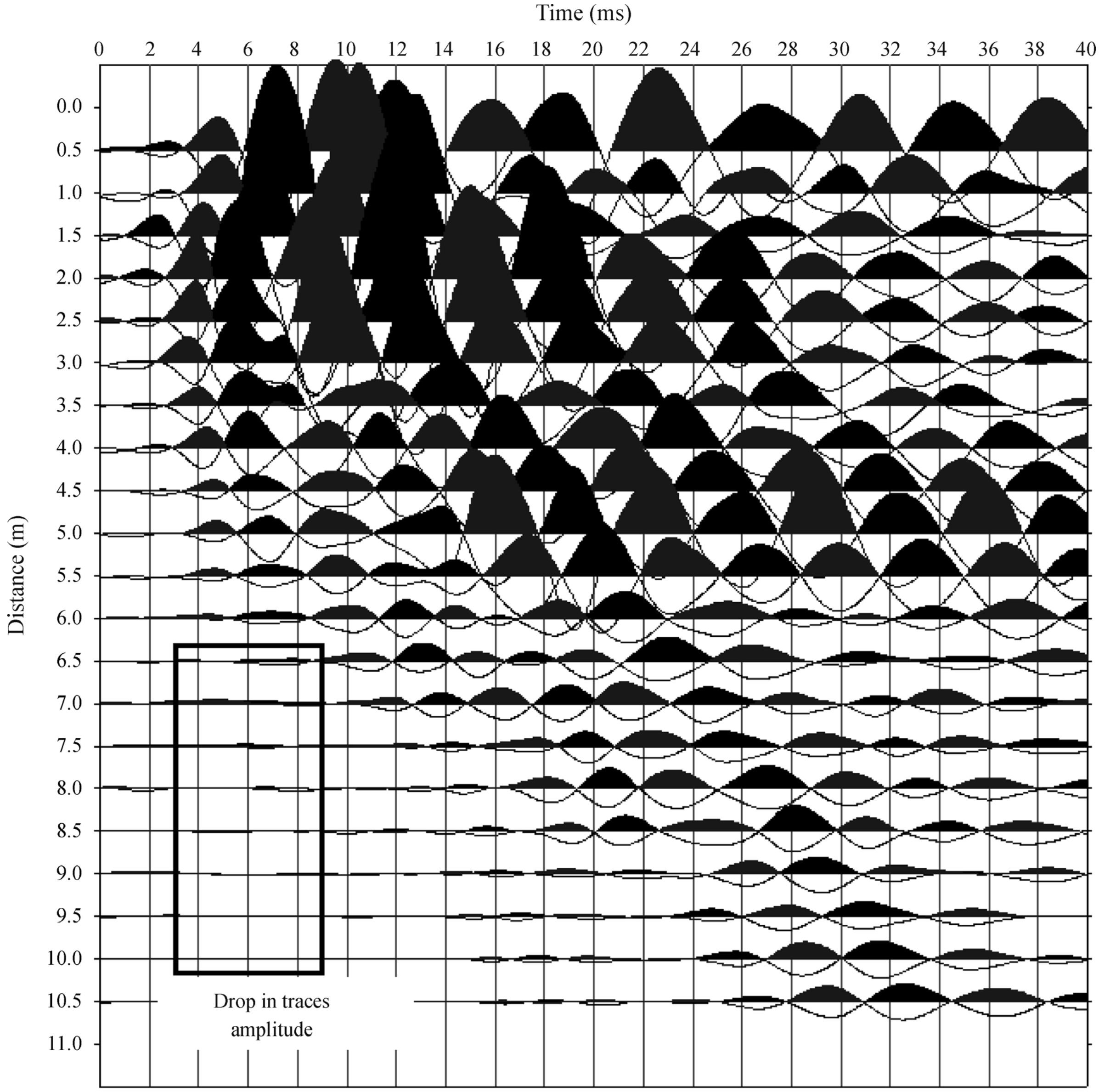

Figure 11 - Parallel seismic test results showing the seismogram for one horizontal component after the application of two S-waves, and visualization of a drop in trace amplitudes occuring at 6.5 m.

The part of the signal that attenuates with depth should show a shift to lower frequencies, whereas the part that is irradiated by the foundation element should maintain the frequency peak, attenuating only below the base of the foundation element.

5. Conclusions

The parallel-seismic (PS) and induction-logging (IL) tests were performed on a 25-cm diameter root-pile embedded in altered meta-sandstone rock. The foundation element was part of the foundations of a telecommunication tower located in Santana de Parnaíba, São Paulo, Brazil. At this site, both tests were performed under challenging conditions. The presence of altered rock surrounding the relatively slender root-pile resulted in low contrast in stiffness, and a seismograph that did not exhibit the two-adjustable line pattern. Nevertheless, the seismograph interpretation method of verifying the depth at which significant signal attenuation occurs allowed to estimate the root-pile depth as ranging from 6.5 to 7.5 m, which was later found to be in agreement with the root-pile as-built documentation.

For the induction logging (IL) test, the amplitude envelope profile exhibited a pattern that was not expected, rendering the test inconclusive in terms of an estimate for the pile depth. A possible interpretation in this case was that the electromagnetic noise generated by the antenna interfered with the measured electromagnetic signals in this test. For future work, factors that interfere with good quality sig-

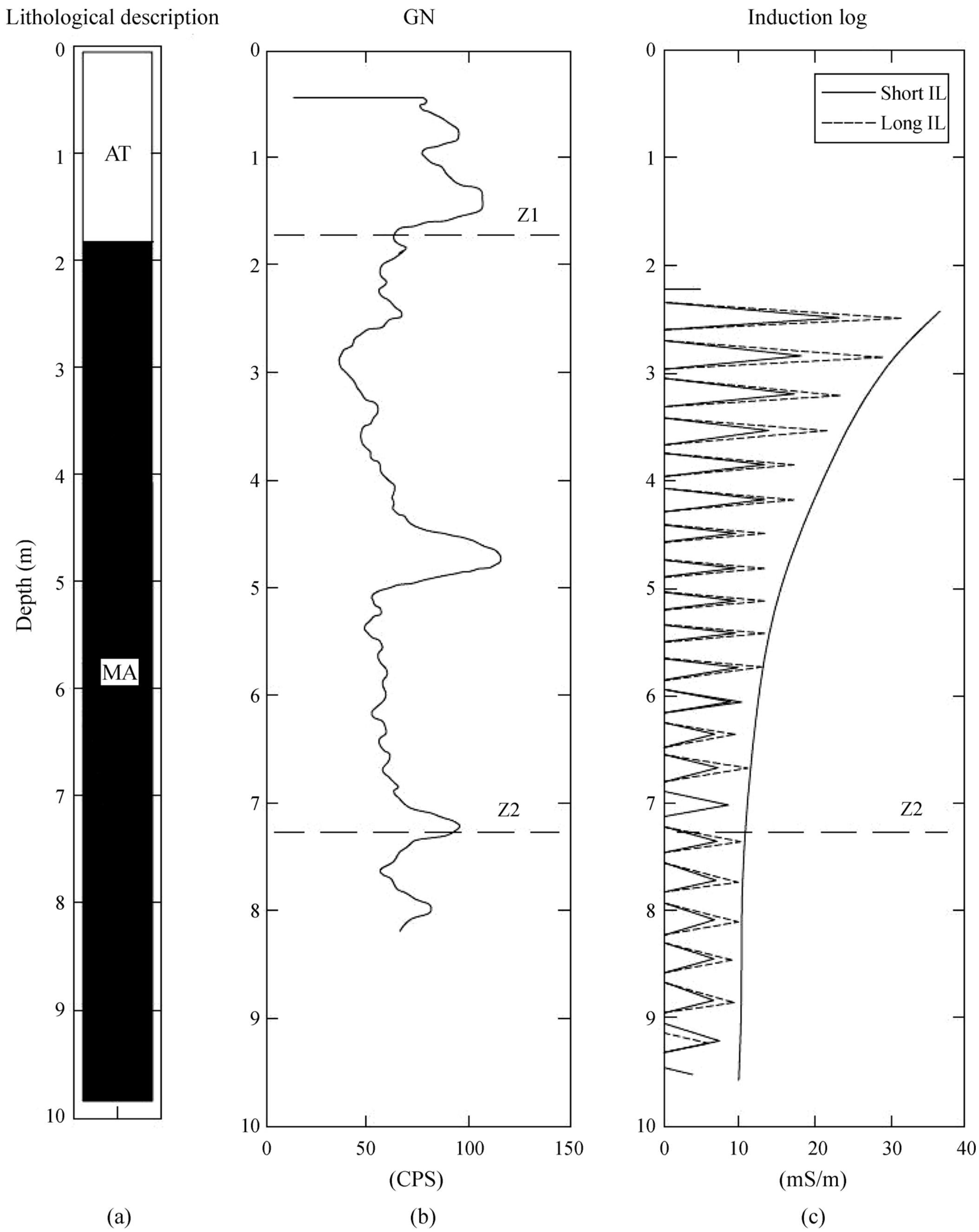

Figure 12 - Induction-logging and gamma-natural sonde results: (a) lithological description, (b) gamma-natural profile in counts per second, and (c) induction-logging profiles in mS m^{-1}.

nal acquisition will be further assessed for each test, procedures to enhance the consistency of the analyses will be studied and, finally, the consistency of the results under different geological settings and foundation typologies will be evaluated.

Acknowledgments

The authors acknowledge the support given by IAG-USP (Geophysical Institute-University of São Paulo), IPT (Technological Research Institute) and thank Dr. Carlos Mendonça for his assistance and comments.

References

ASTM (2007). D4428- Standard Test Methods for Crosshole Seismic Testing, West Conshohocken, PA, USA, 11 p.

ASTM (2008). D7400 - Standard Test Methods for Downhole Seismic Testing, West Conshohocken, PA, USA, 11 p.

Cunha, R.P. & Costa, F.L. (1998). Avaliação da integridade física de estacas assentes na argila porosa de Brasília pelo P.I.T. Proc. XI COBRAMSEG, Brasília, p. 1647-1654.

Cunha, R.P.; Camapum de Carvalho, J. & Silva, C.M. (2002). Controle de qualidade e aceitação de estacas moldadas in loco via utilização de ensaios de integridade de estacas (PIT). Proc. XII COBRAMSEG, São Paulo, v. 3, p. 1569-1579.

de Groot, P.H. (2014). Evaluation of the Parallel Seismic detection of defects in pile foundations. Masters Thesis, Geo Engineering, TU Delft, The Netherlands, 192 p.

Davis, A.G. (1995). Nondestructive evaluation of existing deep foundations. Journal of Performance of Constructed Facilities, 9(1):57-74.

Doll, H.G. (1949). Introduction to induction logging and application to logging of well drilled with oil base mud. Journal of Petroleum Technology, 1(6):148-162.

Ellis, D.V. & Singer, J.M. (2008). Well Logging for Earth Scientists. Springer, The Netherlands, 2nd ed.

Foá, S.B.; Cunha, R.P.; Pereira, J.F.; Camapum de Carvalho, J. & Silva, C.M. (2000). Análise de fundações profundas usando ensaios de PIT. In: Seminário de Engenharia de Fundações Especiais e Geotecnia, SEFE 4, São Paulo, v. 1, p. 349-359.

Gandolfo, O.C.B.; Souza, T.J.; Aoki, P.C. & Hemsi, P.S. (2015). A determinação da profundidade de um elemento de fundação utilizando o ensaio sísmico paralelo (parallel seismic). Fundações e Obras Geotécnicas, year 5, 55:54-58.

Huang, D.Z. & Chen, L.Z. (2007). 3-D Finite element analysis of parallel seismic testing for integrity evaluation of in-service piles. In: Innovative Applications of Geophysics in Civil Engineering, Geo-Denver 2007, Denver, USA, p. 1-9.

Keys, W.S. (1989). Borehole Geophysics Applied to Ground-Water Investigations. National Water Well Association, Dublin, 314 p.

Liao, S.-T.; Tong, J.-H.; Chen, C.-H. & Wu, T.-T. (2006). Numerical simulation and experimental study of parallel seismic test for piles. International Journal of Solids and Structures, 43(7-8):2279-2298.

Luthi, S.M. (2001). Geological Well Logs: Use in Reservoir Modeling, Schlumberger, Log Interpretation, II, Aplications: Schulumberger Ltd. Springer New York, 116 p.

Mondelli, G. (2008). Integração de Diferentes Técnicas de Investigação para Avaliação da Poluição e Contaminação de uma Área de Disposição de Resíduos Sólidos Urbanos. Tese de Doutoramento, Escola de Engenharia de São Carlos, Universidade de São Paulo, São Carlos, 345 p.

McNeill, J.D. (1980). Electromagnetic terrain conductivity measurement at low induction number. Geonics Limited. Technical Note TN-6, Ontario, Canada, 15 p. Available at http://www.geonics.com.

McNeill, J.D. (1990). Use of Electromagnetic Methods for Groundwater Studies. In: Geotechnical and Environmental Geophysics, 1, Ward, S.H. (ed). Review Tutorial, SEG: 191-218.

Moran, J.H. & Kunz, K.S. (1962). Basic theory of induction logging and application to study of two-coil sondes. Geophysics, 27(6):829-858.

Niederleithinger, E. (2012). Improvement and extension of the parallel seismic method for foundation depth measurement. Soils and Foundations, 52(6):1093-1101.

Sack, D.A. & Olson, L.D. (2010). Combined parallel seismic and cone penetrometer testing of existing bridge foundations and levee sheet piles for length and capacity evaluations. Proc. 23th Symposium on the Application of Geophysics to Engineering and Environmental Problems, SAGEEP 2010, Keystone, p. 655-663.

Scott, J.H.; Petersen, J.K.; Osterkamp, T.E. & Kawasaki, K. (1986). Interpretation of Geophysical Well Logs in Permafrost. U.S. Departament of Energy, U.S. Geological Survey, Denver, 130 p.

Souza, T.J.; Aoki, P.C.; Valverde, R.M. & Valverde, S. (2015). Utilização do PIT para o Mapeamento de Fundações em Estruturas de Telecomunicações. In: Seminário de Engenharia de Fundações Especiais e Geotecnia, SEFE 8, São Paulo, p. 117-127.

Telford, V.M.; Geldart, L.P. & Sheriff, R.E. (1990). Applied Geophysics. Cambridge University Press, Cambridge, 792 p.

Shear Strength and Stiffness Degradation of Geomaterials in Cyclic Loading

R. Pytlik, S. Van Baars

Abstract. Cyclic loading on civil structures can lead to a reduction of strength and stiffness in the loaded materials. The life span of many cyclically loaded structures such as wind turbines, high-speed train tracks and bridges strongly depends on the foundation. The soils and rocks in the foundation can be subjected to cyclic loads from natural and human sources. In order to evaluate the fatigue behaviour of geomaterials, this paper presents static and cyclic triaxial test results for several geomaterials. It was concluded that cyclic loading on different geomaterials can cause different types of effects. The shear strength of cohesionless crumbled limestone increases during cyclic loading; while for cohesive materials, such as gypsum and mortar, the strength decreases. The strength decrease can be seen as a degradation of the cohesion. The most significant factor in the cohesion reduction was found to be the number of applied cycles. It was also noticed that the friction angle for sands does not reduce under cyclic loading. A fatigue limit was not found for cohesive geomaterials; neither a dependence of the strength reduction on the cyclic loading ratios.

Keywords: geomaterials, cyclic loading, fatigue, foundation, strength reduction, stiffness reduction.

1. Introduction

The life span of many structures, such as wind turbines, high-speed trains or bridges etc., depends on the fatigue behaviour of the foundation and the surrounding ground mass. An analysis of these structures requires careful planning at the initial stage and a good evaluation of the degradation process in cyclic loading. The impact of the acting forces, both constant and variable, must be taken into account to estimate the strength and stability of the whole structure. Variable forces, due to the repetitive nature of the loads, are known as a cyclic loading, and can significantly reduce the strength and stiffness of materials and lead to an accumulation of strains. Failure of a material due to cyclic loading is known as ‘fatigue’.

The fatigue of the ground is an important mechanism in foundation designs. However, this mechanism has not yet been fully investigated. Except for a limited number of researchers and a few design guidelines for the offshore oil and gas industry (*e.g.* the American Petroleum Institute Recommended Practice - API RP,(2000); or Det Norske Veritas (DNV, 2013), there is no typical civil engineering procedure that describes the effects of cyclic loading on soil and rocks. So far, the most detailed description of the strength reduction due to cyclic loading exists in the field of earthquake engineering (*i.e.* Eurocode 8: Design of structures for earthquake resistance, Part 5, 2004). Yet this procedure is rather unsuitable to adapt for areas where earthquakes do not occur. Even more, the safety factors applied in earthquake engineering are very high, and thus impractical for normal conditions.

Another method for predicting the fatigue of geomaterials is to use the available theoretical models. However, the only available models for cyclic damage that exist in geotechnical engineering focus on the following three aspects: the strain-stress behaviour of the soil, the increase in pore water pressure, and the pile shaft friction degradation.

The stress-strain behaviour has already been investigated by many researchers. To mention only a few of them: Seed & Lee(1966), Matlock *et al.* (1978), Ibsen(1999) and Andersen *et al.* (2013). As these studies focus mainly on strain accumulation, they are not useful for estimating the remaining shear strength. The other limitations of these methods are that they are difficult to use, require many parameters, and cannot be applied for all geomaterials (*e.g.* the model given by Niemunis *et al.*, 2005).

In undrained soils, cyclic loading may generate a high pore pressure which leads to a loss of bearing capacity of foundations by liquefaction (*e.g.* foundations of off-shore wind power turbines, or costal piers). Some formulas to calculate the increase of pore pressure are given by Seed *et al.* (1976), Lee & Albesia(1974) and the DeAlba *et al.* (1976). In order to optimise the control of the effective stresses, all laboratory tests were unsaturated. Thus, the changes in pore pressure due to cyclic loading were omitted.

Currently, no model exists which describes the reduction of the shear strength of geomaterials due to cyclic loading. In order to describe the loss of shear strength due to cyclic loading, and to determine the design values of the soil strength parameters, a proper strength reduction model for both rock and soils is needed. Such a model should pre-

Robert Pytlik, PhD. Student, Faculty of Science, Technology and Communication, University of Luxembourg, Luxembourg, e-mail: PytlikRobert@gmail.com.
Stefan Van Baars, PhD., Full Professor, Faculty of Science, Technology and Communication, University of Luxembourg, Luxembourg, e-mail: Stefan.VanBaars@uni.lu.
Submitted on November 25, 2015; Final Acceptance on November 27, 2016; Discussion open until April 28, 2017.

dict the loss of strength as a function of the number of cycles under cyclic loading, including probability bands in cases where a correct evaluation of the remaining strength and life of geomaterials is required.

2. Shear Strength Degradation

For evaluation of the strength degradation in metals due to cyclic loading a couple of approaches are widely used. The most common approaches include: the simplistic approach (*e.g.* the Palmgren-Miner rule); the damage mechanics approach (*e.g.* Lemaitre brittle damage model); fracture mechanics approach (*e.g.* Paris' Law); the phenomenological (empirical) approach (S-N curve); the remaining strength approach, and others. All of these are well described and have been confirmed in multiple tests (see for example: Pook, 2007).

The Palmgren-Miner rule is a linear damage hypothesis for which failure occurs when the damage parameter reaches a certain value. According to this rule, the damage accumulates linearly with the number of stress cycles, which is usually not true. The Paris law describes the crack growth in cyclic loading based on empirical correlations. The continuum damage mechanics models use state variables to represent the effects of damage on the material, based on *e.g.* thermodynamical aspects of cyclic loading. The most commonly used method for describing fatigue is the phenomenological approach. Therefore, it was decided to apply this approach also to rock and soil mechanics.

In this paper, two, quite similar, approaches for the fatigue tests are investigated and compared:

- the S-N approach
- the remaining strength approach

The basic methodology for these two approaches is the assumption that the initial static strength S_0 will be reduced after N cycles of σ_{cyc} loading.

2.1. S-N approach

The main purpose of the S-N approach is to count the number of cycles N for a given cyclic stress level σ_{cyc}, until the sample reaches a failure state. The failure state is observed when the material is not able to reach the applied cyclic stress level σ_{cyc} anymore. This simply states that the static strength S_0 is reduced to σ_{cyc} for the last cycle N, where N is the sought variable denoting the life of the material at a given cyclic stress level σ_{cyc}. Thus, a single "S-N" curve can be created for each cyclic load σ_{cyc} (S in the S-N formula), and for the corresponding number of cycles leading to failure N. It is usually assumed that the points for N are log-normally distributed – see the standards: American Society for Testing and Materials ASTM E 739 – 91(2006) and Eurocode 3: Design of steel structures - Part 1-9 Fatigue(2006).

For the purpose of the shear strength degradation in the S-N curve, instead of the cyclic stress level σ_{cyc} the ordinate axis is described by a ratio σ_{cyc}/S_0, which is the ratio of the applied deviatoric cyclic stress σ_{cyc} to the deviatoric part of the static strength S_0. The S_0 is given as:

$$S_0 = \sigma_1 - \sigma_3 \tag{1}$$

where σ_1 and σ_3 are the maximum and minimum principal stresses at failure.

The applied cyclic stress is given as:

$$\sigma_{cyc} = \sigma_{max} - \sigma_{min} \tag{2}$$

where σ_{cyc} is the applied cyclic stress level, σ_{max} is the maximum deviatoric cyclic stress and σ_{min} is the minimum deviatoric cyclic stress.

The reason for using the ratio σ_{cyc}/S_0 instead of simply σ_{cyc} is that the shear strength of geomaterials depends on the confining pressure, unlike the properties of metals (see the numerous experiments conducted by Bridgman(1923). In order to be able to compare the loss of the static strength S_0 with the applied cyclic stress σ_{cyc}, the level of the confining pressure has to be taken into account. The tests for a confining pressure of 0 kPa would be similar to tests on concrete (see the procedure in: ACI Committee, 1993) and on steel, but that does not give a full description of the shear strength reduction of geomaterials.

2.2. Remaining strength approach

For the remaining strength approach, a sample is first subjected to a cyclic load σ_{cyc} for a given number of load cycles n. Then, in the last cycle, the sample is loaded until failure.

Since N is the life or the number of cycles until failure, for the remaining strength approach: $n < N$. The predetermined number of load cycles n is given arbitrarily; however, the powers of the number 10 are used to be able to present the results clearer on a semi-logarithmic plot. The theoretical maximum possible value of n (denoted as n_{max}) should be more or less similar to the N value obtained in the S-N tests for the same cyclic stress ratio σ_{cyc}. This would also correspond to the same loss of strength for both the S-N approach and the remaining strength approach ($S_{rem} = \sigma_{cyc}$).

The applied cyclic stress levels σ_{cyc} are the same as for the S-N approach. For each cyclic stress level σ_{cyc}, a single curve can be found. The goal is to describe the remaining strength S_{rem} as a function of the cyclic stress level σ_{cyc}, the number of applied cycles n and the initial static strength S_0, so:

$$S_{rem} = f(\sigma_{cyc}, n, S_0) \tag{3}$$

In the case when $n = 0$, the remaining strength S_{rem} equals the static strength $S_{rem} = S_0$. It was assumed that the remaining strength is a straight line for each cyclic stress level σ_{cyc}, plotted on a semi-logarithmic scale normalised by the static strength S_0. Based on this, Eq. 3 can be written as:

$$\frac{S_{rem}}{S_0} = A(\sigma_{cyc}, S_0) - B(\sigma_{cyc}, S_0) \cdot \log_{10} n \qquad (4)$$

The parameters A and B depend on the cyclic stress σ_{cyc} and S_0, and will be obtained by a linear regression for a semi-logarithmic plot.

A few models have already been proposed in the literature for developing the parameters of remaining strength, see for example: Broutman & Sahu(1972), Reifsnider & Stinchcomb (1986), Gürler (2013), etc. However, these models are more complicated and may not be suitable for geomaterials. Therefore Eq. 4 will be used for comparing the remaining strength model with the S-N curve.

3. Laboratory Testing

3.1 Laboratory equipment

The main components of the triaxial load equipment are presented in Fig. 1. The load frame 28-WF4005 Tritech includes a conventional triaxial cell equipped with an internal load cell and linear transducers for measuring vertical axial displacements. The axial loading capacity is approximately 50 kN, which allows for a deviatoric stress up to 44 MPa on a 38 mm diameter specimen.

The confining pressure is applied by water surrounding the test specimen, which is sealed by the top and bottom plates and a latex membrane. The fluid pressure is applied by a hydraulic actuator and is monitored by a pressure transducer located on the loading frame. The cell pressure levels may vary between 0 and 5 bars and are kept constant during the test.

Figure 1 - Laboratory triaxial machine with pressure controllers.

The static and the cyclic axial loads are applied to the specimen by a servo motor and are monitored by a load transducer. The triaxial servo motor is controlled by a LabVIEW software program written for this purpose. The program was designed to control the load and the data acquisition during cyclic triaxial tests, and to precisely apply the speed of the loading and the level of the cyclic stresses.

3.2. Materials description

The shear strength of geomaterials can be described by the Mohr-Coulomb failure criterion. For the purpose of the laboratory tests, four different kinds of materials were tested (properties are given in Table 1). These are divided into two groups:

a) cohesive

- artificial gypsum
- mortar

b) cohesionless and low-cohesive

- limestone
- sand (crumbled limestone)

All samples had the same diameter d = 38 mm and height h = 78 mm.

The measurement of the loss of strength due to cyclic loading requires many time-consuming tests to be carried out. High accuracy test results would allow reducing the total number of laboratory tests and significantly decrease the testing time. In order to provide a high accuracy of the tests results, highly homogenous material samples are needed. This is not the case, however, for natural geomaterials. The spread of the static and cyclic test results, for natural geomaterials, is usually very high. Therefore, manmade gypsum and mortar samples were used to assure the homogeneity of the materials and therefore consistency of laboratory test results. The results confirmed (see *e.g.* chapter: *S-N approach*) this assumed high accuracy (a value of r^2 = 0.82 for artificial gypsum and r^2 = 0.99 for mortar samples was found for static tests).

Table 1 - Material properties.

Material	dry density ρ_d (g/cm^3)	Porosity n (%)	Void ratio e (-)	D_{50} (-)	C_u (-)	C_c (-)	Density of particles ρ_p (g/cm^3)
Artificial gypsum	1.00	-	-	-	-	-	-
Mortar	1.87	-	-	-	-	-	-
Limestone	1.16	54%	-	-	-	-	-
Crumbled limestone	1.20	53%	1.15	0.2	2.24	0.82	2.74

3.3. Cohesive materials – artificial gypsum and mortar

Gypsum standard samples, were first to be tested (Fig. 2). These were made from gypsum blocks, which are used in the construction of non-load bearing partition walls. These gypsum blocks are composed of gypsum plaster and water. Drilling with a boring machine produced 100 mm long samples which were further trimmed to a 78 mm length. Water cooling during drilling was not necessary because the material was very soft, and the samples were completely dry.

Mortar samples were made in laboratory from a mixture of constant proportions of sand, cement and water. The proportions of sand, cement and water, which gave the most suitable results (with high cohesion and a small data point spread), were 3:3:1. The water-cement (*w*/*c*) ratio was set to 0.33 to provide easy flowing and placement of the mixture into a mould.

The mixture was put in the metal mould for one day, and after its removal from the mould, was left to cure for a period of one month according to the norm EN 12390-2:2000 (2000). Altogether, 6 samples were prepared simultaneously in metal moulds (see Fig. 3).

3.4. Cohesionless and low cohesive materials - limestone and crumbled limestone (sand)

The tested sedimentary limestone was a natural material (carbonate sandstone, also known as Marl or "Mergel") obtained from a construction site at the highway tunnel "Geusselt A2" in Maastricht (Fig. 4). The Maastricht Formation, from which the samples were obtained, is a geological formation in Dutch Limburg, Belgian Limburg and its adjacent areas in Germany. The rock belonging to the Maastricht Formation, is locally called "mergel", and is an extremely weak, porous rock consisting of soft, sandy shallow marine weathered carboniferous limestone (which is in fact chalk and calcareous arenite). The used samples were prepared according to the Eurocode 7, Part 2 (2007). However, it was very difficult to obtain adequate samples for testing, due to their easy cracking and crumbling.

The laboratory tests were conducted on a very young and shallow rock layer. The static shear strength parameters were very low: $\phi = 40.2°$ and $c = 37.4$ kPa (see Pytlik & Van Baars, 2015) so it was decided to treat this material as a very soft rock.

Besides this very weak rock, also cohesionless sand was investigated which was obtained from the crumbled limestone and had the form of fine sand. The dry sand samples were prepared by filling the membrane with sand trough a funnel directly into a 38 mm diameter split form. Hereafter, a compaction was done by hand tamping with a steel rod to obtain a density more or less similar to that of the natural state of the crumbled limestone.

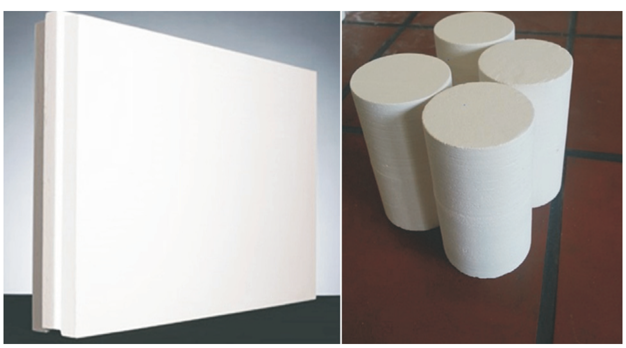

Figure 2 - Artificial gypsum and drilled samples.

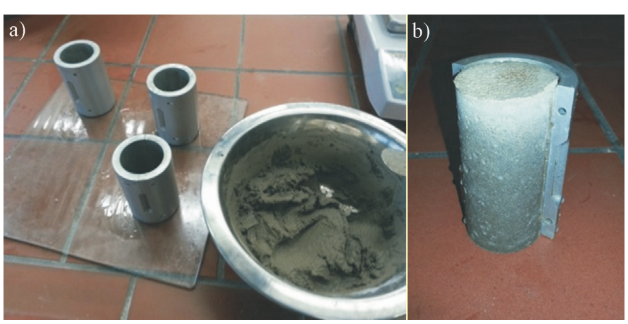

Figure 3 - Mortar samples a) preparation; b) curing.

3.5. Testing procedure

The triaxial laboratory testing was divided into two steps: 1) Static Triaxial Tests; and 2) Cyclic Triaxial Tests

3.5.1. Step 1 - Static tests

The static tests were standard unsaturated triaxial tests. A series of single load tests were conducted in order to determine the parameters of the Mohr-Coulomb failure criterion. The parameters - the cohesion c and the angle of internal friction ϕ - were calculated through a linear least-square regression analysis for the peak stress value.

3.5.2. Step 2 - Cyclic triaxial tests

The cyclic tests were based on multiple loadings and unloadings under a constant cell pressure ($\sigma_2 = \sigma_3$) and a constant strain rate (the speed of the cyclic loading). Three cyclic loadings levels were applied for both the S-N and the remaining strength approach: 40%, 60%, and 80% of the

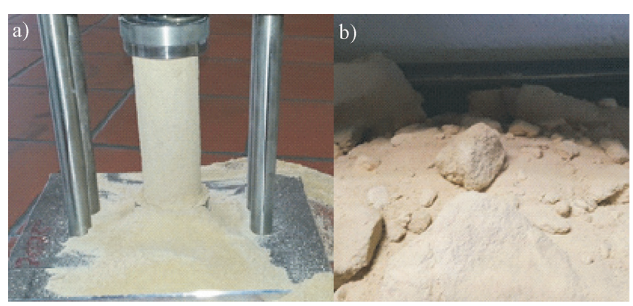

Figure 4 - a) Limestone, b) Crumbled limestone.

maximum static strength. The confining pressure was constant for each test and four values were used 0, 100, 300 and 500 kPa. For all tests, the minimum cyclic loading σ_{min} was equal to 0 kPa, to unload completely the samples. Thus, the cyclic loading is equal to the maximum applied stress:

$$\sigma_{cyc} = \sigma_{max} \tag{5}$$

The σ_{max} can be calculated as follows:

$$\sigma_{max} = \sigma_{1,cyc} - \sigma_3 \tag{6}$$

where $\sigma_{1,cyc}$ is the maximum cyclic principal stress. The $\sigma_{1,cyc}$ is equal to:

$$\sigma_{1,cyc} = \frac{F_{cyc}}{A_s} - \sigma_3 \tag{7}$$

where F_{cyc} is the applied cyclic force, and A_s is the area on which the force F_{cyc} is acting.

The stress ratio R is a parameter for testing steel fatigue, and defined as $\sigma_{min}/\sigma_{max}$. The R had constant value (of 0) for all the tests because σ_{min} = 0 kPa. The shape of the cyclic loading curve was a typical sinusoidal wave.

The speed of the cyclic loading application (the strain rate) in the triaxial apparatus was set to 0.5 mm/min. This assured a slow cyclic loading frequency (f = 0.01 Hz) and an accurate data reading of the force through the LabVIEW software. This also solved the problem of keeping a constant cyclic loading level during the tests, which was an issue for higher frequencies.

4. Laboratory Tests Results

4.1. Tests on cohesive materials

First, the artificial gypsum material was investigated. A total number of 37 cylindrical samples were tested with an unsaturated triaxial test. The obtained static shear strength parameters c and ϕ were compared with the parameters obtained from the cyclic tests. 44 gypsum samples were tested according to the S-N approach and 43 samples according to the remaining strength approach.

4.1.1. S-N approach

Almost all samples selected for the S-N approach were samples which failed prematurely in the remaining strength testing approach (biased samples). Therefore, the accuracy of the S-N approach is questionable. However, for the purpose of a comparison with the remaining strength approach, the results are presented here.

In Fig. 5, a modified S-N plot for the cyclic tests on artificial gypsum is displayed. Additionally, the confidence and prediction bands with a 95% probability have been added, indicating that the uncertainty of the data points spread is high. The spread of the bands is much higher than for metals and for composite materials (*e.g.* the results given by Philippidis & Passipoularidis, 2006). It should

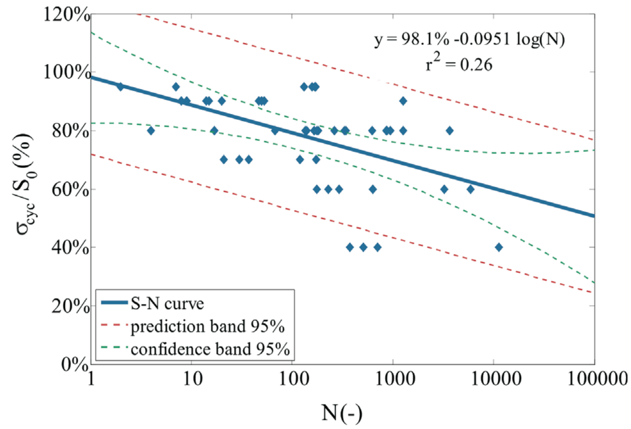

Figure 5 - S-N curve for artificial gypsum samples under cyclic loading.

also be noticed that the inclination of the curve – how fast does the material lose its strength – is again much higher compared to metals (*e.g.* Manson & Halford, 2006). An endurance limit σ_e (the cyclic loading level at which the material can survive an infinite number of cycles) was not found. This means that, for the cohesive geomaterials presented in this paper, even small loads can cause irreversible damage. More importantly, even for low cyclic stress levels (40% of the initial strength), the life of the artificial gypsum was short, not exceeding 100 000 cycles. Therefore, it can be concluded that cohesive geomaterials are more affected by cyclic loading than metals and composites.

4.1.2. Remaining shear strength approach

The linear regression lines for different cyclic stress levels (Fig. 6) were forced to intercept the ordinate at 100%. It can be noticed (Table 2 and Fig. 6) that for the remaining strength S_{rem}, the cyclic loading level is unimportant as all lines are very close to each other, and only the number of cycles n is crucial.

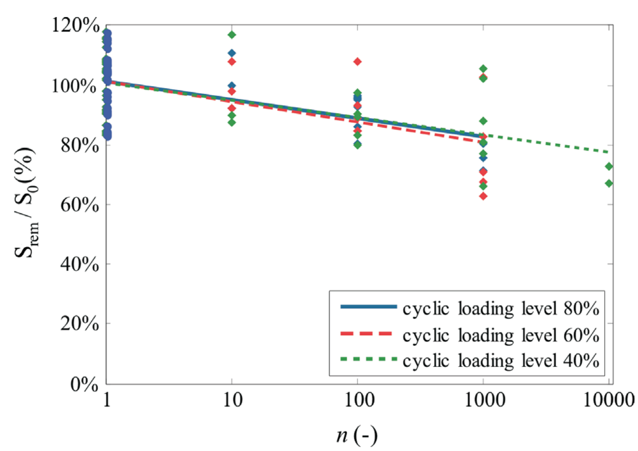

Figure 6 - Remaining strength for artificial gypsum subjected to different cyclic loading levels.

Table 2 - Remaining strength parameters for artificial gypsum subjected to different cyclic loading levels (including static data).

Cyclic loading level	r^2	a	b
40%	0.32	0.068	1.00
60%	0.34	0.086	1.00
80%	0.28	0.072	1.00

If the assumption is made that the strength of the material is greatly dependent on the cyclic level σ_{cyc} then a single log-normal curve for all cyclic tests, with confidence and prediction bands, can be presented. This curve (Fig. 7) fits all samples, both static and cyclic, even though it omits the information about the cyclic loading level. This curve is very similar to the S-N curve. This should be further investigated, because for most materials (*e.g.* composites) different cyclic stress levels cause different reductions in strength. The lack of dependency between the cyclic stress level σ_{cyc} and the remaining strength S_{rem} could be caused by the high scattering of data points, and thus any relationship was hard to find. This also implies that the strength reduction approach loses one of its advantages – the estimation of the life for different cyclic loading ratios. Therefore, the S-N approach seems to be a faster method as it requires fewer tests while giving similar information about the loss of strength as the remaining strength approach. Also, no correlation was found between the remaining strength and the confining pressure σ_3.

The mortar samples gave more accurate static test results than the artificial gypsum samples (higher value of $r^2 > 0.97$). However, the cyclic tests on mortar presented a similar pattern to the results of the artificial gypsum material - with a high spread of cyclic data points (Figs. 8 and 9). Therefore, the high data spread for the S-N approach and the remaining strength approach could be an intrinsic property of cohesive materials. Due to its inhomogeneous internal structure, the cyclic strength results are quite varied.

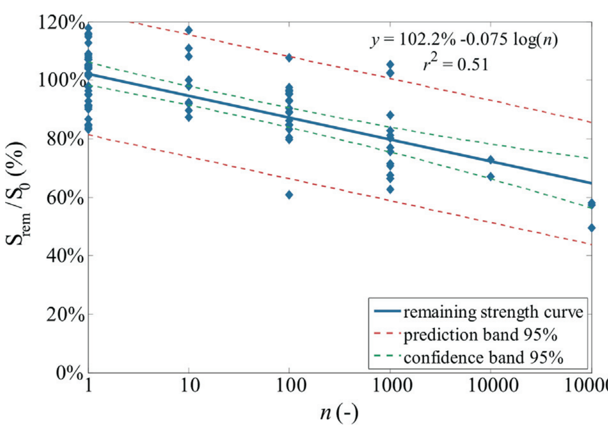

Figure 7 - Remaining strength curve of all cyclic tests for artificial gypsum.

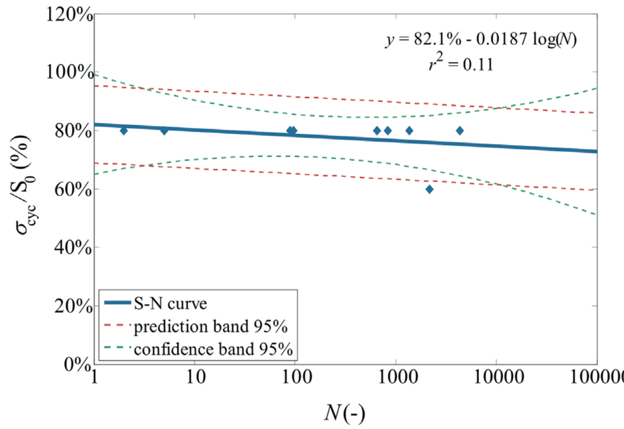

Figure 8 - S-N curve for mortar material.

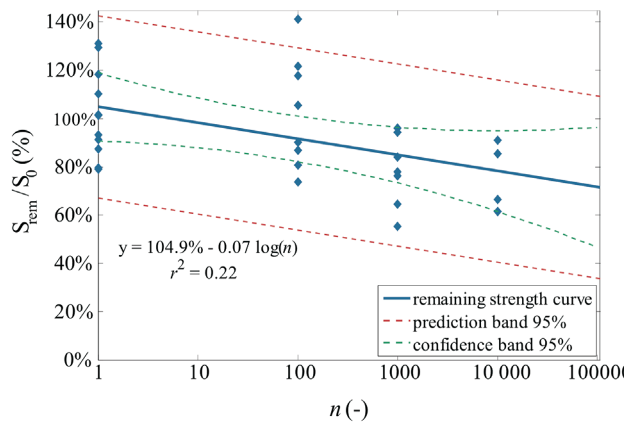

Figure 9 - Remaining strength curve for mortar material.

It was noticed for mortar, that the samples had a longer life than artificial gypsum (based on the S-N approach). This could be related to a higher static strength for mortar than for gypsum ($\phi = 51.4°$, $c = 1.4$ MPa for mortar; and $\phi = 40.9°$, $c = 1.2$ MPa for gypsum). This means that the stronger the material, the longer its life will be, for the same type of cyclic loading.

More importantly, for higher cyclic loading stress levels, a lot of samples failed before reaching the number of predetermined cycles n, before the final loading until failure. Taking into consideration only the remaining samples for the remaining strength approach could result in significantly overestimating of the remaining strength and the life of the material. This is another reason which decreases the usefulness of the remaining strength approach. Moreover, even including the static data points in the remaining strength approach did not increase the accuracy of the model for lower number of cycles (Fig. 7). This could be due to a) the strength reduction being non-linear or b) the logarithmic scale not being the most adequate in terms of shear strength reduction.

4.2. Tests on low-cohesive or cohesionless materials

In order to investigate the fatigue of very weak materials, cyclic triaxial tests were carried out on limestone and on crumbled limestone, with the same procedure as for the cohesive geomaterials. But, due to a low number of available limestone samples, only two cyclic loading ratios were applied: 80% and 40%. Also, the number of applied cycles was rather small – only series of n = 10, 100 and 1000 cycles were carried out. For the remaining strength approach, 9 samples were cyclically loaded (the results are presented in Fig. 10). S-N tests were not conducted due to the lack of samples.

The test results showed that there is no fatigue in limestone at least for a number of cycles up to 1000. The strength of the limestone even increased (Fig. 10). Similar results were found for crumbled limestone and a few other cohesionless geomaterials. The main conclusion regarding the cohesionless and low-cohesive materials is that the strength increases after cyclic loading, due to densification (Youd, 1973). For very dense cohesionless materials, however, the strength can decrease.

The cyclic loading on cohesionless materials, has already been investigated and described by others. The description is usually accompanied by the shakedown theory (*e.g.* by Yu *et al.*, 2007). The basic assumption of the shakedown theory is that below a certain load (named shakedown load) the material will eventually shakedown, *i.e.*, the ultimate response will be purely elastic (reversible) and therefore, there is no more accumulation of plastic strain. If the applied load is higher than the shakedown load, uncontrolled permanent deformations will develop and unstable conditions will progress.

The result for the plastic strain accumulation of the crumbled limestone agrees with the predictions from the shakedown theory. Suiker (2002) found that cohesionless materials influenced by cyclic loading could obtain higher strength parameters than without cyclic loading.

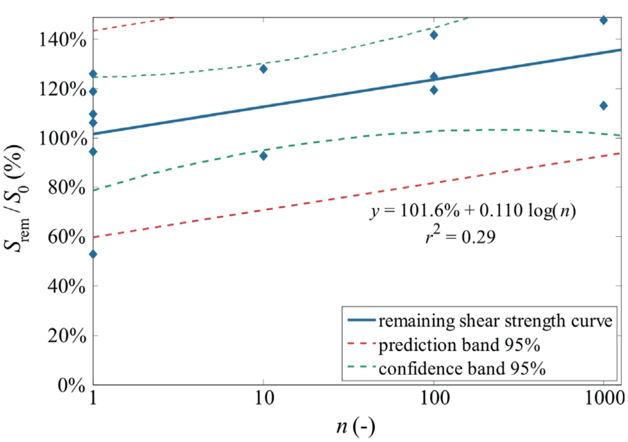

Figure 10 - Remaining strength curve for limestone.

5. Stiffness Degradation

Another interesting phenomenon to investigate is stiffness degradation during cyclic loading, as it requires less laboratory testing than the strength tests, especially because it can be assessed by non-destructive techniques. The stiffness degradation progress can be used as a rough estimation of the material's condition and could improve the assessment of the fatigue life.

One can expect that, a comparison of the initial stiffness E_0 with the stiffness during cyclic loading contains information about the actual life consumption of the sample. Unfortunately, only small number of tests has been conducted on the stiffness degradation for geomaterials, and thus there is not enough reference data and no constitutive model. One of the few examples is offered by Bagde & Petros (2011), who observed the degradation of the stiffness modulus in compressional cyclic tests on sandstone samples.

For the purpose of this investigation, the proportional maximum and minimum limits were taken as 90% and 10% of the maximum strength. The 10% limit was chosen because for lower stresses the readings of the stiffness were not accurate enough. The ratio E_{rem}/E_{max} is denoted as the ratio of the stiffness in the last cycle E_{rem} to the maximum stiffness E_{max} during the whole cyclic loading test. The whole cyclic test run was taken into consideration, as for the first few cycles the stiffness can vary significantly (see Figs. 11 and 13) and the maximum stiffness is not found necessarily at the very beginning. The stiffness data was obtained from the same tests as for the remaining strength approach, because the strains were also measured during these tests.

The cohesive materials lose their stiffness with an increase in the number of cycles, as can be noticed from Fig. 11. The stiffness degradation plot for artificial gypsum, see Fig. 12, is very similar to the corresponding remaining strength plot of artificial gypsum (compare Fig. 7 with Fig. 12).

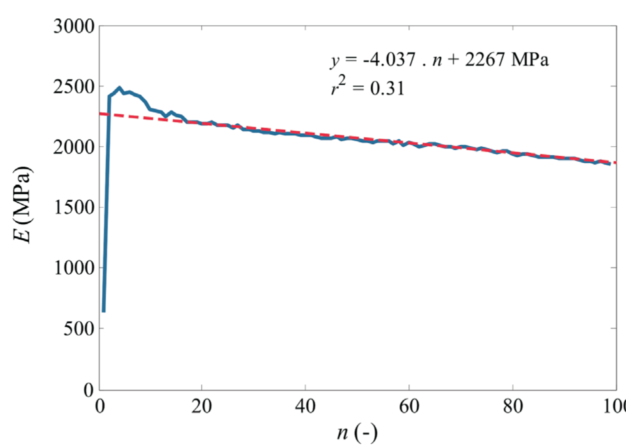

Figure 11 - Stiffness degradation of artificial gypsum sample (100 cycles).

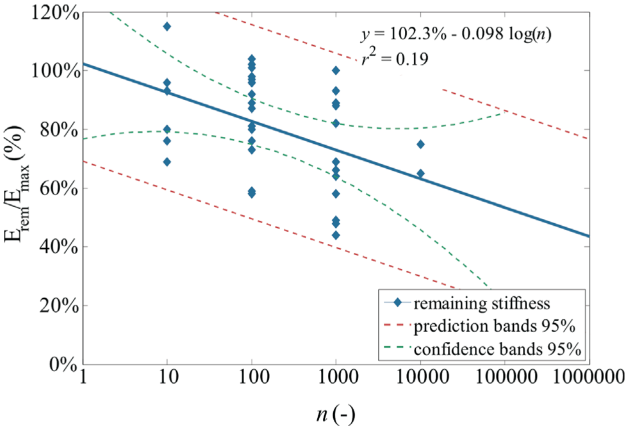

Figure 12 - Stiffness degradation curve for artificial gypsum.

For the low-cohesive materials, it was found that the cyclic loading induced an increase in stiffness, as can be seen in Fig. 13. This also corresponds to the results from the remaining strength tests on the limestone (compare Fig. 10 with Fig. 14).

It can be concluded that, in terms of stiffness reduction, the stiffness changes in cyclic loading are very similar to the shear strength changes. For cohesive materials under cyclic loading, the stiffness decreases; and for cohesionless materials, the stiffness increases. Fortunately, this will be easy to use in practice, because the stiffness reduction is even more significant than the reduction in strength.

6. Parametrisation of a Remaining Shear Strength Model

For a simple shear strength reduction model, the most convenient would be that the parameter which is affected by cyclic loading is only the cohesion c, while the friction angle ϕ remains constant. This assumption of a constant friction angle ϕ was also formulated in the laboratory tests. Vyalov (1978) stated that for rocks, the decrease of strength over time is a result of a decrease in the cohesion c while the

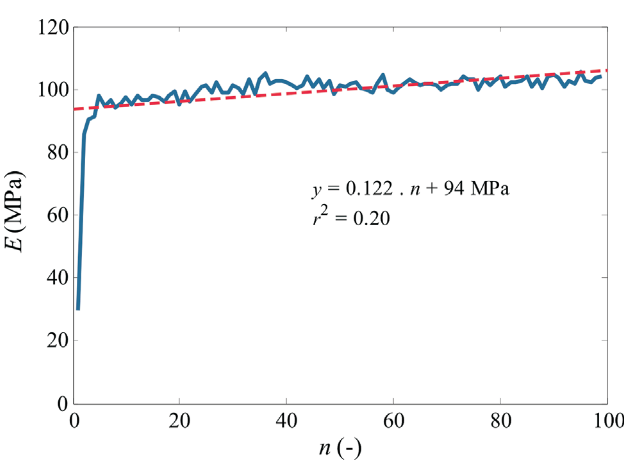

Figure 13 - Stiffness changes of limestone (100 cycles).

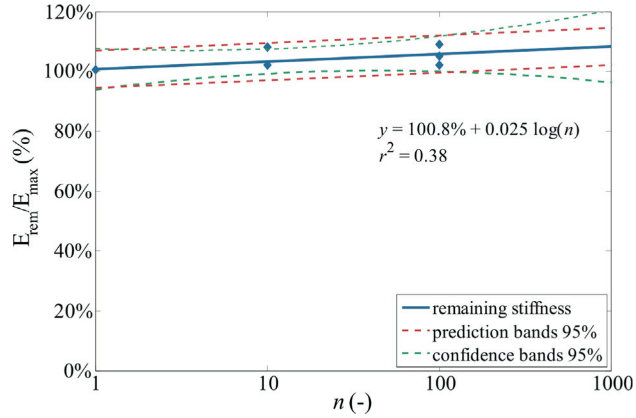

Figure 14 - Stiffness "degradation" curve for limestone.

friction angle ϕ remains constant. This corresponds with a statement from Van Baars (1996) who, based on discrete element modelling, stated that the static strength of a cohesive material depends on the contact strength and the normal force distribution.

Furthermore, Brantut *et al.* (2013) gave a summary of his tests, proving that brittle creep, which is defined by him as permanent deformation due to mechanical stress, reduces the cohesion of rock, but this does not directly affect their internal friction. This indicates that failure which is extended over time is mainly related to reduction of the cohesion. The results of the laboratory tests presented herein also indicate that the cohesive materials lose their strength, while the cohesionless materials do not.

Based on this constant friction angle, one can make a plot, similar to that of the remaining strength - Fig. 5 and, for the S-N approach, Fig. 7 - , in which the remaining strength ratio S_{rem}/S_0 or cyclic stress ratio σ_{cyc}/S_0 is replaced by the remaining cohesion ratio c_{rem}/c.

For each of the tests, the remaining cohesion c_{rem} is obtained by recalculating the cohesion with the Mohr-Coulomb equation. The remaining cohesion for a single test can be calculated from the formula:

$$c_{rem} = \left(\frac{\sigma_1 - \sigma_3}{2}\right)\frac{1}{\cos\phi} - \left(\frac{\sigma_1 + \sigma_3}{2}\right)\tan\phi \qquad (8)$$

where, σ_1 and σ_3 correspond to the maximum and minimum principal stresses at failure.

The interpolated formula of the remaining cohesion can be written as:

$$c_{rem} = c\cdot[B - A\cdot\log(n)] \qquad (9)$$

where A and B are constant parameters obtained from the regression line, and are specific to the material.

In Eq. 9, the parameter which would describe the cyclic loading level is not given. This is because it was found from the laboratory tests for the remaining shear strength approach, that the strength reduction was independent from the cyclic loading level. This requires further investigation however, as mentioned before, because this independency is unexpected.

For the S-N approach, the c_{rem} is obtained in the same way; but, the constants E and F are different here:

$$c_{\text{rem}} = c \cdot [F - E \cdot \log(N)] \tag{10}$$

For the cohesionless materials (*e.g.* sand) no cohesion is present (c = 0 kPa, or it is very low); thus, the shear strength reduction can be neglected for such a material (although the cyclic strain accumulation should be checked anyway). Therefore, a clear distinction has to be made between the cohesive and the cohesionless cyclic behaviour.

For cohesive cyclic behaviour, the updated shear strength τ can be given as:

$$\tau = \sigma \tan \phi + c_{\text{rem}} \tag{11}$$

where the degraded cohesion c_{rem} replaces the "static" cohesion c. Implementing Equation 9 in Eq. 11 yields for the number of applied cycles n (or N):

$$\tau = \sigma \tan \phi + c \cdot [B - A \cdot \log n] \tag{12}$$

In terms of the maximum and minimum principal stresses σ_1 and σ_3, the Mohr-Coulomb failure criterion can then be proposed as:

$$\left(\frac{\sigma_1 - \sigma_3}{2}\right) - \left(\frac{\sigma_1 + \sigma_3}{2}\right) \sin \phi - c_{\text{rem}} \cdot \cos \phi = 0 \tag{13}$$

In order to describe fully the fatigue of geomaterials, one needs to give the life of a material for the remaining strength approach. The number of cycles before failure (life) for the remaining strength approach $n_{max} = N$ can be found from some simple transformations of Eq. 9:

$$\log_{10} n_{\max} = \frac{c \cdot b - c_{\text{rem}}}{\text{c} \cdot \text{a}} \tag{14}$$

and finally:

$$n_{\max} = N = 10^{\frac{c \cdot b - c_{\text{rem}}}{c \cdot a}} \tag{15}$$

To calculate the reduced strength for a combination of different level and number of cyclic loads, an additive rule is needed. Care must be taken to use *e.g.* the simple additive Palmgren-Miner rule, which is the most popular in metal fatigue. This rule could lead, however, to an unsafe foundation because it underestimates the damage at very low load levels and it does not predict well the applied load sequences. Future tests should be conducted to confirm whether the methods from metal fatigue (*e.g.* Palmgren-Miner rule) can be applied for describing the impact of various cyclic loadings in geomaterials.

7. Advantages and Disadvantages of the S-N and Remaining Shear Strength Approach

The biggest advantage of the remaining strength approach, compared to the S-N and the damage accumulation approach (*e.g.* the Paris law), is that the remaining strength approach does not only predict the number of cycles until failure, but gives an indication of the remaining strength as well. The remaining strength is measured directly and in a simple way, and the empirical damage accumulation rule (*e.g.* the Palmgren-Miner linear damage rule) can be replaced by a physical parameter – the shear strength.

Since the number of cycles n is controlled for the remaining strength approach, the laboratory tests for this approach can be easily scheduled, as the time of one cycle is known from the static tests. For the S-N approach it is difficult to predict the life-time of a sample before having finished some of the other cyclic tests. Therefore, the time planning for the S-N approach is more complex.

Another advantage of the remaining strength approach is that the static tests can be included. It was found however, that these results did not necessarily improve the accuracy compared to the S-N curve.

The biggest disadvantage of the remaining strength approach is that it only takes into account the samples which survived the applied number of cyclic loads n. This leads to the conclusion that the remaining strength approach overestimates the strength compared to the S-N approach, and therefore the correlation of the remaining strength approach is questionable. Thus, the standard S-N approach offers more reliable results, and also requires less testing.

For both approaches, the big spread of the resulting data implies that a lot of samples have to be tested to obtain a good accuracy for geomaterials. Unfortunately, these tests are very time consuming.

8. Conclusions

Cyclic loading on geomaterials investigated in this paper can cause different types of effects: for example, the shear strength of crumbled limestone increases during cyclic loading, while for cohesive materials the strength decreases (fatigue). This can be seen as a degradation of the cohesion. The most significant factor in the cohesion reduction was found to be the number of applied cycles.

The fatigue of cohesive geomaterials presented in this paper can be fully described by the remaining cohesion. The existence of a constant friction angle was demonstrated in different ways, for example by tests on low-cohesive and cohesionless materials where the friction angle under cyclic loading was not reduced. Some tests even showed an increase of the value of the friction angle due to densification. Care must be taken however, because the number of tests and the set of investigated materials were limited and the r^2 value in the cyclic tests was rather low.

The amplitude of the cyclic loading does not affect the remaining strength. Also the confining pressure does not affect the remaining strength. Therefore, the remaining strength model proposed in this paper is both simple and effective.

The strength degradation can be linked to the stiffness degradation, which shows a similar pattern. For practical purposes, this could help to estimate the reduction in strength by non-destructive methods, based on changes in the stiffness.

Both the S-N and the remaining strength approach have their advantages and disadvantages. The S-N approach offers, however, a faster and safer solution compared to the remaining strength approach.

References

ACI Committee 2015 (1993). Consideration for design of concrete structures subjected to fatigue loading - ACI 215R-74. In ACI Manual of Concrete Practice Part 1 – 1993, American Concrete Institute, Detroit, pp. 1-24.

American Petroleum Institute (2000). Recommended Practice for Planning, Designing and Constructing Fixed Offshore Platforms—Working Stress Design. API Recommended Practice 2A-WSD (RP 2A-WSD), Washington, 60 p.

Andersen, K.; Puech, A. & Jardine, R. (2013). Cyclic resistant geotechnical design and parameter selection for offshore engineering and other applications. Proceedings of TC 209 Workshop – Design for cyclic loading: piles and other foundations, 18 ICSMGE, Paris, pp. 9-44.

ASTM (2006). E 739-91 - Standard Practice for Statistical Analysis of Linear or Linearized Stress-Life (S-N) and Strain-Life (e-N) Fatigue Data. ASTM, Philadelphia, pp. 1-7.

Bagde, M. & Petros, V. (2011). The Effect of Micro-Structure on Fatigue Behaviour of Intact Sandstone. International Journal of Geoscience, 2:03, pp. 240-247.

Brantut, N.; Heap, M.; Meredith, P. & Baud, P. (2013). Time-dependent cracking and brittle creep in crustal rocks: A review. Journal of Structural Geology, 52:17-43.

Bridgman, P.W. (1923). The compressibility of thirty metals as a function of temperature and pressure, Proceedings of the American Academy of Arts and Science, 58:165-242.

Broutman, L. & Sahu, S. (1972). A new theory to predict cumulative fatigue damage in fiberglass reinforced plastics. Composite Materials: Testing and Design (Second Conference). ASTM STP 497 American Society for Testing and Materials, Philadelphia, pp. 170-188.

DeAlba, P.; Seed, H. & Chan, C. (1976). Sand Liquefaction in Large Scale Simple Shear Tests. Journal of the Geotechnical Engineering Div., 102(GT9), pp. 909-927.

DNV (2013). Design of Offshore Wind Turbine Structures. Det Norske Veritas, Oslo.

EN (2000). 12390-2:2000 - Testing Hardened Concrete. Part 2: Making and Curing Specimens for Strength Tests. CEN, Brussels.

EN (2006). 1993-1-9:2006 Eurocode 3 - Design of steel structures – Part 1-9: Fatigue. CEN, Brussels.

EN (2007). 1997-2 Eurocode 7 - Geotechnical Design, Part 2: Ground Investigation and Testing. CEN, Brussels.

EN (2004). 1998-5: Eurocode 8 - Design of structures for earthquake resistance – Part 5: Foundations, retaining structures and geotechnical aspects. CEN, Brussels.

Gürler, S. (2013). The mean remaining strength of systems in a stress-strength model. Hacettepe Journal of Mathematics and Statistics, 42:2, Ankara, pp. 181-187.

Ibsen, L. (1999). Cyclic Fatigue Model. AAU Geotechnical Engineering Papers: Soil Mechanics Paper, 34:R9916, Aalborg, pp. 1-30.

Lee, K. & Albesia, A. (1974). Earthquake induced settlements in saturated sands. Journal of Geotechnical Engineering ASCE, 100:04, pp. 387-405.

Manson, S. & Halford, G. (2006). Fatigue and Durability of Structural Materials. ASM International, Ohio, pp 123-156.

Matlock, H.; Foo, S.H. & Bryant, L.L. (1978). Simulation of lateral pile behaviour. Proceedings of Earthquake Engineering and Soil Dynamics, ASCE, New York, pp. 600-619.

Niemunis, A., Wichtmann, T. and Triantafyllidis, T. (2005). A high-cycle accumulation model for sand, Computers and Geotechnics, 32:4, pp. 245-263.

Philippidis, T. & Passipoularidis, V. (2006). Residual strength after fatigue in composites: Theory *vs.* experiment. International Journal of Fatigue, 29, pp. 2104-2116.

Pook, L. (2007). Metal Fatigue. Springer, Dordrecht, pp. 35-65.

Pytlik, R. & Van Baars, S. (2015). Triaxiaalproeven op Limburgse mergel leveren verrassende resultaten (in Dutch). Geotechniek, 19(3), Rotterdam, pp. 10-13.

Reifsnider, K.L. & Stinchcomb, W.W. (1986). A critical Element Model of the Residual Strength and Life of Fatigue-Loaded Composite Coupons. Proceedings of the Conference on Composite Materials: Fatigue and Fracture, Philadelphia, pp. 298-303.

Seed, H.B. & Lee, K. (1966). Liquefaction of saturated sands during cyclic loading. Journal of Soil Mechanics and Foundation Engineering, 92(SM6), pp. 105-134.

Seed, H.B., Martin, P., & Lysmer, J. (1976). Pore water pressure changes during soil liquefaction. Journal of the Geotechnical Engineering Division, 102(GT4), pp. 323-346.

Suiker, A. (2002). The Mechanical Behaviour of Ballasted Railway Tracks. Delft University of Technology, Delft, pp. 127-159.

Van Baars, S. (1996). Discrete Element Analysis of Granular Materials. Delft University of Technology, Delft, pp. 61-81.

Vyalov, S. (1978). Rheologic Principles of Soil Mechanics (in Russian). Vysshaya Shkola, Moscow. pp. 285-338.

Youd, T. (1973). Factors controlling maximum and minimum densities of sand. ASTM Special Technical Publications, 523, American Society for Testing and Materials, Philadelphia, pp. 98-112.

Yu, H.; Khong, C. & Wang, J. (2007). A unified plasticity model for cyclic behaviour of clay and sand. Mechanics Research Communications, 34(2):97-114.

List of Symbols

a, b, A, B, and F, E: constants obtained in linear regression
c: cohesion
c_{rem}: remaining cohesion
d: diameter of a sample
h: height of a sample
n: predetermined number of applied load cycles
n_{max}: maximum number of load cycles
A_s: cross-sectional area of a sample
E_{rem}: remaining stiffness
E_{max}: maximum stiffness in the whole test run
F_{cyc}: applied cyclic force
N: life of a sample (the number of cycles until failure)
S_0: static strength
S_{rem}: remaining strength
ϕ: internal friction angle
σ_1: maximum principal stress
σ_3: minimum principal stress
σ_{cyc}: cyclic stress level
$\sigma_{1,\mathrm{cyc}}$: maximum cyclic principal stress
σ_{max}: maximum deviatoric cyclic stress
σ_{min}: minimum deviatoric cyclic stress
τ: shear strength

Determining the Elastic Deformation Modulus From a Compacted Earth Embankment Via Laboratory and Ménard Pressuremeter Tests

R.R. Angelim, R.P. Cunha, M.M. Sales

Abstract. Compacted earth embankments are routinely used in dams and many others infrastructure projects in Brazil. It is common to use fine-grained soils for these embankments, which are placed and compacted in the field at specific values of unit weight and water content. Their design is usually performed using geotechnical parameters from laboratory tests on compacted samples, although in situ tests could emerge as an alternative for determining specific parameters, as such tests can be conducted reasonably rapidly and can somewhat account for local inherent conditions of the soil such as confining stress levels, water content and mineralogical variations. Therefore, this paper explores the application of Ménard-type pressuremeter tests to determine the Young's modulus of compacted soil layers from the side flank of a large-scale earth embankment constructed in the city of Goiânia in the Midwest Region of Brazil. The embankment was compacted under controlled conditions, permitting the extraction of undisturbed soil blocks at distinct levels during its erection. Laboratory tests, such as consolidated isotropic triaxial and oedometer tests, were performed on samples at their natural water content. Young's moduli were derived from these laboratory tests and compared with the elastic moduli measured using the pressuremeter, either directly under different (external) conditions or at normalized levels of the effective confining octahedral stress. This comparison of results enabled the establishment of preliminary statistical correlations between the average (in situ and laboratory) moduli, which will be useful when using the Ménard pressuremeter for a preliminary design or a post-construction check of compacted earth embankments.
Keywords: earth embankment, compacted soil, Ménard pressuremeter, laboratory test, Young's modulus.

1. Introduction

The conventional geotechnical properties of compacted soils fundamentally depend on their mineralogy and physical characteristics. The latter are inherently associated with the local placement conditions (*i.e.*, water content and density) of the compacted layers. In the case of earth embankments, the choice of which soil type to use is restricted to those available from borrowing areas near the site. Compaction tests in the laboratory, and the specifications derived from them, are thus key elements in guiding the design and ensuring that appropriate geotechnical parameters are achieved in the field. Generally speaking, compaction control is adopted as a means of quality assurance during the construction of an embankment, in which the best performance is sought in terms of shearing, compression, seepage and filtering.

In such jobs, quality control is ensured by accounting for the level of compaction energy and uniformity of the earth mass, for instance, by releasing each compacted layer based on the deviation of the soil's moisture content from optimal values and by checking the wet and dry densities. If the construction is well controlled, it is, in principle, assumed that the design values of deformability, strength and permeability will be met.

The presumption that achieving the "desired" range of physical properties during the construction stage of an embankment is sufficient to guarantee its structural stability unfortunately discourages the complementary performance of post-construction field investigations. For instance, in situ testing could be conducted to check the originally estimated geotechnical values or when poorly controlled circumstances are identified.

One additional problem also arises, particularly in Brazil. Several earth dams that have been constructed during the last century for energy generation have never been checked with regard to their actual safety conditions or tested against the newest security standards. The original design parameters from these dams are rarely known, but they could certainly be reestablished through on-site investigations.

This paper advocates one particular method of doing so, at least in regard to the soil stiffness. This method has

Renato Resende Angelim, Ph.D., Associate Professor, Escola de Engenharia Civil e Ambiental, Universidade Federal de Goiás, Praça Universitária, 1488, 74605-220 Goiânia, GO, Brazil. email: tecnoeng@gmail.com.
Renato Pinto da Cunha, Ph.D., Associate Professor, Departamento de Engenharia Civil e Ambiental, Universidade de Brasília, Campus Universitário Darcy Ribeiro Asa Norte, ENC/FT, 70910-900, Brasília, DF, Brazil. e-mail: rpcunha@unb.br.
Maurício Martines Sales, Ph.D., Associate Professor, Escola de Engenharia Civil e Ambiental, Universidade Federal de Goiás, Praça Universitária, 1488, 74605-220, Goiânia, GO, Brazil. e-mail: sales.mauricio@gmail.com.
Submitted on January 13, 2016; Final Acceptance on November 27, 2016; Discussion open until April 28, 2017.

the ability to determine the deformability parameters of an existing compacted earth embankment solely via on-site investigation, specifically through the Ménard pressuremeter test (PMT). The PMT is an attractive approach in addressing this challenge because it can be used to test large volumes of soil, when compared with standard soil samples, and can enable the establishment of parameters already influenced by local placement conditions. The use of the PMT during the initial construction phase can eventually be adopted to guide routine modifications to compaction procedures, thus truly serving as a quality assurance/control mechanism.

The PMT research presented here is related to a real construction case of an earth embankment located at the lateral edge of a roller-compacted concrete dam, with 389 m of extension and erected to a maximum height of 52 m. This dam, named Ribeirão João Leite, was built close to the city of Goiânia, Brazil, and forms the João Leite reservoir that serves this same city.

In a zone within one of the lateral compacted earth embankments, an experimental testing area was established, where pressuremeter tests (along with tests using other in situ devices) were performed together with the retrieval of undisturbed block samples. This was done as the embankment was raised, at specific layers and levels. The entire testing program was part of a thesis (Angelim, 2011) supervised by the Universities of Brasília and Goiás, the major geotechnical institutions of the Brazilian Midwest.

This paper thus provides an overall picture of the earth embankment and its testing site, presenting its main geotechnical characteristics and describing several of the reference laboratory tests conducted on the retrieved samples. It also fully addresses the PMT investigation program. The deformation modulus derived from each laboratory technique was calculated and converted into the corresponding Young's modulus, enabling a cross-comparison with the elastic modulus typically derived through the PMT.

This study is innovative in the sense that the comparative relationship between in situ and laboratory data on real compacted earth structures has rarely been investigated or reported on.

2. Site Location and Details

The city of Goiânia is the capital of the state of Goiás, a large crop-raising frontier (for soybeans, among other grains) with vast flat areas of farmland. A cattle meat industry for export is also well established there. Its metropolitan area has a total population of approximately 2.4 million, being the second largest city in this central region of Brazil and the 12th largest in the country. The Ribeirão João Leite dam was constructed to supply water to this city through the formation of a 10.4 km^2 reservoir, as depicted in Fig. 1.

The crest of the dam lies at an elevation of 752.55 m above sea level, with two laterally confined flank embankments made of compacted soil. In one of them, in a flat zone near the downstream slope (el. 746.00 m), an experimental testing area was established where several in situ tests were conducted. These tests were performed approximately 30 m downstream from the embankment axis, as part of the same doctoral research program. Figure 2 depicts the testing area in the context of the embankment.

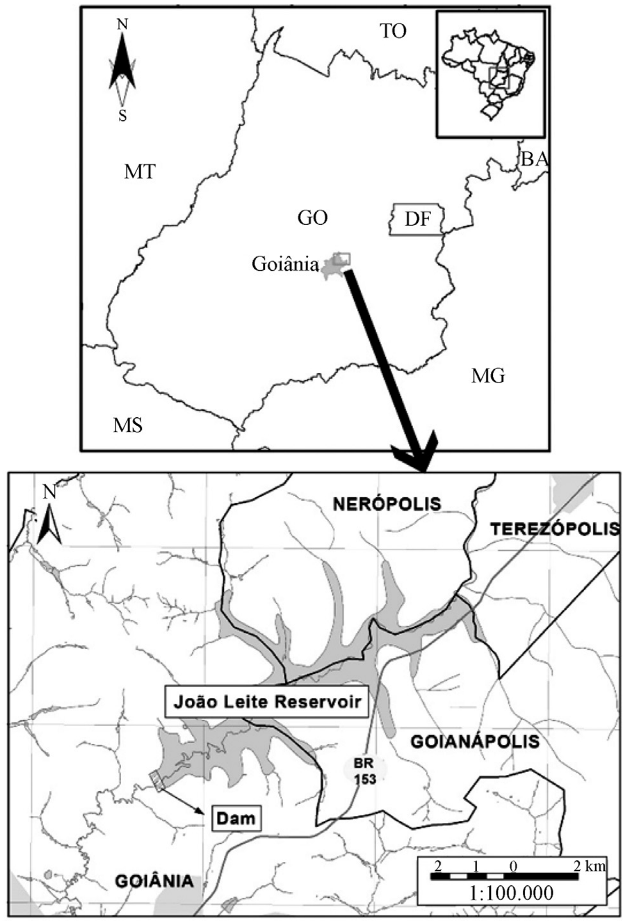

Figure 1 - Location of embankment within Brazilian Midwest.

The embankment was erected in successive layers of approximately 200 mm compacted to the standard Proctor energy, by means of 6 to 8 passages of vibratory sheep foot compaction rollers. Figure 3 presents cross section AA from the testing area. Orientation points A to H can be seen, as well as depth levels. Undisturbed 300 x 300 x 300 mm blocks were retrieved from alternating positions in each representative layer of 1 m in thickness.

For the retrieval of 2 blocks per layer, a trench of approximately 600 mm in depth and dimensions of 2 x 4 m was excavated using a tractor backhoe as each meter of the embankment was completed. The reference level for each sample refers to the depth of the mid-height section of the extracted blocks, as shown in Fig. 3. Once extraction was complete, the trench was manually recompacted, and the erection of the embankment continued.

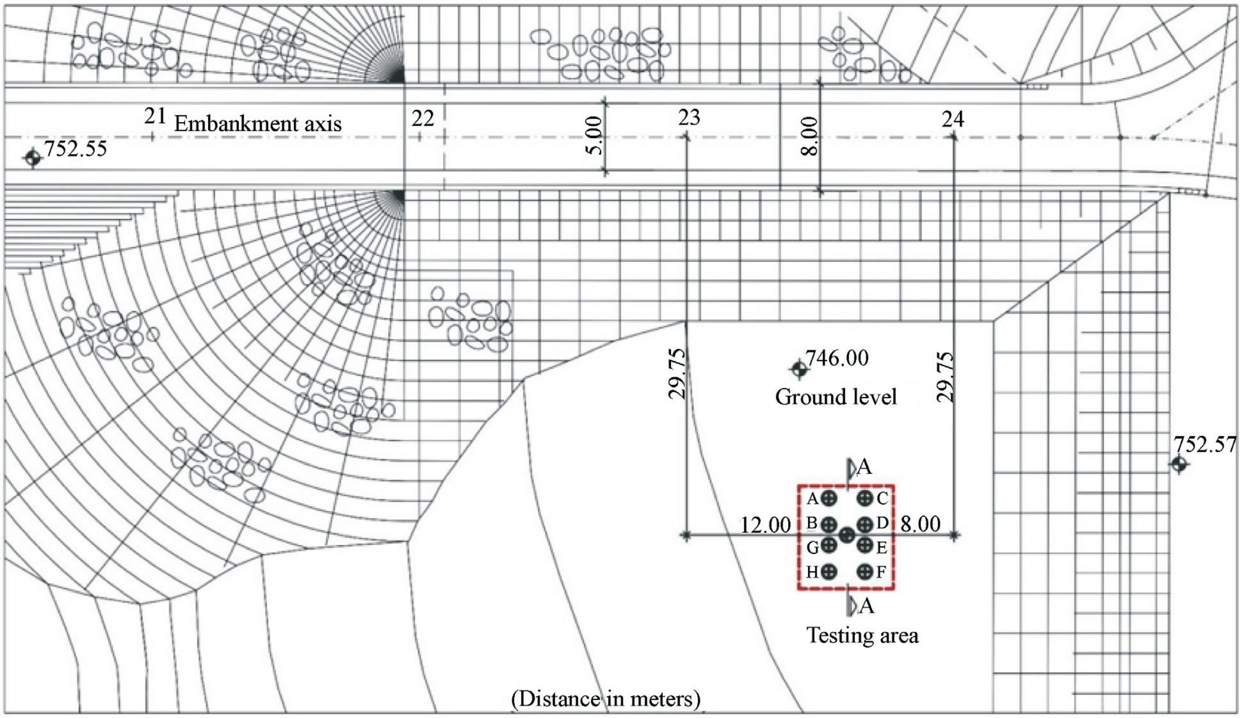

Figure 2 - Sampling and testing location close to the embankment's axis.

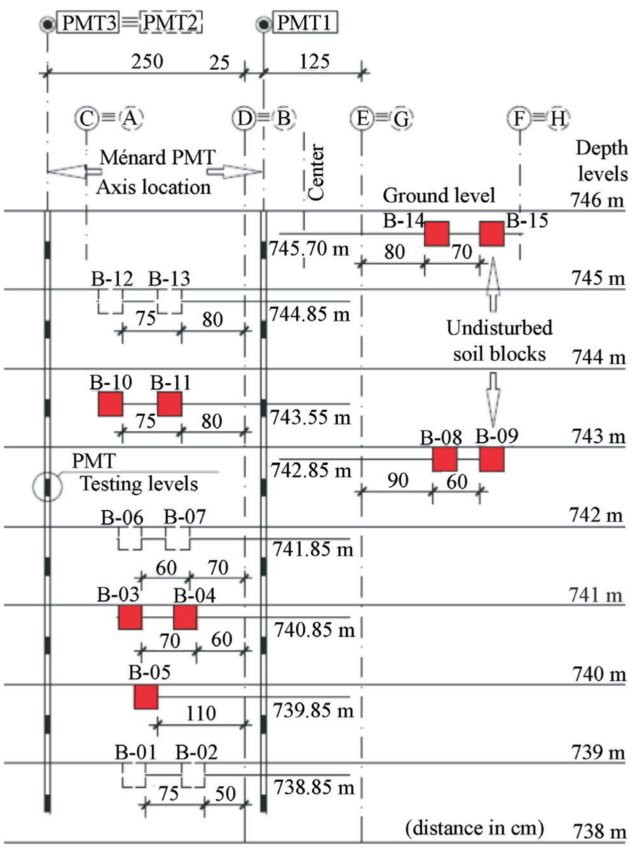

Figure 3 - Cross section AA from testing area.

After finishing the block extraction, in situ tests were conducted near the center of the testing area, as shown in Fig. 4. Several types of tests were performed, including plate load and cone penetration tests. This paper, however, focuses on the results of 24 pressuremeter tests performed in three pre-bored holes (PMT 1 to 3). As depicted in this and the previous figure, PMTs were performed in all representative layers, at horizontal distances that were less than 2 m from the corresponding undisturbed blocks. The reference level of each pressuremeter test refers to the depth of the mid-height section of the central expanding membrane.

3. Sampling and Laboratory Program

3.1. Characterization and compaction

Three samples retrieved from each undisturbed block were investigated in the laboratory to determine the physical characteristics of the soil. Figure 5 presents the results along the depth direction for the water content (*w*), degree of saturation (*S*), unit weight (γ), dry unit weight (γ_d) and void ratio (*e*). Note the existence of three data points per representative layer and the over all average value for the entire profile (considering all points). As a general rule, layers with above-average water content had a unit weight below the respective average, and the converse was also true.

Table1 extends the physical properties along the depth direction based on additional tests performed on samples from the undisturbed blocks. Compaction tests yielded

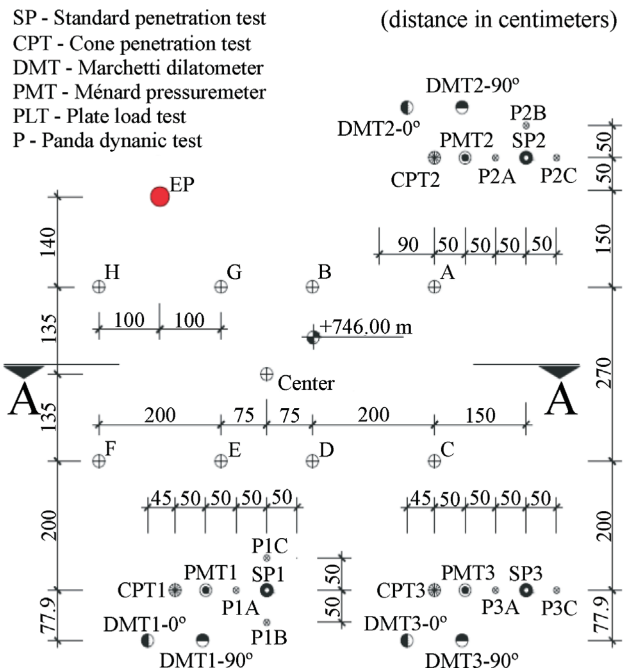

Figure 4 - Detailed location of in situ tests in testing area.

knowledge of the optimum water content (w_{opt}) and maximum dry unit weight (γ_{dmax}) of each layer. On-site control of the embankment using the Hilf (1959) methodology yielded knowledge of the water content and the relative compaction (*RC*) of the layers. Quality control during construction demanded that each layer had a minimum *RC* of 96% and a maximum deviation of w_{opt} of -1 to +2% by means of either on-site or laboratory control. The Atterberg limits and indices were determined at each layer, indicating an inactive soil of medium plasticity. The unified classification system (D2487-11 ASTM, 2011a) indicated clay layers intermingled with clayey silt layers of low plasticity.

These results can be explained in terms of the mineralogy of the material, as extracted from a nearby borrowing area. X-ray tests, presented in Angelim (2011), indicate a major presence of gibbsite with minor traces of caulinite minerals in this soil. Oxides and hydroxides of aluminum and iron are present. These minerals are typical of superficial, highly weathered tropical soils. They also explain the observed low values of activity and plasticity.

Tropical soils also have another intrinsic feature: their granulometric composition tends to change depending on whether tests are performed with or without a dispersing agent. Figure 6 presents the results obtained with and without such a component (sodium metaphosphate, based on the Brazilian standard (NBR 7181- ABNT, 1988). According to Table1, with the dispersing agent, the average content of clay particles is 36.6%. Without it (not shown in this table), this content drops to 0.0%. The agent promotes the breakage of particle aggregates into micro- and macro-concretions, thereby changing the grain size. For instance, based on granulometry tests in the presence of the dispersing agent, the soil can be classified as sandy clay. In tests without the agent, the classification changes to silty sand.

3.2. Oedometertests

Oedometer tests were also performed on undisturbed samples at their natural water content. One sample with dimensions of 100 x 30 mm (diameter x height) was tested per layer, following the Brazilian standard (NBR 12007 -

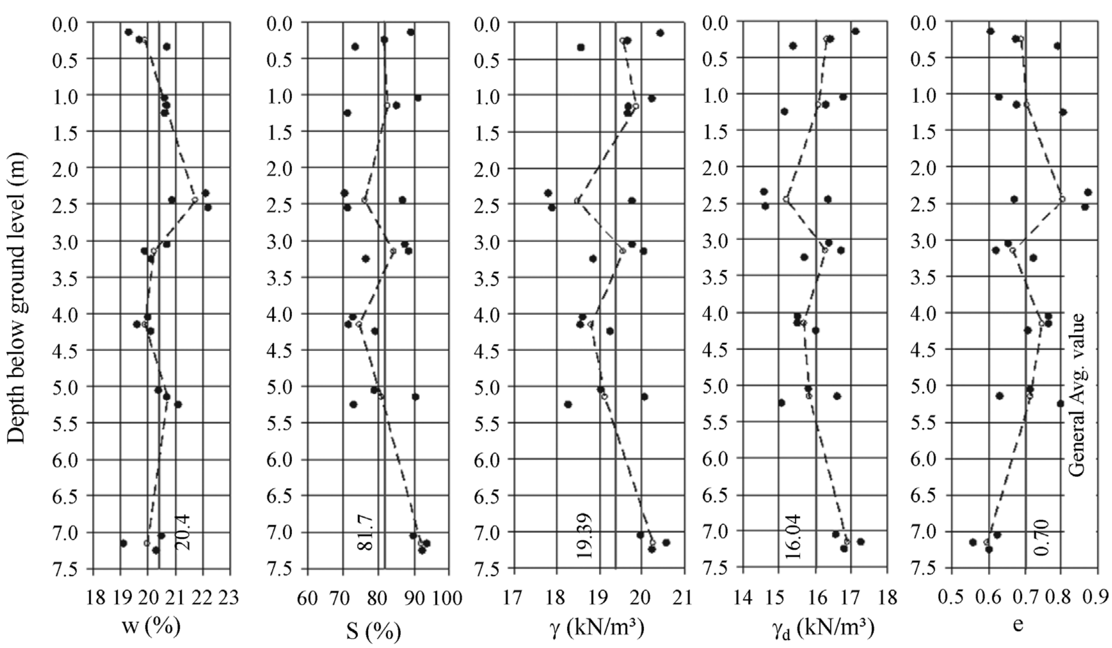

Figure 5 - Main physical indices for the compacted soil along depth (levels 738.85 to 745.70 m).

Table 1 - General physical indices for the compacted embankment along depth.

Depth level (m)	USCS*	Clay content* (%)	Laboratory† compaction tests		Field on-site tests‡		Atterberg Limits and soil indices§			
			w_{opt}(%)	γ_{dmax}(kN/m^3)	w(%)	RC(%)	w_L(%)	w_P(%)	I_P(%)	I_a(%)
745.70	CL	40.1	20.4	16.6	19.6	98.7	45	26	19	0.47
744.85	ML	36.6	20.6	16.5	21.1	100.4	47	29	18	0.49
743.55	ML - CL	35.7	21.1	16.3	20.7	100.9	46	28	18	0.50
742.85	ML - CL	37.8	20.5	16.4	19.1	98.2	46	28	18	0.48
741.85	CL - ML	27.5	20.8	16.2	18.3	98.6	46	27	19	0.69
740.85	ML - CL	39.0	19.9	16.5	19.5	96.3	46	28	18	0.46
739.85	CL	37.5	18.6	17.0	19.7	96.7	43	25	18	0.48
738.85	CL	38.7	18.8	16.7	19.1	99.3	44	25	19	0.49
Average		36.6	20.0	16.5	19.6	98.6	45.3	27	18.3	0.50

Note: *USCS = Unified Soil Classification System and clay content from grain size analyses with dispersing agent; †Tests performed on disturbed soil samples retrieved in the embankment after its construction (w_{opt} = optimum water content, γ_{dmax} = maximum dry unit weight); ‡Tests performed with undisturbed samples retrieved in the embankment just after each layer construction (w = water content of the soil, RC = relative compaction); §Standard characterization tests with disturbed soil samples retrieved in the embankment (w_L = liquid limit, w_P = plastic limit, I_P = plastic index, I_a = soil activity).

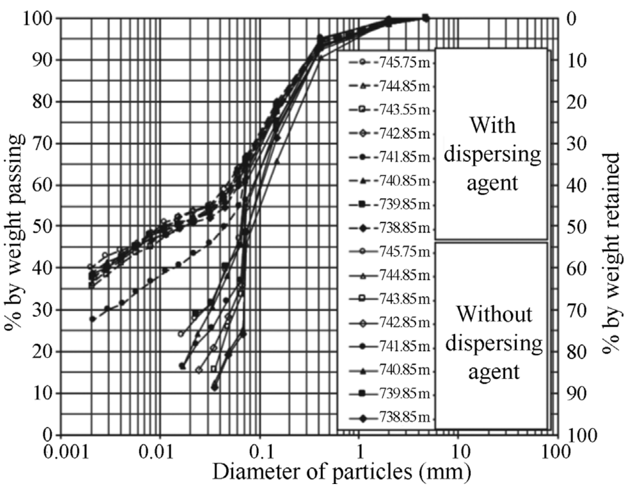

Figure 6 - Grain size curves of soil along depth.

ABNT, 1990). Figure 7 presents plots of the logarithm of the vertical pressure (σ_V) *vs.* the void ratio. Pressure was applied from 12.5 to 1600 kPa, in both the increasing and decreasing directions. Measurements were acquired from 6 sec to 8 h at each pressure level. A humid rag on top of the sample maintained a constant water content throughout the loading sequence. The values of the (virtual) preconsolidation pressure (σ_P), effective overburden pressure (σ'_{V0}), compression index (C_c) and overconsolidation ratio (OCR) were determined. The σ'_{V0} values were calculated considering the final height of the embankment, assuming average values of unit weight. The value of σ_P was determined using the empirical technique proposed by Pacheco Silva (1970) based on a simple graphical method.

Table 2 presents these variables together with the interpreted values of the soil constrained modulus (M) and Young's modulus (E_{YO}) at four distinct pressure levels. M and E_{YO} are defined in accordance with Eqs. 1 and 2:

$$M = \frac{\Delta\sigma_V}{\Delta\varepsilon_V} \tag{1}$$

$$E_{YO} = \frac{M(1+\nu)(1-2\nu)}{(1-\nu)} \tag{2}$$

where ε_V and ν are the volumetric strain and the Poisson's ratio, respectively. Note that E_{YO} is the Young's modulus derived by applying an elastic equation to raw oedometer values. The average value and the corresponding coefficient of variation (CV) are also given for the series of E_{YO} values.

The pressure intervals were chosen in accordance with the typical behavior of oedometric curves. Two intervals were in the preconsolidated range (0-200 and 200-400 kPa), and two were in the normally consolidated range (400-800 and 800-1600 kPa). The values in the final stages of the curve were considered to be truly in the virgin state (OCR = 1) based on estimations of σ_P and the shape of the oedometric curves.

The values of the preconsolidation pressure were well above those of the overburden pressure at each layer, yielding the conclusion that they were indeed a direct result of the applied compaction energy. Queiroz (2008) also reached a similar conclusion based on dilatometer tests performed on this same earth embankment.

Figures 8 to 10 present the relationship between the Young's modulus derived from constrained modulus and

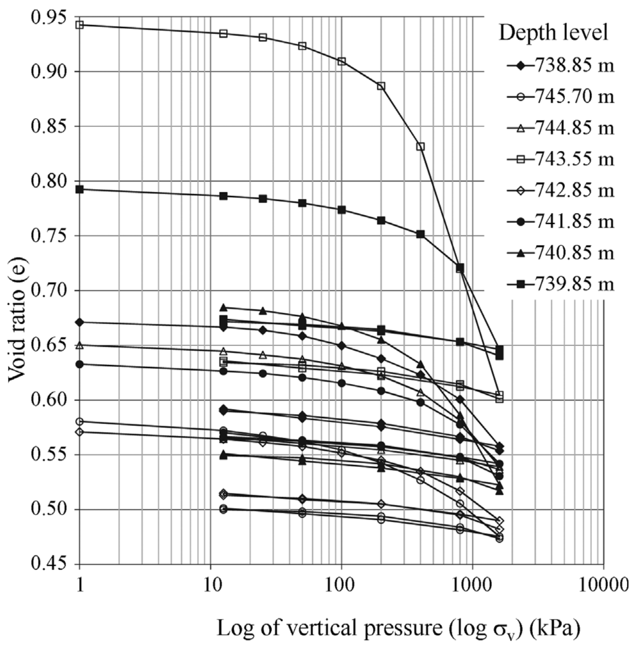

Figure 7 - Oedometric curves of soil along depth.

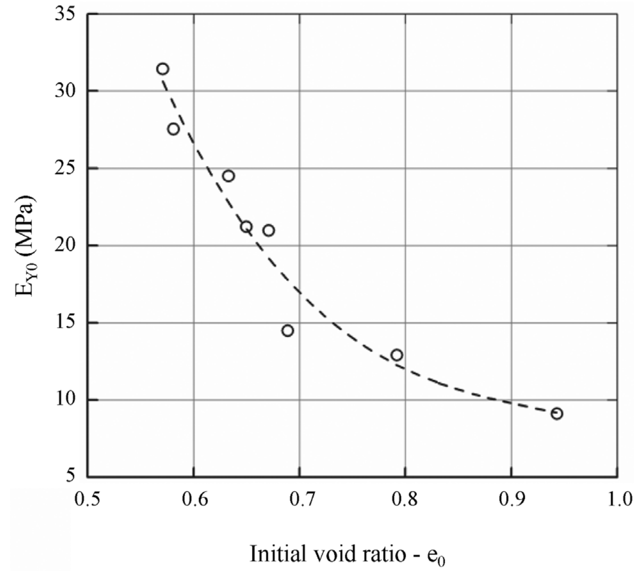

Figure 8 - Relationship between initial void ratio and Young's modulus calculated from oedometric test results at the stage of 800-1600 kPa.

the initial e, γ, and RC values of the samples. A clear nonlinear behavior was observed in all curves.

3.3. Triaxial tests

Triaxial tests were also performed on undisturbed samples at their natural water content. One sample with dimensions of 50 x 100 mm (diameter x height) was tested per layer, following the D7181-11 standard (ASTM, 2011b). Figure 11 presents plots of the deviatoric stress (σ_D) *vs.* the axial strain (ε_a) for a particular isotropic confining pressure (σ_C). This latter pressure was varied from 49 to 392 kPa in the tests, in accordance with the previously presented ranges of preconsolidation and vertical overburden pressures.

All triaxial tests were performed in two successive stages, *i.e.*, isotropic consolidation followed by drained shear. The shear velocity was taken to be 0.009 mm/min to avoid any eventual build-up of pore pressure. An external load cell was used to measure the applied load. The vertical

Table 2 - Results from oedometer tests on undisturbed samples at natural water content.

Depth level (m)	σ'_{v0} (*) (kPa)	σ_P (†) (kPa)	C_C (‡)	OCR	Constrained modulus§ (MPa)				Young's modulus# (MPa)			
					M_1 (MPa)	M_2 (MPa)	M_3 (MPa)	M_4 (MPa)	E_{YO1} (MPa)	E_{YO2} (MPa)	E_{YO3} (MPa)	E_{YO4} (MPa)
745.70	5	295	0.103	59	8	20	30	41	6	13	20	28
744.85	23	440	0.140	19	12	22	25	31	8	15	17	21
743.55	49	300	0.382	6	7	7	7	14	5	5	5	9
742.85	63	380	0.090	6	12	31	35	47	8	21	24	31
741.85	83	475	0.120	6	13	33	33	36	9	22	22	24
740.85	103	435	0.209	4	10	15	14	21	7	10	10	14
739.85	123	600	0.249	5	13	28	24	19	9	19	16	13
738.85	143	455	0.143	3	10	22	30	31	7	15	21	21
Average	-	423	0.179	-	11	22	25	30	7	15	17	20
CV (%)									19	38	38	38

Note: *Effective vertical pressure at the center of the undisturbed block at depth level; †Preconsolidation pressure; ‡Compression index at the virgin compression zone of the curve; §Constrained modulus directly from oedometer ($\Delta\sigma_V/\Delta\varepsilon_V$) inclinations at distinct ranges of vertical pressureσ_V (M_1@0-200 kPa, M_2@200-400 kPa, M_3@400-800 kPa, M_4@800-1600 kPa); #Young's modulus derived with constrained values at same pressure levels ($E_{YO} = M(1+\nu)(1-2\nu)/(1-\nu)$, where ν = 0.33, Poisson'sratio).

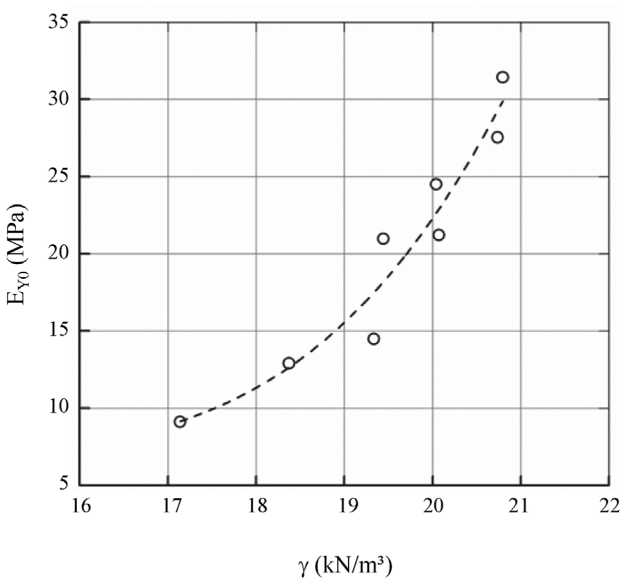

Figure 9 - Relationship between unit weight and Young's modulus calculated from oedometric test results at the stage of 800-1600 kPa.

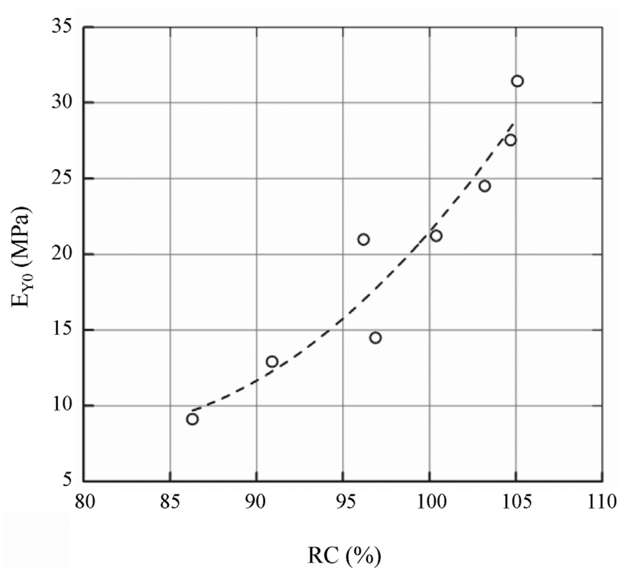

Figure 10 - Relationship between relative compaction and Young's modulus calculated from oedometric test results at the stage of 800-1600 kPa.

and horizontal strains were obtained using a mechanic deflectometer and the water volume control into the chamber, respectively.

As a general rule, it was observed that the stress-strain curves for low confining pressures exhibited behavior characteristic of a strain-softening mode, typical of overconsolidated clays and dense sands. As the σ_c value approached the virgin state of the soil (upper range of values), as seen in Fig. 11, there was a tendency toward homogenization of the results in a strain-hardening mode.

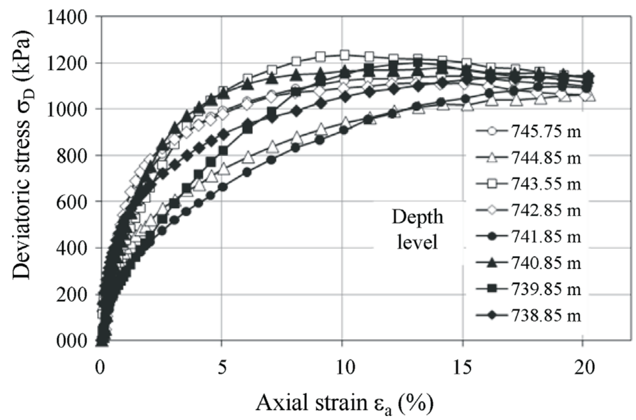

Figure 11 - Typical CID triaxial curves (σ_c = 392 kPa).

Table 3 presents the results of the consolidation stage for four distinct σ_c intervals chosen to represent the entire spectrum of pressures. The directly measured values of the bulk modulus (B) and the interpreted values of the Young's modulus (E_{IST}) are defined in accordance with Eqs. 3 and 4:

$$B = \frac{\Delta\sigma_C}{\Delta\varepsilon_V} \tag{3}$$

$$E_{IST} = 3B(1-2\nu) \tag{4}$$

As expected, the modulus values increased with increasing confining pressure because of the simple fact that a higher pressure resulted in a lower void ratio of the sample, thereby increasing the contact between particles and the stiffness of the soil structure.

Table 4 presents the results for the subsequent shearing stage, at the same confining pressures as before. Three levels of deviatoric stress were used to define the Young's modulus, which was directly calculated in accordance with Eq. 5:

$$E_T = \frac{\Delta\sigma_D}{\Delta\varepsilon_a} \tag{5}$$

The tangent modulus (E_{TI}) in the initial stage (2 to 3 initial data points) and the secant moduli at 25 and 50% of the maximum σ_D value (E_{T25} and E_{T50}, respectively) were determined at each layer, as seen in this table. The tangent modulus was easier to determine and less subject to variations among the data points at each level. Nevertheless, as observed by Angelim (2011), the tangent and secant moduli tended to be quite similar.

The Young's modulus decreased as the level of deviatoric stress at which it was determined increased. The values at 50% (E_{T50}) were consistently lower than those at 25% (E_{T25}) or in the initial stage (E_{TI}). This table also presents the effective cohesion intercept and the angle of internal friction derived from the drained failure envelope in the triaxial test.

Table 3 - Results from consolidated isotropic triaxial drained tests (CID) at natural water content – shearing stage.

Depth level (m)	Bulk modulus* (MPa)				Young's modulus† (MPa)			
	B_1 (MPa)	B_2 (MPa)	B_3 (MPa)	B_4 (MPa)	E_{IST1} (MPa)	E_{IST2} (MPa)	E_{IST3} (MPa)	E_{IST4} (MPa)
745.70	3	4	25	21	3	4	26	21
744.85	3	5	5	7	3	5	5	7
743.55	2	4	4	6	2	4	5	7
742.85	3	4	7	14	3	4	8	15
741.85	2	3	5	8	2	3	5	8
740.85	4	5	9	27	4	5	9	28
739.85	4	6	10	16	5	6	10	17
738.85	6	7	7	14	6	7	7	15
Average	4	5	9	14	3	5	9	15
CV (%)					32	25	72	49

Note: *Bulk modulus directly from isotropic compression curve ($\Delta\sigma_C/\Delta\varepsilon_V$) inclinations at distinct values of isotropic confining pressure σ_C (B_1@49 kPa, B_2@98 kPa, B_3@196 kPa, B_4@392 kPa); †Young's modulus derived with bulk values at same pressure levels ($E_{IST} = 3B(1 - 2\nu)$, where $\nu = 0.33$, Poisson's ratio).

By comparing Tables3 and 4, one observes that in regard to the Young's modulus alone, there was a mild tendency for the value to increase along the depth direction. This behavior was perhaps more pronounced for the moduli in the isotropically consolidated case. This behavior can, in some sense, be attributed to the levels of pressure adopted in the laboratory, which were well below the estimated values of σ_P (Table 2) and overlapped with the range of the effective overburden pressures.

The tables also show the average Young's modulus and the corresponding coefficient of variation (*CV*) for each series. The shear-derived values were distinctly more erratic (with higher *CVs*) than those obtained in the isotropically consolidated case. By comparing these data with those presented in Table 2, one also observes that the oedometer-derived Young's moduli were less subject to variations, *i.e.*, exhibited slightly less sensitive values (lower scatter).

The extent of variability along the depth direction for all deformation moduli can be attributed to a combination of factors. Minor effects of disturbances during sampling and typical experimental errors (trimming, assembling, and position of load cell and techniques of strain measurements for triaxial tests) may contribute to scatter results. However, the effects of soil heterogeneity into each compacted layer seems to be the key point for these results, since the sample height was less than half of layer thickness (200 mm).

Tables 2 to 4 indicate a highly overconsolidated profile (with an OCR of approximately 60 at the surface), in which the OCR decreases with increasing depth. The layers behave as cohesive-frictional materials, with very high cohesion intercepts and friction angles typical of medium-dense silty sands (as classified according to grain size distribution without a dispersing agent). Depending on the laboratory test, the derived Young's moduli are typical of loose or medium-dense sands (with the exception of the E_{TI} values). These results appear to be consistent with the amount of applied compaction energy and the nature of the material in its local state.

4. Pressuremeter Testing Program

The major attraction of the PMT is the fact that it constitutes a simple boundary-value problem of soil mechanics, being the only in situ test that can be theoretically modeled as an expansion of an infinitely long cylindrical cavity. This offers the possibility of simultaneously deriving both the in situ deformation and strength parameters when applying any of the several available cavity expansion models.

Cunha (1994) has demonstrated the potential use of this tool for deriving parameters from alluvial deposits. Nevertheless, the Brazilian experience is still nascent and is restricted to the validation of international experience under local conditions.

With regard to tropical or compacted soils, previous work is rather limited. Ortigão *et al.* (1996) performed one of the first PMT in the Midwest Region of Brazil for the underground project of the city of Brasília. This successful experience has encouraged further tests for the design of Goiânia's metro line (Cunha *et al.*, 2004), this time using traditional interpretation methods, such as those presented by Baguelin *et al.* (1978).

For the present embankment, Ménard pressuremeter tests (PMT 1 to 3) of the G-BX type were performed, as shown in Figs. 3 and 4. They were performed in pre-bored holes excavated to the testing depth using a 63.5 mm diam-

Table 4 - Results from consolidated isotropic triaxial drained tests (CID) at natural water content - shearing stage.

Depth level (m)	c' (*) (kPa)	ϕ' (†) (°)	Initial Tangent Young's‡ Modulus E_{Ti} (MPa)				25% Tangent Young's$ Modulus E_{T25} (MPa)				50% Tangent Young's# Modulus E_{T50} (MPa)			
			Conf. pressure σ_c (kPa)				Conf. pressure σ_c (kPa)				Conf. pressure σ_c (kPa)			
			49	98	196	392	49	98	196	392	49	98	196	392
745.70	148	27	107	251	268	77	11	24	25	60	10	16	20	28
744.85	80	30	195	257	135	191	44	257	36	40	20	11	12	10
743.55	69	33	178	243	226	187	11	5	9	27	3	4	6	23
742.85	93	30	422	398	149	134	422	398	47	55	53	39	35	35
741.85	114	30	308	163	188	51	308	15	22	16	28	5	15	7
740.85	134	30	112	263	162	83	29	58	89	40	9	39	42	28
739.85	142	29	58	191	310	67	45	41	32	17	7	15	13	13
738.85	72	32	72	130	68	316	69	57	51	56	40	36	14	15
Average	107	30	181	237	188	138	35	33	39	39	21	21	20	20
CV (%)			69	34	41	64	64	66	63	45	83	72	63	50

Note: *Eff. cohesion intercept from failure envelope; †Eff. angle of internal friction – inclination from failure envelope; ‡Tangent Young's modulus directly from triaxial ($\Delta\sigma_D/\Delta\varepsilon_a$) inclination of deviatoric stress *vs.* axial strain at initial stage of the curve; $Similar modulus but derived with σ_D @ 25% of max. value; #Similar modulus but derived with σ_D @ 50% of max. value.

eter auger that resulted in good quality holes. Figure 12 presents some views of the used auger.

The tests were performed in equal pressure increments at each representative layer once the entire embankment was completed. All of these tests were performed in accordance with the procedures prescribed by the French standard (XP P94-110-2- AFNOR, 1999). The initial data reduction also followed this standard; it was performed by applying calibration-related corrections regarding the membrane resistance and system compliance to the raw data and by removing the initial recompression stage of the PMT curve (up to the in situ horizontal stress).

Figure 13, for instance, presents the cavity pressure *vs.* volume curves at all testing depths for the PMT1 test. It is evident that the linear "pseudo elastic" phase was followed by a plastic regime, in which the limit pressure was approached.

For each PMT, two unload-reload cycles were performed. Figure 14 presents a typical corrected curve in which the pseudo elastic phase and the first unload-reload loop are well defined by pressure points (p_1-p_2 and p_3-p_4, respectively).

Figure 12 - Auger used to excavate pre-bored holes to perform PMT tests.

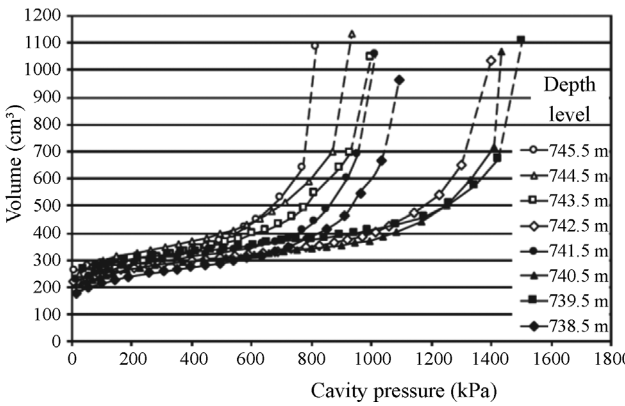

Figure 13 - Pressure *vs.* volume curves – PMT1 tests.

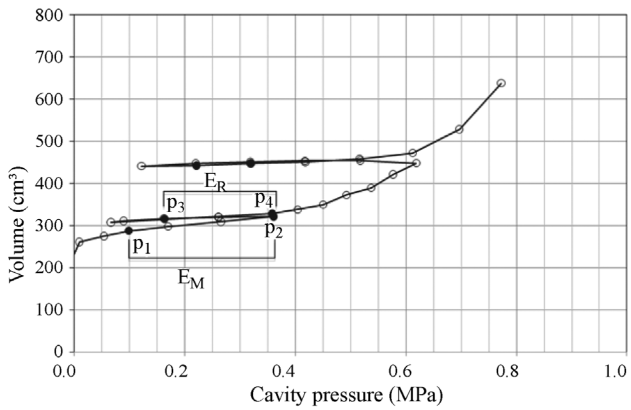

Figure 14 - Definition of pressure points and moduli from Ménard PMT curves.

Using the defined pressures (p_1 to p_4) and the corresponding volumes (v_1 to v_4), it was possible to derive the elastic moduli of the PMT in both the pseudo elastic phase (elastic modulus E_M) and the first loop cycle (E_R). For instance, according to Baguelin *et al.* (1978), Eq. 6 can be used to derive the pressuremeter modulus:

$$E_M = 2(1+v)\left(v_s + \frac{v_1 + v_2}{2}\right)\frac{(p_2 - p_1)}{(v_2 - v_1)} \tag{6}$$

where v_s is the initial volume of the expanding membrane (5.077 x 10^5 mm^3). This same equation can be used to derive E_R by simply replacing v_s with the appropriate pressure and volume variables.

Figure 15 presents plots of the pressuremeter moduli E_M and the loop moduli E_R along the depth direction for the three PMT tests. It also shows the average trend (thick line) calculated based on all results. As is typical, the loop moduli tended to be considerably higher than the standard PMT moduli as a result of several factors, including disturbance effects and the average applied pressure level (Cunha, 1994).

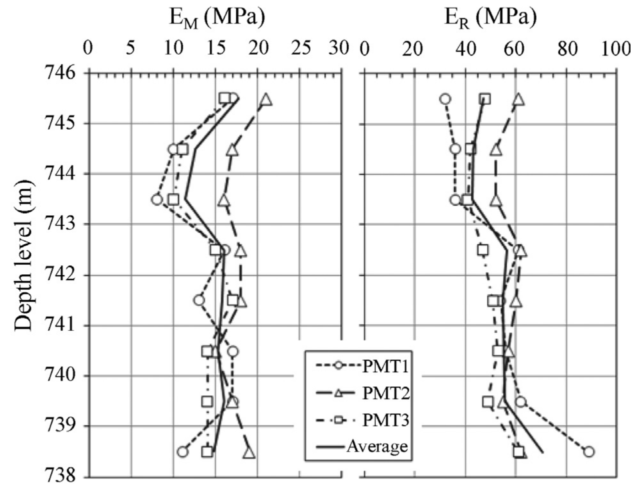

Figure 15 - Elastic moduli from PMT along depth.

Although they are not shown, the *CVs* from the PMT series corresponding to this latter figure varied from 10.5 to 26.2% (valid only for the average E_M), *i.e.*, lower than the equivalent values obtained using the laboratory techniques.

5. Results and Discussion

5.1. Direct comparison of moduli

The average value of the elastic pressuremeter modulus E_M (Fig. 15) was adopted as the reference against which all of the results from the laboratory tests were compared. This stiffness calculated using this in situ device is the value that is generally used in design or to evaluate empirical correlations.

In fact, E_M was originally defined as a Menárd modulus, according to Baguelin *et al.* (1978), being "something roughly equivalent to a Young's modulus". It is certainly an elastic property of the soil, is directly used by these and other authors, and is sometimes corrected using an empirical (α) factor in settlement equations in the framework of the theory of elasticity.

Figures 16 to 18 present direct comparisons of the reference modulus with the values derived from the oedometer measurements and from the triaxial tests (both the consolidation and shearing stages). It is clearly apparent that there is no clear trend among the comparisons, *i.e.*, either the PMT E_M modulus fits better with the upper range of the laboratory results (in the case of the consolidation stage of the triaxial tests) or it lies within the derived spectrum of the data (in the case of the oedometer tests). At certain specific depths, it falls into the lower range of the results, such as at depths of 742/743 m in the shearing stage of the triaxial tests.

Direct comparisons between pressuremeter results and the soil properties deduced from laboratory tests are inevitably misleading. As stated by Mair & Wood (1987), "exact equality of aspects of stress-strain behavior such as

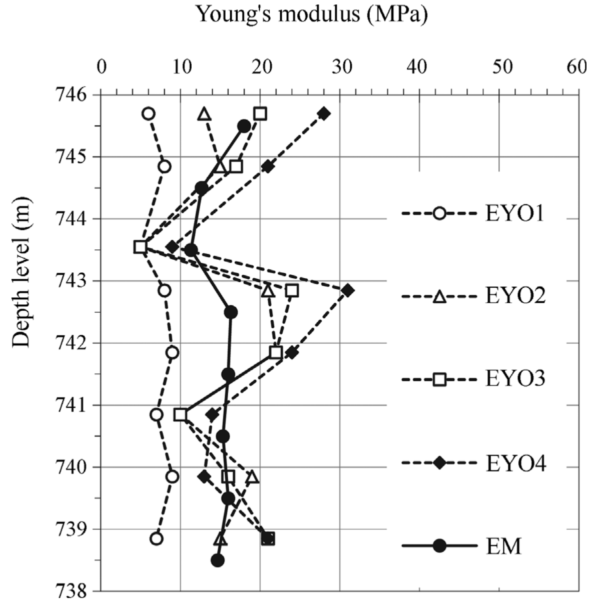

Figure 16 - Comparison of Young's moduli from PMT and oedometer tests.

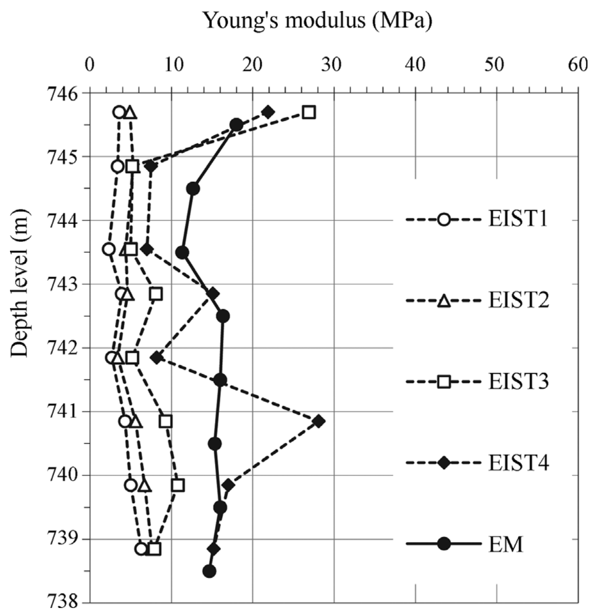

Figure 17 - Comparison of Young's moduli from PMT and triaxial tests – consolidation stage.

stiffness or strength deduced from tests which subject soils to different modes of deformation should not be expected, as most soils are anisotropic in their stress-strain behavior as a result of their depositional and subsequent history".

Indeed, the deformation around the pressuremeter corresponds to the deformation that could be imposed in a plane-strain compression or extension test on a horizontal sample, as previously noted by Mair & Wood (1987) and experimentally demonstrated by Cunha (1994) by means of

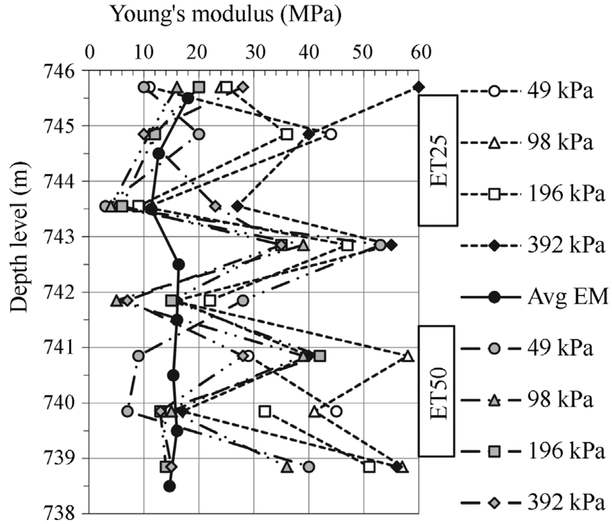

Figure 18 - Comparison of Young's moduli from PMT and triaxial tests – shearing stage.

comparable results for a sedimentary granular deposit in Canada.

The deformation mode of the PMT clearly deviates from typical modes imposed on soil samples in oedometer tests or the compression and shearing stages of triaxial tests, as graphically illustrated by Wood & Wroth (1977). It also shears the soil at rather different stress and strain rates compared with those in the laboratory. Moreover, the compacted layers of an earth embankment are truly anisotropic in nature, given their rather peculiar mode of execution. According to Ortigão *et al.* (1996), for PMT tests in a tropical soil, the PMT moduli are an "index" of the soil stiffness under shearing in a pseudo elastic manner with strains below 0.1% in the horizontal direction.

In essence, there are several factors that hamper the direct comparisons presented in Figs. 16 to 18, such as the inherent anisotropy and heterogeneity of the soil, the distinct deformation modes, and the stress and strain levels associated with each testing technique. The aforementioned comparisons are included to illustrate the difficulties one would typically encounter in practice when benchmarking field data. They clearly expose the average differences and variations exhibited by the in situ (elastic) moduli derived using a pressuremeter with respect to the results of the "known" techniques applied in the laboratory to undisturbed samples. In this sense, these comparisons are didactically illustrative of a practical problem.

The influence of the levels of stress and strain under the same test and soil conditions can also be observed when comparing the pressuremeter E_R and E_M values, as done previously in Fig. 15. Such a comparison clearly highlights the difficulties expressed above, indicating that any comparison of soil moduli obtained using different techniques should attempt to account, whenever possible, for inherent differences in the tests (stress and strain levels, representativeness of samples) and the soil (anisotropy, structure, in situ stresses).

In average terms, however, these differences are not striking, perhaps because different influences may tend to "cancel out" the disparities in the data. For instance, Fig. 19 presents a direct comparison between the average Young's moduli determined using the tested techniques (pressuremeter E_M or E(PMT), oedometer E_{YO} or E(OED), and triaxial E_{IST} and E_{T50}) together with the corresponding ranges of the results. This figure also presents the coefficient of variation (*CV*) for each series.

The presented averages include all data for each test, regardless of the depth or strain/stress levels. The differences in the average results among the PMT and the other laboratory tests are not large.

Because the PMT also tests a large volume of soil surrounding the probe, it appears to yield a more homogeneous (average) modulus, with lesser differences between the maximum and minimum results. Consequently, its coefficient of variation was the smallest among all derived *CVs*, possibly indicating a beneficial feature of this test despite the difficulties in referencing its data to known levels of stress or strain. The triaxial data, on the other hand, tended to exhibit a large scatter in the results. This is reflected in *CVs* above 50%, as presented in the same figure.

5.2. Comparison at a reference stress level

To further investigate the influence of a given external variable on the derived modulus, an additional set of analyses was performed.

In this case, the stress level associated with each modulus was defined and compared with respect to a unique reference value. This value was the octahedral stress, which is defined in accordance with Eq. 7 (Smith, 2013):

$$\sigma_{OCT} = \frac{\sigma_1 + \sigma_2 + \sigma_3}{3} \tag{7}$$

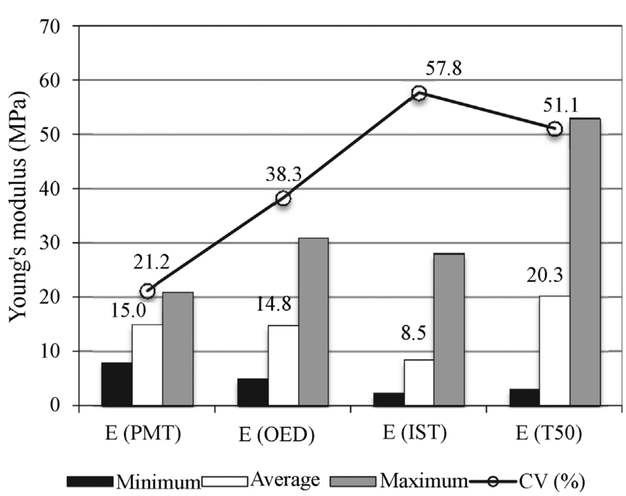

Figure 19 - Overall comparison of range and average values of Young's modulus.

where σ_1, σ_2 and σ_3 are the principal stresses in an element of soil. The octahedral stress represents the normal stress on the octahedral plane, a plane that represents the stress space formed by the three principal stress axes. σ_{OCT} is also the mean value of the three principal stresses in the applied (external) stress system (Smith, 2013) and thus is a true benchmark variable.

The results of the pressuremeter test at each depth were then related to the corresponding values of the effective octahedral stress (σ'_{OCT}) in the absence of a saturated medium. This was done using Eqs. 8 and 9:

$$\sigma'_{OCT} = \frac{(\sigma'_{v0} + 2p_m)}{3} \tag{8}$$

$$p_m = \frac{(p_1 + p_2)}{2} \tag{9}$$

where p_1 and p_2 are the limits of the pseudo elastic phase of the PMT and p_m is the related average cavity pressure. Values in the range of 234 to 451 kPa were calculated for all test levels.

Likewise, the Young's modulus values derived from the triaxial tests in the shearing stage were also associated with their respective σ'_{OCT} levels, using Eq. 10:

$$\sigma'_{OCT} = \frac{(\Delta\sigma_D + 3\sigma_C)}{3} \tag{10}$$

where σ_D and σ_C are the deviatoric and isotropic confining stresses, respectively. This calculation was performed solely for the E_{T50} modulus.

In the case of the results from the consolidation stage of the triaxial tests, the values of E_{IST4} for a confining pressure of 392 kPa (see Table 3) were used directly, as this pressure lies within the field range of the octahedral stresses. For this reason, one also could expect less scatter in the comparison between this variable and the PMT results. This is apparent, for instance, in Fig. 17, where a reasonable comparison between E_{IST4} and the average E_M is observed.

Once the corresponding σ'_{OCT} was established for each test (PMT and triaxial), a simple calculation procedure was performed at each depth level. In the case of the PMT, the average E_M value for PMT 1 to 3 was determined along with the normalized modulus E_M/σ'_{OCT}. In the case of the shearing stage of the triaxial tests, the normalized modulus E_{T50}/σ'_{OCT} was determined for each considered level of σ_C. In the case of the consolidation stage of the triaxial tests, the values of E_{IST4} for a σ_C of 392 kPa were used directly.

Thus, for each depth level, the normalized values of E_M/σ'_{OCT} were plotted together with E_{T50}/σ'_{OCT}, including the best fit (or tendency) determined from the triaxial data. This direct comparison enabled the determination of the values of E_{T50} that were closer to or within the range of the field levels of the PMT σ'_{OCT} values. For instance, Fig. 20 shows the comparison for a depth level of 738.85 m, where one ob-

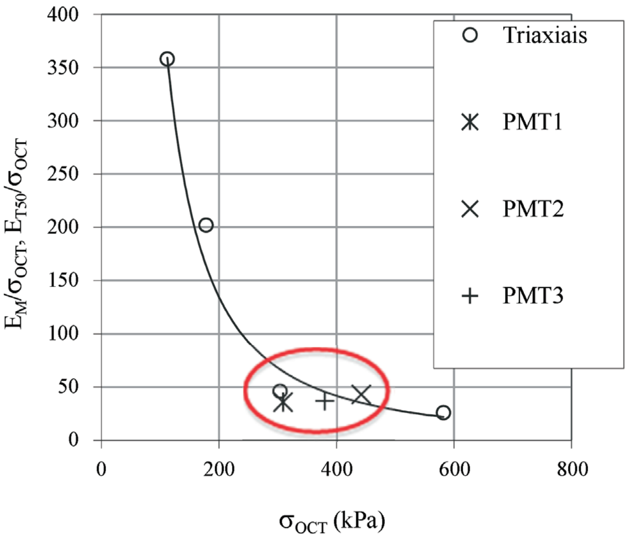

Figure 20 - Normalized moduli from triaxial and PMT data (738.85 m).

serves that only one value of E_{T50} could be considered for further comparison (in this case, the value relative to a σ_C of 196 kPa, *i.e.*, 14 MPa, according to Table 4). This procedure enabled the selection of the 12 data points in Table 4 from among the 32 total results or E_{T50}.

With respect to the consolidation stage, all 8 data points for E_{IST4} in Table 3 were used in the following calculations, as previously noted.

With the knowledge of the triaxial E_{IST} and E_{T50} moduli and the PMT modulus E_M that were related to similar (but not equal) values of the effective octahedral stress at each depth, it was possible to derive an "overall" average value for the profile as a whole. Figure 21 presents the corresponding comparison between the data, presented in a similar fashion as in Fig. 19 for the direct, non-corrected results. The former figure also highlights the minimum and maximum values and the coefficient of variation (*CV*) for each series.

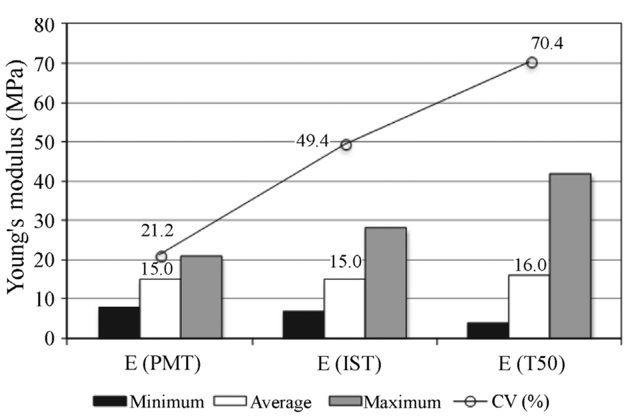

Figure 21 - Overall comparison of range and average values of Young's modulus.

By comparing Figs. 20 and 19, one observes that in general, the average Young's modulus values derived from the triaxial tests using both approaches tend to approximate the average PMT elastic modulus E_M when the stress level effect is taken into account. Nevertheless, the individual series of triaxial moduli E_{T50} or E_{IST} continue to exhibit high variations (or scatter) in the results because the *CV* values do not change considerably when the data are corrected to enable the comparison at the same stress level (in fact, the *CV* for E_{T50} increases instead of decreasing). This observation clearly indicates that other phenomena, such as differences in the testing modes and soil characteristics, continue to play a role in influencing the results.

Another source of variability might also be related to the size of the tested samples. Given the heterogeneity inherently associated with thin layers of an earth embankment (differences in anisotropy, compaction energies, water content, void ratio, mineralogy, and so on), the testing of small samples along the depth direction will certainly lead to more scatter in the results than would the testing of larger samples. This is exactly what the pressuremeter accomplishes with its expanding central membrane, 210 mm in height (compared to laboratory samples of no more than 100 mm in height).

5.3. Empirical relationships among the data

The amount of data, or the data population, considered in this research was rather limited for any attempt to extract reliable relationships among the results. Nevertheless, several prospective empirical trends among the average results can be identified, as a simple means of deriving useful design parameters for a preliminary design.

Table 5 therefore summarizes the relationships between the average values of the triaxial moduli E_{IST} and E_{T50} in regard to the pressuremeter modulus E_M, both under different conditions and at similar reference stress levels. The *CVs* are also shown.

As previously noted, these relationships tend to exhibit a high variability in the results, as indicated by high *CV* values. For instance, for the most common practical case, the average E_{T50}/E_M ratio can vary from 0.26 to 3.24 (a high *CV* of approximately 64%). However, these data allow the practitioner to be aware beforehand of the range of variation to expect when adopting this procedure.

In essence, these correlations will invariably assist in calculating various design variables of interest (such as settlement) based solely on PMT results. Of course, care must be taken given the restricted scope (and associated errors) of these data. In certain special cases, however, such as existing dams where soil sampling is difficult or impossible, the use of post-construction PMT data coupled via relationships similar to those presented in this table can be convenient, at least for a preliminary performance evaluation or to check the original design parameters.

Table 5 - Summary of empirical relationships between Young's modulus and average EM.

Stageof triaxial CID test	Number of data points (*)	Stress level (†)	Relationship E_{T50}/E_M				Relationship E_{IST}/E_M			
			Avg.	Min.	Max.	CV (%)	Avg.	Min.	Max.	CV (%)
Isotropic consolidation	8	Similar	-	-	-	-	0.98	0.5	1.83	43.7
Shearing	12	Similar	1.05	0.36	2.8	67.6	-	-	-	-
Shearing	32	Distinct	1.33	0.26	3.24	63.6	-	-	-	-

Note: *Number of triaxial testing points at different levels used to establish the relationship. The average elastic E_M modulus was determined with 24 PMT values; †Either at similar eff. octahedral stress level (σ'_{OCT}) or at regular levels referenced for each particular test. In the case of the isotropic consolidation stage, values of E_{IST} are related to a σ_C of 392 kPa.

6. Conclusions

According to Giacheti & Cunha (2013), site characterization using in situ testing techniques has changed considerably over the last two decades with the rapid transformation of and advances in the relevant technology. According to these authors, it is clear that in the 21st century, proper investigation and soil behavior prediction for geotechnical design cannot rely solely on one isolated test but must rather take advantage of a combination of techniques.

This paper has emphasized the potential use of the pressuremeter as a complementary field investigation tool to derive elastic parameters from existing compacted earth embankments, thereby enabling an independent check on a geotechnical variable that is typically defined based on conventional laboratory tests of undisturbed soil samples.

The approach proposed in the present paper also extends the significance of field surveys, especially for existing embankments, enabling a post-construction check on their construction quality, original design parameters (especially stiffness), and safety conditions.

Specially devised laboratory tests were performed on undisturbed samples from a real earth embankment acquired from representative layers of 1 m in thickness. These tests enabled the establishment of conventional Young's moduli against which the field PMT data could be compared. Nevertheless, the obtained results clearly reflected the extent of variability along the depth direction that one can observe using the employed laboratory techniques. This variability is undoubtedly caused by a combination of factors, such as the effects of soil heterogeneity (different compaction energies, water contents and mineralogy), disturbances during soil sampling, typical experimental errors during trimming and assembly, and data reduction.

Direct comparisons between the laboratory-derived Young's moduli and the elastic pressuremeter modulus were performed under two conditions, *i.e.*, directly along the compacted layers and between selected data from similar ranges of levels of the effective (confining) octahedral stress. These comparisons yielded several major conclusions:

- Differences in the elastic moduli at equivalent depths expose the external influence of several factors on the derived stiffness of the soil, such as different deformation modes, stress or strain rates, confining stress levels, strain ranges, soil anisotropy and sample volumes, among other factors. Indeed, the variability in the derived data, as quantified by the coefficient of variation of the average modulus, was quite high for all techniques.

- In average terms, however, the differences among the elastic moduli obtained using the considered techniques were not striking, perhaps because the different external factors tended to “cancel out” the disparities in the data.

- By further readjusting the data to similar levels of octahedral stress, an approximate equivalence of the average elastic moduli obtained from both the PMT and triaxial testing techniques could be clearly observed.

- Independently of the stress level, it appears that for earth embankments, the PMT can yield more homogeneous results, *i.e.*, values with lesser differences between the maximum and minimum values, and hence a lower statistical variability in the average modulus. This conclusion can be explained by the fact that the PMT tests a rather large volume of soil compared with standard laboratory techniques, which seems to be advantageous for the analysis of earth embankments constructed in successive layers.

- Empirical correlations for a preliminary estimation of the Young's modulus of the soil, benchmarked by the results of the triaxial tests and the elastic PMT modulus, were established. Although limited by the restrictions of the data population and many other factors, as previously discussed, such correlations can assist in the definition of design variables of interest based solely on PMT data. As previously noted, this approach can serve as a preliminary means of checking the design of an embankment or assessing the quality of its construction.

As a final note, the procedure proposed in the present paper may be a quite good technique available, for many existing dams in Brazil that is capable of providing, at least, a partial check of their actual safety conditions.

Acknowledgments

The authors are grateful to the ANEEL Agency (Agência Nacional de Energia Elétrica) and to Furnas Centrais Elétricas Laboratory in the city of Goiânia for the financial aid and experimental tests kindly provided throughout this research. The first author also acknowledges the support provided by the Brazilian research sponsorship organizations CNPq (Conselho Nacional de Desenvolvimento Científico e Tecnológico) and CAPES (Coordenação de Aperfeiçoamento de Pessoal de Nível Superior) for his Doctoral Thesis at the University of Brasília.

References

ABNT (1990). NBR 12007 – Soil - Unidimensional Consolidation Tests - Testing Method. Rio de Janeiro, Brazil, 15 p. (In Portuguese).

ABNT (1988). NBR 7181 – Soil – Granulometric Analysis. Rio de Janeiro, Brazil, 13 p. (In Portuguese).

AFNOR (1999). XP P94-110-2 Soil: Investigation and Testing – Ménard Pressuremeter Test – Part 2: Test with Unload-Reload Cycle. Ass. Française de Normalisation, Paris, 8 p. (In French).

Angelim, R.R. (2011). Assessment of Pressuremeter Tests in Earth Compacted Dams to Determine Geotechnical Parameters. D.Sc. Thesis, Department of Civil and Env. Engineering, University of Brasília, Brasília, 291 p. (In Portuguese).

ASTM (2011a). D2487-11 Standard Practice for Classification of Soils for Engineering Purposes (Unified Soil Classification System), ASTM International, West Conshohocken, USA, 12 p.

ASTM (2011b). D7181-11 Method for Consolidated Drained Triaxial Compression Test for Soils, ASTM International, West Conshohocken, USA, 11 p.

Baguelin, F.; Jezequel, J.F. & Shields, H. (1978). The Pressuremeter and Foundation Engineering. Trans Tech Publication, Clausthal, 617 p.

Cunha, R.P. (1994). Interpretation of Selfboring Pressuremeter Tests in Sand. Ph.D. Thesis, Department of Civil Engineering, The University of British Columbia, Vancouver, 279 p.

Cunha, R.P.; Sales, M.M.; Souza Pinto, C. & Sampaio Júnior, J.L.C. (2004). Pioneering selfboring pressuremeter tests in soils of the city of Goiânia – GO. Proc. 5th Special Seminar of Eng. Found. and Geot. – SEFE V, São Paulo, v. 1, p. 521-532 (In Portuguese).

Giacheti, H.L. & Cunha, R.P. (2013). General report for TC 102: *In-situ* testing. Proc. of the 18th Int. Conf. on Soil Mechanics and Geot. Engineering - ICSMGE, Paris, v. 1, p.471-478.

Hilf, J.W. (1959). A Rapid Method of Construction Control for Embankments of Cohesive Soils. Available from the United States Dept. of the Interior. Bureau of Reclamation, Denver, Engineering Monograph no. 26, 35 p.

Mair, R.J. & Wood, D.M. (1987). Pressuremeter Testing - Methods and Interpretation. CIRIA Ground Engineering Report: In-situ Testing. Butterworths, London, 160 p.

Ortigão, J.A.R.; Cunha, R.P. & Alves, L.S. (1996). *In situ* tests in Brasilia porous clay. Canadian Geotechnical Journal, 33(1):189-198.

Pacheco Silva, F. (1970).A new graphical construction for determination of the pre-consolidation stress of a soil sample. Proc. of the 4th Brazilian Conference on Soil Mechanics and Foundation Engineering, Rio de Janeiro, Vol. 2, No.1, p. 225-232 (In Portuguese).

Queiroz, A.C.G. (2008). Use of the DMT in the Assessment of Compacted Embankments. M.Sc. Thesis, Department of Civil and Env. Engineering. University of Brasília, Brasília, 96 p. (In Portuguese).

Smith, I. (2013). Smith's Elements of Soil Mechanics. John Wiley and Sons Ed., New York, 552 p.

Timoshenko, S. & Goodier, J.N.(1951). Theory of Elasticity. McGraw Hill Book Co., New York, 263 p.

Wood, D.M. & Wroth, C.P.(1977). Some laboratory experiments related to the results of pressuremeter tests. Géotecnique, 27(2):181-201.

List of Symbols

B: Bulk modulus
c': Effective cohesion intercept from failure envelope
C_C: Compression index
CID: Isotropically consolidated drained
CV: Statistical coefficient of variation
e: Void ratio
E: Young's modulus
E_{IST}: Young's modulus determined via the consolidation stage of a triaxial test
E_M: Elastic or pressuremeter modulus
E_{YO}: $E(OED)$:Young's modulus determined via an oedometer test
E_R: Elastic modulus determined from a pressuremeter loop
E_{T25}, E_{T50}: Secant Young's moduli determined via the shearing stage of a triaxial test
E_{TI}: Tangent Young's modulus determined via the shearing stage of a triaxial test
I_a: Soil activity
I_P: Plastic index
M: Constrained modulus
Max.: Maximum
Min.: Minimum
OCR: Overconsolidation ratio
p_1 to p_4: Pressure points from a pressuremeter curve
p_m: Average pressuremeter cavity pressure
PMT: Ménard pressuremeter test
RC: Relative compaction
S: Degree of saturation
USCS: Unified Soil Classification System
v_1 to v_4: Volume points from a pressuremeter curve

v_s: Initial volume of the expanding membrane
w: Water content
w_L: Liquid limit
w_{opt}: Optimum water content
w_P: Plastic limit
α: Empirical pressuremeter factor
γ: Unit weight
γ_d: Dry unit weight
γ_{dmax}: Maximum dry unit weight
ε_a: Axial strain
ε_V: Volumetric strain
ν: Poisson's ratio
σ_1 to σ_3: Principal stresses in an element of soil
σ_C: Isotropically applied confining pressure
σ_D: Deviatoric stress
σ_{OCT}: Total octahedral stress
σ'_{OCT}: Effective octahedral stress
σ_P: Virtual preconsolidation pressure
σ_V: Total applied vertical pressure
σ'_{V0}: Effective overburden pressure
ϕ': Effective angle of internal friction

Field Permeability Tests Using Organic Liquids in Compacted Brazilian Soils

S.L. Machado, Z.S. Carvalho, M.F. Carvalho, D.F. Mariz

Abstract . This paper presents results of field and laboratory permeability tests aimed at evaluating the performance of mineral barriers for the containment of organic liquids (Non Aqueous Phase Liquids, NAPL). Experimental landfills were constructed following optimal ranges of variation of soil index properties proposed previously and the performance of the landfills was evaluated under two distinct weather conditions (rainy and dry periods). A primary test campaign was performed during the rainy period (March to August). Then a second testing campaign was performed from November 2013 to January 2014 (months of low rainfall). The obtained results corroborate several results published in the technical literature: fluids with a low dielectric constant (non polar) tend to present higher intrinsic permeability (K) than polar fluids and the presence of water, the most wettable fluid, reduces the NAPL permeability. Soils with a higher plasticity index, I_P, presented higher K_w/K_{NAPL}, (ratio water/NAPL intrinsic permeability) showing that the values of K are dependent on the interactions between solid particles and interstitial fluid. Based on laboratory and field results, optimal ranges of variation of soil index properties are proposed for the construction of mineral barriers for organic liquid containment.
Keywords: intrinsic permeability, hydrocarbons, compacted soil barriers, NAPL.

1. Introduction

Leakage of organic fluids such as aromatic solvents, liquid fuels and polycyclic aromatic hydrocarbons (PAHs) from storage tanks and distribution/transport structures has been identified as one of the most important sources of contamination of soils and water (CETESB, 2013). As well as this, petroleum derivates are most frequently Light Non Aqueous Phase Liquids (LNAPL) whose characteristics such as density, surface tension, viscosity and polarity (or dielectric constant) differ substantially from water. If these substances are released into the environment a NAPL plume will migrate downward in the subsoil, eventually reaching the capillary fringe and the ground water table. Once in contact with the groundwater, LNAPL will form a volume of free phase that can depress the water table and move laterally in the direction of the groundwater flow. In addition, the soluble constituents of LNAPL can dissolve in the water and migrate under advection, dispersion and retention phenomena.

It is also worth noting that Brazilian gasoline normally contains 24% anhydrous alcohol. When in contact with soil interstitial water and mainly when the contamination plume reaches the ground water table, the alcohol is stripped to water bringing together many gasoline compounds such as BTEX (Benzene, Toluene, Ethyl-benzene and Xylene) which are recognized as carcinogenic. This phenomenon is normally referred to as co-solvency. Fate and transport of petroleum derivates have been studied in Brazil by several authors such as Corseuil & Marins (1997), Kaipper (2003), Silveira (2004), Schneider (2005) and Amorim Jr. (2007), N. Filho *et al.* (2013), among others.

Mineral liners are the most commonly used containment structures for storage terminals of oil derivates and they are perhaps the most evident example of soil structures where soil permeability is of paramount importance. To protect the environment from possible contamination by pollutants, oil storage areas must be lined. Mineral layers of compacted soil with or without additives are often used because of their relatively low cost, accessibility, durability, high resistance to heat and other factors (Wang & Huang, 1984). However, parameters such as shear strength, shrinkage susceptibility and the compatibility between the contained species and the barrier materials should be addressed in the design of soil liners (Daniel & Benson, 1990, Daniel & Wu, 1993, Shackelford, 2014). Based on Brazilian standards for sanitary landfill construction, compacted soil liners must present water coefficients of permeability values, $k_w < 1 \times 10^{-9}$ m/s (NBR 13896, 1997), while in the case of emergency levees for petroleum derivate storage areas the NBR 17505-1 (2006) recommends $k_w < 1 \times 10^{-8}$ m/s.

The use of water as a reference fluid for such structures mostly induces the use of clayey soils. On the other hand, the coefficient of permeability of clayey soils is affected by factors such as specific surface, particle arrangements, degree of saturation, porosity, chemistry and concentration of electrolytes, clay electro-chemical properties and external pressure (Mitchell, 1976). In the case of NAPL flow, the relationship between permeability and the

Sandro Lemos Machado, D.Sc., Full Professor, Escola Politécnica, Universidade Federal da Bahia, Salvador, BA, Brazil. e-mail: smachado@ufba.br.
Zenite da Silva Carvalho, M.Sc., Researcher, Escola Politécnica, Universidade Federal da Bahia, Salvador, BA, Brazil. e-mail: zenite.esa@gmail.com.
Míriam de Fátima Carvalho, D.Sc., Professor, Universidade Católica do Salvador, Salvador, BA, Brazil. e-mail: mfcmachado@gmail.com.
Digna de Faria Mariz, D.Sc., Safety and Environment Division, Petróleo Brasileiro (Petrobras), Rio de Janeiro, RJ, Brazil. . e-mail: digna@petrobras.com.br.
Submitted on February 22, 2016; Final Acceptance on November 27, 2016; Discussion open until April 28, 2017.

physical and chemical properties of the fluid is even more complex, mainly because the dielectric nature of these fluids is very often quite different from water. Petroleum derivates usually have non-polar compounds which have low relative dielectric constants, ε_r (ε_r represents the ratio between the dielectric constant of the medium and the dielectric constant of the vacuum). Water, a high polarity fluid, presents values of $\varepsilon_r = 80$ whereas most organic fluids present smaller ε_r values. In clayey soils, the electrical phenomena that take place around the clay particles make the properties of the fluids present in the pores an important factor in its permeability (Budhu *et al.*, 1991; Goodarzi *et al.*, 2016). Table 1 summarizes the properties of some common liquids which are stored in petroleum industrial areas.

The most widely accepted conceptual model to represent the interactions between the fluid and the clay surface is the diffuse double layer system. This model was developed from the theory proposed by Helmholtz-Smoluchowski and was improved by Gouy-Chapman and Quinke. The diffuse double layer system consists of clay particles, adsorbed cations and water molecules in one layer, while the other is a diffuse layer with the presence of counterions. Although this model ignores the effect of the potential energy in the oriented molecules of water that surround the clay particles, it is useful to explain some basic phenomena in a clay-water-electrolyte system (Fang, 1997). Eq. 1 can be used to predict the double layer thickness, t, based on the Gouy-Chapman theory,

$$t = \sqrt{\frac{\varepsilon_r \cdot K_b \cdot T}{8\pi \cdot n_e \cdot e^2 \cdot \nu^2}} \tag{1}$$

where K_b is the Boltzmann constant, T is the temperature, n_e is the electrolyte concentration, e is the elementary charge and ν is the ionic valence.

As can be seen from Eq. 1, a decrease in the fluid dielectric constant reduces the double layer thickness. As part of the double layer thickness is fixed, reducing its thickness will provide more space in the voids of the soil for fluid flow, increasing the soil permeability. Although this is a very simplistic approach, it is completely corroborated by profuse experimental evidence. Fig. 1 illustrates the effect of the fluid dielectric constant on the soil permeability. According to Anandarajah (2003) among others, the shrinkage

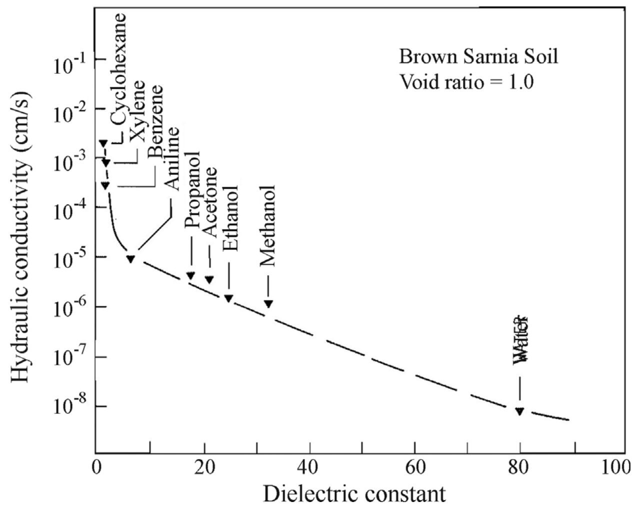

Figure 1 - Hydraulic conductivity *vs.* dielectric constant for a void ratio of unity (Fernandez & Quigley, 1985).

of clusters resulting in localized cracks in the soil can also explain part of the wide variations in the measured coefficient of permeability.

The concept of intrinsic permeability, K [L^2], Eq. 2, was proposed by Nutting (1934) and assumes that it depends solely on the soil properties. It is normally used to convert water permeability values in the expected value of permeability for another fluid in the same soil. Eq. 1 normally provides good results in the case of coarse soils, without the presence of considerable amounts of clay. As the clay content of the soil increases, however, the intensity of the solid surface/fluid interactions also increases and begins to play an important role in the values of K (Brown & Anderson, 1983; Brown & Thomas, 1984; Fernandez & Quigley, 1985; Schramm *et al.*, 1986; Budhu *et al.*, 1991; Amarasinghe *et al.*, 2012; Parker *et al.*, 1986 and Oliveira, 2001).

$$k = \frac{K \cdot \rho \cdot g}{\mu} \tag{2}$$

where g [LT^{-2}] is gravity acceleration, ρ [ML^{-3}] is the fluid density and μ is fluid dynamic viscosity [$ML^{-1}T^{-1}$].

The influence of the liquid polarity (or ε_r) on the K value has been recognized by many authors (Mesri & Ol-

Table 1 - Liquid properties at 20 °C (Carvalho, 2015).

Liquid	Density ρ (gcm^{-3})	Dynamic viscosity μ ($gcm^{-1}s^{-1}$)	Mobility (ρ/μ) (scm^{-2})	Relative dielectric constant - ε_r (-)	Surface tension ($mN.m^{-1}$)
Water	0.998	0.0107	93.03	80.08	72
Bio-diesel	0.883	0.0630	14.02	4.5	23.85
Commercial diesel	0.829	0.0351	23.62	2.13	27.3
Brazilian commercial gasoline	0.767	0.0123	62.36	9.06	22.23

son, 1971; Fernandez & Quigley, 1985; Schramm *et al.*, 1986; Fernandez & Quigley, 1988; Graber & Mingelgrin, 1994; Kaya & Fang, 2000; Oliveira, 2001; Anandarajah, 2003; Kaya & Fang, 2005; Amorim Jr., 2007; and Cardoso, 2011; Akinwumi et. al. 2014). As a general rule, the higher the fluid ε_r, the lower the soil K. Eq. 3 was proposed by Budhu *et al.* (1991) in order to take into account the influence of the fluid dielectric constant (ε_{rf}) in the soil intrinsic permeability. ε_{rw} is the water relative dielectric constant. According to Budhu *et al.* (1991), λ, the parameter that reflects this influence varies with soil type, although there is no indication as to which soil properties affect the value of λ.

$$\frac{K_f}{K_w} = e^{\lambda\left(1-\frac{\varepsilon_{rf}}{\varepsilon_{rw}}\right)} \tag{3}$$

where K_f [L^2] is the soil intrinsic permeability concerning the fluid used and K_w [L^2] is the soil intrinsic permeability for water.

Eq. 4 was proposed by Oliveira (2001) in order to predict soil permeability (k) for different soils and fluids. However, in this work the variable B, with a dimension of [L^2] was not physically related to any measurable parameter of soil.

$$k = \rho \frac{g}{\mu}\left(\frac{1}{5}\right)\left[\frac{n^3}{(n-1)^2}\right]\frac{B}{\varepsilon^N} \tag{4}$$

where n [-] is the soil porosity, B [L^2] seems to reflect the surface activity of the soil particles and N seems to be dependent on the clay content of the soil.

According to Cardoso (2011), creating a model to predict soil permeability values for different fluids must take into account the dielectric constant of the fluid and some parameter that reflects soil activity or specific surface. Cardoso (2011) and subsequently Machado *et al.* (2016) proposed equations to introduce fluid/particles interaction in the Nutting equation. Eq. 5 presents the equation proposed by Machado *et al.* (2016).

$$k_f = \frac{\rho_f}{\mu_f}\cdot\frac{\mu_w}{\rho_w}\cdot k_w \cdot 10^{\left\{a\cdot\left(\frac{\varepsilon_w}{\varepsilon}-1\right)^b\left[1-\exp\left(\frac{-c\cdot I_p}{c+I_p}\cdot\log\left(\frac{k_{ref}}{k_w}\right)\right)+\frac{I_p}{c+I_p}\left\{d\cdot\log\left(\frac{k_{ref}}{k_w}\right)+\frac{e}{(1-Sr_w)}\right\}\right]\right\}} \tag{5}$$

where I_P [-] is the soil plasticity index, k_{ref} [LT^{-1}] is a reference permeability, k_w [LT^{-1}] is the water soil permeability, Sr_w [-] is the soil water saturation, ε_{rw} [-] is the water relative dielectric constant, ε_{rf} [-] is the NAPL fluid dielectric constant. a, b, c, d, e [-] and k_{ref} [LT^{-1}] are model fitting constants. Water and fluid density and viscosity are also required.

In the model, I_P and $\log(k_w)$ were used to represent the ability of the soil to interact with fluids and the variable ($\varepsilon_{rw}/\varepsilon_{rf}$ - 1) was used to represent the ability of the fluid to interact with soil particles. The fourth variable used in the model was (1 - Sr_w). It reflects the influence of the soil water content on the soil NAPL permeability. As water is normally the most wettable fluid, an increase in Sr_w will reduce the void space for NAPL to flow. In other words, this variable takes into account the fact that in most of the tests performed to evaluate NAPL permeability there is a considerable amount of water in the soil (as in the case of compacted soils, optimum moisture content). Therefore, the measurement being made is the soil effective permeability (multiphase flow) rather than soil permeability.

In the case of miscible fluids, such as ethanol, Sr_w must be set to zero. On the other hand, the mixture of fluids inside the pore spaces will change the ε_{rf} value, which should be calculated using Eq. 6.

$$\varepsilon_{rf} = \varepsilon_{rw}\cdot Sr_w + (1-Sr_w)\cdot\varepsilon_{rf} \tag{6}$$

The following values were used for fitting parameters by Machado *et al.* (2016): a = 0.263, b = 0.20, c = 5.00, d = 1.19, e = -0.259 and k_{ref} = 1.34 x 10 $^{-4}$ m/s (I_P values in %). A value of R^2 = 0.915 was obtained considering a data set of 541 tests (133 average values) embracing soils of very different textures. Considering a confidence interval of 90% the error obtained was around 6.4. For the sake of comparison, errors higher than 100,000 were obtained when directly using the Nutting equation on the data set.

From our earlier discussion it can be concluded that using k_w as the base permeability for performance evaluation of mineral barriers for containment of petroleum derivates (ABNT NBR 17505-1, 2006) is not reliable. k_{NAPL} experimental values might surpass in several magnitude orders the values estimated using k_w and the Nutting equation.

Another noteworthy aspect is that mineral barriers designed to contain organic fluids must be specified differently from those for water. Clayey soils are not effective in the containment of organic fluids because of the less effective particle/fluid interactions. In this case, the clay fraction must act as filler, complementing the grain size curve of the soil.

In this paper some soil specifications based on laboratory tests results are compared with the field performance of mineral barriers in water and organic fluids containment. Experimental landfills were constructed and field and laboratory tests were performed in order to evaluate the behavior of the barriers over a period of about one year. Field values were used to test the validity of Eq. 5 and to improve the proposed ranges of soil properties for mineral barrier construction focusing on NAPL containment.

2. Previous Studies: Laboratory Tests

Previous to the field tests, a laboratory research program was performed sponsored by Brazilian Petroleum Company, PETROBRAS. Two typical soils of the Metropolitan Region of Salvador were used: the residual soil from Granulite/Gneiss and the sand clayey sedimentary soil from tertiary formation denominated *Barreiras*. These soils were used alone (first laboratory phase) and as part of mixtures in varying proportions (second laboratory phase). The first set of permeability tests was performed using the normal and modified Proctor energies, varying soil moisture and water, diesel and alcohol as permeating fluids. 47 permeability tests were performed using Barreiras soil (BS) and 50 tests for residual soil from Granulite/Gneiss (RSG). The main purpose of these tests was to evaluate the effect of the soil structure and moisture content on NAPL soil permeability. Eight mixtures were prepared using different proportions of BS and RSG, resulting in 144 permeability tests (second laboratory phase). Table 2 provides a summary of the soil-mixture characteristics and the average permeability values obtained for different fluids. Fig. 2 shows the variation in the soil permeability in such tests with some soil index parameters. For all the test results in Fig. 2 the modified Proctor energy was used because no sample compacted with normal energy reached the target permeability value of $k_{NAPL} < 1 \times 10^{-8}$ m/s, as required by the Brazilian Standard ABNT NBR 17505-1 (2006).

For the same mixture, the use of modified Proctor energy and the resulting increase in the dry density (ρ_d) of the soil compared to normal Proctor energy, reduced the k_{NAPL} by around two orders of magnitude. Considering the results presented in Table 2 and Fig.2, both the k_{NAPL} and k_w decreased as the ρ_d increases. This can be explained by the decrease in the mixture clay content, as well known from principles of soil mechanics. However, the effect of the ρ_d or clay content in the k_{NAPL} is less evident.

As expected, diesel (non polar fluid, $\varepsilon_r = 2.13$) leads to critical results (larger permeability values) in most cases thus requiring the construction of mineral barriers for organic fluid containment. Alcohol presented an intermediate behavior. It can be observed in Fig. 2 that values of $k < 1 \times 10^{-8}$ m/s are obtained for clay contents higher than 26%. However, from this point on, the effect of the clay content on the soil diesel permeability is much less pronounced. Considering that high plasticity soils present high volume variations and have associated shrinkage cracks due to wetting/drying cycles, it is prudent to adopt an upper limit for the clay content of the soil.

A similar behavior can be observed considering the soil optimal moisture content, w_{opt}, and the plasticity index,

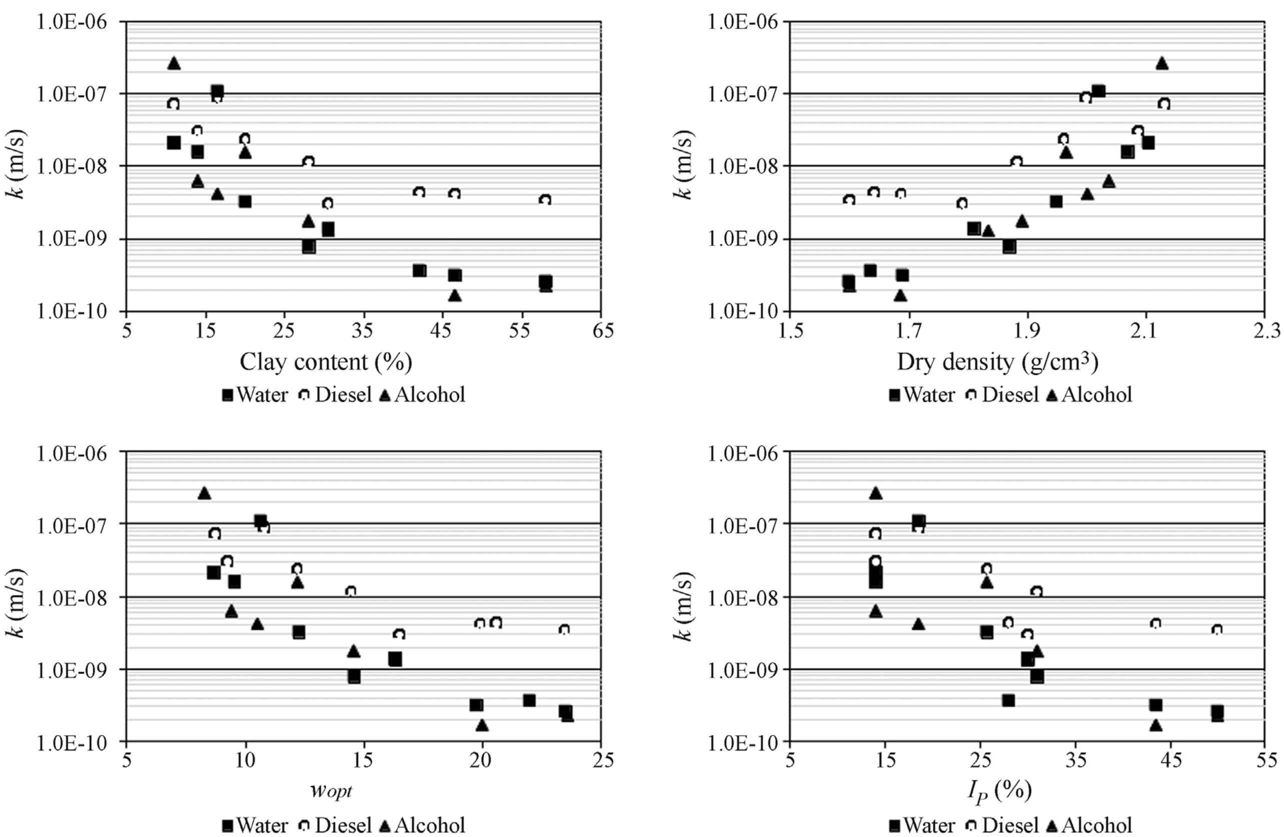

Figure 2 - Coefficient of permeability (*k*) as a function of some index properties - Laboratory tests.

Table 2 - Characterization of soil-mixtures and average permeability values for different fluids. Second phase of laboratory tests.

Mixture ID	Grain size distribution				Consistence limits			Specific mass (g/cm^3)	Compaction PM energy		SUCS classification	Permeability (m/s)		
	Gravel	Sand	Silt	Clay	w_L	w_P	I_P		w_{opt}	ρ_{dmax}		Water	Diesel	Alcohol
Mix. 01	5	76	5	14	31	16	15	2.662	9.41	2.036	SC	1.59E-08	3.04E-08	6.32E-08
Mix. 02	9	74	6	12	27	16	12	2.660	8.6	2.069	SC	2.11E-08	7.13E-08	2.68E-07
Mix. 03	4	68	8	20	46	20	26	2.674	12.15	1.951	SC	3.23E-09	2.34E-08	1.58E-08
Mix. 04	6	70	7	17	38	19	19	2.662	10.57	1.994	SC	1.09E-07	8.65E-08	4.15E-09
Mix. 05	1	47	22	30	58	29	29	2.713	16.18	1.792	CH/MH	1.38E-09	2.98E-09	1.28E-09
Mix. 06	0	41	13	47	80	36	44	2.727	19.84	1.676	CH	3.12E-10	4.17E-09	1.66E-10
Mix. 07	2	59	11	28	56	26	30	2.698	14.7	1.857	SC	7.79E-10	1.16E-08	1.76E-09
Mix. 08	0	28	14	58	91	41	50	2.764	23.26	1.594	MH	2.58E-10	3.43E-09	2.28E-10

I_P. Considering the dry density (ρ_d) values reached in the compaction curves, admissible k_{NAPL} values are obtained for values of $\rho_d < 1.9$ g/cm^3. Based on these results, the specifications presented in Table 3 were proposed for the construction of mineral barriers for the containment of organic fluids. These ranges of variations were the basis on which the construction of the experimental landfills experiment were made.

3. Materials and Methods

In order to check the validity of the ranges proposed in Table 3, field landfills were constructed using mixtures of RSG/BS soils. Six landfills were constructed using different proportions of RSG and BS and a seventh landfill was constructed using soil borrowed from a sedimentary *Barreiras* layer which had a relatively high clay content. The activities performed in field are discussed below.

3.1. Field location and weather characteristics

The experimental area is located about 21 km from Salvador, Bahia (12°50'50.4" S 38°22'42.4" W), Brazil. The rainfall was about 2,100 mm per year in the period from 1998 to 2014 (measurements from a weather station close to the area). Rainfall is seasonal, usually from April to July. The average temperature is 25.2 degrees Celsius, with little variation throughout the year.

3.2. Materials and compaction process

Table 4 summarizes the properties of the soil-mixtures used to construct the landfills. The following ABNT standards were used in the tests: NBR 6457 (1986); NBR 6508 (1984); NBR 7181 (1984); NBR 6459 (1984); NBR 7180 (1984) and NBR 7182 (1986). The RSG/BS proportions were chosen in such a way that mixtures 1 to 4 fit the *Fc* criterion presented in Table 3. Mixtures 5 to 7 were made with coarse soils. The idea was to study not only the soil hydraulic behavior just after compaction, but also the long term behavior of the landfills. Fine grained mixtures tend to have a better short term behavior (before first drying cycle), however, since coarse soils are less sensitive to changes in environmental conditions, the long term performance tends to be more effective for coarse soils.

Table 3 - Optimal ranges of index properties for the construction of mineral barriers for organic fluid containment.

Index property	Proposed range
Plasticity Index (I_P)	28%-42%
Fine (clay + silt) content (Fc)	33%-60%
Clay content (Cc)	27%-45%
Sand content (Sc)	34%-57%
Optimal moisture content (w_{opt})	14%-20%
Maximum dry density (ρ_{dmax})	1.65-1.83 (g/cm^3)

All the RSG and BS soils used in the experiments were homogenized prior to mixing using a backhoe and the total amount of soil used in each landfill was calculated based on the landfills geometry and physical indices of the compacted mixture. The landfills were compacted in four layers with a final total height of 0.6 m (4 layers of 0.15 m). The nominal dimensions of the landfills were 2.2 x 5.0 m, except for mixture 6 which had nominal dimensions of 2.2 x 10 m. Fig. 3 provides a sketch of the experimental landfills. The filled gray area represents the area used for the field tests and undisturbed blocks sampling. RSG/BS proportions were used to calculate the amount of dry mass of each soil to be used in the compaction process.

Using the field moisture content, the mass of compacted soil used in layers was calculated. This mass was converted into an equivalent number of backhoe shells. In order to do this, the mass of the empty backhoe along with the mass of the backhoe filled with each soil was determined using the field balance of 20 Mg. The necessary amount of soil for each layer was then mixed and water was added to reach the desired water content. After the mixing and wetting procedures, the soil layers were allowed to settle for 24 h so that the moisture would become uniform.

The soil layers were then compacted using a 24 Mg sheepsfoot roller going over it 9 to 10 times. Compaction control was made based on moisture content (w_{opt} - 1% < w < w_{opt} + 3%) and compaction efficiency, CE = $\rho_{dfield}/\rho_{d\max}$ > 0.95. The water content was determined in the field using *speedy test* and infrared balances and in the laboratory (24 h later) using standard procedures. Density was determined crimping a beveled cylinder of known internal volume and mass and determining the mass of soil + cylinder after crimping. Fig. 4 illustrates some of the field procedures. More details concerning the field activities can be found in Carvalho (2015).

3.4. Performance evaluation of the landfills

Landfill performance was evaluated using laboratory and field tests at two distinct moments. The first field campaign started just after the compaction of the landfills and took place from March to August of 2013 (rainy period). The second testing campaign was performed between November 2013 and January 2014 (dry season). Fig. 5 shows the daily rainfall during the field test periods. The first and second campaign periods are also highlighted in the figure and field test days are represented by a vertical line. As can be observed, during most of the first campaign there were rainy days. As the soil was close to 100% saturation just after compaction, the rain in this period reduced the occurrence of shrinkage and cracks. In the case of the second campaign, the opposite weathering conditions could be observed. Water, diesel, biodiesel and commercial gasoline were the percolation fluids. Two tests were performed for each fluid making up eight tests for each landfill, 56 tests in each campaign and 112 tests in total.

Field permeability tests were performed using Guelph permeameter which meets the requirement of ASTM D5126/D5126M-90 (2010)e1. The Guelph permeameter problem of flow was solved by Reynolds & Elrick (1985), using Richards' equation and the assumption of steady state flow in a cylindrical cavity, taking into account the soil matric suction:

$$Q = \left(\frac{2\pi \cdot H^2}{C} + \pi \cdot a^2\right) \cdot k_{fs} + \left(\frac{2\pi \cdot H}{C} + \pi \cdot a^2\right) \cdot \varphi_m \quad (7)$$

where Q [L^3T^{-1}] is the flow rate entry into the soil; H [L] is the hydraulic head inside the cavity; C is a shape factor; a [L] is the cavity radius; k_{fs} [LT^{-1}] is the soil permeability and φ_m [L^2T^{-1}] corresponds to the water flow due to soil matric potential (see Eq. 8).

$$\varphi_m = \int k(\psi) \cdot d\psi \quad (8)$$

where $k(\psi)$ [LT^{-1}] is the hydraulic conductivity function and ψ [L] is the matric potential.

The Guelph permeameter was developed by Reynolds *et al.* (1983) to carry out field permeability tests in steady state conditions. A Mariotte tube is used to assure a constant hydraulic head (H) inside the bore hole and the flow rate, Q, is measured using the reservoir tubes. The inner tube is used for low permeability soils. The shape factor, C, can be obtained using Fig. 6. Unfortunately, the use of the rigorous method (use of two H values) sometimes leads to unrealistic (negative) values of k_{fs}. This occurs normally when the assumptions adopted for solving Eq. 7 (homogeneous porous material and matric potential in the unsaturated flow zone) are not present in the field. In order to overcome this, Elrick et *al*. (1989) suggest the use of the α [L^{-1}] parameter in order to estimate k_{fs} using a single head

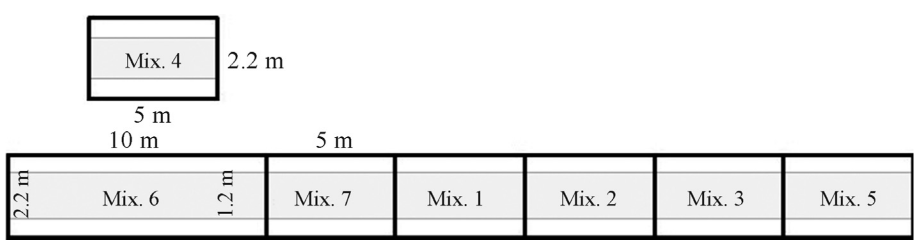

Figure 3 - Sketch of the field experimental landfills.

(Eq. 9). Table 5 presents α values suggested by the authors for different types of soils.

$$\alpha = \frac{k_{fs}}{\varphi_m} \tag{9}$$

$$k_{fs} = \frac{CQ}{\left(2\pi \cdot H^2 + \pi \cdot a^2 \cdot C + 2\pi \cdot \frac{H}{\alpha}\right)} \tag{10}$$

A standard permeameter was used for water whereas a modified permeameter, developed in the UFBA Geo-environmental Laboratory (GEOAMB), was used for commercial gasoline, diesel and biodiesel. The modified permeameter was developed for testing organic and/or aggressive fluids and is made of mostly steel and glass. Its design prevents direct contact with fluid (the permeameter is filled from bottom to top using a vacuum pump) and the measurements can be taken visually from the glass tubes or be seen on a LCD panel of a pressure transducer (measures are stored in a datalogger). This is particularly useful in the case of opaque fluids. The internal tube of the permeameter has a smaller inner diameter compared to standard models which makes it more appropriate for low permeability soil testing. Both permeameters were checked exhaustively against leaks before tests. During the tests, the annular gap between the permeameter rod and the wall of the boreholes was covered by a cardboard sheet to prevent evaporation (Fig. 7a). Furthermore, tests were performed to estimate the evaporation rate and correct field reading. All the tests were performed at a depth of 20 cm and used two hydraulic heads. More details can be found in Carvalho (2015).

Field permeability was calculated according to Eq. 10 and the adopted k was the average value for the two heads used. Laboratory permeability tests were also performed using undisturbed blocks (0.3 x 0.3 x 0.3 m). Blocks were extracted from landfills at a depth of 0.1 m. The extraction of the blocks occurred in the period from January 24th to March 12th, 2014, just after the second field campaign (see Fig. 5). The landfill borders were avoided for the extraction of undisturbed blocks because of the bad compaction conditions. Flexible permeameters (triaxial chambers) were used and the falling head procedure was adopted (NBR 14545, 2000). Samples had nominal dimensions of 0.05 x

Table 5 - α values proposed by Elrick *et al.* (1989) for different soil types

α (cm^{-1})	Soil type
0.01	Compacted clays
0.04	Unstructured clays
0.12	Clay to fine sand (or structured soils)
0.36	Coarse sand. structured soils with cracks and macro pores

Table 4 - Characterization and compaction control results (average values for the four layers).

Mixture ID	RSG/BS	Grain size distribution				Consistence limits			Specific mass (g/cm^3)	Compaction PM energy		SUCS classification	w_{field}	ρ_{field}	Compaction efficiency (%)
		Gravel	Sand	Silt	Clay	w_L	w_P	I_P		w_{opt}	ρ_{dmax}				
Mix. 01	100/0	1	54	17	28	41	20	20	2.701	12.54	1.936	SC	17.6	1.820	94.7
Mix. 02	90/10	2	58	17	23	31	18	13	2.685	11.08	1.966	SC	15.1	1.872	95.2
Mix. 03	79/21	3	60	14	23	30	17	13	2.683	10.29	1.998	SC	13.4	1.942	97.2
Mix. 04	69/31	1	64	13	22	28	16	12	2.685	10.6	2.013	SC	12.1	1.968	97.8
Mix. 05	58/42	0	67	12	21	28	17	11	2.672	10.16	2.008	SC	11.6	1.930	96.1
Mix. 06*	0/100	0	82	6	12	NL	NP		2.673	9.39	1.964	SM	9.0	1.860	94.7
Mix. 07*	-	1	72	8	19	25	15	10	2.693	10.24	2.018	SC	11.2	1.957	97.0

* Fine content out of the proposed range of variation.

Figure 4 - (a) weighing the backhoe filled with soil; (b) layer being released and allowed to settle for 24 h for moisture equalization (c) compaction process and (d) compaction control.

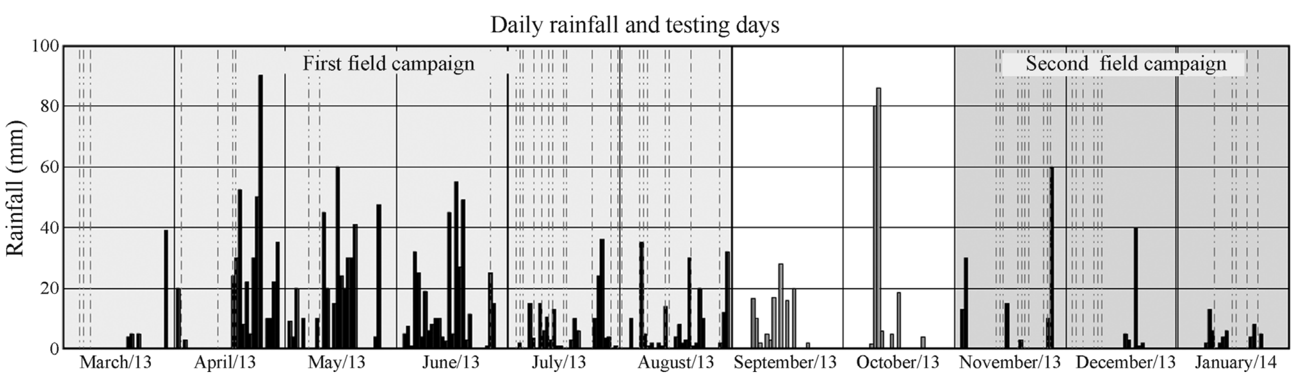

Figure 5 - Daily rainfall during the field tests.

0.10 m. Fig. 8 illustrates undisturbed block extraction, sample trimming and one of the flexible wall permeameters used.

4. Results and Analysis

Fig. 9 compares the field results for water and diesel (all the mixtures considered) with the results presented in Fig. 2. As can be observed, both the field and laboratory results are consistent. The field results plotted in Fig. 9 correspond to the first campaign as the laboratory tests were performed using w_{ot} and ρ_{dmax} conditions. Considering the obtained results, the landfills were able to achieve good results even for relatively lower I_P and w_{ot} values. These results make possible the refinement of the previously pro-

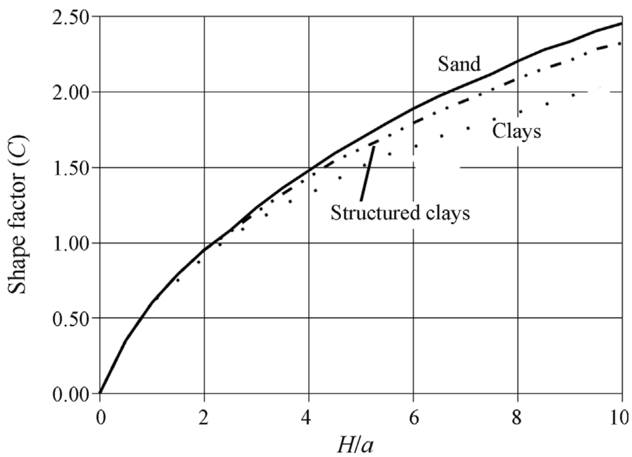

Figure 6 - Shape factor, C, as a function of the ratio H/a. Reynolds *et al.* (1983).

posed ranges. Tables 6 to 8 present the coefficient of the permeability results obtained in field. Values of $k \leq$ to 1 x 10^{-8} m/s are highlighted. Some observations can be made concerning the results presented in Tables 6 to 8:

a) Mixtures 1 to 5 and 7 showed good performance in the first field campaign. Only for Brazilian gasoline $k > 1$ x 10^{-8} m/s, which is probably due to its higher mobility (see Table 1). Besides this, commercial gasoline contains about 24% ethanol which will be stripped to the pore water during flow (Corseuil & Marins, 1997; Kaipper, 2003). However, even in this case, mixtures present k around 1 x 10^{-8} m/s. Mixture 2 presents $k \leq 1$ x 10^{-8} m/s for all the tested fluids. The obtained results are consistent with the previous phase of study because mixtures 1 to 5 meet the fine content criteria (see

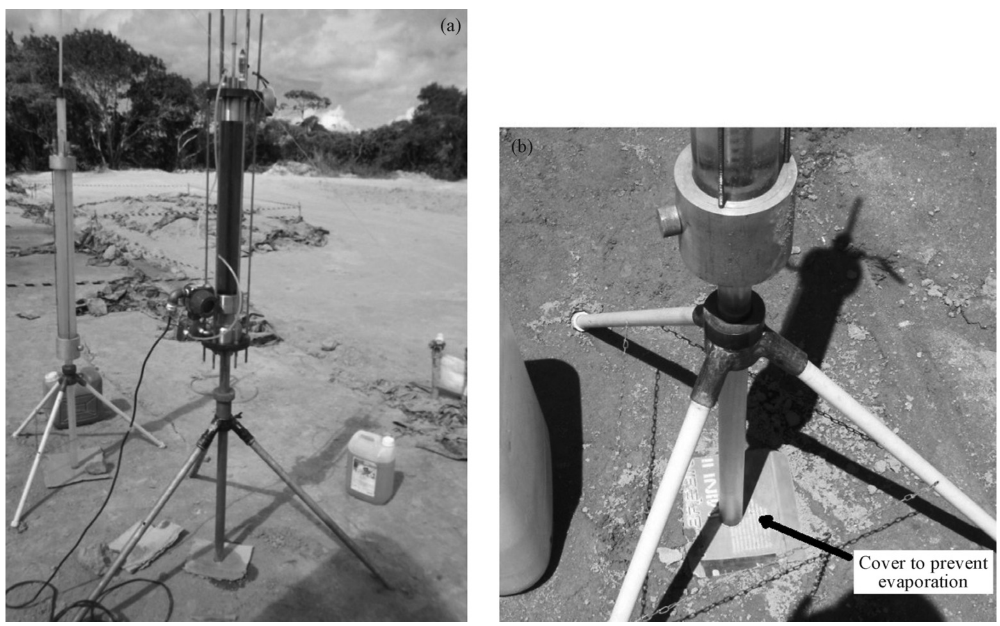

Figure 7 - a) Permeability tests using water and diesel and b) details of the cover adopted to reduce evaporation.

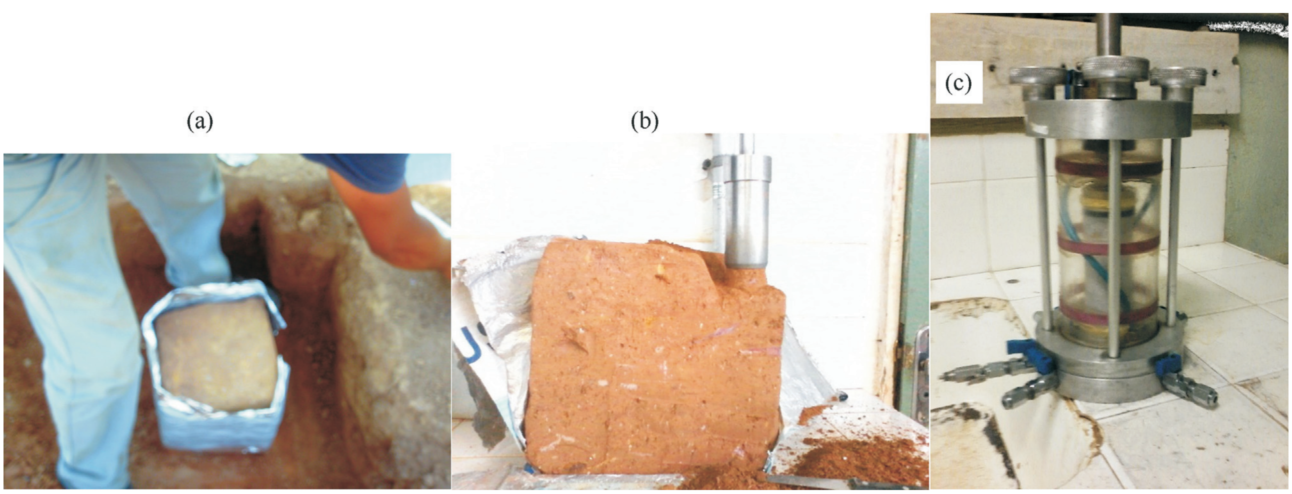

Figure 8 - a) Undisturbed blocks extraction; b) samples trimming and c) flexible wall permeameter.

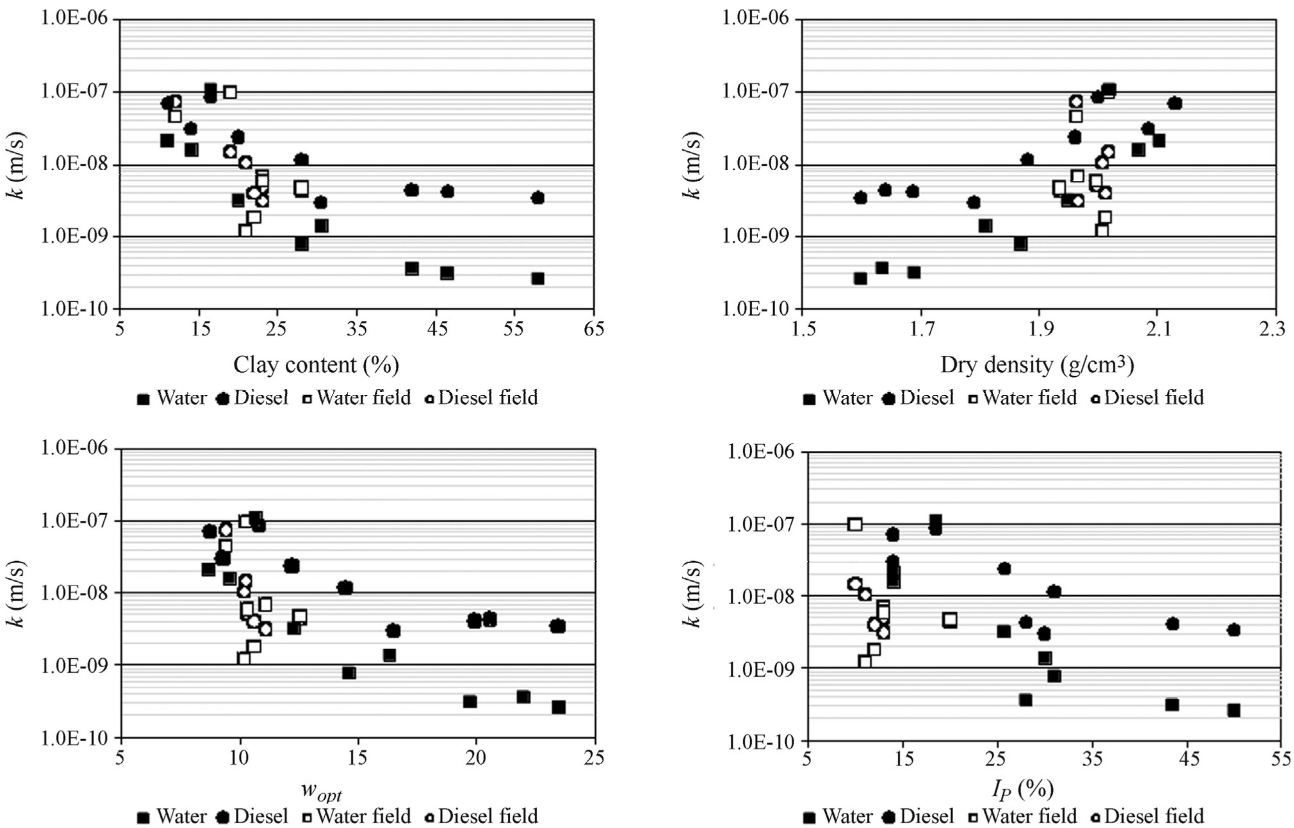

Figure 9 - Comparison between field (first campaign) and laboratory (previous research phase) results.

Table 6 - Field permeameter results. First field campaign.

Fine content (*Fc*)/mixture	45%	40%	37%	35%	33%	18%	27%
	Mix. 1	Mix. 2	Mix. 3	Mix. 4	Mix. 5	Mix. 6	Mix. 7
Water	5E-07	7E-07	6E-07	2E-07	1E-07	5E-06	1E-05
Commercial diesel	4E-07	3E-07	5E-07	4E-07	1E-06	7E-06	1E-06
Brazilian gasoline	3E-06	1E-06	2E-06	2E-06	2E-06	5E-06	7E-07
Bio-diesel	3E-07	3E-07	1E-07	9E-07	1E-07	4E-06	1E-06

Table 7 - Field permeameter results. Second field campaign.

Fine content (*Fc*)/mixture	45%	40%	37%	35%	33%	18%	27%
	Mix. 1	Mix. 2	Mix. 3	Mix. 4	Mix. 5	Mix. 6	Mix. 7
Water	5E-06	1E-06	7E-07	1E-05	1E-06	2E-05	1E-06
Commercial diesel	2E-06	8E-07	3E-06	6E-06	2E-06	2E-05	8E-07
Brazilian gasoline	4E-06	1E-05	6E-07	7E-05	5E-06	4E-05	4E-06
Bio-diesel	4E-06	2E-06	1E-06	2E-06	4E-06	7E-06	1E-05

Table 8 - Values of k_2/k_1.

Fine content (Fc)/mixture	45%	40%	37%	35%	33%	18%	27%
	Mix. 1	Mix. 2	Mix. 3	Mix. 4	Mix. 5	Mix. 6	Mix. 7
Water	11.03	2.11	1.19	57.55	9.17	3.34	0.11
Commercial diesel	5.23	2.56	5.39	14.33	2.22	3.33	0.52
Brazilian gasoline	1.59	11.81	0.30	32.70	2.54	8.82	6.62
Bio-diesel	13.24	5.67	14.98	2.59	35.52	1.69	8.75

Tables 3 and 4) and mixture 7 has a fine content of 27% which is close to the minimum fine content of the proposed range (33%).

b) The second campaign, performed during the dry period, presented higher k values compared to the first one. The only exceptions were the results for mixture 7, water and diesel fluids. As expected, because of their higher fine content, mixtures 1 and 2 presented higher permeability ratios between the second and the first campaigns (k_2/k_1). The presence of shrinkage cracks was more evident in these soils. Mixture 4 behaved unexpectedly with the highest permeability ratios between the first and second campaigns. It is worth pointing out, however, that this landfill was constructed away from the other landfills, resulting in a larger exposed area for evaporation and shrinkage (a larger number of shrinkage cracks could be observed in field). Despite the increase in the permeability values over time, the authors consider the obtained k_2/k_1 ratios to be quite acceptable, since there are many variables that could affect the obtained results in field. 29% of the k_2/k_1 ratios values presented in Table 8 are higher than 10.

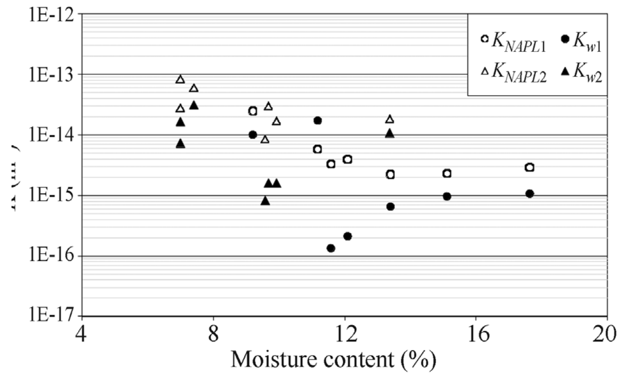

Figure 10 - Intrinsic permeability values calculated based on water, K_w and NAPL (gasoline, diesel and bio-diesel), K_{NAPL} and their variation with soil water content.

Fig. 10 shows how the intrinsic permeability, K, varies as a function of the fluid and the water content of the soil. In this graph, K_w refers to the average soil intrinsic permeability calculated using water as the base fluid whereas K_{NAPL} refers to the average value calculated using diesel, biodiesel and gasoline. As expected, because NAPL has a lower dielectric constant relative to water, K_{NAPL} values are higher than K_w, for the same water content. On the other hand, because water has a higher wettability than NAPL (water is the most wettable fluid), lower moisture contents will increase available spaces for NAPL flow, increasing the K_{NAPL} value. The subscripts *1* and *2* refer to the first and second field campaign, respectively. These results emphasize the need for barrier specifications not to be based on water permeability but rather on results obtained from testing the same fluids as those to be stored in the field.

Table 9 and Fig. 11 compare the laboratory and field results (second campaign). Note that the undisturbed blocks were collected in the same period as the second field campaign. Besides the coefficient of permeability, this ta-

Table 9 - Laboratory x field coefficient of permeability.

Mix.	$k_{diesel2}\alpha_{orig}$ (m/s)	$k_{w2}\alpha_{orig}$ (m/s)	w (%)	α_{orig} (cm^{-1})	$k_{diesel2}\alpha_m$ (m/s)	$k_{w2}\alpha_m$ (m/s)	α_m (cm^{-1})	$k_{diesellab}$ (m/s)	w (%)	k_{wlab} (m/s)	w (%)
Mix. 1	2E-08	5E-08	13.37	0.010	6E-08	1E-07	0.033	3E-09	13.62	1E-09	13.52
Mix. 2	8E-09	1E-08	9.68	0.010	3E-08	5E-08	0.045	1E-07	9.77	8E-09	9.74
Mix. 3	3E-08	7E-09	9.58	0.010	1E-07	4E-08	0.077	2E-08	9.39	3E-09	9.80
Mix. 4	6E-08	1E-07	7.51	0.010	5E-07	8E-07	0.211	1E-07	8.75	1E-08	8.46
Mix. 5	2E-08	1E-08	7.93	0.010	4E-08	2E-08	0.020	1E-07	7.80	1E-08	8.07
Mix. 6	2E-07	2E-07	7.00	0.010	1E-06	6E-07	0.054	1E-06	6.80	1E-06	7.26
Mix. 7	8E-09	1E-08	7.00	0.010	6E-08	7E-08	0.144	1E-08	7.40	4E-09	7.21

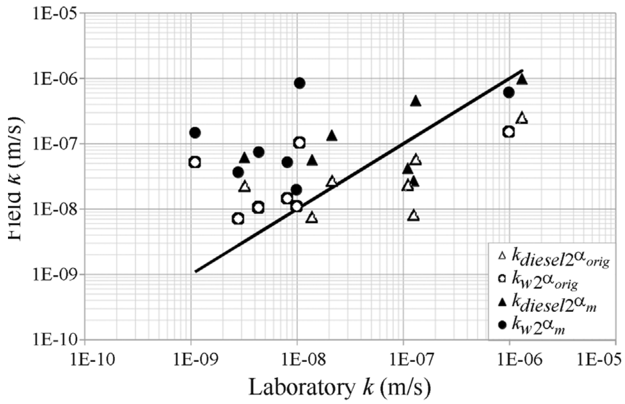

Figure 11 - Laboratory x field permeability results.

ble shows the initial moisture content of the soil and the α value adopted when computing field permeability. In this table α_{orig} means the adoption of the α values suggested in Table 5 (α = 0.01) and α_m means the average α value obtained considering the valid field permeability results for each landfill. The subscript *2* refer to the second field campaign. As can be seen, the laboratory and field *samples* had similar moisture contents before the tests. Laboratory and field permeability values showed fair agreement. Discarding the three most discrepant results, the maximum difference between the values is around 10.

Fig. 12 compares the field and laboratory results predicted by Eq. 5 and obtained experimentally. In Fig. 12(a) the field results were calculated assuming $\alpha = 0.01$ whereas Fig. 12(b) presents the field results calculated using the values of α_m shown in Table 9. As can be observed, the use of the α_m values improved the performance of the model compared to the adoption of a single value for all the landfills ($\alpha = 0.01$). However, the number of experimental points located outside the confidence interval is larger than 10%. A higher scattering in the field results had been expected because field tests are less controlled than those in a laboratory environment and the landfills undergo the influence of changes in the weather, which causes the appearance of shrinkage cracks.

Table 10 - Optimal ranges of index properties for the construction of mineral barriers for containment of organic fluids.

Index property	Proposed range
Plasticity Index (I_p)	12%-25%
Fine (clay + silt) content (*Fc*)	25%-45%
Clay content (*Cc*)	20%-35%
Sand content (*Sc*)	45%-70%
Optimal water content (w_{ot})	10%-17%
Maximum dry density (ρ_{dmax})	1.65-2.0 (g/cm^3)

As discussed earlier, second field campaign was performed during the dry season when the soil had a lower moisture content and after the soil had undergone the first wetting/drying cycle. This resulted in higher k values compared to the first campaign. On the other hand, the laboratory results tended to be lower than the field results of the second campaign. This is probably due to the hydraulic anisotropy of the compact soil, which presents higher *k* values in the horizontal direction compared to the vertical. Laboratory tests measured the vertical coefficient of permeability whereas Guelph permeameter measured flow rate in both directions.

Table 10 shows the proposed refinement for the ranges of index properties presented earlier in Table 3. As can be observed, all the indexes were changed toward the use of coarser soils. These changes reflect the good response of the landfills constructed using mixtures with fine contents close to the minimum value of the original range (33%) or even lower than stipulated, as in the case of mixture 7, in which a fine content of 27% was used. The new range is based on the expected long-term performance of the barriers, since clayey soils tend to increase k over time in a more pronounced way than coarse soils.

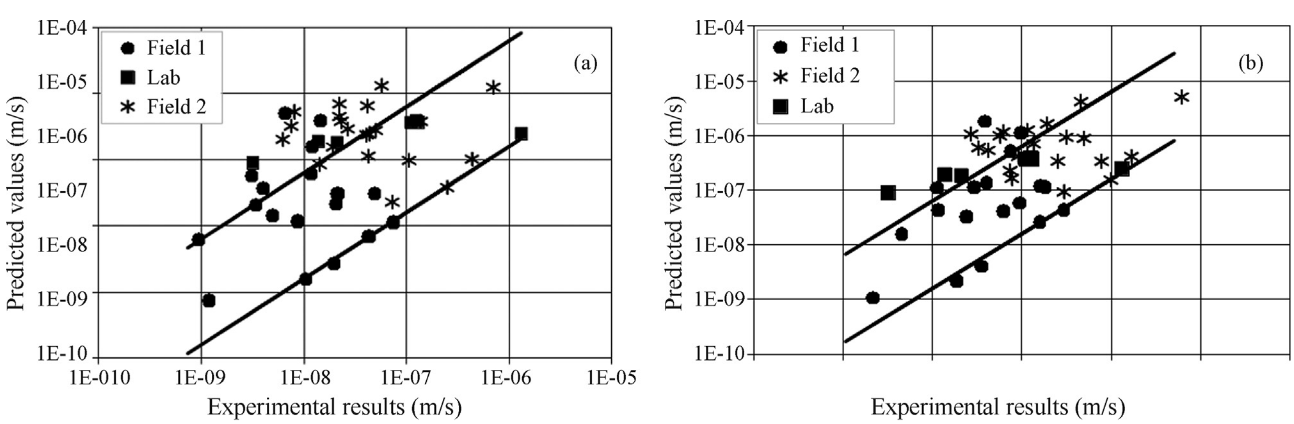

Figure 12 - Experimental and predicted permeability values by Eq. 5.

5. Conclusions

This paper presents the results of field permeability tests that were carried out in landfills constructed using optimal ranges of soil index properties for mineral barriers for the containment of organic fluids. The obtained results corroborate several results published in the technical literature (Fernandez & Quigley, 1985; Budhu *et al.*, 1991; Oliveira, 2001; Amarasinghe *et al.*, 2012 and Cardoso, 2011): fluids with low dielectric constants (non polar) tend to present higher intrinsic permeabilities than polar fluids because they reduce the double layer thickness, providing more space in the voids of the soil for NAPL flow. On the other hand, the presence of water, the most wettable fluid, reduces the permeability of NAPL as interstitial water reduces the available pore spaces for NAPL (Machado *et al.*, 2016 and Cardoso, 2011).

Clayey soils tend to have a lower long term performance due to field wetting/drying cycles and the consequent appearance of cracks and fissures. Despite the increase in the permeability values over time, however, the authors consider the obtained k_2/k_1 ratios quite acceptable, as soil permeability is perhaps the most sensitive soil parameter and there are many variables that could affect the obtained results in the field. Only 29% of the values presented in Table 8 are higher than 10.

The obtained field results are coherent with previous studies performed in the laboratory in order to establish optimal ranges of index properties. However, considering the obtained results as a function w_{opt} and I_P, the landfills showed good results even for relatively low I_P and w_{opt} values.

Although there was good agreement between the fine content range proposed previously and the obtained results in the field, some changes were required to improve the soil index ranges. These indexes were changed towards the use of coarser soils relative to the original specifications obtained in laboratory and were proposed based on the expected long-term performance of the barriers, since clayey soils tend to increase k over time in a more pronounced way than coarse soils.

The results presented in this paper emphasize the need for the design and construction of barriers not to be based on water permeability but rather on results obtained from testing the specific fluid that they will be required to contain in the field. As low polarity fluids tend to present higher permeabilities than water in clayey soils, the use of water as a base fluid for calculation may lead to the poor performance of the mineral barriers in the field.

References

Amarasinghe, P.M.; Katti, K.S. & Katti, D.R. (2012). Insight into role of clay-fluid molecular interactions on permeability and consolidation behavior of Na-montmorillonite swelling clay. Journal of Geotechnical and Geoenvironmental Engineering, 138(2):138-146.

Amorim Jr. (2007). Evaluation of Criteria for Waterproofing of Levees for Containement Proposed by ABNT NBR 17505-2/2006. M.Sc. Dissertation, UFSC, Florianópolis, 114 p. (In Portuguese).

Akinwumi I.I.; Diwa D. & Obianigwe N. (2014). Effects of crude oil contamination on the index properties, strength and permeability of lateritic clay. Int. Journal of Applied Sciences and Engineering Research, 3(4):816-824.

Anandarajah, A. (2003). Mechanism controlling permeability change in clays due to changes in pore fluid. J. of Geotechnical and Geoenvironmental Engineering, 129(2):163-172.

ASTM D5126/D5126M-90 (2010)e1. Standard Guide for Comparison of Field Methods for Determining Hydraulic Conductivity in Vadose Zone. Annual Book of ASTM Standards. ASTM International, West Conshohocken, USA.

Brown, K.W. & Anderson, D.C. (1983). Effects of Organic Solvents on the Permeability of Clay Soils. Environmental Protection Agency (U.S.), EPA-600/S2-83-016.

Brown, K.W. & Thomas, J.C. (1984). Conductivity of three commercially available clays to petroleum products and organic solvents. J. of Hazardous Wastes, 1(4):546-553.

Budhu, M.; Giese Jr. R.F.; Campbell, G. & Baumgrass, L. (1991). The permeability of soils with organic fluids. Can. Geotechnical Journal, 28(1):140-147.

Cardoso, L.S.P. (2011). NAPL Transport in Soils. Ph.D. Thesis, Federal University of Bahia, Salvador, BA, 149 p. (In Portuguese).

Carvalho, Z.S. (2015). Performance of Mineral Barriers of Compacted Soils Using Optimal Grain Size Distributions. M.Sc. Dissertation, Federal University of Bahia, Salvador, BA, 127 p. (In Portuguese).

Corseuil, H.X. & Marins, M.D. (1997). Subsurface water contamination by gasoline: This is a serious problem?. Revista de Engenharia Sanitária e Ambiental, 2(2):50-54 (In Portuguese).

CETESB - Companhia de Tecnologia de Saneamento Ambiental. Relation of Contaminated Areas in the State of São Paulo. December 2013. http://www.cetesb.sp.gov.br/userfiles/file/areas-contaminadas/2013/texto-explicativo.pdf.

Daniel D. & Benson, C. (1990). Water content-density criteria for compacted soil liners. Journal of Geotechnical Engineering, ASCE, 116(12):1811-1830.

Daniel D.E. & Wu Y.K. (1993) Compacted clay liners and covers for arid sites. J Geotech Eng, 119(2):223-237.

Elrick, D.E.; Reynolds, W.D. & Tan, K.A. (1989). Hydraulic conductivity measurements in the unsaturated zone using improved well analysis. Ground Water Monitoring Review 9(3):184-193.

Fang, H.Y. (1997). Introduction to Environmental Geotechnology. CRC press LLC, 670 p.

Fernandez, F. & Quigley, R.M. (1985). Hydraulic conductivity of natural clays permeated with simple liquid hydrocarbons. Can. Geotechnical Journal, Volume 22(2):205-214.

Fernandez, F. & Quigley, R.M. (1988). Viscosity and dielectric constant controls on the hydraulic conductivity of clayey soils permeated with water-soluble organics. Can. Geotechnical Journal, 25(3):582-589.

Graber, E.R. & Mingelgrin, U. (1994). Clay swelling and regular solution theory. Environ. Sci. Technol, 28(13):2360-2365.

Goodarzi, A.R.; Fateh, S.N. & Shekary, H. (2016). Impact of organic pollutants on the macro and microstructure responses of Na-bentonite. Applied Clay Science, 121:17-28.

Kaipper, B.I.A. (2003) The influence of Ethanol in the Aromatic Hydrocarbon Solubility in Diesel Contamined Aquifers. Ph.D. Thesis, Federal University of Santa Catarina, Florianópolis, SC, 199 p. (In Portuguese).

Kaya, A. & Fang, H.Y. (2000). The effects of organic fluids on physicochemical parameters of fine-grained soils. Can. Geotechnical Journal, 37(5):943-950.

Kaya, A. & Fang, H.Y. (2005). Experimental evidence of reduction in attractive and repulsive forces between clay particles permeated with organic liquids. Can. Geotech. Journal, 42(2):632-640.

Machado, S.L.; Cardoso, L.S.P.; Oliveira, I.A.; Mariz, D.F.M. & Karimpour-Fard, M. (2016). Modeling soil permeability when percolated by different soil. Transport in Porous Media, 111(3):763-793.

Mesri, G. & Olson, R.E. (1971). Mechanisms controlling the permeability of clays. Clays and Clay Minerals, 19(3):151-158.

Mitchell, J.K. (1976). Fundamentals of Soil Behavior. John Wiley and Sons, Inc., New York.

NBR 14545 (2000). Soil Permeability Determination. Falling Head (In Portuguese).

NBR 13896 (1997). Non Dangerous Materials Landfills (In Portuguese).

NBR 17505-1 (2006). Storage of Flammable and Combustible Liquids (In Portuguese).

NBR 6457 (1986). Soil Samples Preparation for Compaction and Characterization (In Portuguese).

NBR 6459 (1984). Liquid Limit Determination (In Portuguese).

NBR 6508 (1984). Specific Mass of Soil Grains Passing on 4.8 Sieve (In Portuguese).

NBR 7180 (1984). Plasticity Limit Determination (In Portuguese).

NBR 7181 (1984). Grain Size Analysis (In Portuguese).

NBR 7182 (1986). Compaction Test (In Portuguese).

N. Filho, I.; Vieceli, N.C.; Cardoso, E.M. & Lovatel, E.R. (2013). Analysis of BTEX in experimental columns containing neat gasoline and gasoline-ethanol. J. Braz. Chem. Soc., 24(3):410-417.

Nutting, P.G. (1934). Physical analysis of oil sands. Am. Assoc. Petroleum Geologists Bull, 14(10):1337-1349.

Oliveira, J.C.S. (2001). Clayey Sediments Contamination by Automotive Fuels: The Problem of the Permeability Assessment. Ph.D. Thesis, Federal University of Bahia, Salvador, BA, 116 p. (In Portuguese).

Parker, F.; Benefield, L.D. & Marshall, N.M. (1986). Effect of Organic Fluids on Clay Permeability. In: Proceeding of the 41st Industrial Waste Conference, Purdue University, pp. 283-292.

Reynolds, W.D. & Elrick, D.E. (1985). In situ measurement of field saturated hydraulic conductivity, sorptivity, and the [alpha]-parameter using the Guelph permeameter. Soil Science, 140(4):292-302.

Reynolds, W.D.; Elrick, D.E. & Topp, G.C. (1983). A reexamination of the constant head well permeameter method for measuring saturated hydraulic conductivity above the water table. Soil Science, 36(4):250-268.

Schneider, M.R. (2005) Weathering of Contaminated Sources in Aquifers Impacted by Gasoline and Alcohol and the Influence on the Human Health. Ph.D. Thesis, Federal University of Santa Catarina, Florianópolis, SC, 192 p. (In Portuguese).

Schramm, M.; Warrick, A.W. & Fuller, W.H. (1986). Permeability of soils to four organic liquids and water. Hazardous Waste & Hazardous Materials, 3(1):21-27.

Shackelford, D.C. (2014). The ISSMGE Kerry Rowe Lecture: The role of diffusion in environmental geotechnics. Can. Geotechnical Journal, 51(11):1219-1242.

Silveira, C.S. (2004) Infiltration and Transport in the Unsaturated Zone of a Forest Soil - Tijuca Park. Ph.D. Thesis, Federal University of Rio de Janeiro, Rio de Janeiro, RJ, 217 p. (In Portuguese).

Wang M.C. & Huang C.C. (1984) Soil compaction and permeability prediction models. J Environ Eng, ASCE, 110(6):1063-1083.

Technical Notes

The Effect of Not Fully Grouted Rock Bolts on the Performance of Rock Mass

H. Xu, Y. C. Zhao, W. K. Bu

Abstract. According to the characteristics of rock bolts in mining engineering, a mechanical model for not fully grouted rock bolt is presented to obtain the expression of shear displacement, the axial force and the shear stress along the anchor section. On these bases, the effect of the length of anchor section on the performance of rock mass and the effect of the axial force at the free end of the bolt on the performance of rock mass are analyzed by COMSOL Multiphysics. According to the results of numerical simulations, there are some conclusions as following: (1) a moderate length of anchor section, such as the length of 1.0 m~1.4 m, is favorable in mining supporting design, which can make sure grout and rock in coupled state and reduce the construction cost; (2) the favorable distance between the rock bolts is from 0.9 m to 1.3 m; (3) more rock bolts should be installed if the rock mass has larger deformation, which also can make sure grout and rock in coupled state. Conversely, less rock bolts should be installed if the rock mass has smaller deformation, which also can reduce the construction cost.

Keywords: not fully grouted, rock bolt, supporting design, coal roadway, mining engineering.

1. Introduction

Rock bolts have been widely used for rock reinforcement in underground engineering for a long time, especially in mining engineering in China. In order to improve the rock bolting effect, it is necessary to have a good understanding of the effect of rock bolts on the performance of rock mass.

Since the 1970s, numerous researchers have carried out field monitoring (Freeman, 1978; Björnfot & Stephansson, 1984a,b; Sun, 1984; Choquet & Miller, 1988), laboratory tests (Hawkes & Evans, 1951; Farmer, 1975; Stillborg, 1994; Stjern, 1995; Benmokrane *et al.*, 1995; Hyett *et al.*, 1995; Hagan, 2004; Moosavi *et al.*, 2005; Marthin *et al.*, 2011), analytical approaches (Farmer, 1975; Yazici & Kaiser, 1992; Hyett *et al.*, 1995; Pellet & Egger, 1996; Li & Stillborg, 1999; Cai *et al.*, 2004; Ren *et al.*, 2010; Marthin *et al.*, 2011; Fahimifar & Ranjbarnia, 2011; He *et al.*, 2015) and numerical simulations (Larson & Olofsson, 1984; Fuller *et al.*, 1996; Ivanovic & Neilson, 2009; Deb & Das, 2010) for a better understanding of the load transfer mechanism between the rock bolts and the surrounding rock mass. Some concepts such as "neutral point", "pick-up length" and "anchor length", clearly outline the behavior of fully grouted rock bolts in a deformed rock formation. Undoubtedly, these studies contribute to a better comprehension of the mechanical behavior of fully grouted rock bolts.

Nevertheless, the characteristics of rock bolts in mining engineering are not the same as the characteristics of fully grouted rock bolts in civil engineering or other underground engineering in China. These differences are in two aspects: (1) the rock bolts in mining engineering are not fully grouted. A single rock bolt is divided into "anchor section" and "freedom section" as shown in Fig. 1. Here, the anchor section means the bolt section within grouted layer and the freedom section means the bolt section without grouted layer; (2) the faceplate is installed at the free end of the bolt, which can provide effective support to the rock mass and generate an axial force at the free end of rock bolt. These differences must be taken into account in developing analytical models for not fully grouted rock bolts.

The aim of this paper is to analyze the effect of not fully grouted rock bolts on the performance of rock mass. A mechanical model for not fully grouted rock bolt is presented first, and then the shear displacement, the axial force and the shear stress along the anchor section are obtained. On these bases, numerical simulations are carried out by COMSOL Multiphysics for analyzing the effect of the length of anchor section on the performance of rock mass and the effect of the axial force at the free end of the bolt on the performance of rock mass.

2. Theoretical Analysis

Windsor (1997) proposed the concept that a reinforcement system comprises four principal components: the rock mass, the reinforcing element, the internal fixture and the external fixture. For reinforcement with a rock bolt in mining engineering, the reinforcing element refers to the rock bolt and the external fixture refers to the faceplate and

Hui Xu, PhD. Student, State Key Laboratory for Geomechanics & Deep Underground Engineering, School of Mechanics & Civil Engineering, China University of Mining & Technology, Xuzhou, Jiangsu, China and Heze University, Heze, Shandong, China. e-mail: xu_hui521@126.com.
Yu Cheng Zhao, Full Professor, Doctoral Supervisor, State Key Laboratory for Geomechanics & Deep Underground Engineering, School of Mechanics & Civil Engineering, China University of Mining & Technology, Xuzhou, Jiangsu, China. e-mail: zhaoyc1972@163.com.
Wan Kui Bu, PhD, Associate Professor, Resources and Environment Department, Heze University, Heze, Shandong, China. e-mail: bwk239@126.com.
Submitted on June 3, 2015; Final Acceptance on May 3, 2016; Discussion open until December 30, 2016.

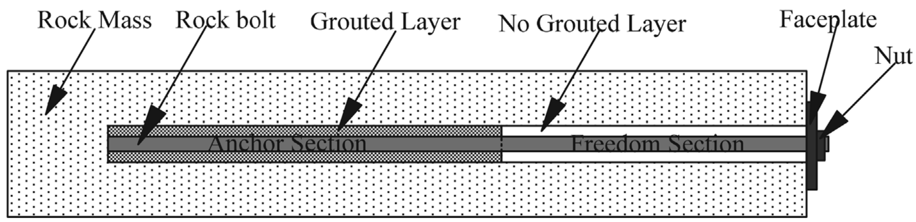

Figure 1 - A not fully grouted rock bolt in surrounding rock mass.

nut. The internal fixture is the grouted layer, which usually uses epoxy resin in mining engineering in China. The internal fixture provides a coupling condition at the interface. When grouted bolts are subjected to an axial pull load, failure may occur at the bolt-grout interface, or at the grout-rock interface. However, in this study we concentrate on the effect of rock bolts on the performance of rock mass, which is based on the hypothesis that there is no failure at the bolt-grout interface, or at the grout-rock interface. In other words, the decoupling at the interface is not considered in this paper.

It is well known that the faceplate restrains the deformation of the rock mass, and at the same time, there is an axial force in the rock bolt. For keeping balance, the anchor section of rock bolt is induced shear stress at the bolt-grout interface. And then the shear stress at the bolt-grout interface transfers into grouted layer, which also induces shear stress at the grout-rock interface. Finally, the shear stress transfers into rock mass. When the shear stress at the bolt-grout interface and the shear stress at the grout-rock interface are both lower than the shear strength, there is no slippage at the bolt-grout interface and the grout-rock interface, which is called coupling stage or compatible deformation stage.

The concept of the mechanical model of a single rock bolt and grouted layer is drawn in Fig. 2 and the equilibrium balance of the infinitesimal element in anchor section is shown in Fig. 3. According to the balance of the infinitesimal element of the rock bolt and grouted layer in anchor section, the equilibrium equation is written as,

$$N(x+dx) - N(x) - \pi D \tau(x) dx = 0 \tag{1}$$

where, dx is the length of the infinitesimal element; $N(x)$ and $N(x+dx)$ are the axial force at left side and right side of the infinitesimal element, respectively; D is the diameter of the borehole and $\tau(x)$ is the shear stress at the grout-rock interface.

According to Taylor expansion and ignoring high-order remainders, Eq. 1 can be expressed as below,

$$\frac{dN(x)}{dx} = \pi D \tau(x). \tag{2}$$

The geometrical equation of the infinitesimal element in anchor section is expressed as,

$$\Delta u = \frac{4N(x)}{\pi D^2 E_a} dx \tag{3}$$

where, Δu is the extension of the infinitesimal element, which can be expressed as Eq. 4; E_a is the composite elastic modulus of rock bolt and grouted layer, which can be calculated as Eq. 5.

$$\Delta u = u(x+dx) - u(x) \tag{4}$$

where, $u(x)$ and $u(x+dx)$ are the axial displacement at left side and right side of the infinitesimal element, respectively.

$$E_a = \left\{ E_g \left(\frac{\pi D^2}{4} - A \right) + E_b A \right\} / \left(\frac{\pi D^2}{4} \right) \tag{5}$$

where, E_b and E_g are elastic modulus of rock bolt and grouted layer, respectively; A is the area of the cross-section of the rock bolt (He & Li, 2006).

Combining Eq. 3 and Eq. 4, and ignoring high-order remainders, the following equation can be obtained.

$$u'(x) = \frac{4N(x)}{\pi D^2 E_a}. \tag{6}$$

After differential and substituting Eq. 2 into Eq. 6, it turns to Eq. 7.

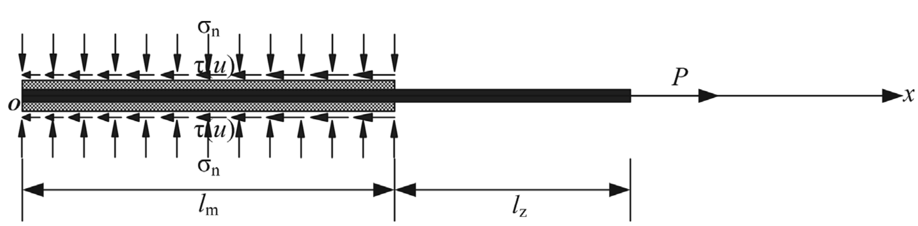

Figure 2 - Mechanical model of a single rock bolt and grouted layer.

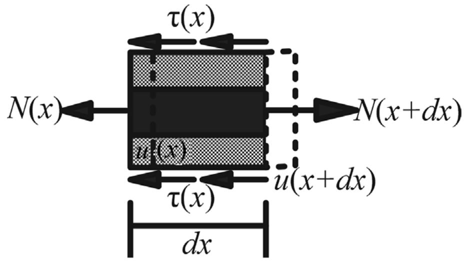

Figure 3 - Equilibrium element of the rock bolt and grouted layer in anchor section.

$$u''(x) - \frac{4\tau(x)}{DE_a} = 0. \tag{7}$$

When the reinforcement system is in coupling stage, the constitutive equation for grouted layer can be expressed as,

$$\tau(x) = Ku(x) \tag{8}$$

where, K is shear stiffness.

Substituting Eq. 8 into Eq. 7, it can be written as,

$$u''(x) - \frac{4Ku(x)}{DE_a} = 0. \tag{9}$$

The solution for Eq. 9 can be expressed as,

$$u(x) = C_1 e^{\beta x} + C_2 e^{-\beta x} \tag{10}$$

where, $\beta = \sqrt{\dfrac{4K}{DE_a}}$.

Substituting Eq. 10 into Eq. 6 and Eq. 8, the expressions for $N(x)$ and $\tau(x)$ can be written as,

$$N(x) = \frac{\pi D^2 E_a}{4}(C_1 \beta e^{\beta x} - C_2 \beta e^{-\beta x}) \tag{11}$$

$$\tau(x) = K(C_1 e^{\beta x} + C_2 e^{-\beta x}). \tag{12}$$

According to Fig. 2, the boundary conditions are expressed as Eq. 13,

$$x = l_m, \quad N(l_m) = P, \tag{13a}$$

$$\int_0^{l_m} \tau(x)\pi D dx = P \tag{13b}$$

where, l_m is the length of anchor section, P is the axial force at the free end of rock bolt.

Combining Eq. 11-Eq. 13, the expressions for $u(x)$, $N(x)$ and $\tau(x)$ can be expressed as following:

$$u(x) = \frac{4P}{\pi \beta D^2 E_a (e^{\beta l_m} - e^{-\beta l_m})}(e^{\beta x} + e^{-\beta x}) \tag{14}$$

$$N(x) = \frac{P}{e^{\beta l_m} - e^{-\beta l_m}}(e^{\beta x} - e^{-\beta x}) \tag{15}$$

$$\tau(x) = \frac{\beta P}{\pi D(e^{\beta l_m} - e^{-\beta l_m})}(e^{\beta x} + e^{-\beta x}). \tag{16}$$

3. Numerical Simulation Model

The deformation of rock mass before rock bolts supporting and after rock bolts supporting are shown in Fig. 4. An effective region, such as the red region in Fig. 4, is selected as the research object. Here, the range of effective region is wider than the influence range of a single rock bolt. Considering the unloading effect of excavation, the mechanical model of the effective region is proposed in Fig. 5. The left and right boundaries in Fig. 5 are fixed as the same as top boundary. The bottom boundary in Fig. 5 is uniform stress boundary, which simulates the unloading of excavation. Since the model is axisymmetric, it is sufficient to analyze only half of the model in Fig. 5, which is named simplified model shown in Fig. 6. The boundaries of simplified model are the same as the boundaries of model in Fig. 5 except the left boundary. The left boundary of simplified model is divided into two parts, which are called anchor section boundary and freedom section boundary, respectively. For anchor section boundary, the horizontal dis-

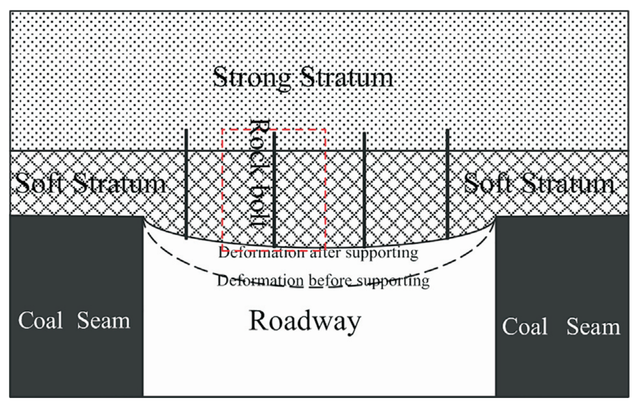

Figure 4 - Deformation of rock mass in coal roadway.

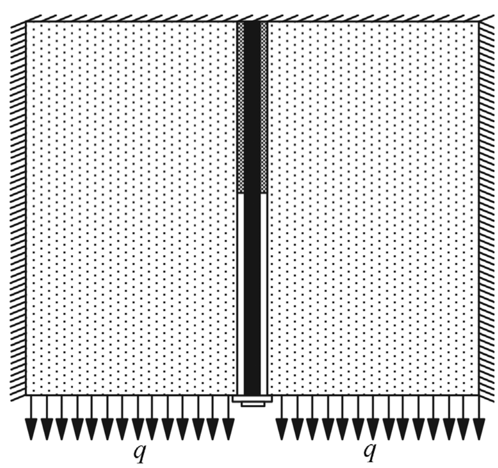

Figure 5 - Mechanical model of the effective region.

placement is zero and the vertical displacement is calculated according to Eq. 17; for freedom section boundary, the horizontal displacement is also zero but the vertical displacement is obtained according to Eq. 18. Thus, the numerical simulation model is built by COMSOL Multiphysics with free mesh, in which the height is 2.4 m and the width is 2 m. The boundary conditions of numerical simulation model and the coordinate system are shown in Fig. 7.

$$u(y_1) = -\frac{4P}{\pi\beta D^2 E_a (e^{\beta l_m} - e^{-\beta l_m})}(e^{-\beta y_1} + e^{\beta y_1}) \quad -l_m \le y_1 \le 0 \tag{17}$$

$$u(y_2) = \frac{P(y_2 + l_m)}{E_b A} - \frac{4P}{\pi\beta D^2 E_a (e^{\beta l_m} - e^{-\beta l_m})}(e^{\beta l_m} + e^{-\beta l_m}) \quad -l \le y_2 \le -l_m \tag{18}$$

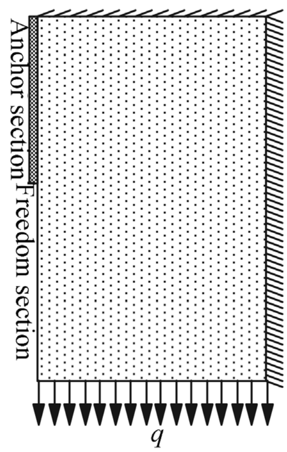

Figure 6 - Simplified model.

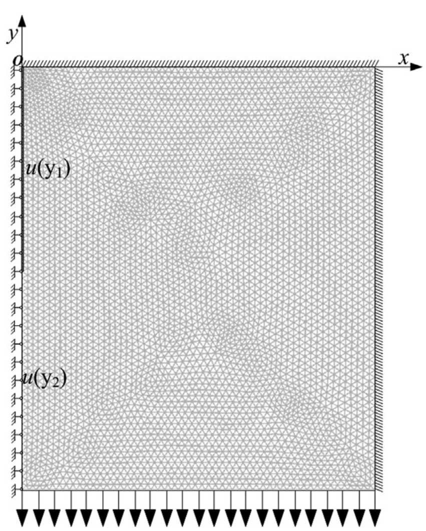

Figure 7 - Numerical simulation model.

where, l_m is the length of anchor section, P is the axial force at the free end of rock bolt.

4. Analysis on the Influence of Not Fully Grouted Rock Bolt on the Performance of Rock Mass

According to the proposed model, the performance of rock mass mainly depends on the axial force P at the free end of rock bolt and the length of anchor section l_m. The uniform load on the bottom boundary in Fig. 6 equals to 20×10^6 Pa and the other basic parameters are listed in Table 1.

4.1. Influence of the length of anchor section

For researching the effect of the length of anchor section l_m on the performance of rock mass, the axial force P at the free end of rock bolt should be a constant. Here, the axial force P equals to 80×10^3 N and the length of anchor section l_m changes from 0 m to 2.2 m in the proposed simulation model. The expression $l_m = 0$ m means that there is no rock bolt supporting.

The numerical results including vertical displacement, vertical stress and vertical strain are shown in Fig. 8. The vertical displacement of bottom boundary in simulation model is shown in Fig.9, which means the vertical displacement of rock mass at the roof of roadway. When the length of anchor section increases from 0 m to 0.6 m, the vertical displacement of rock mass at the faceplate decreases from 67.8×10^{-3} m to 3.63×10^{-3} m, which means that the vertical displacement of rock mass decreases significantly if the rock mass is supported by rock bolt. But on the other side, when the length of anchor section increases from 1.4 m to 2.2 m, the vertical displacement of rock mass at the faceplate decreases from 2.02×10^{-3} m to 1.18×10^{-3} m, which means that the supporting performance of rock bolt cannot improve significantly only by increasing the length of anchor section.

Compared with no rock bolt supporting, the relative reduction of vertical displacement of rock mass is shown in

Table 1 - Basic parameters of rock mass and rock bolt.

Rock mass's deformation modulus E_m	0.5×10^9 Pa
Poisson's ratio of rock mass μ_m	0.30
Density of rock mass ρ_m	2200 kg/m^3
Young's modulus of rock bolt E_b	210×10^9 Pa
Length of rock bolt l	2.4 m
Diameter of rock bolt D_b	24×10^{-3} m
Diameter of borehole	36×10^{-3} m
Deformation modulus of grouted layer	15×10^9 Pa
Grouted layer's shear stiffness	0.6×10^9 Pa/m

 Soils and Rocks, São Paulo, 39(3): 317-324, September-December, 2016.

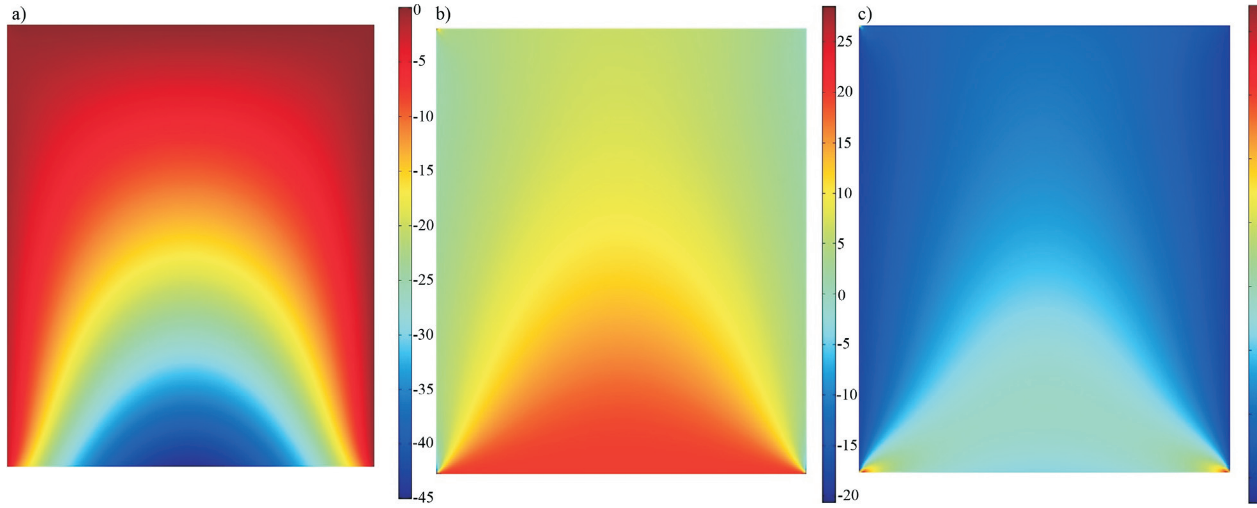

Figure 8 - Numerical results (l_m = 1.4 m). (a) Vertical displacement/$\times 10^{-3}$ m. (b) Vertical stress/$\times 10^6$ Pa. (c) Vertical strain.

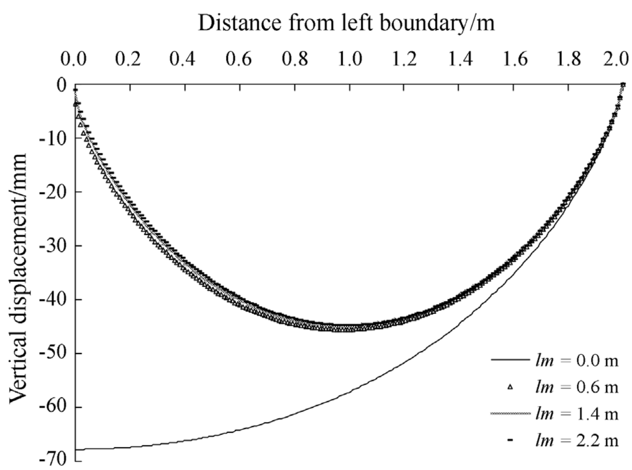

Figure 9 - Vertical displacement of rock mass at the roof of roadway.

Fig. 10. The distance from left boundary increases from 0 m to 1.4 m while the relative reduction of vertical displacement of rock mass decreases from about 90% to about 10%. If the range in which the relative reduction of vertical displacement of rock mass is more than 10% is defined as the influence range of a single rock bolt, the corresponding distance from the left boundary is defined as the influence radius of a single rock bolt. The influence radius of a single rock bolt with different length of anchor section is shown in Fig. 11. When the length of anchor section increases from 0.2 m to 2.2 m, the influence radius of a single rock bolt increases from 1.37 m to 1.49 m, which indicates that increasing the length of anchor section will increase the influence radius of a single rock bolt, however, the influence radius of a single rock bolt keeps almost constant if it exceeds certain length.

The shear stress at the grout-rock interface with different length of anchor section is also obtained in Fig. 12. According to the curves in Fig. 12, the shear stress at the grout-rock interface has not uniform distribution along the axial direction of rock bolt. Taking l_m = 1.8 m for example, the value of shear stress at the end of anchor section is 0.28×10^6 Pa while the value of shear stress at the point between anchor section and freedom section is 0.64×10^6 Pa, which shows that decoupling behavior occurs more easily at the point between anchor section and freedom section than at the end of anchor section. On the other hand, when the axial force P equals to 80×10^3 N and the length of anchor section increases from 0.2 m to 2.2 m, the minimum and the maximum shear stress decreases from 3.52×10^6 Pa to 0.20×10^6 Pa and from 3.57×10^6 Pa to 0.61×10^6 Pa, respectively, which means that increasing the length of anchor section will reduce the value of shear stress at the grout-rock interface. In other words, increasing the length of anchor section can make sure grout and rock in coupled state.

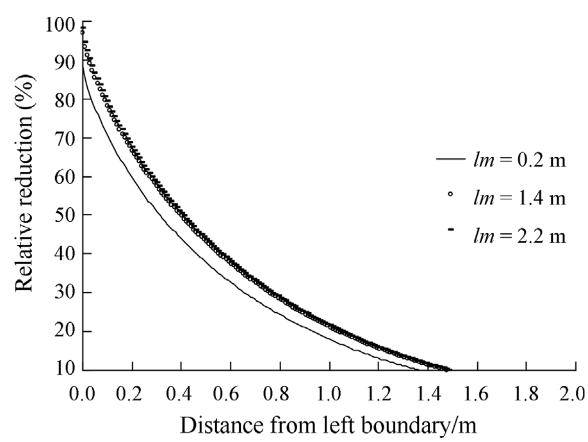

Figure 10 - Relative reduction of vertical displacement of rock mass at the roof of roadway.

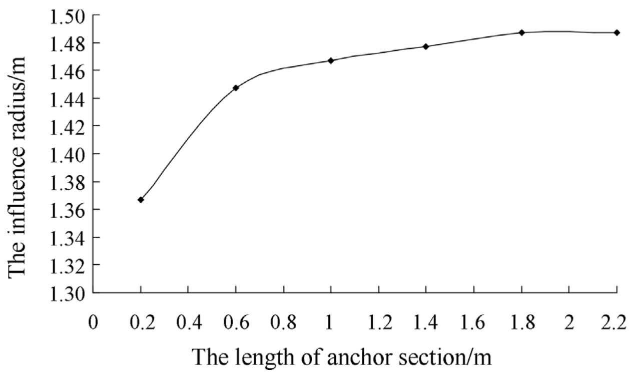

Figure 11 - Influence radius of a single rock bolt.

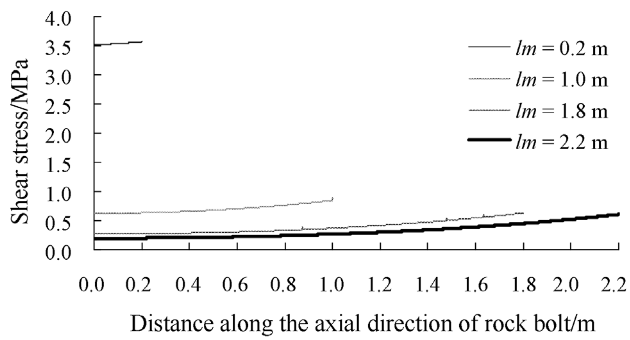

Figure 12 - Shear stress at the grout-rock interface.

4.2. Influence of the axial force at the free end of rock bolt

For researching the effect of the axial force P at the free end of rock bolt on the performance of rock mass, the length of anchor section l_m should be a constant. Here, the length of anchor section l_m equals to 1.4 m and the axial force P at the free end of rock bolt changes from 20×10^3 N to 160×10^3 N in the proposed simulation model.

The vertical displacement of rock mass at the roof of roadway is shown in Fig. 13. When the axial force at the free end of rock bolt increases from 20×10^3 N to 160×10^3 N, the vertical displacement of rock mass at the faceplate increases from 0.50×10^{-3} m to 4.03×10^{-3} m, which indicates that increasing the axial force at the free end of rock bolt will increase the vertical displacement of rock mass. However, the vertical displacement of rock mass cannot be significantly increased. On the other hand, the increasing axial force at the free end of rock bolt only influences the performance of rock mass in a small region, in which the distance from left boundary is less than 1 m.

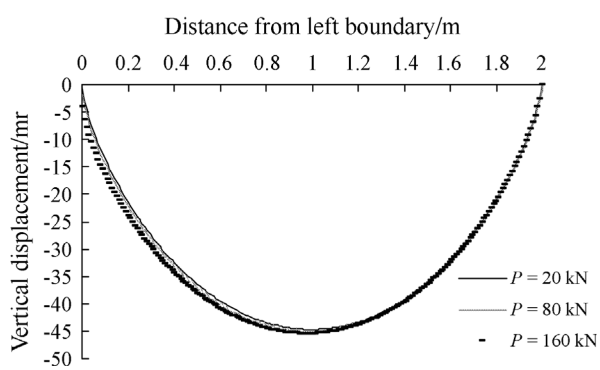

Figure 13 - Vertical displacement of rock mass at the roof of roadway.

The axial force at the free end of rock bolt is very important for mining engineering. According to the axial force at the free end of rock bolt, researchers can optimize the design of rock bolt supporting. The vertical displacement of rock mass at the faceplate with different axial force is shown in Fig. 14. Obviously, the vertical displacement of rock mass at the faceplate linearly increases with the increasing of axial force at the free end of rock bolt, which agrees well with the theoretical analysis. Therefore, more rock bolts should be installed if the rock mass has larger deformation, which also can make sure grout and rock in coupled state. Conversely, less rock bolts should be installed if the rock mass has smaller deformation, which also can reduce the construction cost.

The shear stress at the grout-rock interface with different axial force is also calculated in Fig. 15. When the axial force at the free end of rock bolt increases from

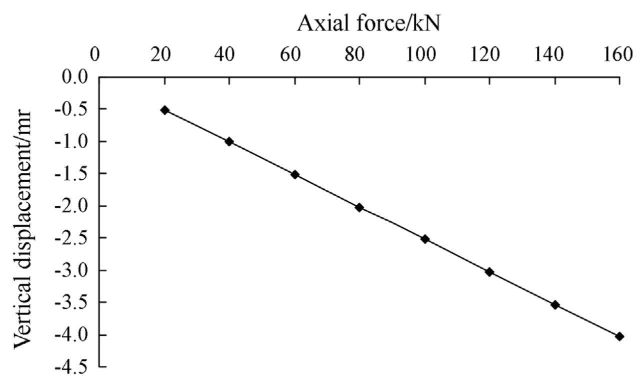

Figure 14 - Vertical displacement of rock mass at the faceplate.

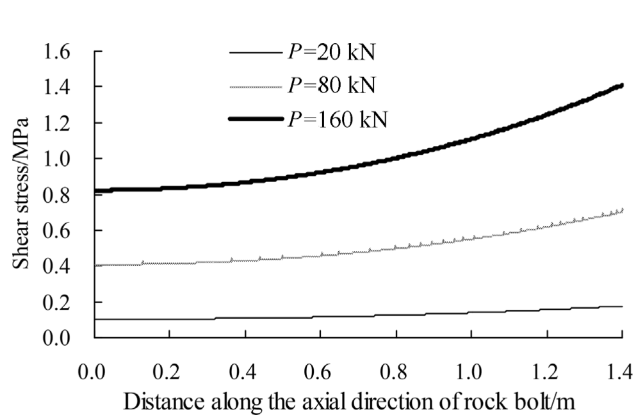

Figure 15 - Shear stress at the grout-rock interface.

20×10^3 N to 160×10^3 N, the minimum and the maximum shear stress increases linearly from 0.103×10^6 Pa to 0.824×10^6 Pa and from 0.176×10^6 Pa to 1.41×10^6 Pa, respectively, which also agrees well with the theoretical analysis. It indicates that decoupling behavior can more easily happen with bigger axial force. Thus, more rock bolts are installed in this case for reducing the axial force of rock bolts and preventing the decoupling behavior.

5. Conclusions

A mechanical model is proposed for not fully grouted rock bolts in rock mass and the effect of not fully grouted rock bolts on the performance of rock mass is discussed based on a numerical simulation model. It supplies a sufficient way to analyze the influence of not fully grouted rock bolts on the performance of rock mass for mining engineering. According to the model, the performance of rock mass mainly depends on the length of anchor section and the axial force at the free end of rock bolt, and the following findings are obtained.

1) Increasing the length of anchor section will reduce the vertical displacement of rock mass and reduce the value of shear stress at the grout-rock interface. However, the influence radius of a single rock bolt keeps almost constant if the length of anchor section exceeds certain length. Thus, a moderate length of anchor section, such as the length of 1.0 m~1.4 m, is favorable in mining supporting design, which can make sure grout and rock in coupled state and reduce the construction cost.
2) For improving the effectiveness of rock bolts supporting, the distance between the rock bolts should be less than the influence radius of a single rock bolt. Therefore, the favorable distance between the rock bolts is from 0.9 m to 1.3 m, which can explain the phenomenon that the distance between the rock bolts is about 1.1 m in the roadway supporting of mining engineering.
3) The increasing axial force at the free end of rock bolt only influences the performance of rock mass in a small region, moreover, it will increase the value of shear stress at the grout-rock interface. Thus, more rock bolts should be installed if the rock mass has larger deformation, which also can make sure grout and rock in coupled state. Conversely, less rock bolts should be installed if the rock mass has smaller deformation, which also can reduce the construction cost.

Acknowledgments

Financial support for this work, provided by National Undergraduate's Scientific Research Foundation in China (No.201310290009) and the Scientific Research Foundation of Heze University (No.XY14KJ01 & No.XYPY02) are gratefully acknowledged.

References

Benmokrane, B.; Chennouf, A. & Mitri, H.S. (1995). Laboratory evaluation of cement-based grouts and grouted rock anchors. International Journal of Rock Mechanics and Mining Sciences & Geomechanics, 32(7):633-642.

Björnfot, F. & Stephansson, O. (1984). Interaction of grouted rock bolts and hard rock masses at variable loading in a test drift of the Kiirunavaara Mine, Sweden. Proceedings of the International Symposium on Rock Bolting, Balkema, Rotterdam, pp. 377-395.

Björnfot, F. & Stephansson, O. (1984). Mechanics grouted rock bolts-field testing in hard rock mining. Swedish Rock Engineering Research Foundation.

Cai, Y.; Esaki, T. & Jiang, Y. (2004). An analytical model to predict axial load in grouted rock bolt for soft rock tunneling. Tunnelling and Underground Space Technology, 19(6):607-618.

Choquet, P. & Miller, F. (1988). Development and field testing of a tension measuring gauge for cable bolts used as ground support. CIM Bulletin, 81(914):53-59.

Deb, D. & Das, K.C. (2010). Bolt-grout interactions in elastoplastic rock mass using coupled FEM-FDM techniques. Advances in Civil Engineering, pp. 1-13.

Fahimifar, A. & Ranjbarnia, M. (2011). Analysis of circular reinforced tunnels by analytical approach. Journal of Structural Engineering, 1(1):1-5.

Farmer, I.W. (1975). Stress distribution along a resin grouted rock anchor. International Journal of Rock Mechanics and Mining Sciences & Geomechanics, 12(11):347-351.

Freeman, T.J. (1978). The behaviour of fully-bonded rock bolts in the Kielder experimental tunnel. Tunnels and Tunnelling International, 10(5):37-40.

Fuller, P.; Hume, B. & Hume, R. (1996). Bolt load simulation and its practical application. Proc. 2nd North American Rock Mechanics Symposium, Montreal, pp. 187-193.

Hagan, P.C. (2004). Variation in load transfer of a fully encapsulated rockbolt. Proc. 23rd International Conference on Ground Control in Mining, Morgantown, pp. 33-49.

Hawkes, J.M. & Evans, R.H. (1951). Bond stresses in reinforced concrete columns and beams. Journal of the Institute of Structural Engineers, 24(10):323-327.

He, L.; An, X.M. & Zhao, Z.Y. (2015). Fully grouted rock bolts: An analytical investigation. Rock Mechanics and Rock Engineering, 48(3):1181-1196.

He, S.M. & Li, X.P. (2006). Study on mechanism of prestressed anchor bolt. Chinese Journal of Rock Mechanics and Engineering, 25(9):1876-1880 (In Chinese).

Hyett, A.J.; Bawden, W.F.; Macsporran, G.R. & Moosavi, M. (1995). A constitutive law for bond failure of fully-grouted cable bolts using a modified Hoek cell. International Journal of Rock Mechanics and Mining Sciences & Geomechanics, 32(1):11-36.

Ivanovic, A. & Neilson, R.D. (2009). Modelling of debonding along the fixed anchor length. International Journal of Rock Mechanics and Mining Sciences, 46(4):699-707.

Larsson, H. & Olofsson, T. (1984). Bolt action in jointed rock. Proc. International Symposium on Rock Bolting, Abisko, pp. 33-46.

Li, C. & Stillborg, B. (1999). Analytical models for rock bolts. International Journal of Rock Mechanics and Mining Sciences, 36(8):1013-1029.

Martin, L.B.; Hassen, F.H.; Tijani, M. & Noiret, A. (2011). A new experimental and analytical study of fully grouted rockbolts. Proc. 45th US Rock Mechanics/Geomechanics Symposium, San Francisco, pp. 11-242.

Moosavi, M.; Jafari, A. & Khosravi, A. (2005). Bond of cement grouted reinforcing bars under constant radial pressure. Cement and Concrete Composites, 27(1):103-109.

Pellet, F. & Egger, P. (1996). Analytical model for the mechanical behaviour of bolted rock joints subjected to shearing. Rock Mechanics and Rock Engineering, 29(2):73-97.

Ren, F.F.; Yang, Z.J.; Chen, J.F. & Chen, W.W. (2010). An analytical analysis of the full range behaviour of grouted rockbolts based on a tri-linear bond-slip model. Construction and Building Materials, 24(3):361-370.

Stillborg, B. (1994). Professional Users Handbook for Rock Bolting. Trans Tech Publications, Germany, 268 p.

Stjern, G. (1995). Practical Performance of Rock Bolts. PhD Thesis, Norwegian Institute of Technology Trondheim, Norway, 178 p.

Sun X. (1984). Grouted rock bolt used in underground engineering in soft surrounding rock or in highly stressed regions. Proc. the International Symposium on Rock Bolting, Balkema, Rotterdam, pp. 93-101.

Windsor, C.R. (1997). Rock reinforcement systems. International Journal of Rock Mechanics and Mining Sciences, 34(6):919-951.

Yazici, S. & Kaiser, P.K. (1992). Bond strength of grouted cable bolts. International Journal of Rock Mechanics and Mining Sciences & Geomechanics, 29(3):279-292.

Hydraulic and Diffusive Behavior of a Compacted Cemented Soil

E.P. Korf, P.D.M. Prietto, N.C. Consoli

Abstract. The study evaluated, through a series of permeability and diffusion tests, the hydraulic and the attenuation behavior of a compacted clayey soil, with and without the addition of Portland cement (0 to 2%). To evaluate the diffusive response, the specimens were subjected to a vertical static load (100 to 500 kPa), simulating the action of a waste mass, and to an acidic solution enriched with toxic metals Pb or Cd, prepared with pH varying from 1 to 6. The reactive behavior analysis indicated that retention by adsorption increased with the increase of pH, but was not affected by the applied static load. The combination of higher cement contents with higher pH caused precipitation to prevail over adsorption reactions.

Keywords: diffusion, lead, cadmium, acidic leachate, transport of contaminants, hydraulic conductivity.

1. Introduction

Leachates from industrial and mining solid wastes are a major source of environmental impact due often to the presence of toxic metallic species and/or their acidic constitution. Some examples are the disposal in the ground of sludge and waste from electroplating and smelters activities, mining tailings from coal and minerals beneficiation, as well as accidental spills. In many cases, the managing of such leachates is inadequate, without any engineered solution to provide adequate containment and treatment of pollutants. The most aggravating aspect is that these wastewaters have the natural ground as their main destination, which unfortunately does not represent the endpoint for such toxic substances.

In this context, the improvement of technical solutions to ensure mitigation and prevention of environmental impacts plays a fundamental role. For instance, the use of reactive, compacted soil barriers, with low hydraulic conductivity, is a traditional technique used to reduce contaminant transport through side slope and bottom sealing in waste disposal facilities. Nevertheless, studies have shown that these barriers might be enhanced by the addition of small amounts of materials like Portland cement, lime, and bentonite, reducing hydraulic conductivity and compound mobility, and increasing adsorption/precipitation reactions (Lo *et al.*, 1997; Lee, 1998; Tsai & Vesilind, 1988; Wu & Li, 1998; Basta *et al.*, 2001; Elzahabi & Yong, 2004; Bartelt-Hunt *et al.*, 2006; Adebowale *et al.*, 2006; Lemos, 2006; Giannakopoulou *et al.*, 2007; Knop *et al.*, 2008; Thomé *et al.*, 2014).

The objective of this research was therefore to evaluate, through a series of permeability and diffusion tests, the hydraulic response and the attenuation capacity of a compacted clayey soil, with and without the addition of Portland cement, aiming at its use as containment barriers for industrial and mining solid waste disposal facilities. To evaluate the diffusive behavior, specimens were submitted to the action of a static vertical load and to an acidic solution enriched with cadmium or lead.

2. Material and Methods

Laboratory experiments were planned, conducted, and analyzed to assess the effects of three main control variables - cement addition (0 and 2%), contaminant solution pH (1 and 6), and static vertical load (0 and 500 kPa) - on the attenuation capacity of a compacted clayey soil, subjected to the diffusive transport of an acidic contaminant solution enriched with cadmium or lead. In addition, the effect of cement content on the hydraulic conductivity of the compacted soil was evaluated.

The experimental program for the diffusion tests was conducted in two separate blocks, identically and independently for each of the metallic species investigated (cadmium and lead). For each block a 2^3 factorial experimental design was used: three control variables at two levels each, with the addition of a central point (1% cement, pH 3.5, static vertical load of 250 kPa). Overall, the experimental design resulted in 9 combinations or treatments (8 factorial points and 1 central point) for each metal investigated (cadmium and lead). It should be noticed that replicates (n = 4) were performed only at central point, totalizing 12 tests for each metal. Further details about the experimental design used in present work can be found in the specific literature (*e.g.* Montgomery, 2005, Box *et al.*, 1999).

Eduardo Pavan Korf, Dr., Professor, Programa de Pós-Graduação em Ciência e Tecnologia Ambiental, Universidade Federal da Fronteira Sul - Campus Erechim, Erechim, Rio Grande do Sul, Brazil. e -mail: eduardo.korf@uffs.edu.br.
Pedro Domingos Marques Prietto, Dr., Associate Professor, Programa de Pós-Graduação em Engenharia Civil e Ambiental, Universidade de Passo Fundo, Passo Fundo, Rio Grande do Sul, Brazil. e -mail: pdmp@upf.br.
Nilo Cesar Consoli, Ph.D., Professor of Civil Engineering, Programa de Pós-Graduação em Engenharia Civil, Universidade Federal do Rio Grande do Sul, Porto Alegre, Rio Grande do Sul, Brazil. e-mail: consoli@ufrgs.br.
Submitted on February 8, 2016; Final Acceptance on November 27, 2016; Discussion open until April 28, 2017.

2.1. Soil sampling and characterization

The soil utilized was a basalt residual soil sampled from the Geotechnical Experimental Site at the University of Passo Fundo, located in the city of Passo Fundo, in southern Brazil. The sample was obtained by disturbed extraction from the B horizon (1.2 m depth).

The soil is classified as sandy clay (68% clay, 27% sand, and 5% silt), according to the NBR-7181 (ABNT, 1984c), has a specific gravity of 2.67 and a plastic index of 11, according to the NBR-6459 (ABNT, 1984a) and the NBR-7180 (ABNT, 1984b), respectively. It presents pH 5.4, low organic matter content (< 0.8%), and low cation exchange capacity (CEC = 8.6 cmolc/dm3), according to Tedesco (1995), as well as 33.86 m^2/g of soil specific surface (EMBRAPA, 1997), typical of soils with the predominance of kaolinite minerals. The soil is also classified as humic oxisoil (Streck *et al.*, 2008). According to X-ray diffraction analysis and chemical composition by X-ray fluorescence analysis, it is a kaolinite-based clay, with a significant presence of hematite (Fe_2O_3 content of 11.7%) and quartz.

The compaction characteristics of the residual soil, determined according to NBR-7182 (ABNT, 1984d) for the modified Proctor energy, are: maximum dry unit weight of 15.7 kN/m^3, optimum moisture content of 24.5%, and degree of saturation at optimum moisture content of 94.8%.

The background concentrations (natural levels) of cadmium and lead available in the soil, as determined by the method of extraction by digestion (USEPA, 1996), are 1.63 and 30.74 mg/kg, respectively.

2.2. Cement and contaminant solution

Portland cement of high early strength [Type III, according to ASTM (2007)] was adopted as the cementing agent and also as a neutralizing element, because of its alkaline nature. The average cement composition is 0-5% of mineral admixtures and 95-100% of clinker, with nominal compressive strength at 28 days of 40MPa. According to the X-ray fluorescence analysis, the cement has a significant presence of CaO (66.2%) and SiO_2 (18%). The chemical composition of the mixture of soil with 2% hydrated cement indicated the presence of SiO_2 (45.1%), Fe_2O_3 (12.1%), Al_2O_3 (27.5%), and CaO (1.8%).

The contaminant solutions were prepared by diluting a 1000 mg/L standard solution of cadmium or lead (at 5% of nitric acidic by volume) into a solution of 10 mg/L. The metallic species concentrations were equivalent to extrapolating 3333 times and 1000 times, respectively for cadmium and lead, the values recommended by the World Health Organization (WHO, 2011). The solutions were prepared at different values of pH in the acidic range, adjusted with a sodium hydroxide and nitric acid solution.

2.3. Diffusion testing device

The testing device comprised a stainless steel cell, which functions as a rigid wall, downward-flow permeameter, allowing hydraulic conductivity determination as well as contaminant transport parameter evaluation. The device is described by Knop *et al.* (2008) and followed the requirements of the ASTM-D 4874 standard (ASTM, 1995) with modifications. The diffusion cell had dimensions of 100 mm in height and 70 mm in diameter and was adapted to a conventional consolidation frame to allow the application of a static vertical load to the specimen, simulating the action of a waste mass over a containment barrier (Fig. 1).

2.4. Specimens preparation and saturation

Mixture specimens with cement contents of 0, 1, and 2% of dry mass of soil, and nominal dimensions of 20 mm in height and 70 mm in diameter, were compacted into the diffusion cell at the specific unit weights and optimum moisture contents obtained in the modified Proctor compaction test (15.7 kN/m^3 and 24.5%, respectively). The water/cement ratios for the cemented specimens were 24.5 and 12.25, respectively for the 1% and 2% cement contents.

To approximate saturation, the following procedure was carried out for all specimens: (1) distilled water percolation from an inlet pressurized cylinder connected to the top of the diffusion cell; (2) application of a hydraulic head equivalent to 80 kPa; (3) measurement of the volume percolated in a graduated burette attached to the bottom of the diffusion cell until steady flow was reached. The saturation procedure was complete in approximately seven days and the saturation degree resulted in values greater than 95%. This procedure was validated by measuring the degree of saturation of the specimens after the tests.

2.5. Diffusion tests

The procedures described below were adapted from Barone *et al.* (1989).

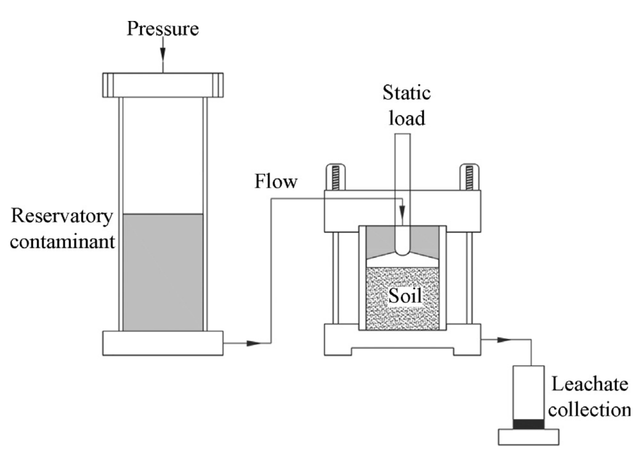

Figure 1 - Diffusion cell adapted to a conventional consolidation frame.

Once the saturation phase was finished and the hydraulic conductivity measured, the outlet valve connected to the bottom of the diffusion cell was closed and remained so throughout the test. Subsequently, the distilled water inside the inlet cylinder was replaced by the contaminant solution, without any pressure applied, but subjected to constant agitation, with the aid of a pump, to maintain homogeneity. The diffusion cell was then coupled to a conventional consolidation frame and the vertical pressure applied. Then, the inlet valve connected to the top of the diffusion cell was opened and the contaminant diffusion phase initiated and conducted for seven days. After each diffusion test, the specimens were sectioned in four slices approximately 5 mm in height, by means of a steel cutting tool. The available metal concentration in each slice was then extracted by acidic digestion (USEPA, 1996) and analyzed in the atomic absorption spectrophotometer.

2.6. Determination of the contaminant transport parameters

In diffusion tests, the retardation factor (R_d) was calculated from Eq. 1, in which ρ_d is the specimen dry density, n is the specimen porosity (n), and K_d is the partition coefficient. The partition coefficient K_d was obtained (Eq. 2) by determining the adsorption (S) for each slice of the tested specimens and calculating the equilibrium concentration of pore water (C) by means of a mass balance.

$$R_d = 1 + \frac{\rho_d}{n} K_d \tag{1}$$

$$K_d = \frac{S}{C} \tag{2}$$

The effective diffusion coefficient (D^*) was determined by back analyzing each slice of the tested specimens and fitting the experimental data to the analytical solution proposed by Carslaw and Jaeger (Shackelford, 1991), which is shown in Eq. 3, along with their initial and boundary conditions, and applies to the testing assembly previously described.

$$\frac{c}{c_0} = \exp\left[\frac{nR_d x}{H_f} + \left(\frac{n}{H_f}\right)^2 D^* R_d t\right] \times \operatorname{erfc}\left(\frac{x}{2\sqrt{\frac{D^* t}{R_d}}} + \frac{n}{H_f}\sqrt{D^* R_d t}\right) \tag{3}$$

Initial condition:

$$c(x,0) = 0 \rightarrow x \geq 0$$

Boundary conditions:

$$c(0,t) = c_0 \rightarrow t \geq 0$$

$$c(\infty,t) = 0 \text{ and } \frac{\partial c(\infty,t)}{\partial x} = 0 \rightarrow t \geq 0$$

In Eq. 3, c is the contaminant concentration at the depth x from the top of the specimen; n is the specimen porosity; t is the time; c_0 is the initial concentration of the contaminant solution; H_f is the effective height of the contaminant solution in the inlet cylinder; R_d is the retardation factor; D^* is the effective diffusion coefficient; and erfc is the complementary error function.

Figure 2 shows an example of fitting experimental data to the analytical solution in order to calculate the D^* parameter.

2.7. Statistical analysis

The results were statistically analyzed by using the Analysis of Variance (ANOVA) method, with a significance level of 5%.

3. Results and Discussion

3.1. Hydraulic conductivity

The average hydraulic conductivity (only for distilled water percolation) decreased with increasing cement content: 5.70 x 10^{-10} m/s for 0% cement, 2.45 x 10^{-10} m/s for 1% cement, and 1.96 x 10^{-10} m/s for 2% cement, with coefficients of variation in the range of 56 to 60%. It should be noticed that the values observed are in the same order of magnitude, and vary within a range that could be most likely explained by experimental error. However, the trend observed is consistent with previous studies. Zhang *et al.* (2004), Lemos (2006), and Knop *et al.* (2008), for instance, have shown that the addition of Portland cement might con-

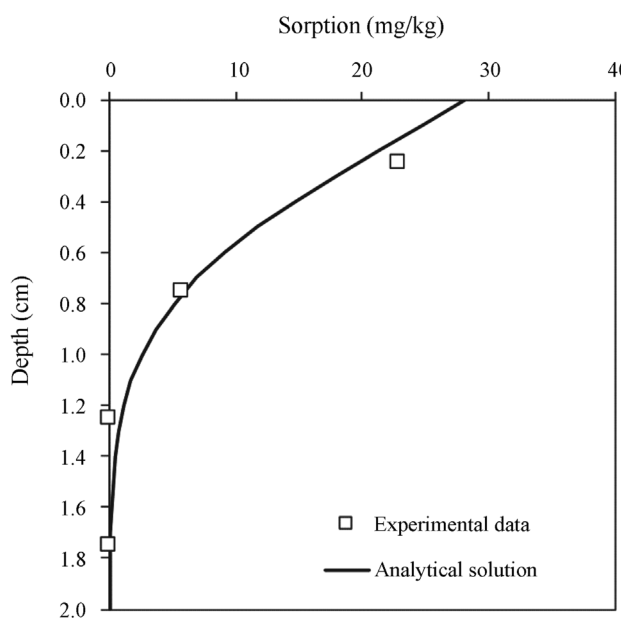

Figure 2 - Example of adjustment for parameters determination.

tribute to hydraulic conductivity reduction, mainly because of the reduction in porosity and changes in microstructure. Moreover, the values obtained are within the range proposed by Daniel (1993) for compacted clay barriers ($< 10^{-9}$ m/s).

Figure 3 shows the hydraulic behavior observed in two tests carried out with 2% cement content and percolation of contaminant solutions at pH 1. It can be noticed that after the seventh day, when contaminant percolation initiated, the hydraulic conductivity showed a slight increase followed by a consistent decline, showing the presumable effect of the acidic percolation on the cemented soil structure. Dissolution and transport of soil particles was not observed in these tests. Similar results were obtained by Lemos (2006), who worked with a mixture of soil, cement, and bentonite subjected to sulfuric acid percolation over 20 weeks. Both results, however, are in disagreement with Daniel (1993), who points out that strong acids can dissolve soil compounds, forming preferential channels and increasing hydraulic conductivity. What probably occurred was the acidic dissolution of hydrated cement particles at first, resulting in the observed slight increase in hydraulic conductivity immediately after the contaminant solution insertion, followed by soil structure reorganization and collapse, which caused the reduction in hydraulic conductivity. However, the results presented herein should be interpreted cautiously, since long-term permeability tests are necessary to establish a complete pattern of behavior with time.

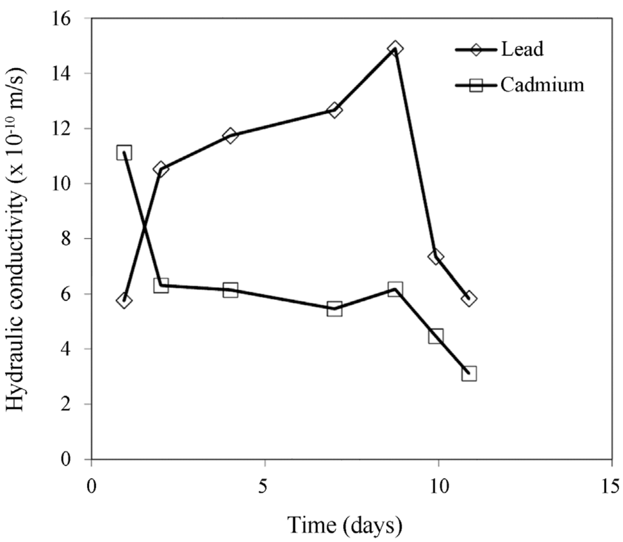

Figure 3 - Hydraulic behavior of the 2% cement content under the pH 1.

3.2. Contaminant transport parameters

The contaminant transport parameters obtained from diffusion tests and the corresponding statistical analysis (ANOVA) are summarized in Tables 1, 2, and 3. In Tables 2 and 3, the so-called *p-values* represent the probability or the margin of error associated to the conclusion that a control variable (cement content, pH, static load) has a significant effect on the response variable (R_d or D^*).

The statistical analysis indicated that the vertical static load had no effect whatsoever on the transport parameters for both metals, possibly because there is no flow in diffusion tests and consequently no consolidation occurs. It should be noted, however, that this is not usually the case with field conditions, in which coupled diffusion-advection-consolidation phenomena can be relevant to actual barrier performance. Furthermore, the effective diffusion coefficient (D^*) was influenced only by cement content and only for lead. Consequently, only the average values of D^* for each cement content are presented in Table 1 for lead. For the same reason, only the overall average value of D^* is presented for cadmium. Figure 4 shows the average effect of cement content on the effective diffusion coefficient for lead. A noticeable reduction in D^* is observed as the cement content increases.

Regarding the retardation factor, the statistical analysis showed that it was significantly affected by both cement content and pH, as well as by their interaction. Figures 5

Table 1 - R_d and D^* values obtained from diffusion tests.

Cement content (%)	Solution pH	Retardation factor R_d		Effective diffusion coefficient D^* (m^2/s)	
		Lead	Cadmium	Lead	Cadmium
0	1	4.0	1.4	1.3×10^{-9}	3.5×10^{-10}
0	3.5	150.0	38.7		
0	6	196.3	13.4		
1	1	2.9	2.5	6.7×10^{-10}	
1	3.5	42.0	37.6		
1	6	156.9	147.3		
2	1	16.8	1.5	1.9×10^{-10}	
2	3.5	20.1	131.9		
2	6	15.1	64.8		

Table 2 - Summary of the statistical analysis (ANOVA) for R_d and D^* obtained from diffusion tests for lead.

Control variable	p-value	
	Retardation factor - R_d	Effective diffusion coefficient - D^*
Main effects:		
Cement content	0.02	0.003
pH	0.01	0.10
Static load	0.28	0.40
Interaction effects:		
Cement content *vs.* pH	0.03	0.10
Cement content *vs.* static load	0.34	0.65
pH *vs.* Static load	0.46	0.51

Table 3 - Summary of the statistical analysis (ANOVA) for R_d and D^* obtained from diffusion tests for cadmium.

Control variable	p-value	
	Retardation factor - R_d	Effective diffusion coefficient - D^*
Main effects:		
Cement content	0.06	0.91
pH	0.02	0.62
Static load	0.36	0.84
Interaction effects:		
Cement content *vs.* pH	0.13	0.34
Cement content *vs.* static load	0.89	0.04
pH *vs.* static load	0.97	0.99

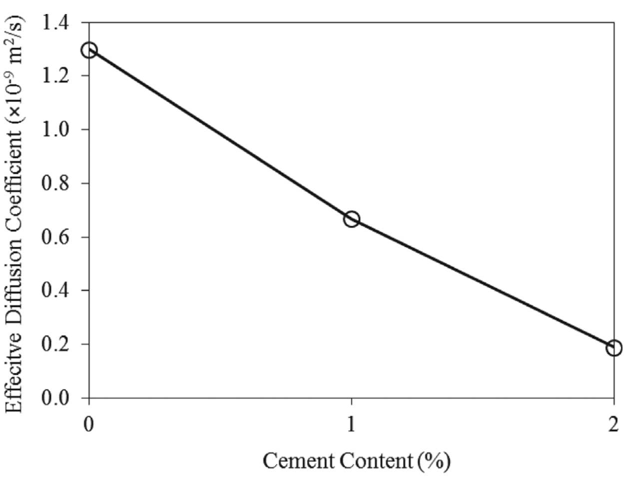

Figure 4 - Effective diffusion coefficient variation with cement content for lead.

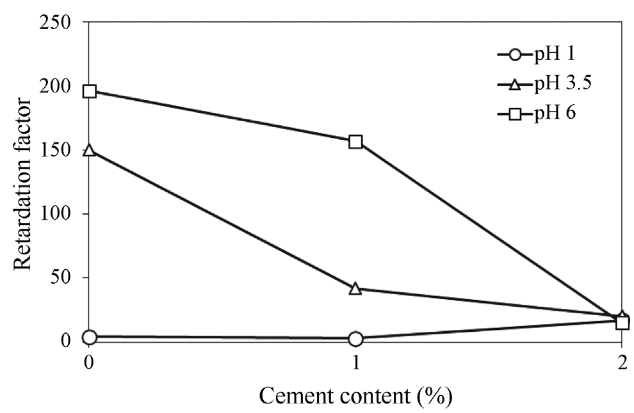

Figure 5 - Retardation factor variation with pH and cement content for lead.

and 6 show the retardation factor (R_d) variation with cement content and pH, for both lead and cadmium, respectively.

It can be readily observed that for the metal lead (Fig. 5) the increase in pH caused an overall increase in R_d. However, with the addition of cement an interaction effect occurred: as the cement content increased from 0 to 1%, the effect of pH on R_d became less pronounced, and for 2% cement no effect was observed. This behavior was probably caused by the immediate rise in pH due to cement addition, which produced a higher rate of precipitation rather than adsorption reactions. Thus, the reduction in the availability of lead to the adsorption process and diffusion resulted in

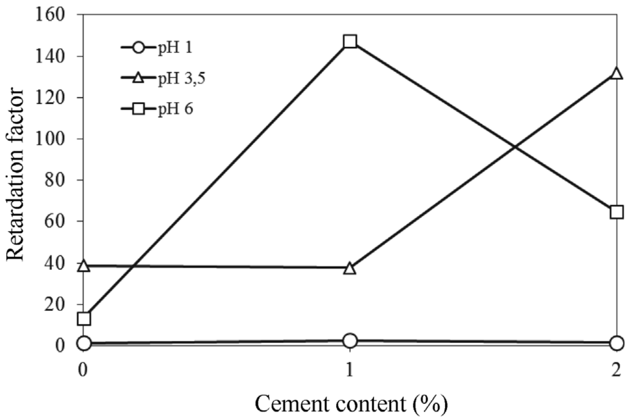

Figure 6 - Retardation factor variation with pH and cement content for cadmium.

the reduction of both R_d and D^*. Regarding the metal cadmium, a different pattern is depicted in Fig. 6. It is likely that precipitation reactions have also occurred, but at lower intensity as compared to lead. As indicated in Fig. 6, it seems that the predominance of precipitation over adsorption reactions occurred only for the combination of pH 6 and 2% cement, which was not sufficient to reduce the effective diffusion coefficient D^*.

Similar findings are reported in the literature. According to Raymond (2001), the metal lead is precipitated in soil at lower pH values when compared to cadmium, which explains the more pronounced effect of pH observed for the tests carried out with lead. This can also be explained by the larger chemical reduction potential of lead when compared to cadmium, resulting in a larger potential to receive electrons and precipitate in the form of salts. In addition, the influence of pH on the adsorption reactions has been investigated by various authors (*e.g.* Lee, 1998; Wu & Li, 1998), who explained that the adsorption is more significant for higher pH values because of the increased negative charges on soil particle surfaces. Also, as indicated by the transport parameters presented in Fig. 6, the metal lead shows lower mobility and greater retention when compared to cadmium (Yong *et al.*, 1992).

4. Conclusion

The present study aimed to contribute to the understanding of the response of geomaterials submitted to boundary conditions similar to those encountered in the field, such as in the case of bottom barriers in industrial or mining waste disposal facilities. The transport parameters investigated are relevant to modeling studies of subsurface contamination plumes and decision-making processes associated with design and management of engineered systems.

The investigated compacted mixtures showed low hydraulic conductivity coefficients ($< 10^{-9}$ m/s), with values that decreased with increasing cement content. Regarding the reactive behavior, the retardation factor (R_d) increased mainly with the increment in the pH of the contaminant solution, thus increasing metal retention. The effective diffusion coefficient D^* was not affected for the metal cadmium, but was reduced for lead. The coupled effect of increasing both pH and cement content caused a higher rate of chemical precipitation reactions, which predominated over adsorption reactions, in particular for the metal lead, allowing the contaminant to remain in solution and favoring its solubilization in acidic conditions.

Further studies are necessary to assess the effects of the variables studied on the long-term hydraulic behavior, advective-diffusive parameters, mechanical response (deformability and strength), and microstructure, such as variations in porosity, as well as chemical and mineralogical modifications.

Acknowledgments

The authors wish to express their gratitude to CNPq/MCT (proc. 480565/2009-0, 486340/2011-2, 309105/2011-0) and DECIT/SCTIE-MS - FAPERGS/CNPq (proc. 10/0030-9 and 11/2041-4) for the financial support to the research group.

References

Adebowale, K.O.; Unuabonah, I.E. & Olu-Owolabi B.I. (2006). The effect of some operating variables on the adsorption of lead and cadmium ion son kaolinite clay. Journal of Hazardous Materials, 134(1-3):130-139.

ABNT (1984a). NBR 6459 - Soil: Determination of liquid limit. Rio de Janeiro, Brazil, 6 p. (in portuguese).

ABNT (1984b). NBR 7180 - Soil: Determination of plasticity limit. Rio de Janeiro, Brazil, 3 p. (in portuguese).

ABNT (1984c). NBR 7181 - Soil: Granulometric Analysis. Rio de Janeiro, Brazil, 13 p. (in portuguese).

ABNT (1984d). NBR 7182 - Soil: Compactation Test. Rio de Janeiro, Brazil, 10 p. (in portuguese).

ASTM (1995). D4874 - Standard Test Method for Leaching Solid Material in a Column Apparatus. ASTM International, West Conshohocken, Pennsylvania, USA.

ASTM (2007). Standard specification for Portland cement - C150. ASTM International, West Conshohocken, Pennsylvania, USA.

Barone, F.S.; Yanful, E.K.; Quigley, R.M. & Rowe, R.K. (1989). Effect of multiple contaminant migration on diffusion and adsorption of some domestic waste contaminants in a natural clayey soil. Canadian Geotech. J., 26(2):189-198.

Bartelt-Hunt, S.; Culver, T.; Smith, J.; Shawn Matott, L. & Rabideau, A. (2006). Optimal Design of a Compacted Soil Liner Containing Sorptive Amendments. J. Environ. Eng., 132(7):769-776.

Basta, N.T.; Gradwohl, R.; Snethen, K.L. & Schroder, J.L. (2001). Chemical immobilization of lead, zinc, and cadmium in smelter-contaminated soils using biosolids and rock phosphate. Journal of Environmental Quality, 30(4):1222-1230.

Box, G.E.P.; Hunter, J.S.; Hunter, W.G. (2005). Statistics for Experimenters: Design, Innovation, and Discovery. 2nd ed. John Wiley & Sons: New York, 629 p.

Daniel, D.E. (1993). Clay liners. Daniel, D.E. (ed) Geotechnical Practice for Waste Disposal. Chapman & Hall, London, p. 33-65.

Elzahabi, M. & Yong, R.N. (2001). pH Influence on sorption characteristics of heavy metal in the vadose zone. Engineering Geology, 60(1-4):61-68.

EMBRAPA. (1997) Handbook of Soil Analysis. 2nd ed. MAPA, Rio de Janeiro, 212 p.

Giannakopoulou, F.; Haidouti, C.; Chronopoulou, A. & Gasparatos, D. (2007). Sorption behavior of cesium on various soils under different pH levels. Journal of Hazardous Materials, 149(3):553-556.

Knop, A.; VanGulck, J.; Heineck, K.S. & Consoli, N.C. (2008). Compacted artificially cemented soil-acid leachate contaminant interactions: Breakthrough curves and transport parameters. Journal of Hazardous Materials, 155(1-2):269-276.

Lee, S.; Chang, L.; Yang, H.; Chena C. & Liua, M. (1998). Adsorption Characteristics of lead onto soils. Journal of Hazardous Materials, 63(1):37-49.

Lemos, R.G. (2006). Estudo do Comportamento Hidráulico, Mecânico e Químico de Barreiras Hidráulicas Verticais, Compostas por Solo Residual, Bentonita e Cimento Sob Ação de Substâncias Agressivas. Dissertação de Mestrado, Programa de Pós-Graudação em Engenharia Civil, UFRGS, Porto Alegre, 310 p.

Lo, I., Mak, R., & Lee, S. (1997). Modified clays for waste containment and pollutant attenuation. J. Environ. Eng., 123(1):25-32.

Montgomery, D.C. (2005). Design and Analysis of Experiments. 6th ed. John Wiley & Sons, New York, 684 p .

Raymond, N. (2001). Geoenvironmental Engineering: Contaminated Soils, Pollutant Fate and Mitigation. CRC Press, Washington, 307 p.

Shackelford, C.D. (1991). Laboratory diffusion testing for waste disposal - A review. J. Cont. Hydrol., 7(3):177-217.

Tedesco MJ (1995). Análise de Solo, Planta e Outros Materiais: Boletim técnico nº 5. Departamento de Solos, Faculdade de Agronomia, Porto Alegre (in portuguese).

Tsai, T. & Vesilind, P. (1998). A new landfill liner to reduce ground-water contamination from heavy metals. J. Environ. Eng., 124(11):1061-1065.

Thomé, A.; Consoli, N. C.; Korf, E.P. & Timbola, R. (2014). Cadmium transport parameters in a clay residual soil with different ranges of contaminant pH. Soils and Rocks, 36(3):311-316.

USEPA - U.S. (1996). Method 3050B - Acid Digestion of Sediments, Sludges, and Soils. USEPA, Washington, D.C., 12 p.

WHO (2011). Guidelines of Drinking Water Quality. 4th ed., v. 1, Recommendation. World Health Organization, Geneva, 541 p.

Wu, G. & Li, L.Y. (1998). Modeling of heavy metal migration in sand/bentonite and the leachate pH effect. Journal of contaminant hidrology, 33(3-4):313-336.

Yong, R.N.; Mohamed, A.M.O. & Warkentin, B.P. (1992). Principles of Contaminant Transport in Soils. Elsevier, Amsterdam, 327 p.

Zhang, K.; Chen, Y.; Deng, F. & Tian, Q. (2004). Retention of clay-solidified grouting curtain to Cd^{2+}, Pb^{2+} and Hg^{2+} in landfill of municipal solid waste. Journal Century South University Technology, 11(4):419-422.

List of Symbols

c: *C*ontaminant concentration at the depth *x* from the top of the specimens
c_0: Initial concentration of the contaminant solution
Cd: Cadmium
CEC: Cation Exchange Capacity
D^*: Effective diffusion coefficient and
erfc: Complementary error function.
H_f : Effective height of the contaminant solution in the inlet cylinder
K_d: Partition Coefficient
n: Specimen porosity
Pb: Lead
R_d: Retardation factor
S: Adsorption
t: Time
x: Distance
ρ_d: Specimen dry density

Assessing the Potential Improvement of Fine-grained Clayey Soils by Plastic Wastes

Hossein Soltani-Jigheh, Arsalan Rasulifard

Abstract. Because of progressively dumping of plastic wastes (PWs) obtained from beverage industry it is of interest to use them as reinforcement material in civil engineering projects. For assessing potential use of plastic wastes in improvement of shear strength of fine-grained soils, two clayey soils were mixed with different amount of plastic wastes (*i.e.* 0.5%, 1.0%, 1.5% and 3.0% by weight) and consolidated undrained triaxial tests were performed on the compacted samples. Test results indicate that variations of shear strength and pore water pressure depend on the amount and type of plastic waste. It is observed that, irrespective of clay plasticity, adding plastic waste to the fine-grained soils improves their shear strength and plastic waste content (PWC) of 3.0%, within the range of used amounts, has the best effect on the shear strength. Moreover, adding plastic waste causes to decrease shear-induced pore water pressure slowly. Furthermore, deformability of samples changes in term of plastic waste content, type of plastic and clay type. It can be concluded that there is a possible usage of clay-plastic waste mixtures as construction materials and, thereby, plastic wastes can be managed by recycling them in the field of geotechnical engineering, thus contributing to clean up the environment.

Keywords: plastic waste, management, undrained behavior, clay mixtures, triaxial test.

1. Introduction

The bottled water is the fastest growing beverage industry in the world. International Bottled Water Association (IBWA) reported that 1.5 million tons of plastic are annually used to bottle water and 1500 bottles are dumped as garbage every second. Polyethylene terephthalate (PET) is one of the most abundant plastics in solid urban waste (de Mello *et al.*, 2009). It has been reported that annual consumption of PET bottles is approximately 10 million tons in the world and it grows about up to 15% every year. On the other hand, the number of recycled or returned bottles is very low (ECO PET, 2007). Global bottled water consumption is estimated about 61.4 billion gallons in 2011 and total consumption swelled by 8.6 percent in 2011. Per capita consumption of 8.8 gallons represented a gain of 1.2 gallons over the course of five years (Rodwan Jr., 2012).

Biodegradation process of plastics is very slow, because plastics mainly are synthesized using non-renewable fossil resources. Therefore, the plastic wastes should be recycled to decrease these effects. For the management of plastic waste, recently their use in the civil engineering projects is taken into consideration. The advantages are the reuse of these materials and the reduction of using natural material like soil in geotechnical engineering applications. Adding polyethylene fibers of waste plastics to soil-cement mixtures showed that it improves the stress-strain response of uncemented and cemented sands (Consoli *et al.*, 2002). A field application of fiber-reinforced cemented sand proposed for increasing the bearing capacity of spread foundations has been reported previously (Consoli *et al.*, 2003). Consoli *et al.* (2004) by performing triaxial compression tests on cemented and uncemented sand reinforced with various types of fibers indicated that the mode of failure changes from brittle to ductile due to inclusion of fibers. Consoli *et al.* (2009) found that both cement and fiber insertions affect dramatically the stress-dilatancy behavior of the sand.

Dutta & Rao (2007) proposed some regression based models for predicting the behavior of sand-waste plastic mixture. Numerical simulation also indicates that pull-out resistance of fibers governs the stress-strain response of random-reinforced soil (Sivakumar Babu *et al.*, 2008). Comprehensive experimental studies on compacted soil-fiber samples showed improvement in strength and stiffness response, reduction in compression indices, reduction in swelling behavior of soil. It is also observed that fibers reduce the seepage velocity of plain soil considerably and thus increase the piping resistance of soil (Sivakumar Babu & Vasudevan, 2008a, b, c). Based on critical state concepts, a constitutive model was proposed to obtain stress-strain response of coir fiber-reinforced soil as a function of fiber content (Sivakumar Babu & Chouksey, 2010). Sivakumar Babu & Chouksey (2011) investigated the effects of plastic waste on the soil behavior by performing a series of triaxial compression and one dimensional compression tests. They found that there is significant improvement in the strength of plastic waste mixed soils due to increase in friction be-

Hossein Soltani-Jigheh, Department of Civil Engineering, Azarbaijan Shahid Madani University, Tabriz-Maragheh Road 35 km, 34327566, Tabriz, Iran. e-mail: hsoltani@azaruniv.ac.ir.
Arsalan Rasulifard, Department of Civil Engineering, Azarbaijan Shahid Madani University, Tabriz-Maragheh Road 35 km, 34327566, Tabriz, Iran. e-mail: arsalan.rasulifard@gmail.com.
Submitted on February 10, 2016; Final Acceptance on November 27, 2016; Discussion open until April 28, 2017.

tween soil and plastic waste and development of tensile stress in the plastic waste. Compression behavior of plastic waste mixed soil indicates significant reduction in compression parameters.

The main objective of the present study is to obtain the geotechnical properties of fine-grained cohesive soils by partially replacing them with plastic waste. To this end, experimental tests were conducted on clayey soils and mixtures of clayey soils with different amount of plastic waste. The tests include a series of consolidated undrained (CU) triaxial tests to determine stress-strain and pore water pressure behavior of plastic waste mixed clayey soils. The obtained results are compared with the associated behavior of plain clays and an analysis is performed in terms of plastic waste content (PWC), type of plastic waste and clay plasticity.

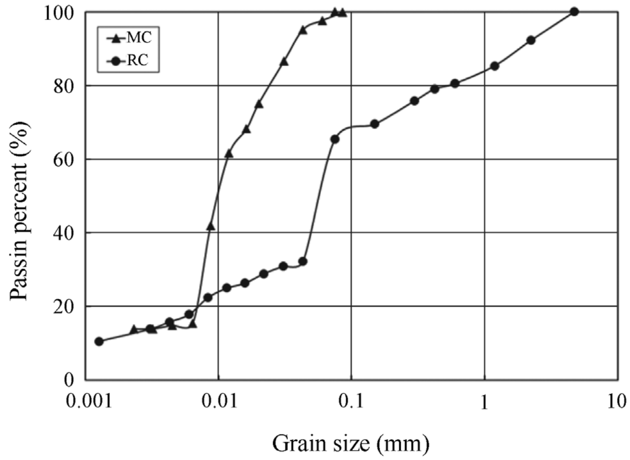

Figure 1 - Grading curve of used clayey soils.

2. Materials and Methods

2.1. Materials

The two fine-grained clayey soils used in this study were retrieved from two distinct borrow areas, namely Malekan and Roshdiyyeh areas in East Azerbaijan province. For abbreviation, these soils were denoted with MC and RC letters, respectively. According to Unified Soil Classification System (USCS), both of the clays were categorized as CL (ASTM, 2011). Some index properties of the clayey soils have been listed in Table 1. As well as, grading curves of these materials have been presented in Fig. 1.

Two types of plastic wastes obtained from water bottles with different flexibility are used as reinforcing material. Plastic wastes chips were named PW1 and PW2, the PW2 type being more flexible than the PW1 type. The size of pieces for both types of plastics were selected 8 mm in length and 4 mm in width, and their specific gravities are 1.452 and 1.36, respectively.

2.2. Sample preparation

Soil mixtures were prepared by mixing clayey soils with 0%, 0. 5%, 1.0%, 1.5% and 3.0% of plastic wastes by dry weight. To study the effect of plastic flexibility, both PW1 and PW2 plastics were added to Malekan clay. In order to model samples for the triaxial tests which would reproduce field conditions as closely as possible, standard Proctor compaction tests were performed on both the clayey soils and mixtures of MC clay with PW2 plastic to determine maximum dry unit weight (γ_{dmax}) and optimum water content (w_{opt}) (ASTM, 2012). Compaction test results showed that plastic waste does not significantly affect compaction parameters of MC clay. Therefore, compaction tests were not performed on the other mixtures. Triaxial samples of MC and RC clays mixed with PW1 plastic were prepared according to 0.98γ_{dmax} and w_{opt} values of MC and RC clays, respectively. Required materials for samples made of MC clay and PW2 plastic were calculated based on 0.98γ_{dmax} and w_{opt} values of associated sample.

To obtain a homogenous mixture, required quantity of plastic wastes was distributed over the soil and mixed uniformly and, then, required water was sprayed onto the surface of the materials and after mixing it was placed in sealed plastic bags and stored overnight in a controlled humidity room. Figures 2(a) and 2(b) show typical photos of PW2 plastic waste chips and mixture of this plastic with MC clay, respectively. The entire mixture was statically compacted in the mold, with 50 mm diameter and 100 mm in height, in four layers, and samples for triaxial testing were obtained. Table 2 shows some specifications of tested samples.

Table 1 - Some index properties of clayey soils.

Index	Clay type	
	MC	RC
Liquid limit (%)	33.0	21.0
Plastic limit (%)	16.0	13.0
Plasticity index	17.0	8.00
Specific gravity	2.771	2.635
USCS classification	CL	CL

2.3. Shear testing

After extruding the samples from the mold, they were set up in triaxial cell and standard consolidated undrained (CU) triaxial testing procedures were followed (ASTM, 2004). To saturate the samples, distilled water was transmitted through them and then incremental backpressure saturation with a pressure differential of 30 kPa was applied. The backpressure was raised to a maximum of 400 kPa and B value was calculated for each increment. Saturation of the samples took approximately 4-6 days to complete until reaching a B value of at least 0.96. The sam-

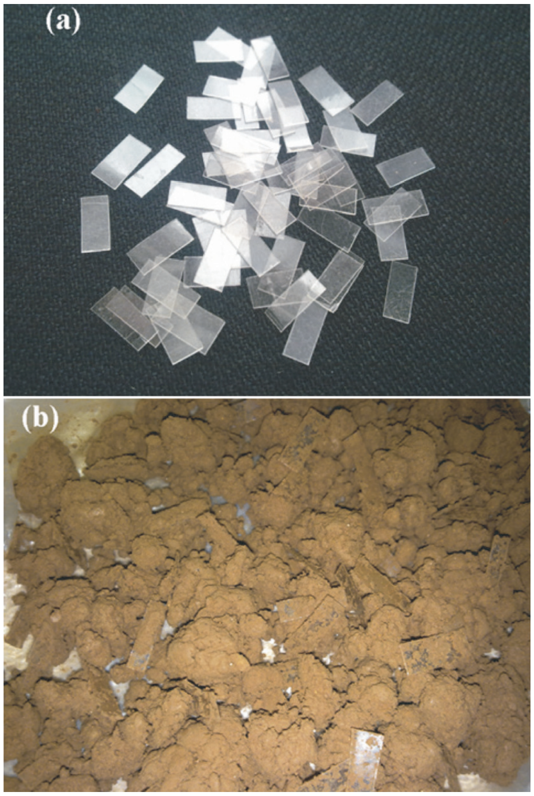

Figure 2 - (a) PW2 plastic chips used in the research, and (b) mixture of MC clay with PW2 plastic before compaction.

ples were consolidated under effective consolidation stresses of 200 kPa and then shearing was applied to the samples at a rate of 0.04 mm/min until reaching up to 20-24% strain by simultaneously measuring shear-induced pore water pressure.

3. Results and Discussions

Figures 3, 4, and 5 illustrate stress-strain curve, changes in pore water pressure and stress paths of MC-PW1, RC-PW1 and MC-PW2 mixtures, respectively. These figures include variations of deviatoric stress *vs.* axial strain (ε_a), excess pore water pressure (Δu) *vs.* ε_a, and deviatoric stress ($q' = \sigma'_1 - \sigma'_3$) *vs.* mean normal effective stress ($p' = (\sigma'_1 + 2\sigma'_3)/3$). It is clearly observed that the plastic waste influences the behavior of natural soils; so that by increasing the plastic waste content the samples exhibit higher shear strength (Figs. 3(a), 4(a) and 5(a)).

3.1. Undrained shear strength

The correlation between undrained shear strength and plastic waste content is shown in Fig. 6(a). The figure shows the shear strength of samples with PWC = 0.5% is approximately equal to the shear strength of plain clay and when the amount of plastic waste changes from 0.5% to 3.0% shear strength increases gradually. The maximum improvement in the shear strength of different mixtures was obtained at plastic content of 3.0%. Maximum increments in shear strength of MC clay mixed with 3.0% PW1 and 3.0% PW2 plastics are about 49.80% and 25.73%, respectively. The increment value for RC clay mixed with 3.0% PW1 plastic was about 55.20%. In addition, this figure illustrates that the effect of PW1 plastic on the improvement of shear strength is almost twice in comparison with that of PW2 plastic.

It is observed that the effect of plastic wastes on the shear strength of clayey soils depends on the clay plasticity so that plastic wastes improve the shear strength of RC clay better than MC clay, but the difference is not noticeable.

Table 2 - List of samples with some specifications.

N°	Clay type	Plastic type	PWC (%)	γ_d (kN/m^3)	*w* (%)
1	MC	-	0	17.15	17.00
2	MC	PW1	0.5	17.15	17.00
3	MC	PW1	1.0	17.15	17.00
4	MC	PW1	1.5	17.15	17.00
5	MC	PW1	3.0	17.15	17.00
6	RC	-	0	19.50	12.70
7	RC	PW1	0.5	19.50	12.70
8	RC	PW1	1.0	19.50	12.70
9	RC	PW1	1.5	19.50	12.70
10	RC	PW1	3.0	19.50	12.70
11	MC	PW2	0.5	17.34	17.00
12	MC	PW2	1.0	17.15	17.80
13	MC	PW2	1.5	17.25	17.60
14	MC	PW2	3.0	17.13	17.20

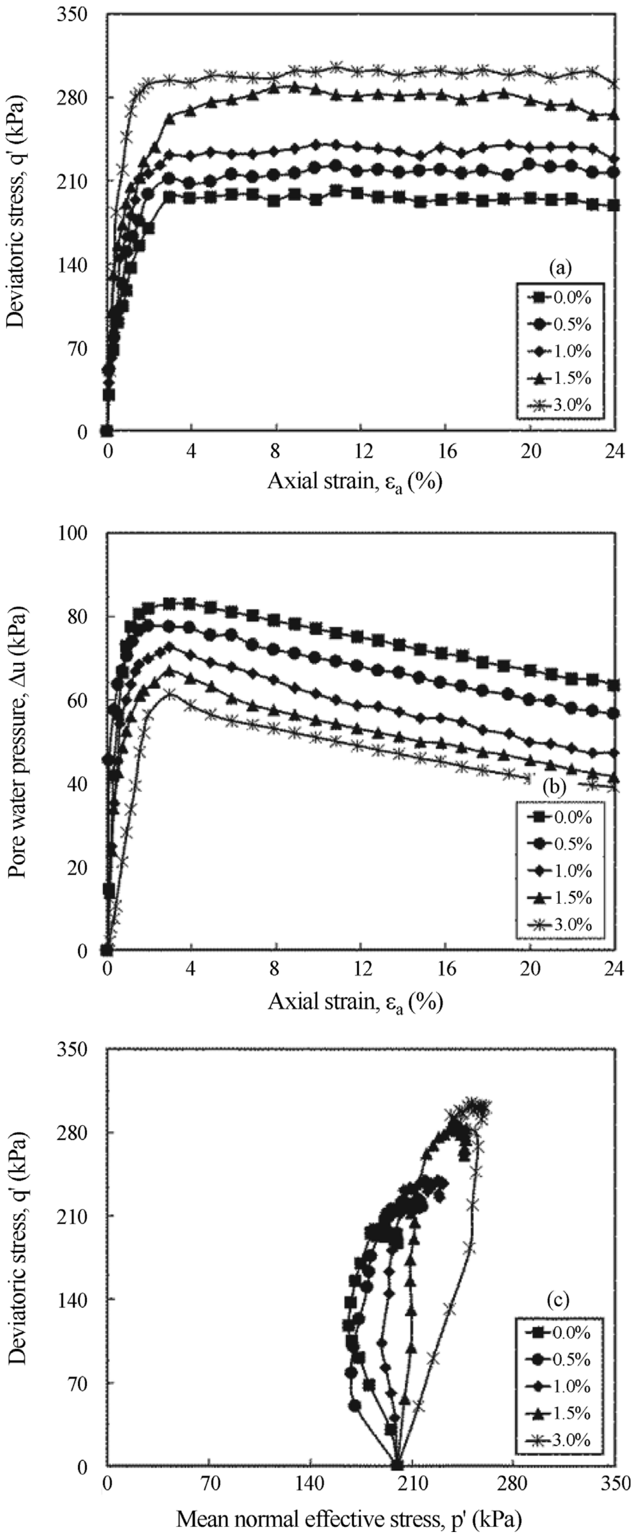

Figure 3 - Results of triaxial tests on MC-PW1 samples: (a) stress-strain curve, (b) pore water pressure changes, and (c) stress paths.

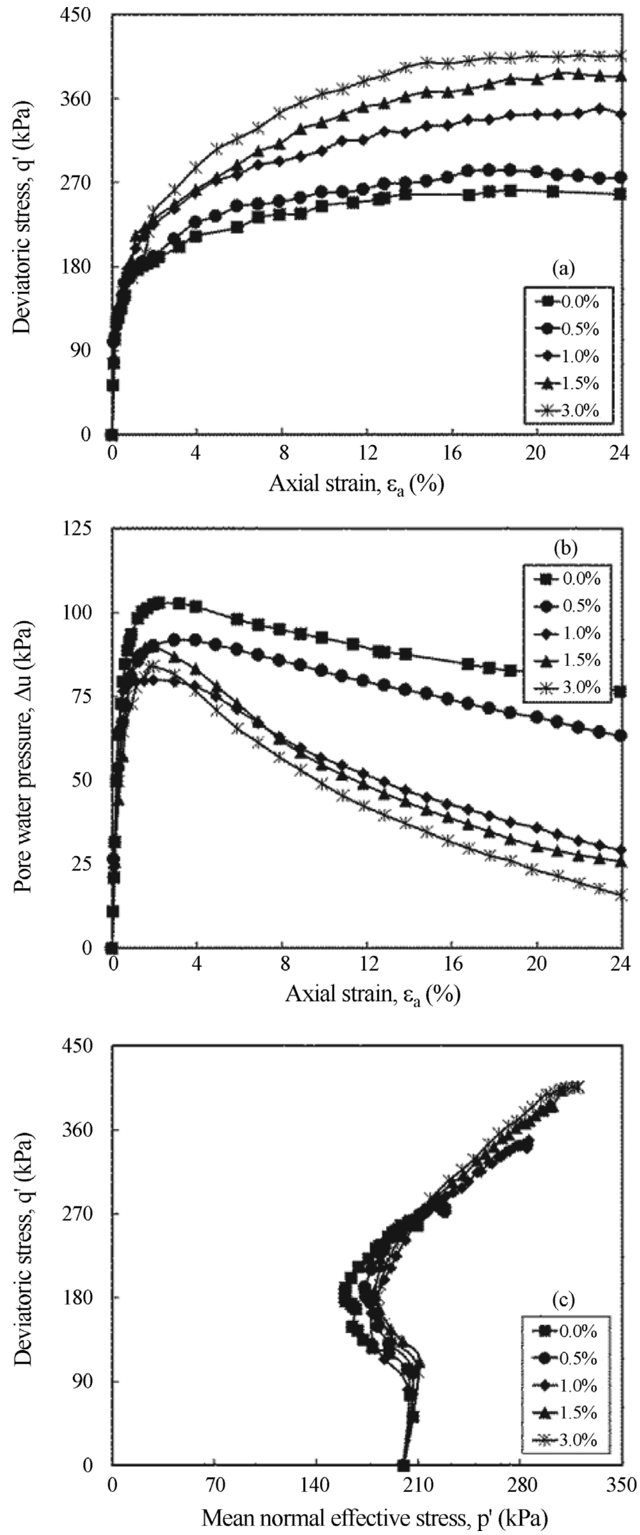

Figure 4 - Results of triaxial tests on RC-PW1 samples: (a) stress-strain curve, (b) pore water pressure changes, and (c) stress paths.

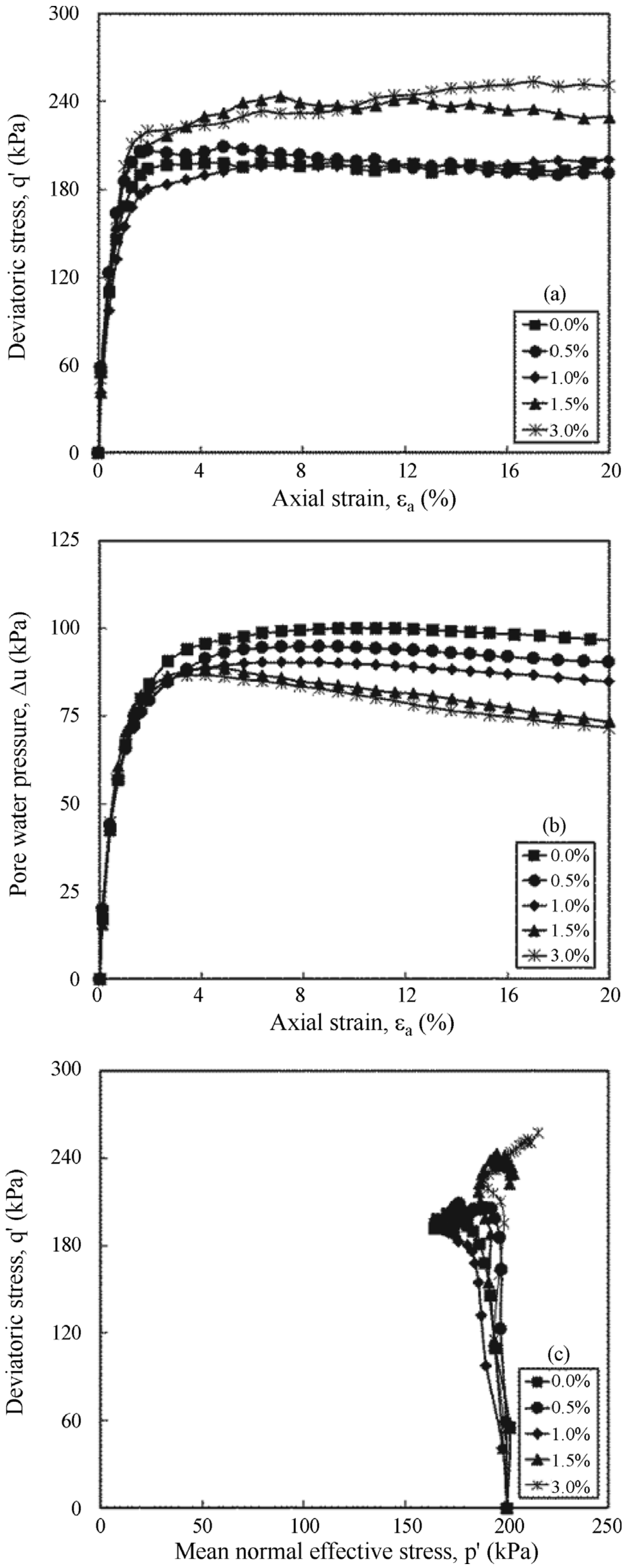

Figure 5 - Results of triaxial tests on MC-PW2 samples: (a) stress-strain curve, (b) pore water pressure changes, and (c) stress paths.

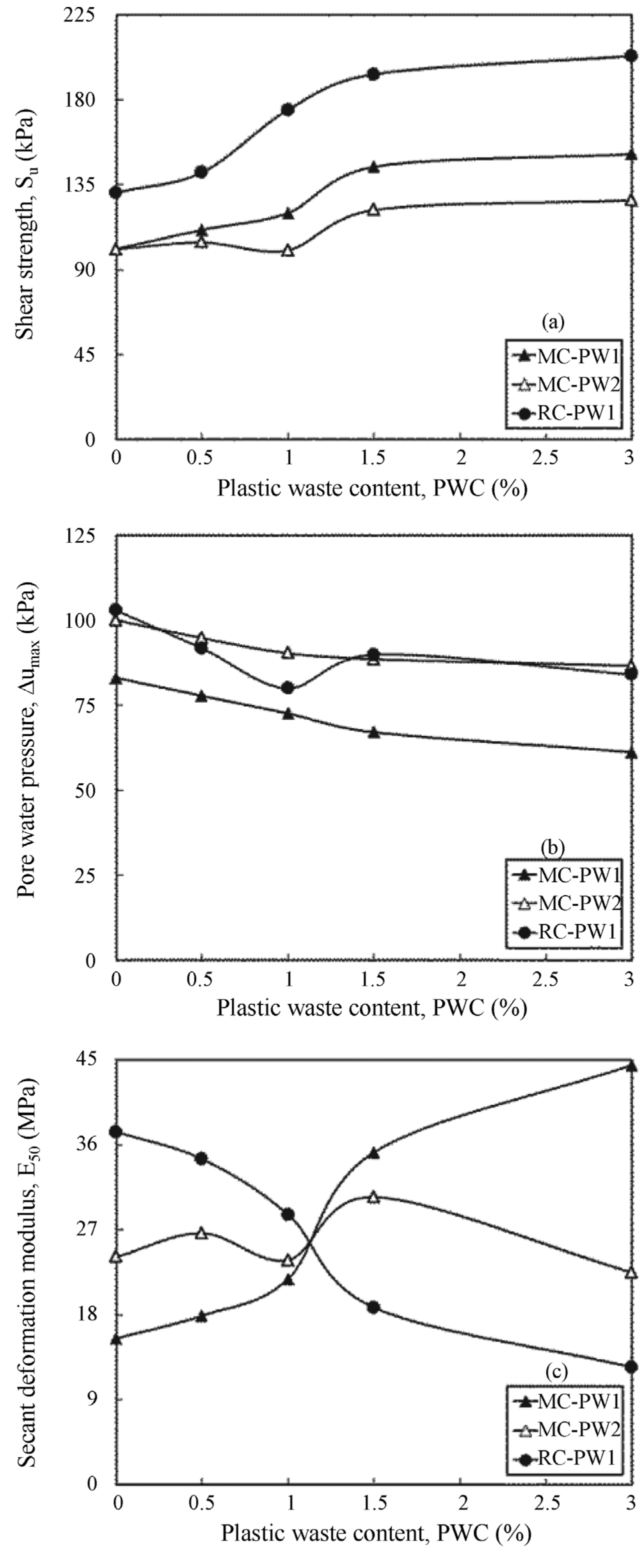

Figure 6 - Effect of plastic wastes on the: (a) shear strength, (b) maximum pore water pressure, and (c) secant deformation modulus.

3.2. Excess pore water pressures (Δu)

Change of pore water pressure during shearing (Δu) is presented in Figs. 3(b), 4(b) and 5(b). It is obvious that as the strain of samples increases to a specific value Δu rises; thereafter its value reduces with straining. The rate of decline is steep in the samples with high plastic content. Also variation of maximum pore water pressure due to shearing (Δu_{max}) (Fig. 6(b)) shows that when PC increases within the samples Δu_{max} decreases gradually. The maximum reduction takes place for MC-PW1, MC-PW2 and RC-PW1 mixtures including 3.0% PW and their values are 26.34%, 15.96% and 18.24%, respectively.

3.3. Stress paths

Stress paths of the tests (Figs. 3(c), 4(c), and 5(c)) explain that, at low level of strain, behavior of all the samples is contractive, but with developing shearing the samples exhibit dilative behavior. Moreover, as plastic waste increases the paths tend to move rightward; *i.e.* they exhibit more dilative behavior. For example, the behavior of MC clay including 3.0% plastic is completely dilative. Therefore, it can be concluded that adding plastic waste to the clay changes the tendency of samples during shearing.

3.4. Deformability

Secant deformation modulus (E_{50}) is an index of soil deformability. Therefore, the values of E_{50} for all the samples obtained from the associated stress-strain curves and their variations *vs.* PWC have been plotted in Fig. 6c. This figure shows that the effect of plastic waste on the values of E_{50} completely depends on the type of clayey soil and type of plastic. In MC clay by adding PW1 the values of secant deformation modulus increases; in other words, the deformability of samples reduces as PWC increases. The rate of increase in E_{50} is considerable and it is about 186%. For the RC clay the trend is quite opposite to that for the MC clay, so that the values of E_{50} decrease by increasing PWC in the mixtures; in other words, the deformability of samples increases as PWC increases. The rate of decrease is about 67% for the sample with 3.0% of PW1 plastic. It can be concluded that the plastic waste increases deformability of relatively stiff clay and reduces deformability of soft clay. A comparison between the curves of MC-PW1 and MC-PW2 in Fig. 6c indicates that plastic type strongly influences the trend of E_{50} variations: while stiff plastic causes E_{50} values of MC clay to increase, flexible plastic does not have any meaningful effect on clay deformability.

Moreover, Figs. 7 and 8 show photographic views of plain and plastic mixed samples after failure, respectively, for mixture of MC and RC clays with PW1 plastic. It can be noted that angle of sliding surface is higher in mixed sample in comparison with those of plain soil. This is a sign of change in behavior from cohesive soil to frictional one.

4. Conclusions

Experiments were conducted to investigate the mechanical behavior of clayey soils mixed with plastic wastes obtained from water bottles. The compaction tests showed that the dry unit weight and optimum water content of mixed samples are not much different from that of associated clay.

The findings from this research show that the maximum shear strength for plain MC clay is 101 kPa, whereas for 3.0% PW1 plastic waste mixed clay it is about 151 kPa. The results indicate that there is 49.8% increase in the shear

Figure 7 - Photo of MC-PW1 samples after testing: a) Plain clay, b) PWC = 0.5%, c) PWC = 1.0%, d) PWC = 1.5%, e) PWC = 3.0%.

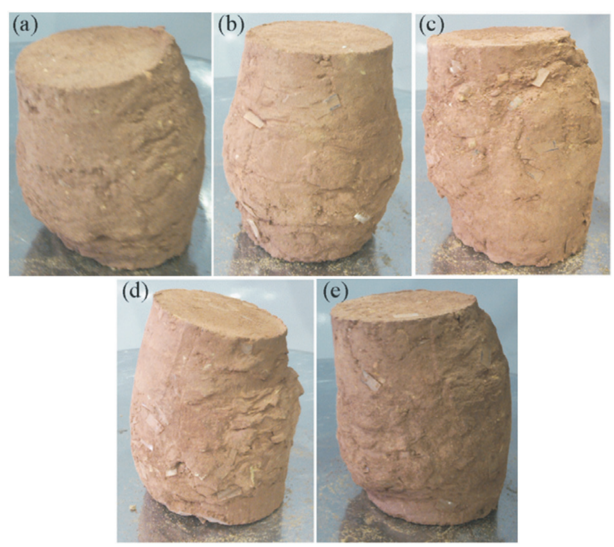

Figure 8 - Photo of RC-PW1 samples after testing: a) Plain clay, b) PWC = 0.5%, c) PWC = 1.0%, d) PWC = 1.5%, e) PWC = 3.0%.

strength of 3.0% plastic waste mixed MC clay as compared with plain clay. The maximum increase in the shear strength of RC clay is 55.20%.

It can be concluded that the plastic wastes influences the behavior of clay but this effect varies depending on the clay plasticity and flexibility of plastic wastes. The increase in the shear strength of soil is mainly due to development of tensile stress in the plastic waste. Pore water pressure due to shearing decreases slowly with an increase in plastic waste content.

The effect of plastic waste on the deformability of natural soils completely depends on the clay plasticity and plastic types. So that for MC clay with intermediate plasticity adding relatively stiff plastic causes a decrease in deformability, while for RC clay with low plasticity adding the same plastic causes an increase in deformability. In addition, it is observed that the type of plastic strongly influences the trend of deformation modulus variations.

Finally, it can be concluded that it is possible to use clay-plastic mixtures as construction materials, because of some increase in shear strength of clayey soils, and thus help to clean up the environment from the waste plastic materials.

References

ASTM (2011). D2487-06 - Standard Practice for Classification of Soils for Engineering Purposes. ASTM International, West Conshohocken, Pennsylvania, USA, 12 p.

ASTM (2012). D698-07 - Standard Test Methods for Laboratory Compaction Characteristic of Soil Using Standard Effort. ASTM International, West Conshohocken, Pennsylvania, USA, 13 p.

ASTM (2004). D 4767-04 - Standard Test Methods for Consolidated Undrained Triaxial Compression Test for Cohesive Soils. ASTM International, West Conshohocken, Pennsylvania, USA, 13 p.

Consoli, N.C.; Montardo, J.P.; Prietto, P.D.M. & Pasa, G.S. (2002). Engineering behavior of a sand reinforced with plastic waste. Journal of Geotechnical and Geoenvironmental Engineering, ASCE, 128(6):462-472.

Consoli, N.C.; Vendruscolo, M.A. & Prietto, P.D.M. (2003). Behavior of plate load tests on soil layers improved with cement and fiber. Journal of Geotechnical and Geoenvironmental Engineering, ASCE, 129(1):96-101.

Consoli, N.C.; Montardo, J.P.; Donato, M. & Prietto, P.D.M. (2004). Effect of material properties on the behavior of sand-cement-fiber composites. Ground Improvement, 8(2):77-90.

Consoli, N.C.; Vendruscolo, M.A.; Fonini, A. & Dalla Rosa, F. (2009). Fiber reinforcement effects on sand considering a wide cementation range. Geotextile and Geomembranes, 27(3):196-203.

de Mello, D.; Pezzin, S.H. & Amico, S.C. (2009). The effect of post-consumer PET particles on the performance of flexible polyurethane foams. Polymer Testing, 28(7):702-708.

Dutta, R.K. & Rao, G.V. (2007). Regression models for predicting the behavior of sand reinforced with waste plastic. Turkish Journal of Engineering and Environmental Science, 31(1):119-126.

ECO PET (2007). Available at http://www.ecopet.eu/Domino_english/ecopet.htm, accessed on 13 September 2010 and downloaded at December 10th 2014.

Rodwan Jr., J.D. (2012). Bottled water 2011: The recovery continues, U.S. and international developments and statistics, BWR, available at www.bottledwater.org, April/May 2012 and downloaded at February 20th 2015.

Sivakumar Babu, G.L.; Vasudevan, A.K. & Haldar, S. (2008). Numerical simulation of fiber reinforced sand behaviour. Geotextiles and Geomembranes, 26(2):181--188.

Sivakumar Babu, G.L. & Vasudevan, A.K. (2008a). Strength and stiffness response of coir reinforced tropical soils. Journal of Materials in Civil Engineering, ASCE, 20(9):571-577.

Sivakumar Babu, G.L. & Vasudevan, A.K. (2008b). Use of coir fibers for improving the engineering properties of expansive soils. Journal of Natural Fibers, 5(1):61-75.

Sivakumar Babu, G.L. & Vasudevan, A.K. (2008c). Seepage velocity and piping resistance of coir fiber mixed soils. Journal of Irrigation and Drainage Engineering, ASCE, 134(4):492-495.

Sivakumar Babu, G.L. & Chouksey, S.K. (2010). Model for analysis of fiber-reinforced clayey soil. Geomechanics and Geoengineering: An International Journal, 5(4):277-285.

Sivakumar Babu, G.L. & Chouksey, S.K. (2011). Stress-strain response of plastic waste mixed soil, Waste Management, 31(3):481-488.

Discussion

Soils and Rocks
v. 39, n. 3

Discussion

On the Interpretation of Bidirectional Loading Tests

Discussion by:
Virginia Maset and **Frederico Falconi**
ZF Engenheiros Associados

The method presented by the author is an evolution from the usual procedure, which is commonly used to interpret the bidirectional test, since it also takes into account the elastic deformations of the pile. However, some considerations must be made.

The author uses, as his main case study to validate the method, a case in which two static load tests were performed in similar and closely spaced piles. The value of y_1, *i.e.* the pile displacement required to trigger non-linear response along the shaft-soil interface, is considered equal to 0,35 mm. This value was probably inferred by identifying, in the load-settlement curve obtained from the conventional test, the point at which the shaft resistance reaches maximum for the first section of the pile. In another section of the article, it is stated that usually y_1 is "of the order of a few millimeters". When the load-settlement curve from the conventional test is not available – which happens very often – it becomes very hard to determine this value. In two other cases to which the method was applied by the author, different values were assumed for y_1: in one, it is stated that "the value of y_1 was large", therefore the pile behaved like a rigid or short pile; in the other, "y_1 was assumed to be 3,8 mm".

The readers applied the method to a case study in Curitiba, PR, and found out that a variation of 2 mm in the value of y_1 could be the difference between classifying the pile as short/rigid or as long/compressible.

It is also of note that the O-cell is not always ideally placed along the pile shaft. In most cases – like the one the author based his proposed method on – there is a huge difference between the shaft and toe movements. When this happens, one of the curves must be extrapolated in order to build the equivalent load x settlement curve from the conventional test. This extrapolation may induce errors and misinterpretation of the pile behavior.

Finally, in Fig. 22 the author presents the download curves from both the conventional test and the equivalent curve from the bidirectional test obtained by the proposed method. He observes that both curves have a remarkable fit up until the full mobilization of the shaft resistance in pile E 46A, but its fictitious toe resistance is much lower than that of E 46 due to an "unknown reason". This suggests that, even if the method is successfully applied to a bidirectional test set of curves, the failure load obtained could be lower than the actual failure load of the pile, thus underestimating the pile capacity.

In conclusion, the method proposed by the author theoretically solves the problems inherent to interpreting the results of the bidirectional tests. Not only it introduces the elastic shortening of the pile shaft, but also corrects it by the ratio *c*/*c*' to simulate the top-down loading of the pile. Nevertheless, the aforementioned practical difficulties – determination of the value of y_1, extrapolation of almost linear curves – make it difficult for the method to be incorporated into foundation design routines.

Article by Faiçal Massad, published in Soils and Rocks, 38(3):249-262 (2015), e-mail: faissal@usp.br.

Closure by author

The author wishes to thank the readers for the comments and questions that surely will help in understanding the basis of the new procedure to find the equivalent curve of the conventional test through the bidirectional test on piles.

1) The new procedure is based on approximate formulas given by Eqs. (17) and (18) of the paper, applicable when one or more expansive interconnected cells are placed near the pile toe. Note that the term y_1 of Fig. 4-a does not appear in these equations, that are an extension of the usual procedure to determine the equivalent curve. Modifications were introduced to take into account the elastic shortening of the shaft induced by the loads in the bidirectional test, just knowing pile elasticity modulus (E), its dimensions and the distribution of lateral load along depth, for example through the *SPT*. The magnitude of the elastic shortening determines pile compressibility: if large the pile is "long" otherwise it is "short". There is no need at all to know the term y_1.

2) The term y_1 was used in the paper associated to the application of the mathematical model developed by the author based on Cambefort Relations (Fig. 4). This model was used both, to show that the coefficients c and c' play an important role to find the equivalent curve and to support and validate the application of the approximate formulas, as it was done, for instance, through Fig. 22 for the two CFA piles E 46 and E 46A. In this figure there are 4 curves, one related to the conventional test on pile E 46 (measured curve) and the 3 others to the bidirectional test on pile E 46A. The last 3 curves were obtained by:

a) the mathematical model (Cambefort) applied to pile E 46A;

b) the equivalent curve for pile E 46A, based on the new procedure using the approximate formulas, Eqs. (17) and (18), that again do not depend on y_1; details of the calculations are shown in Table 3; and

c) the usual procedure for pile E 46A, that ignores pile compressibility, as if it had an infinite stiffness.

The paper stressed that the fittings are remarkable up to the point of full mobilization of the shaft resistance except for the usual procedure, with much smaller settlements because it did not consider the large compressibility of pile E 46A. Fig. 22 shows moreover that the fictitious toe resistance of Pile E 46A is much smaller than the toe resistance of Pile E 46, submitted to the conventional test, due to an unknown reason. One may guess that some problem occurred during the O-Cell installation, supported by the result presented in Fig. 20-b relating toe loads and downward movements of the bidirectional test on pile E 46A.

3) Other models may be used in the above mentioned validation, like the software algorithm UniPile of Fellenius or the Coyle-Reese model, as the author mentioned throughout the paper and in its Appendix, where the Ratio Function (Fig. A2) was considered instead of the Cambefort Relation as the shaft transfer function. In the case histories validated by the mathematical model based on Cambefort Relations, the terms y_1, A_{lr} (total shaft load at failure) and *R.S* (toe stiffness) were estimated using the data measured in the bidirectional tests, in the upward and downward directions. This was the case in determining particularly the term y_1 of the aforementioned pile E 46A, using Figs. 19 and 20, and not in the way speculated by the readers.

4) The readers mentioned difficulties in extrapolations when dealing with the upward and downward curves of the bidirectional tests. In fact this problem may happen and extrapolations are usually done by those who apply the usual procedure to find the equivalent curve. The two procedures, the usual and the new one proposed by the author, require good quality tests. The paper showed various case histories that accomplished this condition. In all of them the O-cells were placed near the pile toe, except for the two short (rigid) Omega Piles in São Paulo City. In all cases the results were very good, revealing the potential and simplicity of the new proposed procedure.

5) Finally, summing up and going to the main point of the readers' arguments, the new procedure does not require the knowledge of the term y_1. It suffices to compute the elastic shortening of the pile shaft in some way, as pointed out by the author in his paper.

SOILS and ROCKS
An International Journal of Geotechnical and Geoenvironmental Engineering

Publication of

ABMS - Brazilian Association for Soil Mechanics and Geotechnical Engineering

SPG - Portuguese Geotechnical Society

Volume 39, N. 3, September-December 2016

Author index

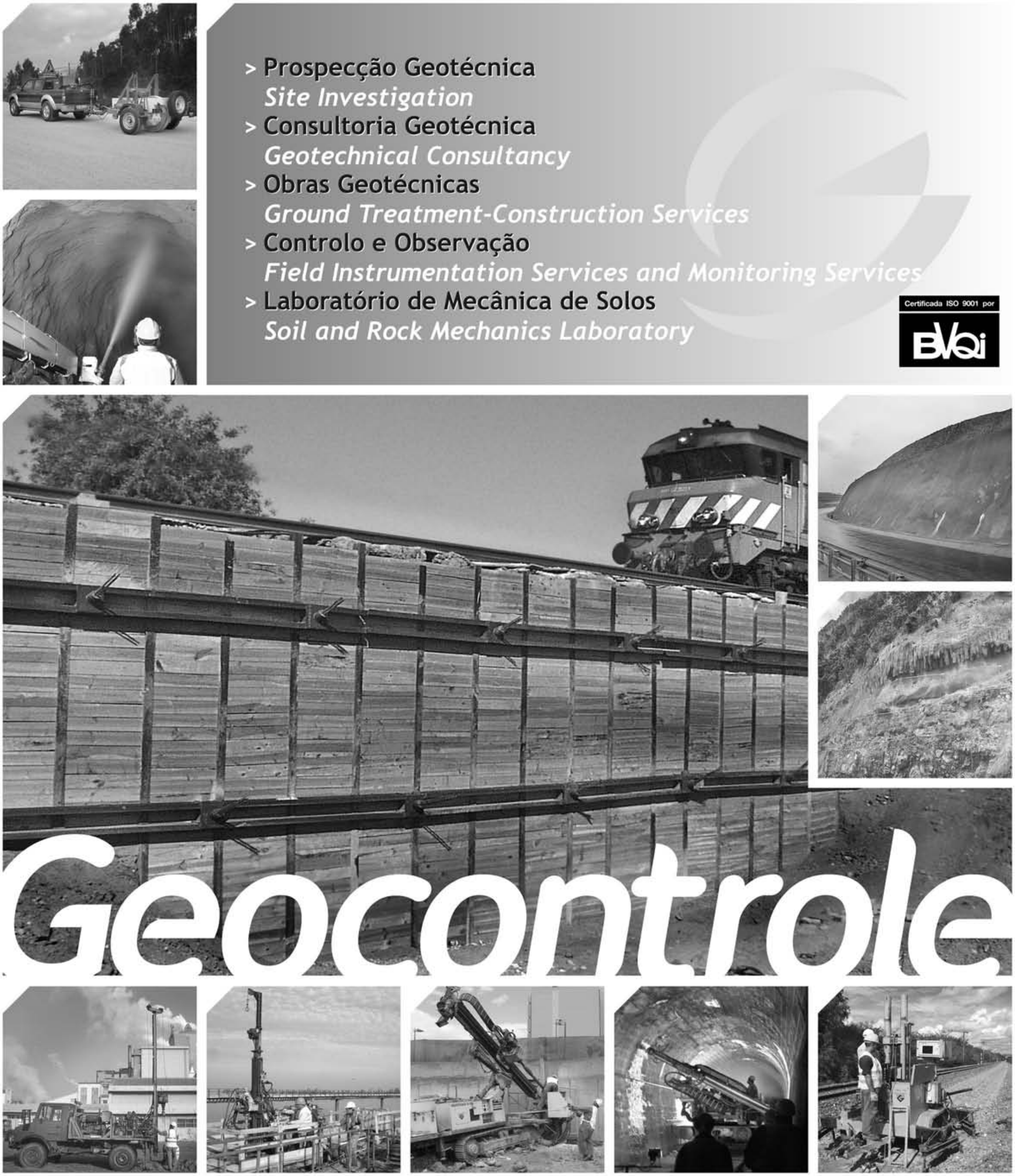

> Prospecção Geotécnica
Site Investigation
> Consultoria Geotécnica
Geotechnical Consultancy
> Obras Geotécnicas
Ground Treatment-Construction Services
> Controlo e Observação
Field Instrumentation Services and Monitoring Services
> Laboratório de Mecânica de Solos
Soil and Rock Mechanics Laboratory
Certificada ISO 9001 por
BVQi
Geocontrole

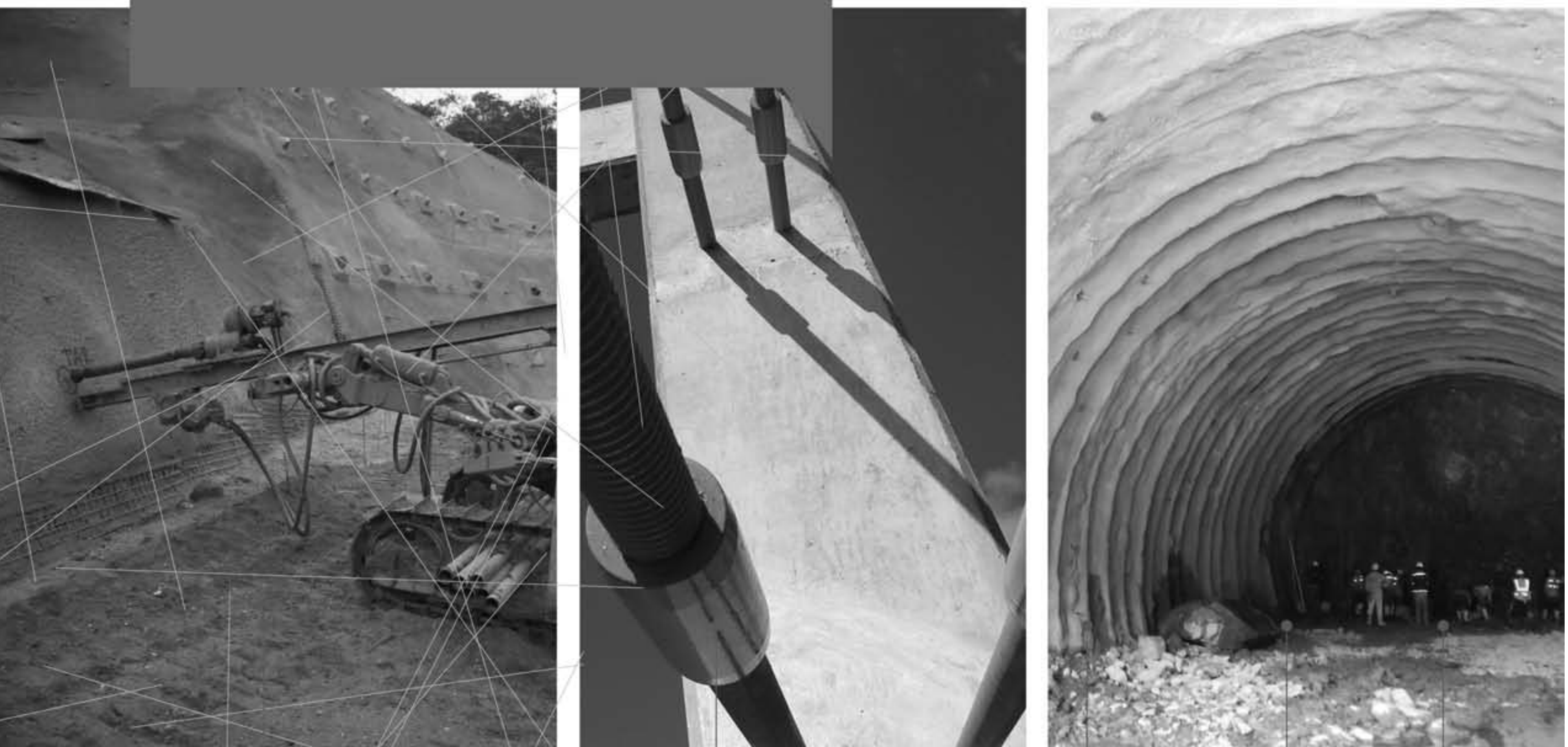

Instructions for Submission of Manuscripts

Category of the Papers

Soils and Rocks is the international scientific journal edited by the Brazilian Association for Soil Mechanics and Geotechnical Engineering (ABMS) and the Portuguese Geotechnical Society (SPG). The aim of the journal is to publish (in English) original research and technical works on all geotechnical branches.

According to its content the accepted paper is classified in one of the following categories: Article paper, Technical Note, Case Study or Discussion. An article paper is an extensive and conclusive dissertation about a geotechnical topic. A paper is considered as a technical note if it gives a short description of ongoing studies, comprising partial results and/or particular aspects of the investigation. A case study is a report of unusual problems found during the design, construction or the performance of geotechnical projects. A case study is also considered as the report of an unusual solution given to an ordinary problem. The discussions about published papers, case studies and technical notes are made in the Discussions Section.

When submitting a manuscript for review, the authors should indicate the category of the manuscript, and is also understood that they:

a) assume full responsibility for the contents and accuracy of the information in the paper;

b) assure that the paper has not been previously published, and is not being submitted to any other periodical for publication.

Manuscript Instructions

Manuscripts must be written in English. The text is to be typed in a word processor (preferably MS Word), **single column**, using ISO A4 page size, left, right, top, and bottom margins of 25 mm, Times New Roman 12 font, and line spacing of 1.5. All lines and pages should be numbered. The text should be written in the third person.

The first page of the manuscript must include the title of the paper followed by the names of the authors with the abbreviation of the most relevant academic title. The affiliation, address and e-mail must appear below each author´s name. An abstract of 200 words follows after the author´s names. A list with up to six keywords at the end of the abstract is required.

Although variations on the sequence and title of each section are possible, it is suggested that the text contains the following sections: Introduction, Material and Methods, Results, Discussions, Conclusions, Acknowledgements, References and List of Symbols. A brief description of each section is given next.

Introduction: This section should indicate the state of the art of the problem under evaluation, a description of the problem and the methods undertaken. The objective of the work should be clearly presented at the end of the section.

Materials and Methods: This section should include all information needed to the reproduction of the presented work by other researchers.

Results: In this section the data of the investigation should be presented in a clear and concise way. Figures and tables should not repeat the same information.

Discussion: The analyses of the results should be described in this section.

Conclusions: The content of this section should be based on the data and on the discussions presented.

Acknowledgements: If necessary, concise acknowledgements should be presented in this section.

References: References to other published sources must be made in the text by the last name(s) of the author(s), followed by the year of publication, similarly to one of the two possibilities below:

...while Silva & Pereira (1987) observed that resistance depended on soil density... or *It was observed that resistance depended on soil density (Silva & Pereira, 1987).*

In the case of three or more authors, the reduced format must be used, *e.g.*: Silva *et al.* (1982) or (Silva *et al.*, 1982). Two or more citations belonging to the same author(s) and published in the same year are to be distinguished with small letters, *e.g.*: (Silva, 1975a, b, c.). Standards must be cited in the text by the initials of the entity and the year of publication, *e.g.*: ABNT (1996), ASTM (2003).

Full references shall be listed alphabetically at the end of the text by the first author´s last name. Several references belonging to the same author shall be cited chronologically. Some examples are listed next:

Papers: Bishop, A.W. & Blight, G.E. (1963). Some aspects of effective stress in saturated and unsaturated soils. Geotechnique, 13(2):177-197.

Books: Lambe, T.W & Whitman, R.V. (1979). Soil Mechanics, SI Version. John Wiley & Sons, New York, 553 p.

Book with editors: Sharma, H.D.; Dukes, M.T. & Olsen, D.M. (1990). Field measurements of dynamic moduli and Poisson's ratios of refuse and underlying soils at a landfill site. Landva, A. & Knowles, G.D. (eds), Geotechnics of Waste Fills - Theory and Practice, American Society for Testing and Materials - STP 1070, Philadelphia, pp. 57-70.

Proceedings (printed matter or CD-ROM): Jamiolkowski, M.; Ladd, C.C.; Germaine, J.T. & Lancellotta, R. (1985). New developments in field and laboratory testing of soils. Proc. 11th Int. Conf. on Soil Mech. and Found. Engn., ISSMFE, San Francisco, v. 1, pp. 57-153. (specify if CD ROM).

Thesis and dissertations: Lee, K.L. (1965). Triaxial Compressive Strength of Saturated Sands Under Seismic Loading Conditions. PhD Dissertation, Department of Civil Engineering, University of California, Berkeley, 521 p.

Standards: ASTM (2003). Standard Test Method for Particle Size Analysis of Soils - D 422-63. ASTM International, West Conshohocken, Pennsylvania, USA, 8 p.

Internet references: Soils and Rocks available at http://www.abms.com.br and downloaded on August 6th 2003.

On line first publications must also bring the digital object identifier (DOI) at the end.

Figures shall be either computer generated or drawn with India ink on tracing paper. Computer generated figures must be accompanied by the corresponding digital file (.tif, .jpg, .pcx, etc.). All figures (graphs, line drawings, photographs, etc.) shall be numbered consecutively and have a caption consisting of the figure number and a brief title or description of the figure. This number should be used when referring to the figure in text. Photographs should be black and white, sharp, high contrasted and printed on glossy paper.

Tables shall be numbered consecutively in Arabic and have a caption consisting of the table number and a brief title. This number should be used when referring to the table in the text. Units should be indicated in the first line of the table, below the title of each column. Acronyms should be avoided. When applicable, the units should come right below the corresponding column heading. Additional comments can be placed as footnotes.

Equations shall appear isolated in a single line of the text. Numbers identifying equations must be flushed with the right margin. International System (SI) units must be used. The definitions of the symbols used in the equations must appear in the List of Symbols. It is recommended that the symbols used are in accordance with Lexicon in 8 Languages, ISSMFE (1981) and the ISRM List of Symbols.

The text of the submitted manuscript (including figures, tables and references) intended to be published as an article paper or a case history should not contain more than 30 pages, formatted according to the instructions mentioned above. Technical notes and discussions should have no more than 15 and 8 pages, respectively. Longer manuscripts may be exceptionally accepted if the authors provide proper explanation for the need of the required extra space in a cover letter.

Discussion

Discussions must be written in English. The first page of a discussion should contain:

The title of the paper under discussion;

Name of the author(s) of the discussion, followed by their position, affiliation, address and e-mail. The author(s) of the discussion should refer to himself (herself/themselves) as the reader(s) and to the author(s) of the paper as the author(s).

Figures, tables and equations should be numbered following the same sequence of the original paper. All instructions previously mentioned for the preparation of article papers, case studies and technical notes also apply to the preparation of discussions.

Editorial Review

Each paper will be evaluated by reviewers selected by the editors according to the subject of the paper. The authors will be informed about the results of the review process. If the paper is accepted, the authors will be required to submit a version of the revised manuscript with the suggested modifications. If the manuscript is rejected for publication, the authors will be informed about the reasons for rejection. In any situation comprising modification of the original text, classification of the manuscript in a category different from that proposed by the authors, or rejection, the authors can reply presenting their reasons for disagreeing with the reviewer comments.

Submission

The author(s) must upload a digital file of the manuscript to the Soils and Rocks website.

Follow Up

The online management system will provide a password to the corresponding author, which will enable him/her to follow the reviewing process of the submitted manuscript at the Soils and Rocks website.

Volume 39, N. 3, September-December 2016

Table of Contents